Composite of microgels and lipids as biofilm to restore skin barrier function

Marion Oudshoorn

Publication of this thesis was financially supported by:

Croda Europe Ltd (UK)

CRODA

Utrecht Institute for Pharmaceutical Sciences, Utrecht, The Netherlands
UIPS

UIPS Utrecht Institute for Pharmaceutical Sciences

Composite of microgels and lipids as biofilm to restore skin barrier function
Marion Oudshoorn
PhD thesis with summary in Dutch
Department of Pharmaceutics, Utrecht University, Utrecht, The Netherlands
October 2008

ISBN: 978-90-393-4872-7

Cover design: Jeroen Hutten. Picture on cover shows a sculpture (‘Music for the eyes’) created by Jan Pater (www.partbeelden.nl).
Printed by PrintPartners Ipskamp, Enschede, The Netherlands

Composite of microgels and lipids as biofilm to restore skin barrier function

Composiet van microgelen en lipiden als biofilm voor het herstel van de huidbarrière-functie

(met een samenvatting in het Nederlands)

Proefschrift

ter verkrijging van de graad van doctor aan de Universiteit Utrecht op gezag van de rector magnificus, prof. dr. J.C. Stoof ingevolge het besluit van het college voor promoties in het openbaar te verdedigen op woensdag 1 oktober 2008 des middags te 4.15 uur

door

Marion Henrica Monique Oudshoorn

geboren op 9 november 1981 te Delft

Promotoren: Prof. dr. ir. W.E. Hennink
Prof. dr. J.A. Bouwstra

The research described in this thesis was financially supported by the Technology Foundation STW (project no. 6117).

TABLE OF CONTENTS

General introduction

1

1. Introduction

The natural function of the skin is the protection of the body against desiccation on the one hand and against various environmental influences on the other hand [1-3]. It mediates a large group of protective functions against, for instance, mechanical stress and UV light but it also keeps microbial pathogens outside the body [2, 4]. Moreover, the skin plays a crucial role in transmitting external environmental information (sensory organ) and in regulating the body temperature. Epidermal barrier perturbation can be a consequence of many factors, such as environmental influences, burns or injuries. Additionally, an impaired barrier function is also encountered in diseased skin and in skin of preterm infants. These infants have an ineffective skin barrier due to a deficient or even absent stratum corneum (SC), which is the outermost layer of the skin [5-7].
It is known that a proper hydration of the SC is essential for barrier repair and also to maintain an optimal skin barrier. The balance of moisture is necessary to preserve flexibility and to provide enough water to allow enzymes to facilitate both normal SC maturation and desquamation (loss of cells from the surface of the SC). An excess or a lack of hydration will interfere with these processes impeding barrier repair [3, 8-11]. Many skin protectants have been developed with the aim to modify the hydration level of the SC and to protect the body against excessive water loss and thus to normalize water levels in SC [3, 5, 12]. These skin protectants increase the moisture content of the SC and thus increase the extent of hydration of SC by either blocking the water loss from the skin surface or by delivering exogenous humectants into the SC. However, upon water release to the environment the structure of these creams, which is markedly different from the structure of SC, changes. This may result in an uncontrolled effect on the water level in the SC. Therefore it is suggested that treatment with creams combining an excellent water holding capacity with a virtually unchanged structure upon water release may help in the development and/or repair of the SC barrier. When mimicking closely the structure of SC, the creams may in addition act as a protective layer (similar as the natural function of SC) on damaged skin where the SC is largely absent.

Vernix caseosa (VC) is a lipid-rich, natural biofilm which coats the skin of the developing fetus during the final stage of the gestational period. The structure of VC is very similar to that of SC [13-16]. A variety of biological properties has been assigned to VC [6, 13, 14, 17-20]: it is, for instance, suggested to act as waterproof film promoting the formation of the horny layer of the fetus. The exact mechanism of action, however, is still unknown but many presumed mechanisms are reported in literature [13, 15]. The multiple biological functions of VC imply that this natural biofilm holds promise as a clinical effective therapeutic agent promoting the repair of the skin barrier of preterm infants [6, 7] or enhancing barrier repair in adult skin [13]. Application of VC to clinical use,

however, is restricted by the limited availability of VC and the risk of transmission of diseases. Therefore, the development of a synthetic VC equivalent could lead to novel biofilms, mimicking closely the unique composition and properties of natural VC. These innovative biofilms may promote barrier repair processes of injured skin in a similar way as has been suggested for VC in the fetus [13, 14]. Hence, the objective of this thesis was to design a new generation of synthetic biofilms combining the structure and properties of natural VC, to protect diseased, dry and premature skin and to facilitate healing of superficial wounds (defined as skin where the SC is largely absent, whereas underlying skin is undamaged).

In the first part of this chapter, the structure and function of the human skin and available models to mimic impaired human skin will be discussed. The second part describes the preparation of crosslinked hydrophilic polymers (hydrogels). These networks are capable of absorbing large amounts of water and are therefore appropriate to mimic the water holding capacity of VC. Finally, the objective and outline of this thesis will be presented.

2. The human skin

2.1. Stratum corneum

The outermost layer of the skin, the stratum corneum (SC; 10-20 µm thick) [1, 3, 4], is the principal physical barrier for diffusion of substances across the skin. The SC consists of flat dead cells, corneocytes, which are filled with keratin filaments and water. The corneocytes are surrounded by densely crosslinked proteins (cornified envelope) and the surface of the corneocytes is coated with lipids chemically bound to the cornified envelope. The corneocytes are embedded in lipid lamellar regions (Fig. 1). This structure is frequently portrayed as a wall-like structure where the corneocytes represent ‘bricks’ that are embedded in a lipid ‘mortar’. Protein structures, referred to as desmosomes, are present to interconnect the corneocytes [1, 21].

The SC covers the viable epidermis. The viable epidermis is 50-100 µm thick and is responsible for generation of the SC. The epidermis is a dynamic, constantly self-renewing tissue, in which a loss of cells from the surface of the SC (desquamation) is balanced by cell growth in the deepest layer of the epidermis. Underneath the epidermis, the dermis is located. The dermis (1-2 mm thick) provides the mechanical support for the skin. Additionally, the blood vessels in the dermis provide the skin with nutrients and oxygen [1, 22]. The subcutis or subcutaneous fat tissue is the deepest layer of the skin. It helps to conserve body temperature and provides mechanical protection.

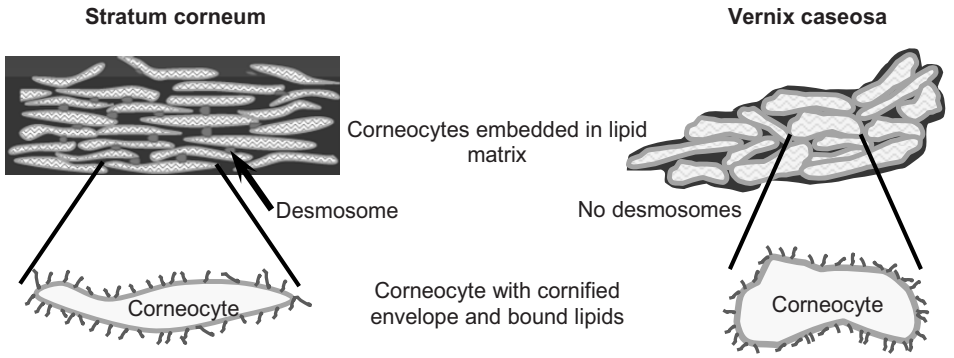

Figure 1. *Schematic drawing of stratum corneum and vernix caseosa. The corneocytes are surrounded by a densely crosslinked protein layer, called the cornified envelope, and a layer of covalently bound lipids. The corneocytes are embedded in a lipid matrix. Desmosomes are interconnecting the corneocytes in stratum corneum. VC lacks these intercorneocyte desmosomal connections and is therefore be referred to as a 'mobile phase' SC.*

2.2. Vernix caseosa

During the last trimester of human pregnancy the highly organized SC is being developed. In this period, the SC of the fetus is protected by a thick, cheesy, white cream (Fig. 2) called vernix caseosa (VC). In premature infants however, this natural surface biofilm is absent [6, 7, 14]. The production of VC is uniquely human and is proposed to be beneficial in postnatal adaptation [14, 15]. VC has a similar structure as SC and consists of hydrated cells (corneocytes) embedded in a lipid matrix (Fig. 1). On the interface between the free lipids and the corneocytes, lipids are covalently bound to the cornified envelope of the cells, similar as in SC. However, in contrast to SC, VC lacks intercorneocyte desmosomal connections and the intercellular lipids are in a less ordered state. As a consequence, VC exhibits a viscous fluid character and is therefore referred to as a mobile phase SC [13-16]. In its natural environment, VC is composed of roughly 80% water, 10% proteins and 10% lipids [7, 13]. The most abundant protein present in VC is keratin, which forms the scaffold of the corneocytes. These dead cells form the main water reservoir of VC and are mostly polygonal and flat in shape, with a diameter varying between 15 and 40 μm and a thickness of 1-2 μm [23]. The VC lipid matrix is composed of both SC and sebaceous lipids [7, 13, 16]. Additionally, VC contains antibiotic peptides and polypeptides with innate immune functions [18, 24, 25].

Figure 2. *Vernix caseosa on the skin of an infant at birth. It covers the skin of the human fetus to varying degrees during the last stage of the gestational period [26].*

A variety of biological properties has been assigned to VC. *In utero* it is suggested to act as a waterproof film promoting the formation of SC of the fetus [13, 14]. Additionally, VC is proposed to act as a lubricant during delivery, while exhibiting anti-infective [18], anti-oxidant [19], skin hydrating [20] and skin cleansing properties postnatally [6]. Moreover, VC shows a temperature-dependent dehydration behavior, enabling the hydration of the newborn's skin in a continuous manner [17]. Because of these multiple excellent properties, VC appears to hold promise as a clinical effective therapeutic agent promoting the repair of the skin barrier of preterm infants [6, 7] or enhancing superficial wound healing of adult skin [13].

2.3. Skin care management of impaired skin

Epidermal perturbation can be caused by many environmental factors, but can also be due to diseases or premature birth [6, 7, 27]. If the natural barrier is immature or damaged, water diffusion increases and transepidermal water loss (TEWL) values can increase up to 5 to 10 times the TEWL of healthy SC, which may result in a dehydration of the SC [28-30]. A proper hydration of the SC, however, is essential to maintain an optimal skin barrier and also for barrier repair. This moisture balance is required to allow enzymes to promote normal SC maturation and desquamation and to preserve flexibility. Either prolonged exposure to moisture or a shortage of hydration will interfere with these processes, impeding barrier repair [3, 8-11]. Currently, many skin protectants are available with the aim to modify the hydration level of the SC and to protect the body against excessive water loss and thus to support epidermal barrier function [3, 5, 12]. However, the precise mechanism of action of how these agents work is still not fully understood. They are designed to increase the hydration level by either reducing the TEWL such as occlusive lipophilic moisturizers (e.g. Vaseline) or by penetrating into the

SC such as hydrophilic moisturizers (e.g. glycerin) [31, 32]. The structure of moisturizer containing creams is in most cases markedly different from that of the SC. Moreover, these creams changes in structure upon water release to the environment, which may result in an uncontrolled effect on the water level in the SC. Therefore it is suggested that treatment with creams combining an excellent water holding capacity with a virtually unchanged structure upon water release may help in the development and/or restoration of the SC barrier. In circumstances where the SC is still present (e.g. dry skin) the application of these new creams might result in a controlled release of water. More importantly, when the SC is largely deficient or even absent (e.g. superficial wound healing or in preterm infants) these new creams may act as a protective layer, similar as the natural function of SC. For this purpose, the unchanged structure upon water release, the water holding capacity and the presence of barrier lipids may play a role in protecting impaired SC and possibly in promoting SC formation as was suggested for natural VC [13, 14]. Consequently, other creams have to be developed that mimic more closely the structure of the SC.

2.4. Models for human skin

In order to test new wound healing strategies there is a need for models to investigate product safety and efficacy. Moreover, the models are essential as the wound healing process is of multifactorial nature and may be influenced by many external factors and compounds [33-35]. Ideally, human studies are considered as the golden standard when studying the effectiveness of wound healing agents [8, 32, 36-38]. Nevertheless, human studies encounter several drawbacks [39]: I) A large group of patients with identical wounds for randomized trials is difficult to obtain. II) There is a restriction to objective measurements as frequent biopsies are necessary for histological evaluation. III) Ethics prevents the application of controls, which will constrain the quality of the data.

Hence, the use of other models (*in vitro* and *in vivo*) is inevitable and in the literature many *in vitro* and *in vivo* wound-healing models have been described [33, 34, 40, 41]. The choice of the models depends on several factors, such as type of investigation (e.g. efficacy or safety) and outcome (e.g. visual assessment or tissue regeneration). Different *in vitro* models exist, varying from human skin and animal skin to cell cultures with increasing complexity from single cell systems to multicellular systems in artificial 3D matrices [42-45]. In recent years, several artificial human skin models have been developed of which several are commercially available (e.g. Epiderm™, SkinEthic™ and Episkin™) [44, 45]. These models are useful to assess skin irritation or injury and to a lesser extend for percutaneous absorption of drugs. For all systems the cellular functions, such as migration, proliferation, protein synthesis and wound contraction, related to the applied stress or compound can be tested. More specific wound healing models are suitable to evaluate key elements of tissue repair, such as angiogenesis and

re-epithelialization [34, 41]. A large diversity of *in vivo* models is also available depending on the part of the healing process that needs to be studied [35]. Small mammals, such as rabbits, guinea pigs, rats and mice, are frequently used in wound healing studies [33, 34, 39, 41]. Selection of a model is based on its accuracy to reflect the biological processes that occur in normal human wound healing. When using animals the wound healing process is faster than observed in humans (i.e. days rather than weeks). Moreover, wound healing in animals show similarities to tissue repair in the clinical practice. Removal and analysis of tissues in rather large amounts is possible as well as the assessment of various parameters, such as macroscopic observations, cellular and immunologic response and measurement of wound healing markers [34, 41]. A common skin wound model is the superficial wound model [34, 46]. In this model, barrier perturbation can be induced by, for instance, sequential tape stripping [27, 29, 36, 47] or various detergents [29, 48], and it is used to evaluate epidermal regeneration. The insults simulate a variety of disturbances that occur during different types of environmental exposure. With the superficial wound model the influence of various types of compounds or drugs can be investigated [30, 49]. Evaluation of skin recovery can be done by means of histology, whereas barrier integrity can be assessed by non-invasively TEWL measurements [29, 36, 40, 48, 50].

3. Hydrogels

3.1. General

One of the key elements in VC are the corneocytes, which are responsible for the water holding properties. In a VC mimic their role can be taken over by hydrogel particles. Hydrogels are hydrophilic, crosslinked polymeric materials, which are capable of absorbing large amounts of water while preserving a three-dimensional (3-D) network structure [51, 52]. Due to this high water-absorbing capacity and their soft and rubbery nature, which is similar to natural tissue, hydrogels ensures good biocompatibility and can therefore be applied for a large variety of applications in the biomedical and pharmaceutical field (e.g. drug delivery devices, artificial organs/implants and contact lenses) [51-55]. To prevent the polymer chains from dissolving in an aqueous environment crosslinks have to be present in the hydrogels [52-54, 56]. This can be achieved by either physical or chemical crosslinking of the hydrophilic polymers [52, 57]. Physical crosslinked gels, involving non-permanent, reversible crosslinks, can be based on e.g. ionic interactions [58], hydrophobic association [59, 60] or hydrogen bonding [61]. Chemical (permanent) crosslinked hydrogels can be obtained by introducing covalent crosslinks between polymer chains, e.g. by radical polymerization of mono- or multifunctional (meth)acrylates [55, 62, 63]. The method of crosslinking used is dependent on the specific application of the hydrogels: physical crosslinked gels can be

formed under mild conditions and can be reversibly broken, although their mechanical strength is often weak, whereas chemical crosslinking results in the formation of reproducible, well-defined gels with a high mechanical strength, though chemical crosslinking agents might damage loaded substances. In addition to the crosslinking method, the degradability of the polymeric networks as well as the formed degradation products can be tailored [54, 55, 64]. Degradability can be established by introducing labile bonds, whereas the formed degradation products can be tailored by selecting the appropriate hydrogel building blocks. As a result a wide and diverse range of polymers, depending on the required properties, can be used to prepare hydrogels. The composition of the polymers can be divided into two groups: natural polymers, such as hyaluronic acid [65, 66], dextran [63, 67] and chitosan [68, 69], and synthetic polymers, including poly(ethylene glycol) (PEG) [70, 71] and poly(hydroxyethyl methacrylate) (pHEMA) [72, 73].

3.2. Hydrogel particles

As mentioned, hydrogels have been widely used for a variety of biomedical applications, such as drug delivery matrices or for tissue engineering purposes, due to their biocompatibility and tissue-like physical properties [51-53, 74]. Microfabrication of hydrogels is used increasingly for various applications, as these structures have more potential compared to the classical macroscopic-sized hydrogels [75-77]. Ideally, the morphology of the gels (i.e. size and shape) should be tailorable in accordance to their aimed application and function. Various techniques, such as phase separation and emulsion/solvent evaporation [78-80], can be applied to prepare polymeric microgels. The obtained spheres can be injected with a syringe or e.g. administrated intranasally when intended for drug delivery, or they can act as substrates for cells and be combined with the scaffold for tissue engineering purposes [38]. The major drawback of these methods, however, is that they are restricted to spherical shapes and that they yield particles with a large size distribution. Hence, new methods are needed to fabricate the next generation of microdevices with requested, well-defined structures and uniform sizes that have potential applications in tissue engineering or as multi-functional, ‘intelligent’ drug delivery devices [64, 79, 81]. Methods that are commonly used to prepare well-defined microparticles with uniform sizes are photolithography [74, 75, 77, 82-84] and soft lithographic techniques [76, 79, 85-89]. Photolithography is a simple, inexpensive method that transfers geometric structures from a mask onto a substrate via UV illumination [86]. This mask is usually made of a quartz (glass) plate coated with a thin layer of non-transparent chromium. The desired pattern on the mask can easily be created with computer-aided design (CAD) software and allows structure resolution down to 1-2 µm. Soft lithography comprises a group of techniques (e.g. micromolding, microcontact printing and microfluidic patterning) with one common feature: elastomeric

(soft) materials such as stamps and molds are used at some stage of the process to create 2-D patterns or 3-D structures [74, 86]. Many variations exist on this last technique such as the micro-transfer technique [76] and the PRINT (particle replication in nonwetting templates) process [90, 91]. Also, well-defined 3-D structures have been prepared, using a rapid prototyping technique [92, 93] that uses a computer controlled 3-D printing system. All these techniques have in common that they are able to produce specific, well-defined structures with highly uniform sizes, such as squares, cubes, bars, stacked structures, rings and tubes [79, 84, 87, 89, 92, 94]. Such spatial and surface patterned hydrogels have been used to design biosensors, microfluidic devices, drug delivery devices and structures to mimic the complex 3-D tissue environment [75, 77, 79, 81, 92].

4. Aim and outline of this thesis

The objective of this thesis was to design a new generation of skin-surface biofilms, combining the structure and properties of vernix caseosa, to protect diseased and premature skin and to facilitate superficial wound healing. These biofilms will mimic more closely the properties of the skin than traditional barrier and moisturizing creams.

The base of our biofilms consisted of synthetic corneocytes embedded in a lipid matrix. The development of these biofilms was divided into three parts: I) Preparation and characterization of microscopic particles, which will act as synthetic corneocytes, with size and shape similar to natural corneocytes. II) Generation of a lipid mixture with a very similar composition and organization as found for VC lipids. III) Combining the synthetic corneocytes and lipids to design a biofilm, which was subsequently characterized and tested *in vivo*. This thesis describes the development of the synthetic corneocytes from crosslinked hydrophilic polymers. Combined with the work of Rissmann (presented in thesis R. Rissmann), who focused on the characterization of VC and the development of a synthetic lipid mixture, we were able to prepare a new generation of biofilms. These biofilms were characterized and optimized to mimic VC. Various biofilms were applied topically on disrupted mouse skin to investigate their effect on superficial wound healing.

To mimic corneocytes in the biofilms, synthetic corneocytes were prepared from hydrophilic crosslinked polymers. Hyaluronic acid (HyA) was introduced for this purpose. In **Chapter 2** the synthesis of methacrylate derivatized HyA (HyA-MA) with precise control over the substitution degree (DS) in a suitable aprotic solvent was studied. The DS was determined by high performance liquid chromatography (HPLC). Hydrogels were obtained by crosslinking methacrylated HyA in aqueous solutions using potassium peroxodisulfate (KPS) and *N,N,N',N'*-tetramethylethylenediamine (TEMED). Rheological analysis and swelling experiments were applied to evaluate the characteristics of the hydrogels.

As alternative to HyA, **Chapter 3** reports on the synthesis and characterization of methacrylated hyperbranched polyglycerol (HyPG-MA) and hydrogels obtained after chemical polymerization of this derivatized polymer. The DS of the obtained product was established by nuclear magnetic resonance (NMR) spectroscopy and HPLC. Gel properties were monitored by rheological analysis and swelling experiments.

The preparation and characterization of well-defined HyPG-MA microparticles with uniform sizes and shapes, which will act as synthetic corneocytes, are described in **Chapter 4**. Three different preparation methods were evaluated: rigid micromolding, soft

micromolding and photolithography. Formation of well-defined particles was studied using light microscopy. Additionally, the swelling characteristics of the obtained HyPG-MA microgels were evaluated.

Chapter 5 describes the preparation of biofilms that consist of HyPG-MA microgels, which mimic corneocytes, assembled and mixed with the lipid matrix (described in thesis R. Rissmann). The synthetic corneocytes were embedded in the lipid matrix using various particle/lipid ratios as well as corneocytes with different water content to obtain the most optimal biofilm. The biofilms were characterized for their homogeneity by confocal laser-scanning microscopy. Furthermore, stability, water handling-properties, rheology and thermotropic behavior were studied.

The generation of a reliable model for skin barrier disruption and repair is reported in **Chapter 6**. Therefore, five different levels of skin barrier disruption in mice, accomplished by tape stripping, were assessed. The recovery of extensively damaged skin after VC application was evaluated. Barrier recovery was monitored by TEWL measurements and biopsies were harvested to study the recovery of the SC by histology.

In **Chapter 7** the effect of the biofilms was evaluated *in vivo*. Various biofilms were applied topically on disrupted mouse skin to determine which formulation could improve barrier function, while mimicking VC as closely as possible. Changes in TEWL were selected to monitor barrier recovery. Biopsies were harvested to study the recovery of the SC by histology. Results were compared to VC and to the commonly used oil-based ointments Vaseline and Eucerin.

Chapter 8 focused on the preparation of biodegradable HyPG that may be used in biofilm as well as drug delivery systems. After chemical crosslinking, hydrogels were characterized for their swelling and degradation properties as well as for their rheological behavior.

Chapter 9 is a summarizing discussion of this thesis. Furthermore, perspectives for the application of biofilms in the medical and cosmetic field are presented.

References

1. Bouwstra JA, Ponec M. The skin barrier in healthy and diseased state. *Biochim Biophys Acta* 2006; 1758(12): 2080-2095.
2. Chuong CM, Nickoloff BJ, Elias PM, Goldsmith LA, Macher E, Maderson PA, Sundberg JP, Tagami H, Plonka PM, Thestrup-Pederson K, Bernard BA, Schroder JM, Dotto P, Chang CM, Williams ML, Feingold KR, King LE, Kligman AM, Rees JL, Christophers E. What is the 'true' function of skin? *Exp Dermatol* 2002; 11(2): 159-187.
3. Madison KC. Barrier function of the skin: "la raison d'etre" of the epidermis. *J Invest Dermatol* 2003; 121(2): 231-241.
4. Elias PM. The skin barrier as an innate immune element. *Semin Immunopathol* 2007; 29(1): 3-14.
5. Bautista MI, Wickett RR, Visscher MO, Pickens WL, Hoath SB. Characterization of vernix caseosa as a natural biofilm: comparison to standard oil-based ointments. *Pediatr Dermatol* 2000; 17(4): 253-260.
6. Moraille R, Pickens WL, Visscher MO, Hoath SB. A novel role for vernix caseosa as a skin cleanser. *Biol Neonate* 2005; 87(1): 8-14.
7. Hoeger PH, Schreiner V, Klaassen IA, Enzmann CC, Friedrichs K, Bleck O. Epidermal barrier lipids in human vernix caseosa: corresponding ceramide pattern in vernix and fetal skin. *Br J Dermatol* 2002; 146(2): 194-201.
8. Visscher MO, Hoath SB, Conroy E, Wickett RR. Effect of semipermeable membranes on skin barrier repair following tape stripping. *Arch Dermatol Res* 2001; 293: 491-499.
9. Rawlings AV. Trends in stratum corneum research and the management of dry skin conditions. *Int J Cosmetic Sci* 2003; 25: 63-95.
10. Visscher MO, Tolia GT, Wickett RR, Hoath SB. Effect of soaking and natural moisturizing factor on stratum corneum water-handling properties. *J Cosmet Sci* 2003; 54(3): 289-300.
11. Okan D, Woo K, Ayello EA, Sibbald G. The role of moisture balance in wound healing. *Adv Skin Wound Care* 2007; 20(1): 39-53; quiz 53-35.
12. Rawlings A, Harding C, Watkinson A, Banks J, Ackerman C, Sabin R. The effect of glycerol and humidity on desmosome degradation in stratum corneum. *Arch Dermatol Res* 1995; 287(5): 457-464.
13. Haubrich KA. Role of Vernix caseosa in the neonate: potential application in the adult population. *AACN Clin Issues* 2003; 14(4): 457-464.
14. Pickens WL, Warner RR, Boissy YL, Boissy RE, Hoath SB. Characterization of vernix caseosa: water content, morphology, and elemental analysis. *J Invest Dermatol* 2000; 115(5): 875-881.
15. Hoath SB, Pickens WL, Visscher MO. The biology of vernix caseosa. *Int J Cosmetic Sci* 2006; 28: 319-333.
16. Rissmann R, Groenink HW, Weerheim AM, Hoath SB, Ponec M, Bouwstra JA. New insights into ultrastructure, lipid composition and organization of vernix caseosa. *J Invest Dermatol* 2006; 126: 1823-1833.
17. Rissmann R, Groenink HW, Gooris GS, Oudshoorn MHM, Hennink WE, Ponec M, Bouwstra JA. Temperature-Induced Changes in Structural and Physicochemical Properties of Vernix Caseosa. *J Invest Dermatol* 2008; 128: 292-299.

18. Akinbi HT, Narendran V, Pass AK, Markart P, Hoath SB. Host defense proteins in vernix caseosa and amniotic fluid. *Am J Obstet Gynecol* 2004; 191(6): 2090-2096.
19. Pickens WL, Zhou Y, Wickett RR, Visscher MO, Hoath SB. Antioxidant defense mechanisms in vernix caseosa: potential role of endogenous vitamin E. *Pediatr Res* 2000; 47: 425A.
20. Visscher MO, Narendran V, Pickens WL, LaRuffa AA, Meinzen-Derr J, Allen K, Hoath SB. Vernix caseosa in neonatal adaptation. *J Perinatol* 2005; 25(7): 440-446.
21. Bouwstra J, Pilgram G, Gooris G, Koerten H, Ponec M. New aspects of the skin barrier organization. *Skin Pharmacol Appl Skin Physiol* 2001; 14 Suppl 1: 52-62.
22. Bouwstra JA, Honeywell-Nguyen PL, Gooris GS, Ponec M. Structure of the skin barrier and its modulation by vesicular formulations. *Prog Lipid Res* 2003; 42(1): 1-36.
23. Agorastos T, Hollweg G, Grussendorf EI, Papaloucas A. Features of vernix caseosa cells. *Am J Perinatol* 1988; 5(3): 253-259.
24. Tollin M, Bergsson G, Kai-Larsen Y, Lengqvist J, Sjovall J, Griffiths W, Skuladottir GV, Haraldsson A, Jornvall H, Gudmundsson GH, Agerberth B. Vernix caseosa as a multi-component defence system based on polypeptides, lipids and their interactions. *Cell Mol Life Sci* 2005; 62(19-20): 2390-2399.
25. Tollin M, Jagerbrink T, Haraldsson A, Agerberth B, Jornvall H. Proteome analysis of vernix caseosa. *Pediatr Res* 2006; 60(4): 430-434.
26. Marchini G, Lindow S, Brismar H, Stabi B, Berggren V, Ulfgren AK, Lonne-Rahm S, Agerberth B, Gudmundsson GH. The newborn infant is protected by an innate antimicrobial barrier: peptide antibiotics are present in the skin and vernix caseosa. *Br J Dermatol* 2002; 147(6): 1127-1134.
27. Uhoda E, Piérard-Franchimont C, Debatisse B, Wang X, Piérard G. Repair kinetics of the stratum corneum under repeated insults. *Exog Dermatol* 2004; 3: 7-11.
28. Wilson DR, Maibach HI. Transepidermal water loss in vivo. Premature and term infants. *Biol Neonate* 1980; 37(3-4): 180-185.
29. Yang L, Mao-Qiang M, Taljebini M, Elias PM, Feingold KR. Topical stratum corneum lipids accelerate barrier repair after tape stripping, solvent treatment and some but not all types of detergent treatment. *Br J Dermatol* 1995; 133(5): 679-685.
30. Amano T, Takeda T, Yano H, Tamura T. Olopatadine hydrochloride accelerates the recovery of skin barrier function in mice. *Br J Dermatol* 2007; 156(5): 906-912.
31. Vernon HJ, Lane AT, Wischerath LJ, Davis JM, Menegus MA. Semipermeable dressing and transepidermal water loss in premature infants. *Pediatrics* 1990; 86(3): 357-362.
32. Lane AT, Drost SS. Effects of repeated application of emollient cream to premature neonates' skin. *Pediatrics* 1993; 92(3): 415-419.
33. Dorsett-Martin WA. Rat models of skin wound healing: a review. *Wound Repair Regen* 2004; 12(6): 591-599.
34. Gottrup F, Agren MS, Karlsmark T. Models for use in wound healing research: a survey focusing on in vitro and in vivo adult soft tissue. *Wound Repair Regen* 2000; 8(2): 83-96.
35. Lindblad WJ. Animal models in wound healing research: do we need more? *Wound Repair Regen* 2000; 8(2): 81-82.
36. van de Kerkhof PC, de Mare S, Arnold WP, van Erp PE. Epidermal regeneration and occlusion. *Acta Derm Venereol* 1995; 75(1): 6-8.

37. Zhai H, Poblete N, Maibach HI. Stripped skin model to predict irritation potential of topical agents in vivo in humans. *Int J Dermatol* 1998; 37(5): 386-389.
38. Mano JF, Silva GA, Azevedo HS, Malafaya PB, Sousa RA, Silva SS, Boesel LF, Oliveira JM, Santos TC, Marques AP, Neves NM, Reis RL. Natural origin biodegradable systems in tissue engineering and regenerative medicine: present status and some moving trends. *J R Soc Interface* 2007; 4(17): 999-1030.
39. Sullivan TP, Eaglstein WH, Davis SC, Mertz P. The pig as a model for human wound healing. *Wound Repair Regen* 2001; 9(2): 66-76.
40. Fluhr JW, Feingold KR, Elias PM. Transepidermal water loss reflects permeability barrier status: validation in human and rodent in vivo and ex vivo models. *Exp Dermatol* 2006; 15(7): 483-492.
41. Greenhalgh DG. Models of wound healing. *J Burn Care Rehabil* 2005; 26(4): 293-305.
42. Ponec M, Gibbs S, Pilgram G, Boelsma E, Koerten H, Bouwstra J, Mommaas M. Barrier function in reconstructed epidermis and its resemblance to native human skin. *Skin Pharmacol Appl Skin Physiol* 2001; 14 Suppl 1: 63-71.
43. Ponec M. Skin constructs for replacement of skin tissues for in vitro testing. *Adv Drug Deliv Rev* 2002; 54 Suppl 1: S19-30.
44. Ponec M, Boelsma E, Gibbs S, Mommaas M. Characterization of reconstructed skin models. *Skin Pharmacol Appl Skin Physiol* 2002; 15 Suppl 1: 4-17.
45. Netzlaff F, Lehr CM, Wertz PW, Schaefer UF. The human epidermis models EpiSkin((R)), SkinEthic((R)) and EpiDerm((R)): An evaluation of morphology and their suitability for testing phototoxicity, irritancy, corrosivity, and substance transport. *Eur J Pharm Biopharm* 2005; 60(2): 167-178.
46. Denda M, Wood LC, Emami S, Calhoun C, Brown BE, Elias PM, Feingold KR. The epidermal hyperplasia associated with repeated barrier disruption by acetone treatment or tape stripping cannot be attributed to increased water loss. *Arch Dermatol Res* 1996; 288(5-6): 230-238.
47. Breternitz M, Flach M, Prassler J, Elsner P, Fluhr JW. Acute barrier disruption by adhesive tapes is influenced by pressure, time and anatomical location: integrity and cohesion assessed by sequential tape stripping. A randomized, controlled study. *Br J Dermatol* 2007; 156(2): 231-240.
48. Grubauer G, Elias PM, Feingold KR. Transepidermal water loss: the signal for recovery of barrier structure and function. *J Lipid Res* 1989; 30(3): 323-333.
49. Ikeyama K, Fuziwara S, Denda M. Topical application of neuronal nitric oxide synthase inhibitor accelerates cutaneous barrier recovery and prevents epidermal hyperplasia induced barrier disrupted. *J Invest Dermatol* 2007; 127: 1713-1719.
50. Govil SK, Flynn AJ, Flynn GL, Ackermann C. Relationship of hairless mouse skin surface temperature to wound severity and maturation time. *Skin Pharmacol Appl Skin Physiol* 2003; 16(5): 313-323.
51. Peppas NA, Bures P, Leobandung W, Ichikawa H. Hydrogels in pharmaceutical formulations. *Eur J Pharm Biopharm* 2000; 50(1): 27-46.
52. Hoffman AS. Hydrogels for biomedical applications. *Adv Drug Deliv Rev* 2002; 54(1): 3-12.

53. Hennink WE, van Nostrum CF. Novel crosslinking methods to design hydrogels. *Adv Drug Deliv Rev* 2002; 54(1): 13-36.
54. Hennink WE, van Nostrum CF, Crommelin DJ, Bezemer JM. Hydrogels for the controlled release of proteins, in: Kwon G.S. (Ed.), Polymeric drug delivery systems, Taylor & Francis Group, Boca Raton, FL. 2005; 148: 215-249.
55. Anseth KS, Metters AT, Bryant SJ, Martens PJ, Elisseeff JH, Bowman CN. In situ forming degradable networks and their application in tissue engineering and drug delivery. *J Control Release* 2002; 78(1-3): 199-209.
56. Jeong SH, Fu Y, Park K. Hydrogels for oral administration, in: Kwon G.S. (Ed.), Polymeric drug delivery systems, Taylor & Francis Group, Boca Raton, FL. 2005; 148: 195-214.
57. Oudshoorn MHM, Rissmann R, Bouwstra JA, Hennink WE. Synthesis and characterization of hyperbranched polyglycerol hydrogels. *Biomaterials* 2006; 27(32): 5471-5479.
58. Van Tomme SR, van Steenbergen MJ, De Smedt SC, van Nostrum CF, Hennink WE. Self-gelling hydrogels based on oppositely charged dextran microspheres. *Biomaterials* 2005; 26(14): 2129-2135.
59. van de Manakker F, van der Pot M, Vermonden T, van Nostrum CF, Hennink WE. Self-assembling hydrogels based on beta-cyclodextrin/cholesterol inclusion complexes. *Macromolecules* 2008; 41(5): 1766-1773.
60. Li J, Li X, Ni X, Wang X, Li H, Leong KW. Self-assembled supramolecular hydrogels formed by biodegradable PEO-PHB-PEO triblock copolymers and alpha-cyclodextrin for controlled drug delivery. *Biomaterials* 2006; 27(22): 4132-4140.
61. Noro A, Nagata Y, Takano A, Matsushita Y. Diblock-type supramacromolecule via biocomplementary hydrogen bonding. *Biomacromolecules* 2006; 7(6): 1696-1699.
62. Li L, James Lee L. Photopolymerization of HEMA/DEGDMA hydrogels in solution. *Polymer* 2005; 46(25): 11540-11547.
63. van Dijk-Wolthuis WNE, Franssen O, Talsma H, van Steenbergen MJ, Kettenes-van den Bosch JJ, Hennink WE. Synthesis, characterization and polymerization of glycidyl methacrylate derivatized dextran. *Macromolecules* 1995; 28(18): 6317-6322.
64. Peppas NA, Hilt JZ, Khademhosseini A, Langer R. Hydrogels in biology and medicine: from molecular principle to bionanotechnology. *Adv Mater* 2006; 18: 1345-1360.
65. Masters KS, Shah DN, Leinwand LA, Anseth KS. Crosslinked hyaluronan scaffolds as a biologically active carrier for valvular interstitial cells. *Biomaterials* 2005; 26(15): 2517-2525.
66. Leach JB, Bivens KA, Patrick Jr CW, Schmidt CE. Photocrosslinked hyaluronic acid hydrogels: natural, biodegradable tissue engineering scaffolds. *Biotechnology and bioengineering* 2002; 82(5): 578-589.
67. Van Tomme SR, De Smedt SC, van Nostrum CF, Hennink WE. Degradation behavior of dextran hydrogels composed of positively and negatively charged microspheres. *Biomaterials* 2006; 27: 4141-4148.
68. Berger J, Reist M, Mayer JM, Felt O, Peppas NA, Gurny R. Structure and interactions in covalently and ionically crosslinked chitosan hydrogels for biomedical applications. *Eur J Pharm Biopharm* 2004; 57(1): 19-34.

69. Moura MJ, Figueiredo MM, Gil MH. Rheological study of genipin cross-linked chitosan hydrogels. *Biomacromolecules* 2007; 8(12): 3823-3829.
70. Weber LM, He J, Bradley B, Haskins K, Anseth KS. PEG-based hydrogels as an in vitro encapsulation platform for testing controlled beta-cell microenvironments. *Acta Biomater* 2006; 2(1): 1-8.
71. Bryant SJ, Bender RJ, Durand KL, Anseth KS. Encapsulating chondrocytes in degrading PEG hydrogels with high modulus: engineering gel structural changes to facilitate cartilaginous tissue production. *Biotechnol Bioeng* 2004; 86(7): 747-755.
72. Lu S, Anseth KS. Photopolymerization of multilaminated poly(HEMA) hydrogels for controlled release. *J Control Release* 1999; 57(3): 291-300.
73. Norris P, Noble M, Francolini I, Vinogradov AM, Stewart PS, Ratner BD, Costerton JW, Stoodley P. Ultrasonically controlled release of ciprofloxacin from self-assembled coatings on poly(2-hydroxyethyl methacrylate) hydrogels for Pseudomonas aeruginosa biofilm prevention. *Antimicrob Agents Chemother* 2005; 49(10): 4272-4279.
74. Bryant SJ, Hauch KD, Ratner BD. Spatial patterning of thick poly(2-hydroxyethyl methacrylate) hydrogels. *Macromolecules* 2006; 39(13): 4395-4399.
75. Allcock HR, Phelps MVB, Barrett EW. Ultraviolet photolithographic development of polyphosphazene hydrogel microstructures for potential use in microarray biosensors. *Chem Mater* 2006; 18: 609-613.
76. Wang B, Hong Y, Feng J, Gong Y, Gao C. Rings of hydrogel fabricated by a micro-transfer technique. *Macromol J* 2007; 28: 567-571.
77. Kuckling D, Hoffman J, Plötner M, Ferse D, Kretschmer K, Adler H-JP, Arndt K-F, Reichelt R. Photo cross-linkable poly(N-isopropylacrylamide) copolymers III: micro-fabricated temperature responsive hydrogels. *Polymer* 2003; 44: 4455-4462.
78. Stenekes RJ, Franssen O, van Bommel EM, Crommelin DJ, Hennink WE. The preparation of dextran microspheres in an all-aqueous system: effect of the formulation parameters on particle characteristics. *Pharm Res* 1998; 15(4): 557-561.
79. Guan J, Ferrell N, James Lee L, Hansford DJ. Fabrication of polymeric microparticles for drug delivery by soft lithography. *Biomaterials* 2006; 27(21): 4034-4041.
80. Yun YH, Goetz DJ, Yellen P, Chen W. Hyaluronan microspheres for sustained gene delivery and site-specific targeting. *Biomaterials* 2004; 25(1): 147-157.
81. Hilt JZ, Peppas NA. Microfabricated drug delivery devices. *Int J Pharm* 2005; 306(1-2): 15-23.
82. Hahn MS, Taite LJ, Moon JJ, Rowland MC, Ruffino KA, West JL. Photolithographic patterning of polyethylene glycol hydrogels. *Biomaterials* 2006; 27(12): 2519-2524.
83. Kizilel S, Sawardecker E, Teymour F, Perez-Luna VH. Sequential formation of covalently bonded hydrogel multilayers through surface initiated photopolymerization. *Biomaterials* 2006; 27(8): 1209-1215.
84. Zguris JC, Itle LJ, Koh W-G, Pishko MV. A novel single-step fabrication technique to create hetergoneous poly(ethylene glycol) hydrogel microstructures containing multiple phenotypes of mammalian cells. *Langmuir* 2005; 21: 4168-4174.
85. Khademhosseini A, Suh KY, Jon S, Eng G, Yeh J, Chen GJ, Langer R. A soft lithographic approach to fabricate patterned microfluidic channels. *Anal Chem* 2004; 76(13): 3675-3681.

86. Falconnet D, Csucs G, Grandin HM, Textor M. Surface engineering approaches to micropattern surfaces for cell-based assays. *Biomaterials* 2006; 27(16): 3044-3063.
87. Maynor BW, LaRue I, Hu Z, Rolland JP, Pandya A, Fu Q, Liu J, Spontank RJ, Sheiko SS, Samulski RJ, DeSimone JM. Supramolecular nanomimetics: replication of micelles, viruses, and other naturally occurring nanoscale objects. *Small* 2007; 3(5): 845-849.
88. Campbell CJ, Smoukov SK, Bishop KJ, Grzybowski BA. Reactive surface micropatterning by wet stamping. *Langmuir* 2005; 21(7): 2637-2640.
89. Fukuda J, Khademhosseini A, Yeo Y, Yang X, Yeh J, Eng G, Blumling J, Wang CF, Kohane DS, Langer R. Micromolding of photocrosslinkable chitosan hydrogel for spheroid microarray and co-cultures. *Biomaterials* 2006; 27(30): 5259-5267.
90. Rolland JP, Maynor BW, Euliss LE, Exner AE, Denison GM, DeSimone JM. Direct fabrication and harvesting of monodisperse, shape-specific nanobiomaterials. *J Am Chem Soc* 2005; 127(28): 10096-10100.
91. Gratton SE, Pohlhaus PD, Lee J, Guo J, Cho MJ, DeSimone JM. Nanofabricated particles for engineered drug therapies: A preliminary biodistribution study of PRINT(trade mark) nanoparticles. *J Control Release* 2007; 121(1-2): 10-18.
92. Wang X, Yan Y, Pan Y, Xiong Z, Liu H, Cheng J, Liu F, Lin F, Wu R, Zhang R, Lu Q. Generation of three-dimensional hepatocyte/gelatin structures with rapid prototyping system. *Tissue Eng* 2006; 12(1): 83-90.
93. Yan Y, Wang X, Pan Y, Liu H, Cheng J, Xiong Z, Lin F, Wu R, Zhang R, Lu Q. Fabrication of viable tissue-engineered constructs with 3D cell-assembly technique. *Biomaterials* 2005; 26(29): 5864-5871.
94. Dalton PD, Flynn L, Shoichet MS. Manufacture of poly(2-hydroxyethyl methacrylate-co-methyl methacrylate) hydrogel tubes for use as nerve guidance channels. *Biomaterials* 2002; 23(18): 3843-3851.

Synthesis of methacrylated hyaluronic acid with tailored degree of substitution

Marion H.M. Oudshoorn[a], Robert Rissmann[b], Joke A. Bouwstra[b], Wim E. Hennink[a]

[a] Department of Pharmaceutics, Utrecht Institute for Pharmaceutical Sciences (UIPS), Utrecht University, Utrecht, The Netherlands
[b] Department of Drug Delivery Technology, Leiden/Amsterdam Center for Drug Research (LACDR), Leiden University, Leiden, The Netherlands

Polymer 48 (2007) 1915-1920

2

Abstract

The aim of this work was to develop a new method to derivatize hyaluronic acid (HyA) with polymerizable methacrylate residues with precise control over the substitution degree. The synthesis of methacrylated HyA (HyA-MA) was performed in dimethyl sulfoxide (DMSO) using glycidyl methacrylate (GMA) and 4-(*N,N*-dimethylamino)pyridine (DMAP) as a catalyst. HyA was rendered soluble in DMSO by exchanging the Na^+ ions by the more lipophilic tetrabutylammonium (TBA) ions. HyA-MA with a fully controlled degree of substitution (DS, defined as the number of methacrylate groups per 100 disaccharide units), ranging from 5 to 30, was obtained at 50°C after 48 h. Hydrogels were obtained upon radical polymerization of aqueous solutions of HyA-MA using potassium peroxodisulfate (KPS) as initiator and *N,N,N',N'*-tetramethylethylenediamine (TEMED) as catalyst. Almost complete methacrylate conversion (95%) was achieved for hydrogels obtained by polymerization of HyA-MA with a degree of substitution of 15. At lower DS (DS 8.5 and 5) the methacrylate conversion was 82% and 68%, respectively. Rheological characterization showed that with increasing DS the storage modulus of these HyA-MA hydrogels increased. Swelling experiments showed that HyA-MA gels with a DS of 15 or above were dimensionally stable, whereas HyA-MA gels with DS 5 and DS 8.5 swelled 1.6 and 1.4 times their initial weight, respectively. In conclusion, this paper shows that the DS of HyA-MA can be tailored by the reaction conditions and that consequently HyA-MA hydrogels with different characteristics can be prepared.

1. Introduction

Hyaluronic acid (HyA) is an endogenous polysaccharide, i.e. present in the vitreous body, synovial fluids and the extracellular matrix, which consists of repeating disaccharide units composed of β(1-4)-linked *N*-acetyl-D-glucosamine and β(1-3)-linked D-glucuronic acid [1]. Its biocompatibility, biodegradability and immunoneutrality make HyA an attractive polymer for biomedical and pharmaceutical applications. Currently, HyA is applied to treat joint diseases such as osteoarthritis. It is also used in eye surgery as replacement fluid and under investigation for drug delivery and tissue engineering applications [2-4]. For these applications, besides unmodified HyA, derivatized HyA is also used. Modification of HyA can be performed as hydroxyl and carboxy groups can be used for chemical derivatization [5, 6]. Many chemical modifications of HyA have been described in literature [1]. One chemical modification concerns the derivatization of HyA with polymerizable methacrylate groups. This crosslinkable HyA can be used to form hydrogels for drug delivery and tissue engineering purposes [4, 5, 7, 8]. The synthesis of methacrylated HyA (HyA-MA) is performed in an aqueous environment with an excess of methacrylic anhydride with respect to the hydroxyl groups of HyA [3, 7, 9]. The major drawback of this synthesis lies in the aqueous basic (pH 8) reaction conditions: methacrylic anhydride can react with water to yield methacrylic acid and additionally the covalently linked methacrylic ester can be hydrolyzed during the reaction [10]. This makes it difficult to control the degree of substitution. Hence, there is need for a method in which the DS of methacrylated HyA can accurately be controlled. This has been achieved in the past for the modification of polysaccharides [11-13] allowing the preparation of hydrogels with tailored properties.
This paper reports on the synthesis of methacrylate derivatized HyA with precise control over the substitution degree in a suitable aprotic solvent by substitution of the parent polysaccharide with glycidyl methacrylate. Additionally, the characteristics of the hydrogels obtained with glycidyl methacrylate derivatized HyA are studied.

2. Experimental section

2.1. Materials

HyA sodium salt (from *Streptococcus equi sp.*, M_W ~1,700,000 g/mol), tetrabutylammonium fluoride trihydrate (TBA-F), dimethyl sulfoxide (DMSO, $H_2O \leq 0.005\%$), glycidyl methacrylate (GMA, purity ≥ 97%), methacrylic acid and *N,N,N',N'*-tetramethylethylenediamine (TEMED) were obtained from Fluka (Buchs, Switzerland). 4-(*N,N*-dimethylamino)pyridine (DMAP), 37% hydrochloric acid, 70% perchloric acid and acetic acid were purchased from Acros Chimica (Geel, Belgium). Sodium hydroxide (NaOH) pellets, sodium chloride, potassium peroxodisulfate (KPS)

and ethanol absolute were provided by Merck (Darmstadt, Germany). Diethylether and acetonitrile (HPLC grade) were purchased from Biosolve Ltd. (Valkenswaard, The Netherlands).

2.2. HyA modification in aqueous solution

Methacrylation of HyA was performed following the procedure described by Smeds et al [3]. In brief, 0.5 g HyA sodium salt was dissolved in 25 ml H_2O after which a 20-fold excess of methacrylic anhydride (3.7 ml) relative to primary HyA hydroxyl groups was added. Next, the pH of the reaction mixture was adjusted to 8 with 5 N NaOH and the two-phase system was stirred for 24 h at 5°C. A second synthesis was performed in a similar way as described above, however, at 50°C to prevent phase separation. For both reactions the polymer was precipitated in ethanol and washed with the same solvent for three times. The samples were dried before characterization.

2.3. Dissolution of HyA in DMSO

To render hyaluronic acid soluble in DMSO, the sodium ions of HyA were exchanged with the lipophilic tetrabutylammonium (TBA) ion. Ion-exchange was performed using Dowex® 50W-X8 cation exchange resin (5.1 mmol/g exchange capacity; BioRad Laboratories, Veenendaal, The Netherlands). The Dowex® resin (40 g) was incubated with a large excess of TBA-F (137 g, 435 mmol) dissolved in RO-water (500 ml) for 1 h and washed extensively with water. Next, the resin was transferred into 1000 ml of a 1% (w/w) HyA solution in water and mixed for 2 h at room temperature. The mixture was then centrifuged for 2 min at 5000 rpm to remove the resin. The obtained HyA-TBA solution was lyophilized and used for chemical modification with GMA.

2.4. Synthesis of methacrylated HyA in DMSO

The kinetics of the reaction was studied as follows. A 1% (w/v) solution of HyA-TBA in DMSO (100 ml) was prepared at 50°C. After dissolution of HyA-TBA, 0.2 g of DMAP and 86 µl GMA (corresponding to a molar ratio GMA:primary OH of 0.4:1) were added. At regular time intervals samples of 2 ml were taken, precipitated in diethylether and washed three times with the same solvent. Samples were dried overnight at room temperature prior to determination of the degree of methacrylate substitution (DS, defined as the number of methacrylate groups per 100 disaccharide units; i.e. a DS of 10 indicates that 10 out of 100 hydroxyl groups of a HyA molecule are esterified with methacryloyl groups) by reversed-phase (RP) HPLC (section 2.10.). Based on the results of the kinetic study, the following protocol was used to routinely synthesize methacrylated HyA (HyA-MA). One gram of HyA-TBA salt was dissolved in 100 ml DMSO at 50°C under a nitrogen atmosphere. Subsequently, 0.2 g of DMAP and a calculated amount of GMA (43 µl to 430 µl), depending on the requested degree of

substitution (DS), were added. The solution was stirred for 48 h at 50°C. Next, an equimolar amount of concentrated HCl with respect to DMAP was added to neutralize this catalyst. The reaction mixture was transferred into a dialysis membrane (MWCO 12-14,000 Da, Medicell International Ltd, London, Great Britain) and dialyzed at 4°C for 3 days against 150 mM sodium chloride in RO-water and subsequently for 4 days against RO-water to ensure the exchange of TBA^+ by Na^+ ions and to remove DMSO. Methacrylated hyaluronic acid (HyA-MA) was obtained after freeze-drying and the degree of substitution of the polymer was determined by RP-HPLC analysis (section 2.10.).

2.5. Polymerization kinetics of HyA-MA

Hydrogels were obtained by free radical polymerization of aqueous solutions of HyA-MA initiated by KPS and using TEMED as a catalyst. In detail, a 2% (w/w) solution of the derivatized polymer (17 mg, DS 5, 8.5 or 15) in 750 µl phosphate buffer (10 mM, pH 7.2) was prepared. Subsequently, KPS (60 µl, 50 mg/ml) and TEMED (24 µl, 20% (v/v), adjusted to pH 7 with 2 M HCl) were added to start the polymerization reaction. At regular time intervals, the samples were quickly frozen into liquid nitrogen to stop the polymerization and then lyophilized. The dried samples were rehydrated in 10 ml 0.02 M NaOH and incubated at 37°C for 30 min to hydrolyze unreacted methacryloyl groups. RP-HPLC was used to determine the concentration of methacrylic acid (section 2.10.).

2.6. Preparation of hydrogels

A 2% (w/w) solution of HyA-MA (17 mg, DS varying from 5 to 30) in 750 µl 10 mM phosphate buffer pH 7.2 was prepared and transferred into a cylindrical mould of 10 x 7 mm (diameter x height). The radical polymerization was started after addition of 60 µl KPS (50 mg/ml) and 24 µl TEMED (20% (v/v), adjusted to pH 7 with 2 M HCl). The resulting solution was allowed to polymerize for 1 h at room temperature.

2.7. Rheological analysis of HyA-MA hydrogels

The rheological properties of the polymerizing HyA-MA solutions were determined on a rheometer (AR1000-N, TA instruments, Etten-Leur, The Netherlands) using a 40 mm 1° steel cone geometry. A 2% (w/w) solution of HyA-MA (DS 5, 8.5, 15, 18 or 30) in phosphate buffer (10 mM, pH 7.2) was prepared and directly after addition of the polymerization reagents KPS and TEMED, ~350 µl was placed between the plates. During the polymerization of HyA-MA, the *G'* (shear storage modulus) and the *G"* (loss modulus) were monitored at 20°C maintaining a constant strain of 1% and a constant frequency of 1 Hz. The extent of deformation and recovery of a HyA-MA gel was evaluated by a creep experiment. A shear stress of 10 or 100 Pa was applied on the

system during 2 min while the strain was monitored and after removal of the stress the recovery was analyzed for 2 min.

2.8. Swelling behavior of HyA-MA hydrogels

HyA-MA hydrogels (0.85 g; 2% (w/w); DS 5, 8.5, 15, 18 and 30) were prepared as described in section 2.6. The hydrogels were weighed (W_0) after being transferred into pre-weighed glass vials. Next, 10 ml isotonic 100 mM PBS pH 7.2 with 0.02% NaN_3 was added and the vials were placed in a water bath of 37°C. At regular time intervals, the buffer was replaced by fresh PBS and the gels weighed (W_t) to determine the swelling ratio defined as W_t / W_0.

2.9. ^{1}H NMR spectroscopy

^{1}H NMR spectra were recorded in D_2O (99.9% atom D, Sigma-Aldrich) on a Gemini 300 MHz spectrometer (Varian Associates Inc. NMR Instruments, Palo Alto, CA) using HOD at 4.8 ppm as reference line. A 1% (w/w) solution of HyA-MA in D_2O was prepared for analysis. The substituted methacrylate groups were identified by the signals of the methacryloyl group at 5.6 and 6.0 ppm (protons of the double bond H_a and H_b, respectively) and of the methyl resonance at 1.8 ppm (H_c).

2.10. Reversed phase HPLC analysis

The concentration of methacrylic acid was determined by RP-HPLC as described by Stenekes and Hennink [14]. In brief, HyA-MA (15 mg) was dissolved in 10 ml 0.02 M NaOH and incubated at 37°C for 30 min to hydrolyze the polymer-bound methacrylate groups. Prior to analysis, 2 ml of a 2 M acetic acid solution was added. Ten microlitres of this mixture was injected onto a RP-18 column (Lichrospher, Merck, Darmstadt, Germany). Analysis was carried out with a Waters system (Waters Associates Inc.), including a 600A HPLC pump, a Model 717 autoinjector, and a UV detector Model 2487. The mobile phase consisted of acetonitrile/water (10/90 (w/w)) adjusted to pH 2 with perchloric acid. The flow rate was 1.0 ml/min and the detection wavelength was set at 210 nm. A calibration curve was obtained by injecting varying volumes (0.5 µl to 150 µl) of a 100 µM methacrylic acid in eluent. Empower Pro software (Waters Associates Inc.) was used to determine the peak areas which, in turn, were used to quantify methacrylic acid in the samples.

3. Results and discussion

3.1. Synthesis and characterization of methacrylate modified HyA

The synthesis of methacrylated HyA was previously described by Smeds et al [3]. In their procedure, methacrylated HyA was prepared by reacting a 20-fold excess of methacrylic

anhydride relative to primary HyA hydroxyl groups in an aqueous environment (pH 8) at 5°C. Under these conditions a two-phase system is formed. It was shown that by varying the reaction time and the amount of methacrylic anhydride, methacrylated HyA with 3%, 8%, or 17% degree of substitution could be obtained [3]. Attempts were made by us to reproduce this procedure. In addition, the reaction was carried out at 50°C to prevent phase separation. We were able to obtain methacrylated hyaluronic acid, however, we were unable to control the degree of substitution at both temperatures. Methacrylic anhydride can hydrolyze in water, yielding methacrylic acid, which does not react with HyA. Since this hydrolysis and additionally the hydrolysis of methacrylated HyA are dependent on both pH and temperature, control over the DS is difficult to achieve. Therefore, we developed an alternative method for the synthesis of methacrylated HyA with full control over the DS. Our procedure consists of the reaction of HyA dissolved in DMSO with GMA using DMAP as catalyst, under dry and oxygen free conditions, yielding methacrylated HyA and glycidol (Fig. 1). To render HyA soluble in DMSO, the sodium salt of this polymer was converted into a tetrabutylammonium salt by ion-exchange. Methacrylated HyA, after reaction with GMA, in sodium salt form was obtained following dialysis and freeze-drying after which samples were characterized by ^{1}H NMR spectroscopy. Lack of characteristic signals around 1 ppm showed that TBA^+ [$(CH_3\text{-}CH_2\text{-}CH_2\text{-}CH_2)_4N^+$] ions were fully exchanged by Na^+ ions during dialysis. Methacrylate modification was confirmed by ^{1}H NMR, although the degree of substitution (DS) could not be accurately determined as the signals for the methyl groups of both the polymer backbone and the coupled methacrylate overlapped at 1.8 ppm (spectra not shown). Broadening of signals, which may result in an overlap as in our case, is a normal phenomenon for macromolecules [15]. Also NMR analysis of partially degraded HyA as described in literature [3, 12] did not result in better resolution. Therefore, RP-HPLC was used to determine the DS of the HyA-MA. Hence, the polymer-bound methacrylate groups were hydrolyzed under alkaline conditions and the formed methacrylic acid was quantitatively determined using RP-HPLC.

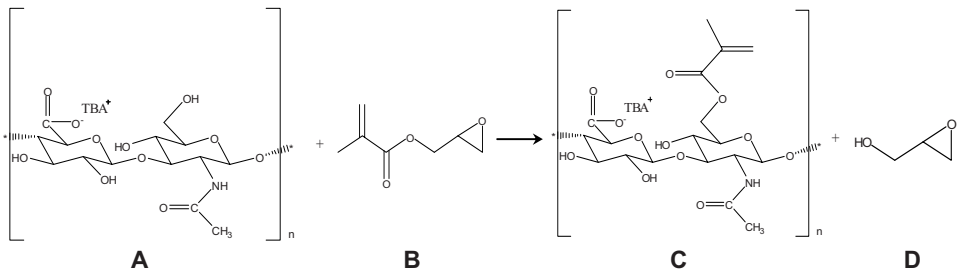

Figure 1. *Synthesis of methacrylated hyaluronic acid. HyA (A) reacted with glycidyl methacrylate (B) in DMSO to obtain the crosslinkable product HyA-MA (C) and glycidol (D).*

A kinetic study showed that the reaction of HyA with GMA, at a feed ratio of 40%, reached a DS of 8.5 within 48 h at 50°C. Modification occurred immediately after addition of GMA and longer incubation time did not result in an increased degree of methacrylate substitution. The relation between the percentage of GMA to the primary hydroxyl group of HyA in the feed and the DS of the modified polymer is presented in Table 1. It is shown that for every feed ratio up to 200%, HyA was derivatized with approximately 20% of the added GMA. This indicates that HyA-MA (DS ranging from 5 to 30) can reproducibly be prepared with good control of the DS. The rather low incorporation of GMA was shown previously in literature [11, 16, 17] and can be attributed to the occurrence of equilibrium during the reaction of HyA with GMA. Rheological analysis (see next section) shows that the *G"* of HyA and HyA-MA (Fig. 2) did not statistically differ from each other, indicating that under the selected reaction conditions no chain scission occurred.

Table 1. *Storage modulus G', loss modulus G'' and tan δ of HyA-MA hydrogels (2% (w/w) initial solid content) as a function of the obtained methacrylate substitution, which is related to the molar ratio of GMA to HyA hydroxyl groups in the feed (%). The data are shown as average ± SD, n = 3.*

Feed ratio (%)	Obtained DS (%)	*G'* (Pa)	*G"* (Pa)	tan *δ*
20	5.4 ± 0.4	1,300 ± 90	2 ± 0.1	0.002 ± 0.000
40	8.5 ± 1.5	2,000 ± 280	2 ± 0.1	0.001 ± 0.000
80	15.4 ± 1.4	3,900 ± 150	4 ± 0.1	0.001 ± 0.000
100	18.0 ± 2.0	4,600 ± 410	28 ± 2.5	0.005 ± 0.001
200	30.0 ± 4.0	10,500 ± 850	34 ± 2.1	0.003 ± 0.001

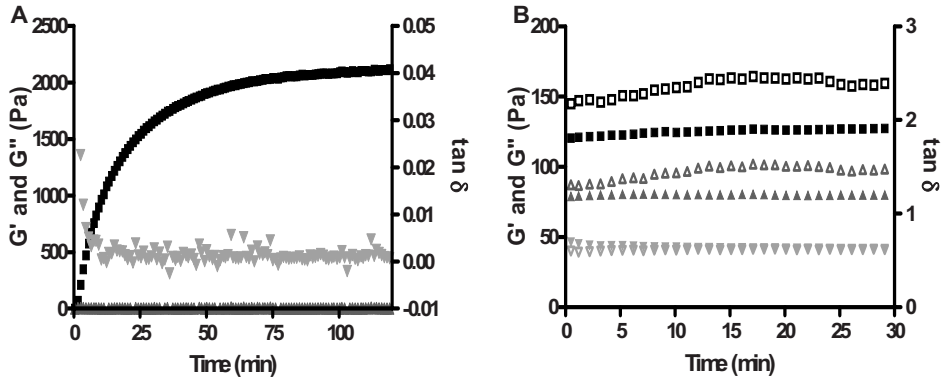

Figure 2. *(A) Storage modulus G' (■), loss modulus G" (▲) and tan δ (▼) of a gelating HyA-MA solution (2% (w/w), DS 8.5) as function of time following radical polymerization using KPS and TEMED. (B) Storage modulus G' (■,□), loss modulus G" (▲,Δ) and tan δ (▼, ▽) of a 2% (w/w) HyA-MA (closed symbols) and 2% (w/w) HyA (open symbols) aqueous solution as function of time.*

3.2. Preparation and characterization of HyA-MA hydrogels

The hydrogels were obtained by crosslinking aqueous solutions of HyA-MA in the presence of KPS and TEMED as initiator and catalyst, respectively. Modified HyA was well soluble in phosphate buffer. The radical polymerization resulted into opaque hydrogels, independent of the DS used. The opacity of the hydrogels indicates that phase separation (i.e. water-poor domains containing relatively hydrophobic polymerized methacrylates and water-rich, hydrated HyA domains) has occurred. The kinetics of the polymerization was studied using RP-HPLC to determine quantitatively the amount of unreacted methacrylate groups. Polymerization started immediately after addition of KPS and TEMED and showed that more than 95% of the methacrylate groups were converted within 1 h for hydrogels containing HyA-MA with a DS of 15. It was observed that with lower degrees of substitution (DS 8.5 and 5) the methacrylate conversion decreased to 82% and 68%, respectively, indicating that with higher DS the methacrylate groups have a higher probability to react with each other.

The viscoelastic properties of the HyA-MA hydrogels (2% (w/w) initial solid content) with various methacrylate substitutions were evaluated using controlled strain experiments. In Figure 2A the formation of an elastic network of HyA-MA DS 8.5 is shown. It can clearly be seen that the storage modulus *G'* gradually increased in time to 2,100 Pa while the loss modulus remained low (2 Pa). Moreover, the tan δ was below 0.01 indicating that the obtained gel was fully elastic. For comparison, a solution of HyA-MA (DS 8.5) with the same solid content was analyzed without the addition of KPS and TEMED (Fig. 2B). It was shown that both *G'* and *G"* remained low at 120 Pa and 100 Pa, respectively, whereas the tan δ was substantially higher at 0.7, which demonstrates that an elastic network does not exist in an aqueous, but viscous, solution of HyA-MA. The results of a creep experiment confirmed that a fully elastic HyA-MA network was obtained upon the addition of a radical polymerization initiator and catalyst (Fig. 3A). It was shown that application of a shear stress (100 Pa) on the system to which KPS and TEMED was added resulted in a deformation up to 5% strain. The hydrogel recovered completely when the stress was removed. On the other hand, an aqueous solution of HyA-MA showed a continuous flow (Fig. 3B) and no recovery after stress removal at a shear stress of already 10 Pa, again demonstrating that it behaved as a viscous solution. In addition, this aqueous solution of HyA-MA showed a similar deformation (>500% strain; Fig. 3B) as an aqueous solution of initial HyA. Rheological analysis also showed that an increasing degree of methacrylation of HyA resulted in gels with increased shear storage modulus and slightly increased loss modulus while the tan δ stayed low (Table 1). As an increased number of methacrylate groups are linked to the hyaluronic acid chains, more covalent crosslinks can be formed resulting in an increased elastic modulus. Nevertheless, the gelation time for all gels remained low: within 1 min *G'* already exceeded *G".*

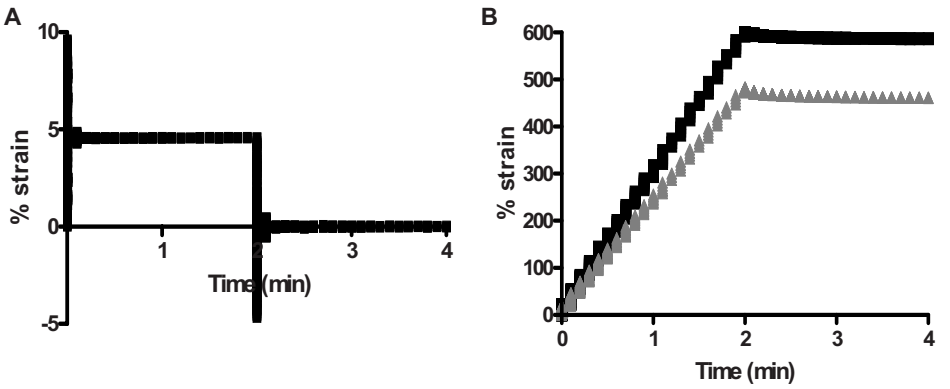

Figure 3. *(A) Creep experiment on a 2% (w/w) HyA-MA hydrogel (DS 8.5, applied stress 100 Pa) as function of time. (B) Creep experiment on a HyA-MA DS 8.5 (■) and a HyA (▲) aqueous solution (2% (w/w), applied stress 10 Pa) as function of time.*

Besides their rheological characteristics, also the swelling behavior of HyA-MA hydrogels was studied. HyA-MA gels with an initial solid content of 2% (w/w) and various degrees of methacrylate substitution were prepared at room temperature and their swelling was evaluated at 37°C and pH 7.2 (Fig. 4). It was observed that with increasing DS the swelling of the gels decreased: HyA-MA gels with DS 5 and DS 8.5 swelled 1.6 and 1.4 times their initial weight, respectively, whereas gels with DS 15, 18 and 30 did not swell. The gels with DS 5 and DS 8.5 started to swell immediately upon immersion in isotonic 100 mM PBS (pH 7.2) and reached their equilibrium swelling within 2 days. The limited swelling at high DS indicates that rather dimensionally stable hydrogels were obtained. Swollen gels reached their equilibrium swelling within 3 days.

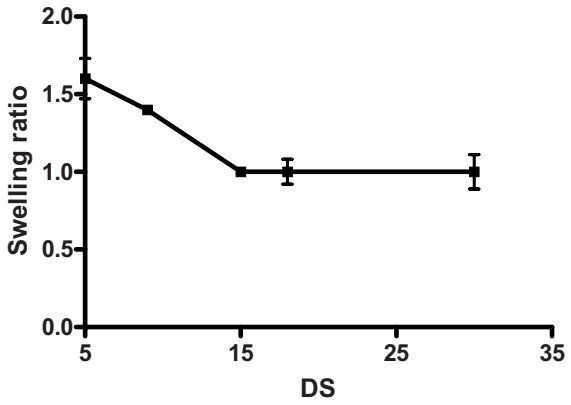

Figure 4. *Swelling ratio of 2% (w/w) HyA-MA hydrogels as function of the DS. The data are shown as average ± SD, n = 3.*

4. Conclusion

In conclusion, a new method is presented to synthesize methacrylated HyA with full control over the DS. Radical polymerization of aqueous solutions of HyA-MA resulted in opaque elastic hydrogels. Characterization of these HyA-MA hydrogels showed that the elastic modulus and the dimensional stability of the gels increased with higher substitution degree. Consequently, this novel method indicates that HyA-MA hydrogels have potential application as drug delivery matrices and for tissue engineering purposes.

References

1. Lapcik L, Jr., Lapcik L, De Smedt S, Demeester J, Chabrecek P. Hyaluronan: Preparation, Structure, Properties, and Applications. *Chem Rev* 1998; 98(8): 2663-2684.
2. Prestwich GD, Marecak DM, Marecek JF, Vercruysse KP, Ziebell MR. Controlled chemical modification of hyaluronic acid: synthesis, applications, and biodegradation of hydrazide derivatives. *J Control Release* 1998; 53(1-3): 93-103.
3. Smeds KA, Pfister-Serres A, Miki D, Dastgheib K, Inoue M, Hatchell DL, Grinstaff MW. Photocrosslinkable polysaccharides for in situ hydrogel formation. *J Biomed Mater Res* 2001; 54(1): 115-121.
4. Park YD, Tirelli N, Hubbell JA. Photopolymerized hyaluronic acid-based hydrogels and interpenetrating networks. *Biomaterials* 2003; 24(6): 893-900.
5. Band PA. Hyaluronan derivatives: chemistry and clinical applications. In: Laurent TC, editor. The chemistry, biology and medical applications of hyaluronan and its derivatives. London; 1998. p. 33-42.
6. Trudel J, Massia SP. Assessment of the cytotoxicity of photocrosslinked dextran and hyaluronan-based hydrogels to vascular smooth muscle cells. *Biomaterials* 2002; 23(16): 3299-3307.
7. Masters KS, Shah DN, Leinwand LA, Anseth KS. Crosslinked hyaluronan scaffolds as a biologically active carrier for valvular interstitial cells. *Biomaterials* 2005; 26(15): 2517-2525.
8. Mori M, Yamaguchi M, Sumitomo S, Takai Y. Hyaluronan-based biomaterials in tissue engineering. *Acta Histochem. Cytochem.* 2004; 37(1): 1-5.
9. Burdick JA, Chung C, Jia X, Randolph MA, Langer R. Controlled degradation and mechanical behavior of photopolymerized hyaluronic acid networks. *Biomacromolecules* 2005; 6(1): 386-391.
10. van Dijk-Wolthuis WNE, Franssen O, Talsma H, van Steenbergen MJ, Kettenes-van den Bosch JJ, Hennink WE. Synthesis, characterization and polymerization of glycidyl methacrylate derivatized dextran. *Macromolecules* 1995; 28(18): 6317-6322.
11. van Dijk-Wolthuis WNE, Kettenes-van den Bosch JJ, van der Kerk-van Hoof A, Hennink WE. Reaction of dextran with glycidyl methacrylate: an unexpected transesterification. *Macromolecules* 1997; 30(11): 3411-3413.
12. Pelletier S, Hubert P, Lapicque E, Payan E, Dellacherie E. Amphiphilic derivatives of sodium alginate and hyaluronate: synthesis and physico-chemical properties of aqueous dilute solutions. *Carbohydr Polym* 2000; 43: 343-349.
13. Coradini D, Pellizzaro C, Miglierini G, Daidone MG, Perbellini A. Hyaluronic acid as drug delivery for sodium butyrate: improvement of the anti-proliferative activity on a breast-cancer cell line. *Int J Cancer* 1999; 81(3): 411-416.
14. Stenekes RJ, Hennink WE. Polymerization kinetics of dextran-bound methacrylate in an aqueous two phase system. *Polymer* 2000; 41: 5563-5569.
15. Varum KM, Anthonsen MW, Grasdalen H, Smidsrod O. Determination of the degree of N-acetylation and the distribution of N-acetyl groups in partially N-deacetylated chitins (chitosans) by high-field n.m.r. spectroscopy. *Carbohydr Res* 1991; 211(1): 17-23.
16. Oudshoorn MHM, Rissmann R, Bouwstra JA, Hennink WE. *Manuscript in preparation*.

17. Oudshoorn MHM, Rissmann R, Bouwstra JA, Hennink WE. Synthesis and characterization of hyperbranched polyglycerol hydrogels. *Biomaterials* 2006; 27(32): 5471-5479.

Synthesis and characterization of hyperbranched polyglycerol hydrogels

Marion H.M. Oudshoorn[a], Robert Rissmann[b], Joke A. Bouwstra[b], Wim E. Hennink[a]

[a] Department of Pharmaceutics, Utrecht Institute for Pharmaceutical Sciences (UIPS), Utrecht University, Utrecht, The Netherlands
[b] Department of Drug Delivery Technology, Leiden/Amsterdam Center for Drug Research (LACDR), Leiden University, Leiden, The Netherlands

Biomaterials 27 (2006) 5471-5479

Abstract

Hyperbranched polyglycerol (HyPG; M_n 2,000 g/mol) was derivatized with glycidyl methacrylate (GMA) in dimethyl sulfoxide using 4-(*N,N*-dimethylamino)pyridine as a catalyst to obtain methacrylated HyPG (HyPG-MA). The degree of substitution (DS, the percentage of derivatized hydroxyl groups), established by NMR and RP-HPLC, was fully controlled in the range of 0.7 to 70 by varying the molar ratio of GMA to HyPG in the reaction mixture. This indicates that for e.g. a DS of 28, 9 out of the 32 hydroxyl groups of a HyPG molecule were esterified with methacryloyl groups. Under the selected conditions, the reaction reached equilibrium within 4 h. Furthermore, it was demonstrated that under the applied conditions the reaction was reversible. Hydrogels were obtained by crosslinking methacrylated HyPG in aqueous solutions using potassium peroxodisulfate (KPS) and *N,N,N',N'*-tetramethylethylenediamine (TEMED) as initiator and catalyst, respectively. Within 10 min, 99% of the methacryloyl groups were polymerized. Rheological analysis showed that the storage modulus of these gels could be tailored by varying the concentration of HyPG-MA in the aqueous solution as well as by the DS. Moreover, the obtained hydrogels have a limited swelling capacity indicating that rather dimensionally stable networks were obtained. As an alternative for radical polymerization with KPS and TEMED, the methacrylated HyPG could also be crosslinked by photopolymerization using Irgacure 2959 as photoinitiator. A methacrylate conversion of 99% was obtained within 3 min of illumination. As for the gels prepared with KPS and TEMED, networks formed by photopolymerization also had a high shear storage modulus and showed limited swelling. Hydrogels based on hyperbranched polyglycerol have great potential as drug delivery matrices and for tissue engineering purposes.

1. Introduction

In recent years, there has been an increasing interest in dendrimers. Unmodified as well as end-group modified dendrimers are under investigation in a variety of applications such as unimolecular nanocarriers for entrapment of catalysts, drugs and other guest molecules, functional crosslinkers and rheology modifiers [1-5]. However, the major drawback of this type of polymers is their multistep synthesis and, therefore, as an alternative for dendrimers, hyperbranched polymers have been introduced. These tree-like structures were until recently regarded as poorly-defined compared to the perfectly structured dendrimers due to their broad molecular weight distribution and random branching. However, recently novel synthetic methods were developed in which substantially better-defined hyperbranched polymers with low molecular weight distributions were obtained [1, 3, 6-8]. As an example, the anionic ring-opening multibranching polymerization (ROMBP) [1, 2, 6, 9] of glycidol resulted in hyperbranched polyglycerol (HyPG). HyPG's were synthesized with molecular weights ranging from 1,000 to 30,000 g/mol and with low polydispersities (M_W/M_n <1.5) [2, 8, 10]. HyPG consists of an inert polyether-backbone with functional hydroxyl-groups at every branch-end. This structural feature resembles the well-known poly(ethylene glycol) (PEG) that is accepted for various biomedical applications [11-15]. The polyether-backbone of HyPG, taking the biocompatibility of aliphatic polyether structures such as PEG into account, makes HyPG an attractive polymer for biomedical and pharmaceutical application [4-9]. Additionally, the hydrophilicity in combination with its hydroxyl functionalities makes HyPG very suitable for the design of hydrogels. Hydrogels, hydrophilic polymeric networks, are of widespread interest for applications in the pharmaceutical, biomedical and biotechnological fields [11, 16-18]. An anticipated advantage of HyPG hydrogels over existing hydrogels is the low viscosity of the hydrogel precursors in water [6, 19], which can lead to gels with high solid contents and consequently excellent mechanical properties. A possible route to obtain HyPG hydrogels is depicted in Figure 1. Here, the hydroxyl groups of HyPG are derivatized with methacrylate groups, which will connect the HyPG molecules with each other by covalent crosslinks. Crosslinking can be achieved by chemical initiation using potassium peroxodisulfate (KPS) and *N,N,N',N'*-tetramethylethylenediamine (TEMED) or by photopolymerization. The first process has been routinely used for the preparation of macroscopic and microscopic hydrogels [20-22]. Photopolymerization is nowadays commonly applied for the preparation of hydrogels, allowing in situ gel formation of patterned gels in a minimal invasive matter [23-25]. However, it is possible that the network properties of the hydrogels may be affected by the polymerization conditions (type of initiating system and concentration of initiators, wavelength of the emitted light and intensity of the UV-lamp). The aim of this

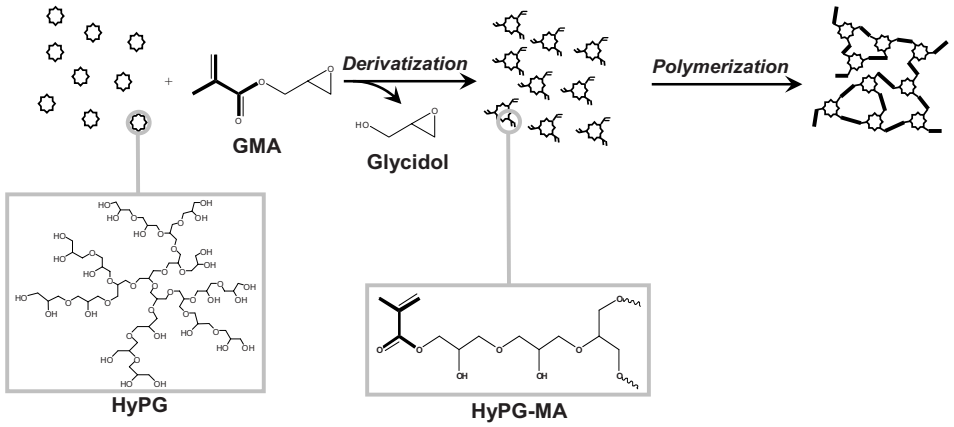

Figure 1. *A schematic representation of the derivatization of HyPG with glycidyl methacrylate (GMA) to yield glycidol as side product and HyPG-MA followed by the formation of HyPG-MA hydrogels by radical polymerization. The depicted polymer structure shows only a small fragment of the large polymer core (M_n 2,000 g/mol).*

study is the synthesis of methacrylated hyperbranched polyglycerol and to study the characteristics of hydrogels derived hereof.

2. Experimental section

2.1. Materials

Hyperbranched polyglycerol (HyPG, M_n 2,000 g/mol, 32 hydroxyl groups per molecule) was purchased from Hyperpolymers GmbH (Freiburg, Germany). Dimethyl sulfoxide (DMSO, $H_2O \leq 0.005\%$), glycidyl methacrylate (GMA), (±)-glycidol, *N,N,N',N'*-tetramethylethylenediamine (TEMED) and methacrylic acid were purchased from Fluka (Buchs, Switzerland). 4-(*N,N*-dimethylamino)pyridine (DMAP), acetic acid and 70% perchloric acid were obtained from Acros Chimica (Geel, Belgium). Methyl sulfoxide-d_6 (99.9% atom D) and 2-hydroxy-4'-(2-hydroxyethoxy)-2-methylpropiophenone (Irgacure 2959, purity 98%) were provided by Sigma-Aldrich (Zwijndrecht, The Netherlands). Sodium hydroxide (NaOH) pellets and potassium peroxodisulfate (KPS) were obtained from Merck (Darmstadt, Germany). Diethylether and acetonitril (HPLC grade) were purchased from Biosolve Ltd. (Valkenswaard, The Netherlands).

2.2. Kinetics of HyPG-MA formation

The synthesis of methacrylated HyPG (HyPG-MA) was based on the method described by van Dijk-Wolthuis et al. for the synthesis of methacrylated dextrans [22, 26]. In detail,

HyPG (1 g) was dissolved in DMSO (9 ml) at room temperature under a nitrogen atmosphere. After dissolution of DMAP (2 g), GMA (251 µl; 2 mmol or 2.51 ml; 20 mmol, corresponding to a molar ratio GMA:OH of 1:1 and 10:1, respectively) was added. Samples of 0.3 ml were taken at regular time intervals, after which HyPG-MA was precipitated in diethylether, washed three times with the same solvent and subsequently dried overnight at room temperature. The degree of substitution (DS, the percentage of derivatized hydroxyl groups) of the HyPG-MA samples was determined by both ^{1}H NMR spectroscopy (section 2.8.) and reversed-phase (RP) HPLC as described by Stenekes et al. [27].

2.3. Large-scale synthesis of methacrylated HyPG

Ten grams of HyPG were dissolved in 90 ml DMSO ($H_2O \leq 0.005\%$) at room temperature under a nitrogen atmosphere. Next, 2 g of DMAP and a certain amount of GMA (0.15 to 7.5 ml), depending on the aimed degree of substitution, were added. After 5 h stirring at room temperature, the HyPG-MA was precipitated in 1 L diethylether. The reaction product was washed three times with the same solvent and dried at room temperature. The DS, defined as the percentage of derivatized hydroxyl groups, of the obtained product was determined by ^{1}H NMR spectroscopy (section 2.8.).

2.4. Reaction of HyPG-MA with glycidol

The reversibility of the reaction of HyPG with GMA was studied as follows. A 10% (w/v) solution of HyPG-MA DS 11 in DMSO (9 ml) was prepared after which 0.2 g DMAP and a 200% or 500% molar excess of glycidol (59 µl; 1 mmol and 146 µl; 2.5 mmol respectively) with respect to hydroxyl groups of HyPG were added. The reaction mixture was stirred at room temperature under a nitrogen atmosphere for 33 days. Samples of 0.3 ml were taken periodically and the polymer was precipitated in 3 ml diethylether. The obtained product was washed with the same solvent, dried overnight at room temperature and subsequently analyzed with ^{1}H NMR spectroscopy (section 2.8.).

2.5. Polymerization kinetics of HyPG-MA

2.5.1. Polymerization kinetics of HyPG-MA polymerized using KPS and TEMED

HyPG-MA (150 mg, DS 11) was dissolved in 315 µl phosphate buffer (10 mM, pH 7.2) to obtain gels with an initial solid content of 30%. Next, KPS (25 µl; 5% (v/v), 50 mg/ml) and TEMED (10 µl; 2% (v/v), 20% (v/v) in 2 M HCl) were added. The polymerization reaction was stopped at various time points by quickly freezing samples of the HyPG-MA solutions in liquid nitrogen. After lyophilization, the dried samples were rehydrated in 10 ml 0.02 M NaOH and kept for 30 min at 37°C to hydrolyze unreacted methacryloyl groups. The concentration of methacrylic acid was determined using RP-HPLC as described by Stenekes et al. [27]. Additionally, the influence of initiator and catalyst

concentration on the polymerization rates of HyPG-MA (DS 11, 30% (w/w)) was evaluated at different concentrations of KPS (2.5% or 10% (v/v)) or TEMED (1% or 4% v/v)).

2.5.2. Photopolymerization kinetics of HyPG-MA

HyPG-MA (75 mg, DS 11) was dissolved in 175 µl phosphate buffer (10 mM, pH 7.2), containing 0.05% (w/v) Irgacure 2959 to obtain gels with an initial solid content of 30%. The influence of initiator concentration on the polymerization kinetics was studied by using different concentrations of Irgacure 2959 (0.025% or 0.1% (w/v)). The solutions were flushed with nitrogen and the HyPG-MA was polymerized (UV light model Bluepoint 4 UVC, Dr. Hoenle AG, UV-Technology, Gräfelfing, Germany; max. UVA intensity 11 mW/cm^2) at a distance of 5 cm above the mould for 0, 0.5, 1, 2, 3, 5 and 7 min in cylindrical moulds of 7 x 5 mm (diameter x height). Unreacted methacryloyl groups were hydrolyzed by incubating the gels in 10 ml 0.02 M NaOH at 37°C for 30 min. The concentration of methacrylic acid was determined using RP-HPLC as described by Stenekes et al. [27].

2.6. Preparation of macroscopic hydrogels

2.6.1. Macroscopic hydrogels prepared using KPS and TEMED

Methacrylated HyPG with varying concentrations (DS 11; 20%, 30%, 50%, 70%, 85%, and 93% (w/w); total volume 465 µl) or varying DS (30% (w/w); DS 1, 1.5, 4, 11, 18, 28; total volume 465 µl) were prepared in 10 mM phosphate buffer pH 7.2, transferred into cylindrical moulds of 10 x 7 mm (diameter x height) and polymerized after the addition of 25 µl (5% (v/v)) KPS (50 mg/ml) and 10 µl (2% v/v) TEMED (20% (v/v) adjusted to pH 7 with 2 M HCl) for 1 h at room temperature. To study the influence of initiator and catalyst concentration for HyPG-MA gels (DS 11, 30% (w/w)), different concentrations of KPS (2.5% or 10% (v/v)) or TEMED (1% or 4% v/v)) were added while preparing the gels.

2.6.2. Macroscopic hydrogels prepared by photopolymerization

Hydrogels were prepared by dissolving various amounts of methacrylated HyPG DS 11 (20%, 30%, 50%, 70%, 85%, and 93% (w/w)) or HyPG-MA with varying DS (30% (w/w); DS 11, 18, 28) in 10 mM phosphate buffer pH 7.2 containing 0.05% (w/v) Irgacure 2959. The solutions were transferred into cylindrical moulds of 7 x 5 mm (diameter x height) and flushed with nitrogen prior to exposure to UV light (UV light model Bluepoint 4 UVC, Dr. Hoenle AG, UV-Technology, Gräfelfing, Germany; max. UVA intensity 11 mW/cm^2) at a distance of 5 cm above the mould for 3 min. The influence of initiator concentration was evaluated by using different concentrations of Irgacure 2959 (0.025% or 0.1% (w/v)) for the preparation of the HyPG-MA hydrogels (DS 11, 30% w/w).

2.7. Characterization of the HyPG-MA hydrogels

2.7.1. Swelling of hydrogels

HyPG-MA gels (0.5 g) with different percentages of solid content (20%, 30%, 50%, 70%, 85%, and 93% (w/w)) were prepared as described in section 2.6.1. and 2.6.2. The hydrogels were transferred into pre-weighed glass vials and their initial weight (W_0) was recorded. Next, the vials were filled with 10 ml isotonic 100 mM PBS, pH 7.2, containing 0.02% NaN_3. The samples were incubated at 37°C and the weight of the gels was measured at regular time intervals (W_t). The buffer was replaced by fresh PBS at regular times. The swelling ratio is defined as the ratio between the weight of the gel at time t and its initial weight (W_t/W_0).

The sol fraction of HyPG-MA (DS 11, 30% (w/w)) hydrogels was determined analytically to evaluate whether after polymerization the gels contain unmodified HyPG-MA. As positive control HyPG-MA (DS 11, 20% (w/w)) hydrogels containing 10% (w/w) unmodified HyPG were prepared (described in section 2.6.1.) and evaluated for their sol fractions. After polymerization, the formed gels were incubated in 2 ml of 100 mM ammonium acetate buffer pH 4 at 37°C to extract the unmodified HyPG. The HyPG concentration present in the extraction solvent was determined by gel permeation chromatography (GPC; consisting of a Waters 2695 pump and injector, a Waters 2414 refractive index detector and a PL aquagel-OH 30 chromatographic column). The eluent consisted of ammonium acetate buffer (100 mM, pH 4), the flow rate was 1.0 ml/min and 50 µl of each sample was injected onto the column. A calibration curve was obtained by injecting varying concentrations (0 to 7.5 mg/ml) of unmodified HyPG in eluent.

2.7.2. Rheological characterization of HyPG-MA hydrogels prepared using KPS and TEMED

Rheological characterization of the hydrogels was performed on an AR1000-N rheometer (TA instruments, Etten-Leur, The Netherlands) equipped with a 1° steel cone geometry of 40 mm diameter. Directly after addition of the polymerizing agents KPS and TEMED, the HyPG-MA solutions were placed between the plates of the rheometer [28]. The rheological properties of the gels were monitored by oscillatory time sweep, frequency sweep, strain sweep and creep experiments at 20°C. The time sweep, carried out with a constant strain of 1% and a constant frequency of 1 Hz, was used to measure the shear storage modulus (G') and the loss modulus (G'') for a period of 1 h. During the frequency sweep and strain sweep experiments the viscoelastic deformation of a 30% (w/w) HyPG-MA hydrogel (DS 11) was evaluated at a frequency range of 10 Hz to 0.1 Hz and a strain range of 0.1% to 10%, respectively. The creep experiment was performed to evaluate the deformation of the samples when applying a shear stress of 100 Pa for 2 min. Subsequently, the stress was stopped and the recovery of the gels followed for 2 more minutes.

2.7.3. Dynamic mechanical analysis

The compression modulus of the HyPG-MA hydrogels after photopolymerization and swelling (see section 2.6.2. and 2.7.1., respectively) was measured at room temperature using a dynamic mechanical analyzer (DMA 2980, TA instruments, Etten-Leur, The Netherlands) in the controlled force mode [29]. Hydrogels of 10 x 7 mm (diameter x height) were placed between the parallel plates (diameter upper plate 6 mm, diameter lower plate 45 mm) and a static force was applied at a rate of 0.05 N/min to 4 N. The Young's modulus (*E*) was determined as described by Meyvis et al. [29]. The shear storage modulus *G'* was calculated as follows [29]:

$$E = 3 \times G' \qquad (1)$$

2.8. ^{1}H NMR spectroscopy

^{1}H NMR spectra were recorded in methyl sulfoxide-d_6 on a Gemini 500 MHz spectrometer (Varian Associates Inc. NMR Instruments, Palo Alto, CA). The reference line of DMSO-d_6 was set at 2.49 ppm. The substituted methacrylate groups were identified by the signals of the methacryloyl group at 5.6 and 6.0 ppm (protons of the double bond H_a and H_b, respectively) and of the methyl resonance at 1.8 ppm (H_c). With the protons of HyPG detected at 3.4 ppm (H_p, on average 6 protons per monomer) the substitution degree is determined as follows:

$$DS = \frac{(H_a + H_b)/2}{H_p/5} \times 100\% \qquad (2)$$

2.9. Calculation of average molecular weight between crosslinks and pore size of the hydrogels

The average molecular weight between crosslinks (M_c) of hydrogel materials can be calculated with the following equation derived from the rubber elasticity theory [30-32]:

$$M_c = \frac{3\rho RT}{E} \qquad (3)$$

where ρ is the specific density of the HyPG hydrogel (g/cm^3), *R* is the gas constant, *T* is the absolute temperature and *E* is the Young's modulus (Pa) obtained from the dynamic mechanical analysis data (section 2.7.3.). The specific density was calculated using the partial specific volume of HyPG (0.75 cm^3/g) [33] and the water content of the gels at equilibrium swelling.

The mesh size ξ of the swollen hydrogel was calculated [34, 35]:

$$\xi = \nu_{2,s}^{-1/3} \sqrt{\overline{r}_o^2} \qquad (4)$$

where $\nu_{2,s}$ is the polymer volume fraction of the gel in the swollen state and $\sqrt{\bar{r}_o^2}$ is the average distance between two adjacent crosslinks in the solvent free state. $\sqrt{\bar{r}_o^2}$, which depends on the molecular weight between crosslinks, was determined as follows [36, 37]:

$$\sqrt{\bar{r}_o^2} = l\sqrt{(2M_c / M_r)}\sqrt{C_n} \qquad (5)$$

where l is the average value of the bond length in the repeating unit, M_c is the average molecular mass between crosslinks, M_r is the molecular mass of the repeating unit (74 g/mol) and C_n is the characteristic ratio, estimated as 4 using poly(ethylene glycol) [36]. A combination of equation 4 and 5 gives:

$$\xi = 0.48 \cdot (\nu_{2,s})^{-1/3}\sqrt{M_c} \qquad (6)$$

3. Results and discussion

3.1. Synthesis and characterization of HyPG-MA

The synthesis of methacrylated HyPG (Fig. 1) was performed using essentially the same synthetic method as described for methacrylated dextrans [22, 26]. ^{1}H NMR analysis of the obtained products demonstrated that under the selected reaction conditions, at room temperature under a nitrogen atmosphere with DMSO as solvent and DMAP as catalyst, the methacryloyl groups are directly linked to the polymer by a transesterification reaction [22, 26, 38] resulting in HyPG-MA. In Figure 2A and 2B the spectra of HyPG and HyPG-MA are displayed, respectively. The ^{1}H NMR spectrum of HyPG (Fig. 2A) shows the methylene and methine protons of HyPG as one broad resonance around 3.4 ppm, whereas the hydroxyl protons give a signal at 4.6 ppm.

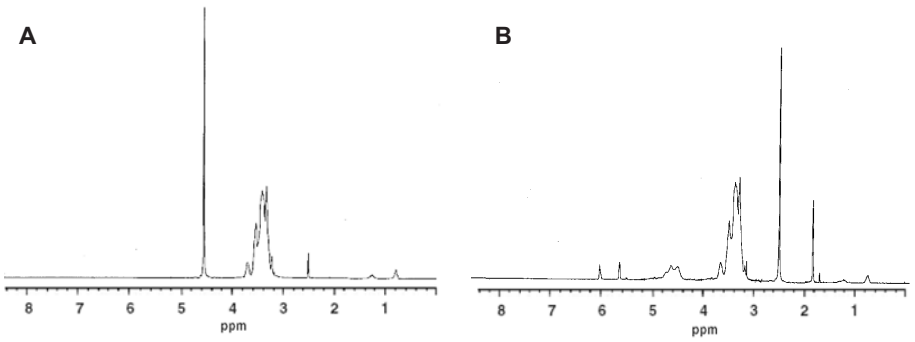

Figure 2. *^{1}H NMR spectra of (A) hyperbranched polyglycerol and (B) methacrylated hyperbranched polyglycerol (DS 11). The polymers were dissolved in DMSO-d_6.*

The two signals observed at 0.9 and 1.2 ppm are due to the methyl and methylene group, respectively, of the initiator 1,1,1-tris(hydroxymethyl)propane used for the synthesis of HyPG [39]. In the spectrum of HyPG-MA (Fig. 2B) the methacryloyl groups give signals at 1.8 ppm (methyl protons, H_c) and at 5.6 and 6.0 ppm (protons of de double bond H_a and H_b), having a ratio of 3:2 as expected. The degree of HyPG methacrylation was determined by both ^{1}H NMR and RP-HPLC; there was excellent agreement between these methods. A study of the kinetics of the reaction of GMA with HyPG (feed ratio of GMA:HyPG hydroxyl groups was 1:1 mol:mol) showed that the degree of methacrylate substitution reached a value of 11 within 25 min after which no further increase in DS was observed. A DS of 11 indicates that ~4 out of the 32 hydroxyl groups of HyPG were substituted with a methacryloyl group. When a feed ratio of GMA:HyPG hydroxyl groups of 10:1 mol:mol was applied, a DS of 55 was obtained within 4 h (data not shown). The higher DS indicates that with an excess of GMA the more inner located OH groups of HyPG have also been substituted with methacrylate groups, which also explains the longer reaction time to reach this DS. In Figure 3 the relation between the ratio of GMA and HyPG in the feed and the degree of substitution of the obtained products is depicted. Under the selected reaction conditions at a feed ratio of GMA:HyPG-OH groups of ≤ 3:1 mol:mol, about 10% of the added GMA had reacted with HyPG. At a feed ratio GMA:HyPG-OH groups of 10:1 mol:mol, the percentage of reacted GMA decreased to 6%. At a feed ratio of 20:1 GMA:HyPG-OH groups a plateau value (DS 70) was reached, which indicated that not all OH groups are available for modification. Likely, the hydroxyl groups buried in the HyPG are not accessible for reaction. Importantly, Figure 3 shows that the degree of methacrylate substitution of HyPG can accurately and reproducibly be tailored in the range of 0.7 to 70. Next, the reversibility of the reaction of HyPG with GMA was studied by addition of glycidol to HyPG-MA in the presence of DMAP. It was shown (Fig. 4) that when no glycidol was added, HyPG-MA was stable as the DS of HyPG-MA was constant in time. Furthermore, it can be observed in Figure 4 that upon incubation with a 200% molar excess of glycidol with respect to the hydroxyl groups of HyPG the DS of HyPG-MA gradually decreased in time. The substitution degree decreased even more rapidly when a 500% molar excess of glycidol was added. These results indicate that the synthesis of HyPG-MA is reversible and that the derivatization occurs via transesterification as reported previously in literature for dextran [26]. Using Figure 3 and 4, the equilibrium constant (K) of the HyPG-MA reaction was determined at 1.04 ± 0.03, which in turn can be used to determine the Gibbs energy change (ΔG^0) of this reaction:

$$\Delta G^o = -RT \ln K \qquad (7)$$

In which R is the gas constant, T the temperature of the synthesis (294 K) and K the equilibrium constant. The ΔG^0 is -96 J/mol.

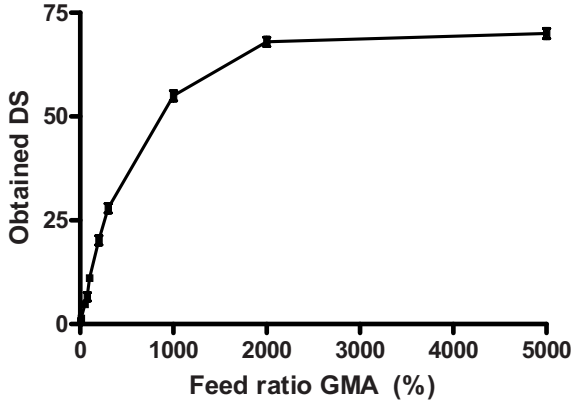

Figure 3. *Relation between the molar ratio of GMA to the hydroxyl groups of HyPG in the feed (in %) and the DS of the obtained material. The data are shown as average ± SD, n = 3.*

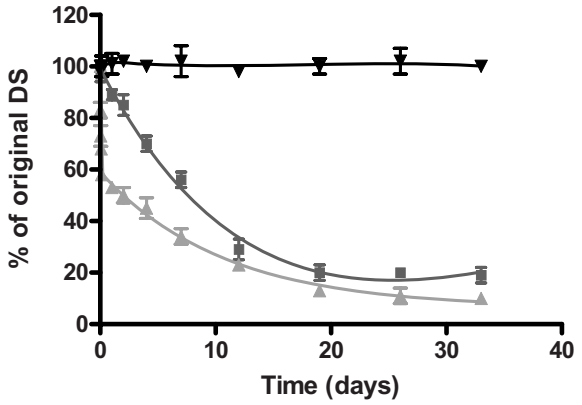

Figure 4. *Reaction of HyPG-MA with glycidol: control (▼) in which no glycidol was added, 200% (■) and 500% (▲) molar excess of glycidol. Data are shown as average (n = 2).*

3.2. Hydrogel formation and characterization

The methacrylated HyPG were crosslinked by radical polymerization, using KPS as initiator and TEMED as catalyst. The polymerization kinetics of HyPG-MA DS 11 dissolved in PB (30% (w/w) solid content) was followed by measuring the conversion of the methacrylates with RP-HPLC. It was observed that within 10 min 99% of the methacrylate groups were converted. Moreover, variation of the initiator and catalyst concentration did not have an influence on the methacrylate conversion (results not shown).

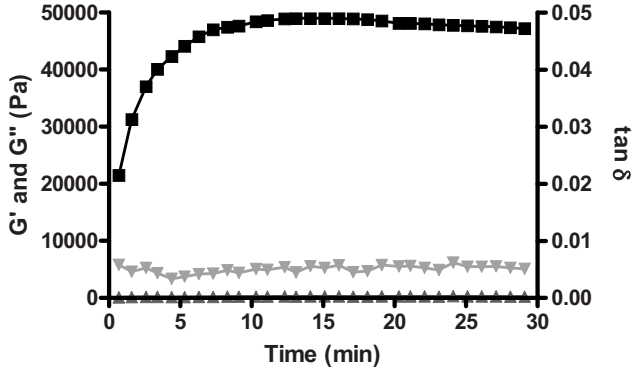

Figure 5. *Storage modulus G' (■), viscous modulus G" (▲) and tan δ (▼) of a 30% (w/w) HyPG-MA DS 11 hydrogel as function of time after addition of KPS and TEMED.*

By rheology measurements it was confirmed that within 10 min a fully elastic network (Fig. 5; *G'* = 49,000 Pa; *G"* = 300 Pa; tan *δ* = 0.005) was obtained independent of the amount of KPS and TEMED used. Before addition of KPS and TEMED, an aqueous solution of HyPG-MA showed mainly viscous behavior (tan *δ* >2.0, and both *G'* and *G"* were low, 0.1 and 0.15 Pa, respectively), demonstrating that the elastic properties of the HyPG-MA gels are due to polymerization of the methacrylate groups by which a network was obtained. After the time sweep experiment, a frequency sweep and strain sweep experiment were performed (results not shown). It was shown that when a frequency of 1 Hz and a strain of 1% were applied, the gel was in the linear viscoelastic deformation range. Both frequency and strain could even be increased up to 10 Hz and 10%, respectively, after which the viscoelastic deformation was still in the linear range. The viscoelastic properties of HyPG-MA gels (DS 11, 30% (w/w) solid content) were also investigated with creep experiments. The hydrogel was deformed up to 0.4% strain when a shear stress of 100 Pa was applied. After removal of the stress the gel recovered completely (data not presented), confirming the fully elastic properties of the network.
In Figure 6 photographs of hydrogels obtained by polymerization of HyPG-MA with DS 11, 18 and 28 (30% (w/w) solid content) are depicted. It was observed that a HyPG-MA DS 11 gel was fully transparent whereas HyPG-MA DS 18 and DS 28 gels were opaque and white, respectively, indicating that in gels with DS 18 and DS 28 phase separation (e.g. water-rich, hydrated hyperbranched polyglycerol domains and water-poor domains rich in relatively hydrophobic polymerized methacrylates) occurred. Rheological analysis showed that, as was observed for HyPG-MA DS 11 gels, also the HyPG-MA DS 18 and DS 28 hydrogels were fully elastic. Figure 7A shows the storage modulus of aqueous solutions of HyPG-MA after addition of KPS and TEMED.

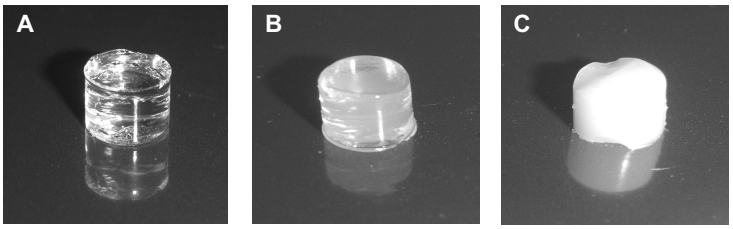

Figure 6. *HyPG-MA hydrogels (30% (w/w) initial solid content) with various substitution degrees: DS 11 (A), DS 18 (B), and DS 28 (C).*

HyPG-MA with low degrees of substitution (DS 1, 1.5 and 4) did not yield hydrogels after addition of KPS and TEMED. This can be ascribed to the low average number of methacrylate groups per HyPG molecule (0.3, 0.5 and 1.3 out of 32 OH groups were substituted for DS 1, 1.5 and 4, respectively), resulting in intramolecular crosslinks due to a minimal overlap of chains. Furthermore, Figure 7A shows that the storage modulus of the HyPG-MA gels increased with increasing degree of methacrylate substitution. Hydrogels consisting of HyPG with a higher modification have a higher crosslink density and consequently higher storage modulus. The HyPG-MA (DS 11) hydrogels were rheologically characterized in more detail by varying the percentages (10%, 20%, 50%, 70%, 85% and 93% (w/w)) of solid material. Figure 7B shows that gelation occurred when the concentration of polymer was at least 20% (w/w). At lower polymer concentrations the overlap of chains is minimal resulting in the formation of intramolecular crosslinks, which do not contribute to network formation [21, 36].

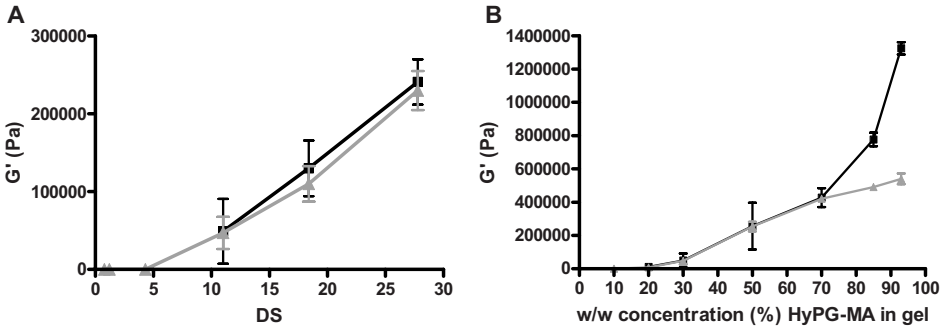

Figure 7. *(A) Storage modulus (G') as function of the substitution degree of HyPG-MA hydrogels (initial solid content of 30% (w/w)) obtained after photopolymerization (■) and polymerization with KPS and TEMED (▲). (B) Storage modulus G' as a function of the solid content of HyPG-MA DS 11 gels obtained after photopolymerization (■) and polymerization with KPS and TEMED (▲). The data are shown as average ± SD, n = 3.*

The gels with 50% to 93% (w/w) of polymer content showed elastic behavior (tan δ about 0.0075; results not shown) as was observed for 30% (w/w) gels. In line with expectations, the storage modulus increased with increasing amount of solid content (Fig. 7B). The swelling behavior of hydrogels with DS 11 and varying percentages of solid content (20% to 93% (w/w)) was evaluated by incubating them in an aqueous buffer of pH 7.2 at 37°C. Within 10 h, equilibrium swelling was obtained and independent of their composition, the hydrogels absorbed 50% water (equilibrium swelling ratio 1.5; see Figure 8 for 30% (w/w) gel). To evaluate the validity of the equilibrium swelling ratio, the sol fraction of HyPG-MA (DS 11, 30% (w/w)) hydrogels was determined analytically [28]. A positive control consisting of HyPG-MA (DS 11, 20% (w/w)) with 10% (w/w) unmodified HyPG was evaluated in parallel. GPC of the extraction liquids indicated that these later hydrogels showed indeed quantitative leakage of unmodified HyPG within 1 day. However, no sol fraction was detected for the 30% (w/w) HyPG-MA hydrogels. The swelling ratio of gels with higher degrees of substitution was also investigated. Figure 8 shows that with increasing DS (DS 18 and DS 28, 30% (w/w) initial solid content) gels swelled less (1.3 and 1.2 times their initial weight, respectively). The limited and controlled equilibrium swelling behavior of HyPG-MA hydrogels has also been reported for gels based on low molecular weight PEG-dimethacrylates. Hydrogels prepared by polymerization of high molecular weight PEG-dimethacrylates, however, always show extensive swelling [15, 40, 41]. Additionally, this limited swelling indicates that rather dimensionally stable hydrogels are obtained, which can be attributed to the rather rigid network of intermolecular crosslinked HyPG-MA molecules as depicted in Figure 1.

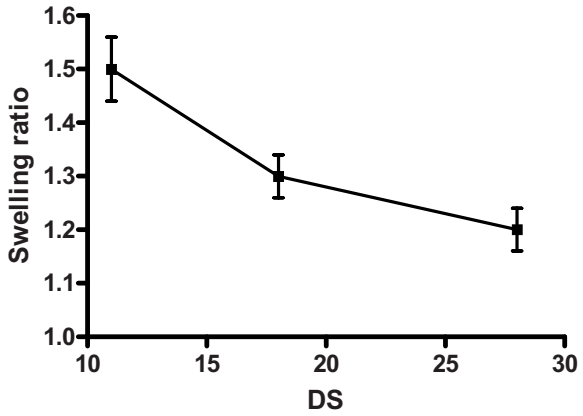

Figure 8. *Swelling ratio of HyPG-MA hydrogels (30% (w/w) initial solid content) as function of the DS: DS 11, DS 18 and DS 28. The data are shown as average ± SD, n = 3.*

3.3. Photopolymerization of HyPG-MA

The photopolymerization of HyPG-MA was investigated using Irgacure 2959 as photoinitiator. It was shown that, independent of the initiator concentration, 99% of the methacrylate groups were converted within 3 min of illumination (results not shown). The obtained hydrogels were analyzed using DMA (dynamic mechanical analysis). As observed for gels prepared using KPS and TEMED, the UV-cured gels showed no alteration in shear storage modulus, *G'*, upon variation of initiator concentration (results not shown). Additionally, the gels showed an increasing *G'* with increasing DS (Figure 7A) and with increasing polymer concentrations (Figure 7B). No significant difference (unpaired *t* test, $p > 0.05$) in *G'* as function of the DS was observed between photopolymerized gels and gels polymerized using KPS and TEMED (Figure 7A). In Figure 7B the shear storage modulus of HyPG-MA gels, obtained after photopolymerization, with various percentages of solid material (20%, 30%, 50%, 70%, 85% and 93% (w/w)) is shown. Up to 70% (w/w) of solid content, gels prepared by both methods showed similar storage moduli. Above this concentration, gels prepared by photopolymerization showed higher storage moduli compared to polymerization using KPS and TEMED (unpaired *t* test, $p < 0.01$). The higher storage modulus observed after photopolymerization may be ascribed to the occurrence of more intermolecular crosslinks, which result in an increased contribution to the network formation. As the mechanical properties can be controlled over a wide range by the hydrogel composition (i.e. water content and degree of methacrylate substitution) it can be anticipated that the right properties can be tailored for tissue engineering and drug delivery purposes.

Additionally, the swelling behavior of HyPG-MA gels (DS 11, solid content varying from 20% to 93% (w/w)) obtained after photopolymerization was evaluated. It was observed that with increasing solid content gels swelled less and reached 1.5 to 1.2 times their initial weight for 20% to 93% (w/w) solid content, respectively. The UV-cured gels showed a lower swelling in particular at high polymer concentration compared to the gels prepared with KPS and TEMED. This indicates that UV-cured gels have a higher crosslink density, which is in agreement with the *G'* observations. This limited swelling implies that the HyPG-MA hydrogels obtained by photopolymerization are dimensionally stable, as was also observed for the gels prepared by chemical polymerization using KPS and TEMED.

3.4. Average molecular weight between crosslinks and hydrogel pore size

The average molecular weight between crosslinks (M_c) of the HyPG-MA hydrogels at maximal swelling was determined using equation 3 (see section 2.9), which was derived from the rubber elasticity theory [30-32]. Subsequently, the calculated M_c values (Table 1) were used to calculate the pore size (ξ) of the hydrogels, as was previously

Table 1. *Characteristics of HyPG-MA hydrogels with varying percentages of solid content and varying degrees of substitution.*

DS	Initial water content (%)	*E* (kPa) (*n*=3)	M_c (g/mol)	$\nu_{2,s}$	ξ (nm)
11	80	37 ± 5	140000	0.11	37.0
11	70	84 ± 22	60000	0.17	21.0
11	50	558 ± 80	10400	0.32	7.2
11	30	688 ± 60	6000	0.47	4.9
11	15	689 ± 70	1600	0.62	2.2
11	7	690 ± 70	1200	0.82	1.8
18	70	200 ± 30	24000	0.28	13.6
28	70	415 ± 60	11500	0.27	9.2

DS = degree of substitution

E = Young's modulus

M_c *= average molecular weight between crosslinks (section 2, equation 3)*

$\nu_{2,s}$ *= polymer volume fraction at maximum swelling*

ξ *= pore size (equation 6, materials and methods)*

performed for star polymers [37], according to equation 6 (see section 2.9). The results of the estimated M_c and ξ are given in Table 1. As expected, with increasing water content both M_c and pore size increased. Additionally, the M_c and pore size increased with decreasing degree of methacrylate substitution. These results, presented in Table 1, show a similar tendency as was previously reported for dextran hydrogels and microspheres [20, 42, 43]. It should be noted that for the used model to calculate M_c it is assumed that the end-to-end distances of the chains are Gaussian, that the network deformation is affine and isothermal and that dangling ends are absent. Likely, the HyPG-MA networks do not fulfill these criteria and consequently, the presented pore size data can only be referred to in a relative way.

4. Conclusions

In this paper we report on the preparation and characterization of methacrylated hyperbranched polyglycerol (HyPG-MA) and hydrogels obtained after chemical polymerization of this derivatized polymer. An efficient method for the synthesis of GMA derivatized HyPG was developed which allowed tailoring of the DS by varying the molar ratio of GMA to HyPG. It was feasible to prepare dimensionally stable hydrogels with high concentrations of solid content. Polymerization of these HyPG-MA gels was very fast as nearly complete conversion was obtained within 10 min after polymerization using

KPS and TEMED and within 3 min after photopolymerization. Moreover, hydrogels with a lower water content or higher DS showed, as expected, a higher elastic modulus and consequently smaller pores. As for the hydrogels prepared with KPS and TEMED, networks formed by photopolymerization showed limited swelling indicating that dimensionally stable hydrogels are obtained. Consequently, these gels offer excellent opportunities for drug delivery and tissue engineering purposes.

References

1. Stiriba SE, Slagt MQ, Kautz H, Klein Gebbink RJ, Thomann R, Frey H, van Koten G. Synthesis and supramolecular association of immobilized NCN-pincer platinum(II) complexes on hyperbranched polyglycerol supports. *Chemistry* 2004; 10(5): 1267-1273.
2. Slagt MQ. Para-functionalized NCN-pincer palladium and platinum complexes as building blocks in organometallic chemistry. Utrecht: Utrecht University; 2002.
3. Haag R, Stumbe JF, Sunder A, Frey H, Hebel A. An approach to core-shell-type architectures in hyperbranched polyglycerols by selective chemical differentiation. *Macromolecules* 2000; 33(22): 8158-8166.
4. Garcia-Bernabe A, Kramer M, Olah B, Haag R. Syntheses and phase-transfer properties of dendritic nanocarriers that contain perfluorinated shell structures. *Chemistry* 2004; 10(11): 2822-2830.
5. Sunder A, Mulhaupt R, Haag R, Frey H. Hyperbranched Polyether Polyols: A Modular approach to complex Polymer Architectures. *Adv Mater* 2000; 12(3): 235-239.
6. Sunder A, Kramer M, Hanselmann R, Mulhaupt R, Frey H. Molecular Nanocapsules Based on Amphiphilic Hyperbranched Polyglycerols. *Angew Chem Int Ed Engl* 1999; 38(23): 3552-3555.
7. Sunder A, Quincy MF, Mulhaupt R, Frey H. Hyperbranched Polyether Polyols with Liquid Crystalline Properties. *Angew Chem Int Ed Engl* 1999; 38(19): 2928-2930.
8. Hyperpolymers. http://www.hyperpolymers.com.
9. Stiriba SE, Kautz H, Frey H. Hyperbranched molecular nanocapsules: comparison of the hyperbranched architecture with the perfect linear analogue. *J Am Chem Soc* 2002; 124(33): 9698-9699.
10. Haag R, Sunder A, Stumbe J. An approach to glycerol dendrimers and pseudo-dendritic polyglycerols. *J Am Chem Soc* 2000; 122: 2954-2955.
11. Drury JL, Mooney DJ. Hydrogels for tissue engineering: scaffold design variables and applications. *Biomaterials* 2003; 24(24): 4337-4351.
12. Hubbell JA. Hydrogel systems for barriers and local drug delivery in the control of wound healing. *J Control Release* 1996; 39(2-3): 305-313.
13. West JL, Hubbell JA. Comparison of covalently and physically cross-linked polyethylene glycol-based hydrogels for the prevention of postoperative adhesions in a rat model. *Biomaterials* 1995; 16(15): 1153-1156.
14. Sperinde JJ, Griffith LG. Synthesis and characterization of enzymatically-crosslinked poly(ethylene glycol) hydrogels. *Macromolecules* 1997; 30: 5255-5264.
15. DiRamio JA, Kisaalita WS, Majetich GF, Shimkus JM. Poly(ethylene glycol) methacrylate/dimethacrylate hydrogels for controlled release of hydrophobic drugs. *Biotechnol Prog* 2005; 21(4): 1281-1288.
16. Smeds KA, Pfister-Serres A, Miki D, Dastgheib K, Inoue M, Hatchell DL, Grinstaff MW. Photocrosslinkable polysaccharides for in situ hydrogel formation. *J Biomed Mater Res* 2001; 54(1): 115-121.
17. Jin Y, Yamanaka J, Sato S, Miyata I, Yomota C, Yonese M. Recyclable characteristics of hyaluronate-polyhydroxyethyl acrylate blend hydrogel for controlled releases. *J Control Release* 2001; 73(2-3): 173-181.

18. Hoffman AS. Hydrogels for biomedical applications. *Ann N Y Acad Sci* 2001; 944: 62-73.
19. Sunder A, Heinemann J, Frey H. Controlling the growth of polymer trees: concepts and perspectives for hyperbranched polymers. *Chemistry* 2000; 6(14): 2499-2506.
20. Stenekes RJ, De Smedt SC, Demeester J, Sun G, Zhang Z, Hennink WE. Pore sizes in hydrated dextran microspheres. *Biomacromolecules* 2000; 1(4): 696-703.
21. Hennink WE, Talsma H, Borchert JCH, De Smedt SC, Demeester J. Controlled release of proteins from dextran hydrogels. *J Control Release* 1996; 39: 47-55.
22. van Dijk-Wolthuis WNE, Franssen O, Talsma H, van Steenbergen MJ, Kettenes-van den Bosch JJ, Hennink WE. Synthesis, characterization and polymerization of glycidyl methacrylate derivatized dextran. *Macromolecules* 1995; 28(18): 6317-6322.
23. Lin-Gibson S, Bencherif S, Cooper JA, Wetzel SJ, Antonucci JM, Vogel BM, Horkay F, Washburn NR. Synthesis and characterization of PEG dimethacrylates and their hydrogels. *Biomacromolecules* 2004; 5(4): 1280-1287.
24. Bryant SJ, Hauch KD, Ratner BD. Spatial patterning of thick poly(2-hydroxyethyl methacrylate) hydrogels. *Macromolecules* 2006; 39(13): 4395-4399.
25. Zhang K, Simon CG, Jr., Washburn NR, Antonucci JM, Lin-Gibson S. In situ formation of blends by photopolymerization of poly(ethylene glycol) dimethacrylate and polylactide. *Biomacromolecules* 2005; 6(3): 1615-1622.
26. van Dijk-Wolthuis WNE, Kettenes-van den Bosch JJ, van der Kerk-van Hoof A, Hennink WE. Reaction of dextran with glycidyl methacrylate: an unexpected transesterification. *Macromolecules* 1997; 30(11): 3411-3413.
27. Stenekes RJ, Hennink WE. Polymerization kinetics of dextran-bound methacrylate in an aqueous two phase system. *Polymer* 2000; 41: 5563-5569.
28. De Smedt SC, Lauwers A, Demeester J, van Steenbergen MJ, Hennink WE, Roefs SPFM. Characterization of the network structure of dextran glycidyl methacrylate hydrogels by studying the rheological and swelling behavior. *Macromolecules* 1995; 28: 5082-5088.
29. Meyvis TK, Stubbe BG, Van Steenbergen MJ, Hennink WE, De Smedt SC, Demeester J. A comparison between the use of dynamic mechanical analysis and oscillatory shear rheometry for the characterisation of hydrogels. *Int J Pharm* 2002; 244(1-2): 163-168.
30. Peppas NA, Bures P, Leobandung W, Ichikawa H. Hydrogels in pharmaceutical formulations. *Eur J Pharm Biopharm* 2000; 50(1): 27-46.
31. Ward IM, Hadley DW. An introduction to the mechanical properties of solid polymers. New York: Wiley & sons; 1993.
32. Flory PJ. Principles of polymer chemistry. In. New York: Cornell University Press; 1953.
33. Garamus VM, Maksimova TV, Kautz H, Barriau E, Frey H, Schlotterbeck U, Mecking S, Richtering W. Hyperbranched polymers: structure of hyperbranched polyglycerol and amphiphilic poly(glycerol ester)s in dilute aqueous and nonaqueous solution. *Macromolecules* 2004; 37: 8394-8399.
34. Peppas NA, Moynihan HJ, Lucht LM. The structure of highly crosslinked poly(2-hydroxyethyl methacrylate) hydrogels. *J Biomed Mater Res* 1985; 19(4): 397-411.
35. Canal T, Peppas NA. Correlation between mesh size and equilibrium degree of swelling of polymeric networks. *J Biomed Mater Res* 1989; 23(10): 1183-1193.

36. Raeber GP, Lutolf MP, Hubbell JA. Molecularly engineered PEG hydrogels: a novel model system for proteolytically mediated cell migration. *Biophys J* 2005; 89(2): 1374-1388.
37. Oral E, Peppas NA. Responsive and recognitive hydrogels using star polymers. *J Biomed Mater Res A* 2004; 68(3): 439-447.
38. Pitarresi G, Palumbo FS, Giammona G, Casadei MA, Micheletti Moracci F. Biodegradable hydrogels obtained by photocrosslinking of dextran and polyaspartamide derivatives. *Biomaterials* 2003; 24(23): 4301-4313.
39. Sunder A, Hanselmann R, Frey H, Mulhaupt R. Controlled synthesis of hyperbranched polyglycerols by ring-opening multibranching polymerization. *Macromolecules* 1999; 32: 4240-4246.
40. Weber LM, He J, Bradley B, Haskins K, Anseth KS. PEG-based hydrogels as an in vitro encapsulation platform for testing controlled beta-cell microenvironments. *Acta Biomater* 2006; 2(1): 1-8.
41. Bryant SJ, Arthur JA, Anseth KS. Incorporation of tissue-specific molecules alters chondrocyte metabolism and gene expression in photocrosslinked hydrogels. *Acta Biomater* 2005; 1(2): 243-252.
42. Chung JT, Vlugt-Wensink KD, Hennink WE, Zhang Z. Effect of polymerization conditions on the network properties of dex-HEMA microspheres and macro-hydrogels. *Int J Pharm* 2005; 288(1): 51-61.
43. de Jong SJ, van Eerdenbrugh B, van Nostrum CF, Kettenes-van den Bosch JJ, Hennink WE. Physically crosslinked dextran hydrogels by stereocomplex formation of lactic acid oligomers: degradation and protein release behavior. *J Control Release* 2001; 71(3): 261-275.

Preparation and characterization of structured hydrogel microparticles based on crosslinked hyperbranched polyglycerol

Marion H.M. Oudshoorn[a], Roel Penterman[b], Robert Rissmann[c], Joke A. Bouwstra[c], Dirk J. Broer[b], Wim E. Hennink[a]

[a] Department of Pharmaceutics, Utrecht Institute for Pharmaceutical Sciences (UIPS), Utrecht University, Utrecht, The Netherlands
[b] Philips Research Laboratories, Department of Biomolecular Engineering, Eindhoven, The Netherlands
[c] Department of Drug Delivery Technology, Leiden/Amsterdam Center for Drug Research (LACDR), Leiden University, Leiden, The Netherlands

Langmuir 23 (2007) 11819-11825

4

Abstract

The aim of this work was to obtain well-defined HyPG-MA (methacrylated hyperbranched polyglycerol) microparticles with uniform sizes. Therefore, three different preparation methods were evaluated. First, we assessed a micromolding technique using rigid SU-8 (a photoresist based on epoxies) grids. Independent of the surface treatment of the SU-8 grid or the type of polymer used, approximately 50% of the microgels remained attached to the SU-8 grid or broke into smaller particles during the release process in which drying of the gels was followed by a sonication process. Although 90% methacrylate conversion could be obtained, this method has some additional drawbacks as the obtained dried microgels did not rehydrate completely after the drying step.

Second, a soft-micromolding technique was evaluated using elastomeric PDMS (poly(dimethyl siloxane)) grids. The use of these flexible grids resulted in a high yield (80 to 90% yield; >90% methacrylate conversion) of microgels with a well-defined size and shape (squares of 100x100x50 µm or hexagons with ∅ 30 µm and a thickness of 20 µm) without the occurrence of water evaporation. However, a number of particles showed less-defined shape as not all grids could be filled well. The microgels showed restricted swelling, implying that these gels are dimensionally stable.

Third, an alternative method referred to as photolithography was evaluated. This method was suitable to tailor accurately the size and shape of HyPG-MA microgels and additionally gained 100% yield. Well-defined HyPG-MA microgels in the size-range of 200-1400 µm (thickness of 6, 20 or 50 µm), with a methacrylate conversion of >90%, could easily be prepared by adding an inhibitor (e.g. 1% (w/v) of vitamin C) to the polymer solution to inhibit dark polymerization. Microgels in the size range of 30-100 µm (>90% conversion) could only be obtained when applying the photomask in direct contact with the polymer solution and using a higher (i.e. 2% (w/v)) concentration of vitamin C. Additionally, the microgels showed limited swelling, indicating that rather dimensionally stable particles were obtained. In conclusion, this paper shows that photolithography and soft-micromolding, as compared to rigid-micromolding, are the most appropriate techniques to fabricate structured HyPG-MA microgels with a tailorable and well-defined size and shape. These microgels have great potential in tissue engineering and drug delivery applications.

1. Introduction

Hyperbranched polyglycerols (HyPG) are randomly branched polymers that can be used as molecular nanocarrier or as support for, for example, catalysts upon selective functionalization [1-3]. Recently, methacrylated HyPG (HyPG-MA) hydrogels [4] were described as potential drug delivery matrices or for tissue engineering purposes [2, 5-9] taking the biocompatibility of the polyether-backbone into account. Although hydrogels may be formed by various polymerization methods including physical and chemical cross-linking [4, 10] a commonly applied method is photopolymerization as it allows for rapid gel formation and in-line production [11]. Ideally, the morphology of the gels (i.e. size and shape) should be tailorable in accordance to their aimed application and function. Various techniques, such as phase separation and emulsion/solvent evaporation [12, 13], are currently applied to prepare polymeric microgels. The major drawback of these methods, however, is that they yield particles with a large size distribution and that they are restricted to spherical shapes. Hence, new methods are needed to fabricate the next generation of microdevices with requested, well-defined structures and uniform sizes that have potential applications in tissue engineering and other soft matter technologies. Methods that are commonly used to prepare well-defined microparticles with uniform sizes are photolithography [14, 15] and soft lithographic techniques (e.g. micromolding, microcontact printing and microfluidic patterning) [13, 16-18]. Photolithography is a simple method that transfers a pattern from a mask onto a substrate via UV illumination, whereas soft lithography is a technology that creates 2-D patterns and 3-D structures using elastomeric materials such as stamps and molds. Many variations exist on this last technique such as the micro-transfer technique [19] and the PRINT (particle replication in nonwetting templates) process [20, 21]. Also, well-defined 3-D structures have been prepared using a rapid prototyping technique [22] that uses a computer controlled 3-D printing system. All these techniques have in common that they are able to produce specific, well-defined structures with highly uniform sizes, such as squares, cubes, bars, stacked structures, rings and tubes [13, 18, 22-24]. Such spatial and surface patterned hydrogels have been used to design biosensors, microfluidic devices, drug delivery devices and structures to mimic the complex 3-D tissue environment [13, 22, 25, 26].

The aim of this study is the fabrication of well-defined HyPG-MA microparticles with uniform sizes by micromolding and photolithography to produce microparticles intended for, for example, drug delivery and tissue engineering. Additionally, the swelling characteristics of the obtained HyPG-MA microgels are studied.

2. Experimental section

2.1. Materials

HyPG (M_n 2000 g/mol, on average 32 hydroxyl groups per molecule) was obtained from Hyperpolymers GmbH (Freiburg, Germany). Dimethyl sulfoxide (DMSO, $H_2O \leq 0.005\%$), glycidyl methacrylate (GMA), methacrylic acid and hydroquinone monomethyl ether (purity ≥98%) were purchased from Fluka (Buchs, Switserland). 4-(*N*,*N*-Dimethylamino)pyridine (DMAP), acetic acid and 70% perchloric acid were purchased from Acros Chimica (Geel, Belgium). 2-Hydroxy-4'-(2-hydroxyethoxy)-2-methylpropiophenone (Irgacure 2959, purity 98%) and methyl sulfoxide-d_6 (99.9% atom D) were provided by Sigma-Aldrich (Zwijndrecht, The Netherlands). 1*H*,1*H*,2*H*,2*H*-perfluorodecyltrichlorosilane (fluorsilane, purity 97%) was obtained from ABCR GmbH and Co. KG (Karlsruhe, Germany). Ascorbic acid (vitamin C, purity 99%) was obtained from BUFA B.V. (Uitgeest, The Netherlands). Sodium hydroxide (NaOH) pellets were purchased from Merck (Darmstadt, Germany). Diethylether and acetonitrile (HPLC grade) were purchased from Biosolve Ltd. (Valkenswaard, The Netherlands).

2.2. Synthesis of hyperbranched polyglycerol derivatized with glycidyl methacrylate

Photocrosslinkable HyPG-MA (Fig. 1) was prepared as described previously [4]. In brief, 10 g of HyPG, 2 g of DMAP and a certain amount of GMA (2.5-7.5 ml), depending on the aimed degree of substitution (DS, the percentage of derivatized hydroxyl groups), were dissolved in 90 ml DMSO.

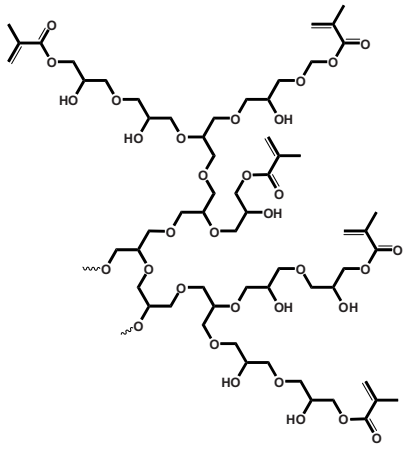

Figure 1. *Chemical structure of photocrosslinkable HyPG-MA.*

The reaction was conducted for 5 h at room temperature. The methacrylated HyPG was obtained after precipitation in 1 L diethylether, washed three times with the same solvent and dried at room temperature. The DS of the obtained product was determined by ^{1}H NMR spectroscopy (Gemini 500 MHz spectrometer, Varian Associates Inc. NMR Instruments, Palo Alto, CA) in methyl sulfoxide-d_6.

2.3. Preparation and characterization of structured HyPG-MA microparticles obtained by micromolding

2.3.1. Preparation of HyPG-MA microparticles by rigid-micromolding

The process for the fabrication of HyPG-MA microparticles using rigid-micromolding is shown in Figure 2A. The SU-8 (photoresist based on epoxies) grids received different surface treatments to enable easy filling of the microwells as well as the release of the formed microparticles. The first treatment consisted of oxygen plasma treatment (300-E plasma system, TePla Technics Plasma GmbH, Munich, Germany) for 20 seconds on the grid surface. The second pretreatment consisted of deposition of fluorsilane (1*H*,1*H*,2*H*,2*H*-perfluorodecyltrichlorosilane; purity 97%) via chemical vapor deposition (CVD) for 30 min using a vacuum desiccator. As third pretreatment, oxygen plasma treatment (20 seconds) was followed by fluorsilane treatment (30 min under vacuum). As a control, one grid did not receive any treatment. The water contact angle on the various treated SU-8 grids was measured using a goniometer (A-100, Ramé-hart, Inc., Netcong, NJ, USA).

Pure HyPG-MA (DS 11; 100% (w/w)) and aqueous solutions of HyPG-MA with various solid content (DS 11; 30% and 50% (w/w)) or with various DS (50% (w/w); DS 11, 18, 28) were prepared in phosphate buffer (10 mM, pH 7.2) also containing 1% (w/v) Irgacure 2959. The polymer solution was applied and spread over the various pretreated SU-8 grids (squares with width of 100 µm and height of 20 µm; pre-fabricated at Philips Research, Eindhoven, The Netherlands) using a doctor blade technique. Filling of the microwells was verified using an optical microscope (Olympus BX60, Olympus Optical Co. GmbH, Hamburg, Germany) before exposure to UV light. After photopolymerization (irradiation time of 15 min; light intensity of 8 mW/cm^2 in the range of 300-450 nm; Oriel 1000 W Hg(Xe) short arc lamp, model no. 92531, Oriel Instruments, Stratford, USA) under continuous nitrogen flow, the grid was placed for 1 h in a vacuum oven (Gallenkamp, Loughborough, UK) at 90°C to evaporate water in the microparticles in order to facilitate their release from the grid. The microparticles were released by placing the grid into a water bath followed by sonication at room temperature for several hours.

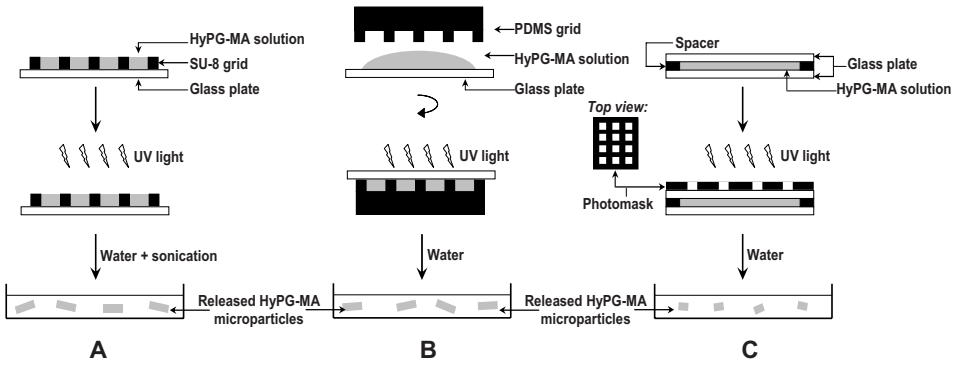

Figure 2. *Schematic representation of the fabrication processes of HyPG-MA structured microparticles using three different methods. (A) This micromolding technique uses a non-flexible SU-8 grid which is filled with aqueous HyPG-MA solution. After exposure to UV light, the microparticles are released by sonication in water. (B) Soft-micromolding is carried out with a flexible PDMS grid that is compressed onto a drop of aqueous HyPG-MA solution deposited on a glass plate. Following exposure to UV light, the grid can be peeled off and the particles obtained by rinsing the plate with water. (C) Photolithography is performed by applying an aqueous HyPG-MA solution between two glass-plates, which are separated by spacers, and polymerizing through a patterned mask. When removing the upper glass plate, microparticles are collected by rinsing the plate with water.*

2.3.2. Preparation of HyPG-MA microparticles by soft-micromolding

The preparation of HyPG-MA microparticles using the soft-micromolding technique is depicted in Figure 2B. Both a flexible poly(dimethyl siloxane) (PDMS) grid (squares of 100x100x50 µm or hexagons with ∅ 30 µm and a thickness of 20 µm, pre-fabricated at Philips Research, Eindhoven, The Netherlands) and a glass plate were treated for 10 min with UV-ozone (UV-ozone photoreactor PR-100, UVP, NTE Electronics Inc., Bloomfield, NJ, USA) and subsequently placed for 10 min in a vacuum desiccator. Next, an aqueous solution of HyPG-MA (50% (w/w); DS 11) in phosphate buffer (10 mM, pH 7.2) also containing 1% (w/v) Irgacure 2959 was flushed with nitrogen prior to application on the glass plate. The PDMS grid was pressed on top of the glass plate by hand to allow the grid to be filled with polymer solution. Subsequently, the grid filled with polymer solution was exposed to UV light (intensity of 8 mW/cm^2 in the range of 300-450 nm; Oriel 1000 W Hg(Xe) short arc lamp, model no. 92531, Oriel Instruments, Stratford, CT, USA) for 5 min maintaining the grid covered with the glass plate to prevent water evaporation. After photopolymerization, the PDMS grid was peeled off and the microparticles were collected by rinsing the glass plate with water.

2.3.3. Photopolymerization kinetics of HyPG-MA prepared by micromolding

Aqueous solutions of HyPG-MA (30% or 50% (w/w), DS 11) in phosphate buffer (10 mM, pH 7.2) also containing Irgacure 2959 (0.5% or 1% (w/v)) were prepared and flushed with nitrogen. The solutions were applied and spread on a SU-8 or PDMS surface that did not contain grids. For the polymerization kinetics on PDMS, a glass plate was put on top of the polymer solution to prevent water evaporation and to mimic as closely as possible the particle preparation method. After exposure to UV light (light intensity of 8 mW/cm^2 in the range of 300-450 nm; Oriel 1000 W Hg(Xe) short arc lamp, model no. 92531, Oriel Instruments, Stratford, CT, USA) for various time periods (from 30 to 900 seconds) under continuous nitrogen flow, the polymer films were released from their SU-8 or PDMS surface and incubated in 10 ml 0.02 M NaOH at 37°C for 30 min to hydrolyze the unreacted methacryloyl groups. The concentration of methacrylic acid was determined using RP-HPLC as described by Stenekes and Hennink [27].

2.4. Preparation and characterization of structured HyPG-MA microparticles obtained by photolithography

2.4.1. Preparation of HyPG-MA microparticles by photolithography

In Figure 2C, the fabrication process of HyPG-MA microparticles by photolithography is illustrated. A solution of 50% (w/w) HyPG-MA DS 11 in phosphate buffer (10 mM, pH 7.2) also containing 1% (w/v) Irgacure 2959 was prepared and flushed with nitrogen. Similarly, two other aqueous HyPG-MA solutions were prepared that contained additionally 1% (w/v) hydroquinone monomethyl ether or 1% (w/v) vitamin C, respectively, to inhibit the polymerization reaction in the non-illuminated areas. Moreover, a 50% (w/w) HyPG-MA DS 11 solution in phosphate buffer (10 mM, pH 7.2) was prepared and not flushed with nitrogen to keep the solution saturated with oxygen, which inhibits radical polymerization reactions. The different solutions were applied between two glass plates (40x40x0.7 mm; treated with UV-ozone for 10 min), separated by 50 µm, 20 µm or 6 µm spacers, and polymerized through a patterned mask (Philips Research, Eindhoven, The Netherlands; patterns of 700x1400 µm, rectangles of 200x400 µm or hexagons of Ø 100 µm or Ø 30 µm) via exposure to UV light (intensity of 8 mW/cm^2 in the range 300-450 nm; Oriel 1000 W Hg(Xe) short arc lamp, model no. 92531, Oriel Instruments, Stratford, CT, USA) for various time periods (160, 330 or 900 seconds). Subsequently, the upper glass plate was removed and the microparticles were collected by rinsing the plate with water.

2.4.2. Photopolymerization kinetics of HyPG-MA prepared by photolithography

HyPG-MA (30 mg or 50 mg, DS 11) was dissolved in 10 mM phosphate buffer pH 7.2 (70 µl or 50 µl, respectively) also containing Irgacure 2959 (0.5% or 1% (w/v)) and either non-flushed or flushed with nitrogen. The solution also contained either 1% (w/v)

hydroquinone monomethyl ether or 1% (w/v) vitamin C. Polymerization was performed between two glass plates (40x40x0.7 mm; pretreated with UV-ozone for 10 min), separated by spacers (50 µm, 20 µm or 6 µm thickness), for various time spans (30 to 900 seconds). After UV illumination, the films were released from the glass plates and incubated in 10 ml 0.02 M NaOH at 37°C for 30 min to hydrolyze the unreacted methacryloyl groups. The concentration of methacrylic acid was determined using RP-HPLC as described by Stenekes and Hennink [27].

2.5. Swelling of microscopic hydrogel particles

Structured microscopic HyPG-MA particles with different DS (DS 11, 18 and 28) and different percentages of solid content (30% (30 mg in 70 µl 10 mM phosphate buffer pH 7.2) and 50% and 100% (w/w)) were prepared using different techniques as described previously (see section 2.3.1., 2.3.2. and 2.4.1.). Structured microparticles prepared by rigid-micromolding (section 2.3.1.) had to be dried to be released from the SU-8 grid. Therefore, the diameter of these dried particles was used as initial size to calculate the swelling ratio. As drying of the structured HyPG-MA particles obtained by soft-micromolding and photolithography (see section 2.3.2. and 2.4.1., respectively) was not necessary, the diameter of the grids or patterns, respectively, was used as an initial size to calculate the swelling ratio.

The microparticles were transferred into a Petri dish and incubated with 1 ml isotonic 100 mM PBS (pH 7.2, containing 0.02% NaN_3) on a thermoplate (model MATS-U505R20, Tokai Hit Co., Ltd. Shizuoka-ken, Japan) at 37°C. The diameters of the dried and incubated microparticles were measured using an optical microscope (Nikon TE200U, Nikon Instruments Europe B.V., Badhoevedorp, The Netherlands). The swelling ratio (D_t/D_0) is defined as the ratio between the diameter of the hydrated gel at time t (D_t) and its initial diameter (D_0) and therefore indicates the swelling of microgels in one-dimension. Assuming that the hydrogel particles are isotropic, the total swelling and equilibrium water content of the particles can be calculated from the data of the 1-D swelling.

3. Results and discussion

3.1. Particle preparation by micromolding

The important steps in the fabrication of HyPG-MA microparticles using the rigid-micromolding technique are shown in Figure 3. An SU-8 grid, consisting of 100 µm wide and 20 µm deep square microstructures (Fig. 3A), was used as a template to obtain structured HyPG-MA particles with a uniform and predetermined size. Since difficulties were encountered to fill the wells (due to the hydrophobicity of the well surfaces) and to

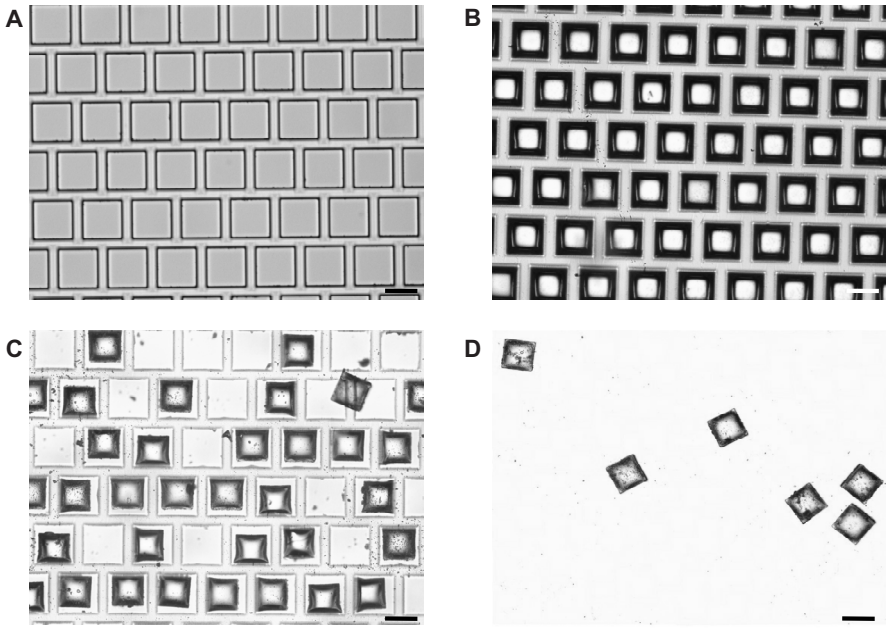

Figure 3. *Optical micrographs of the various phases in the rigid-micromolding technique using HyPG-MA. The empty SU-8 grid (A) was filled with an aqueous HyPG-MA solution (B) and exposed to UV light. Following photopolymerization, the grid was placed in a vacuum oven to shrink the microparticles (C) to facilitate their release. The microparticles were released by sonication in water (D). Scale bar is 100 µm.*

release the formed microparticles from untreated grids, several surface treatments (oxygen plasma or fluorsilane treatment) were investigated. These treatments resulted in major effects on the surface characteristics of SU-8 surfaces. The water contact angle after the various surface treatments are listed in Table 1. Treatment with oxygen plasma resulted in a very hydrophilic (i.e. a water contact angle of 10°) grid surface as compared to untreated grids (water contact angle of 63°). On the other hand, a more hydrophobic (i.e. a higher contact angle; 81°) surface was obtained after deposition of a fluorsilane coating on the SU-8 grids. An increased hydrophobicity was observed as well when fluorsilane was deposited after the oxygen plasma treatment (contact angle of 76°). The altered surface characteristics had a major effect on the filling of the microwells and the release of the formed microparticles after UV-polymerization (Table 1). A hydrophobic (i.e. water contact angle of 81°) grid surface repelled the aqueous HyPG-MA solution (50% (w/w)) resulting in empty or not well-filled wells. In contrast, the microwells were filled relatively easily with a 30 or 50% (w/w) HyPG-MA solution when the grids were rather hydrophilic.

Table 1. *Contact angle and filling and release characteristics of SU-8 grids after various surface treatments.*

O_2 plasma	Fluorsilane	Contact angle	Filling[a]	Release[a]
no[b]	no	63° ± 2	+	+
yes	no	10° ± 2	+	±
no	yes	81° ± 4	-	n.a.[c]
yes	yes	76° ± 3	±	+

[a] *Filling / release: assessed as good (+), moderate (±) or bad (-).*

[b] *No: specific treatment was not applied. Yes: specific treatment was applied.*

[c] *n.a. = not applicable.*

These wells could also be filled well with HyPG-MA containing 1% (w/v) Irgacure 2959 but without solvent, although it took some time before the wells were fully filled, likely due to the absence of solvent to facilitate entrapment into the microwells [13, 28]. Figure 3B shows well-filled microwells due to an increased hydrophilicity of the grid surface.

After filling and subsequent photopolymerization, the kinetics of the polymerization were studied by measuring the conversion of the methacrylates using RP-HPLC. It was shown (Fig. 4) that the conversion of the methacrylate groups was dependent on both polymer and initiator concentrations; at lower polymer concentration and lower initiator concentration the methacrylates were converted more slowly. However, in all circumstances >90% conversion was obtained within 15 min of illumination.

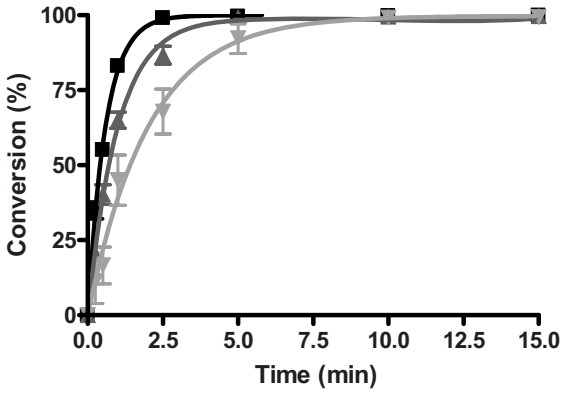

Figure 4. *Methacrylate conversion of polymerizing HyPG-MA as function of the illumination time: 50% (w/w) HyPG-MA in phosphate buffer containing 1% (w/v) Irgacure 2959 (■), 30% (w/w) HyPG-MA in phosphate buffer containing 1% (w/v) Irgacure 2959 (▲) and 50% (w/w) HyPG-MA in phosphate buffer containing 0.5% (w/v) Irgacure 2959 (▼). Data are shown as average ± SD, n = 3.*

Next, microparticles were allowed to shrink (Fig. 3C) before sonication was performed for at least 3 h. As a result, microparticles were released (Fig. 3D) and collected by centrifugation. Release from hydrophobic grids (i.e. water contact angle of 81°) was not evaluated as empty or not well-filled wells were obtained due to repelling of the polymer solution. Release of the hydrogel particles was relatively easy from rather hydrophilic grids (Table 1). However, even from these grids not all particles were released. Independent of the type of polymer solution about 50% of the microparticles remained adhered to the SU-8 grid (see Fig. 3C) or broke into smaller particles during the drying and sonication process.

Preparation of microparticles using this rigid-micromolding technique has some drawbacks as water evaporation occurs during filling of the SU-8 grids and UV-polymerization. As a result the final solid content concentration of the microparticles is not controlled. Moreover, only 50% of the particles could be released in their intact form from the grid. Therefore, an alternative method was developed to obtain a high yield of microparticles with a predetermined size and water-content. This procedure, referred to as soft-micromolding [13], uses an elastomeric (soft) grid to create the polymeric structures. It was essential to keep these PDMS grids under vacuum for at least 10 min before use to remove traces of oxygen that otherwise inhibited the UV-polymerization. After photopolymerization, the PDMS grid was carefully removed; the microparticles were stuck onto the glass plate and could easily be collected by rinsing the plate with water. Independent of the type of polymer solution (varying DS or solid content) and the size/shape of the microwells, a high yield (80 to 90%; >90% conversion) was obtained. Figure 5 shows optical micrographs of square (100 µm wide and 50 µm thick; Fig. 5A) and hexagonal (Ø 30 µm and 20 µm thick; Fig. 5B) microparticles released from PDMS grids. Nevertheless, a number of particles showed a less-defined shape as filling of the wells was not optimal.

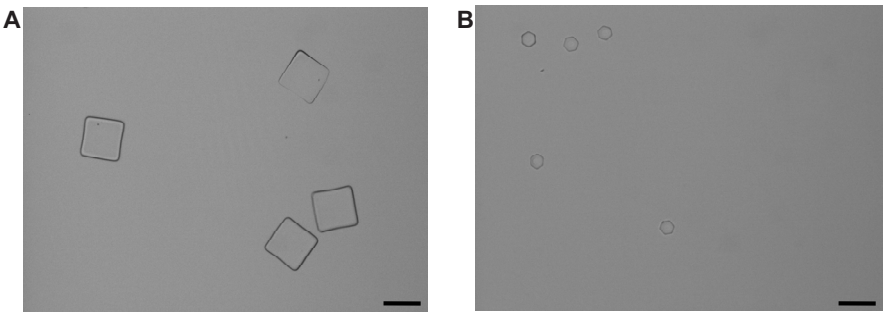

Figure 5. *Optical micrographs of HyPG-MA hydrogel microparticles obtained after soft-micromolding: (A) squares of 100x100 µm and (B) hexagons of ∅ 30 µm. Scale bar is 100 µm.*

3.2. Particle preparation by photolithography

Besides the micromolding techniques, photolithography was also investigated to prepare HyPG-MA microparticles. As the polymer solution is applied between two glass plates, uncontrolled water-loss is essentially prevented, resulting in microparticles with a controllable water content. When a solution of HyPG-MA (50% (w/w) containing 1% (w/v) Irgacure 2959) was flushed with nitrogen and photopolymerized, it turned out that hydrogel microparticles (700x1400 µm; 50 µm spacer) were obtained up to 60 seconds of illumination. However, independent of the polymer or photoinitiator concentration, prolonged exposure to UV light resulted in hydrogel films rather than microparticles. This indicates that polymerization also occurred in the dark areas likely due to the diffusion of radicals from the UV-exposed areas. At 60 seconds of illumination, however, a methacrylate conversion of only 50 to 83% was obtained depending on the polymer and initiator concentration (Table 2). When a 50% (w/w) aqueous solution of HyPG-MA was not flushed with nitrogen (leaving the solution saturated with oxygen), the dark polymerization was indeed inhibited and hydrogel microparticles (700x1400 µm; 50 µm spacers) were obtained up to exposure times of 120 seconds. As the amount of oxygen is hard to control and therefore impedes the reproducibility, other inhibitors (hydroquinone monomethyl ether or vitamin C, both added at a concentration of 1% (w/v)) were evaluated.

Table 2. *Maximal UV exposure time to obtain hydrogel microparticles by photolithography and the corresponding methacrylate conversion for various HyPG-MA solutions with or without the inhibitor vitamin C.*

HyPG-MA % (w/w)	Irgacure 2959 % (w/v)	Inhibitor	Maximal exposure time (sec)	Conversion (%)
50	1	no[a]	60	83 ± 1
		MEHQ[b]	300	>90 ± 2
		vitamin C[c]	330	>90 ± 1
30	1	no	60	67 ± 3
		MEHQ	300	>90 ± 1
		vitamin C	330	>90 ± 2
50	0.5	no	60	50 ± 2
		MEHQ	300	>90 ± 2
		vitamin C	330	>90 ± 1

[a] *No: no inhibitor added to polymer solution*

[b] *MEHQ: hydroquinone monomethyl ether; final concentration of 1% (w/v) in HyPG-MA solution*

[c] *Vitamin C: final concentration of 1% (w/v) in HyPG-MA solution*

The addition of the inhibitors resulted in microstructures (patterns of 700x1400 µm; 50 µm spacer) when exposed to UV for up to 300 or 330 seconds, respectively. However, at longer UV-illumination times the polymerization in the dark areas was not inhibited sufficiently and hydrogel films were obtained rather than hydrogel particles. It was observed that the kinetics of the methacrylate conversion was dependent on both initiator and polymer concentration; lower initiator and polymer concentration resulted in slower polymerization kinetics. Nevertheless, a conversion of >90% was obtained in all circumstances at maximal illumination time (300 or 330 seconds for hydroquinone monomethyl ether and vitamin C, respectively; Table 2).

Besides structures of 700x1400 µm, it was also possible to obtain smaller particles by photolithography using other photomasks. Therefore, the polymerization in the dark areas still needed to be inhibited. Vitamin C was selected for further optimization of the preparation of smaller hydrogel particles, since it is more biofriendly than hydroquinone monomethyl ether. Additionally, vitamin C was described previously in the literature as a radical scavenger to optimize the preparation of nanogels with uniform sizes [29]. When exposing a 50% (w/w) solution of HyPG-MA (containing 1% (w/v) Irgacure 2959 and 1% (w/v) vitamin C) through a photomask containing patterned rectangles of 200x400 µm (20 µm spacers; Fig. 6A or 6 µm spacers) microstructures were obtained already after 160 seconds of illumination.

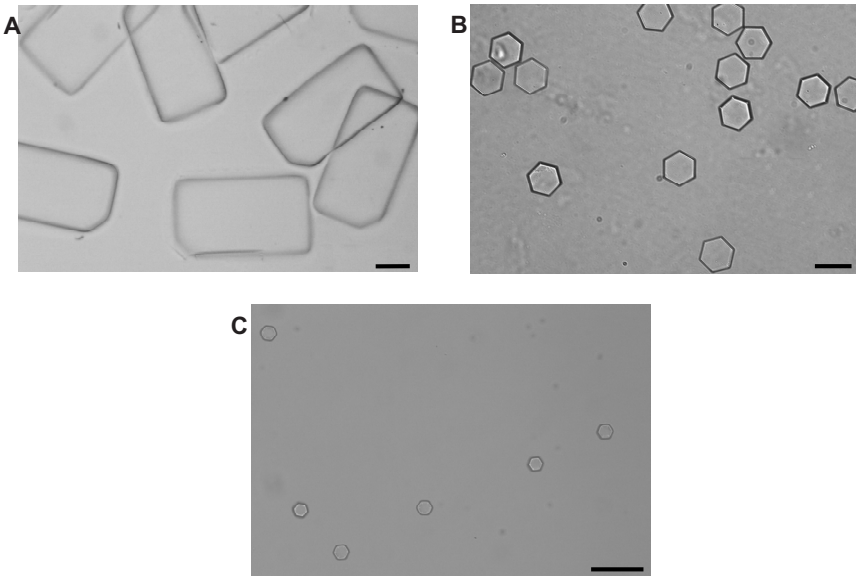

Figure 6. *Optical micrographs of HyPG-MA hydrogel microparticles obtained after photolithography: (A) rectangles of 200x400 µm, (B) hexagons of ∅ 100 µm and (C) hexagons of ∅ 30 µm. Scale bar is 100 µm.*

At longer UV-exposure times, hydrogel films were obtained due to insufficient inhibition of the polymerization in the dark areas. Nevertheless, a high methacrylate conversion (>90%) was obtained independent of the thickness of the spacer. However, when a photomask was applied with smaller patterned structures (hexagons of Ø 100 µm or Ø 30 µm; 20 or 6 µm spacers) short illumination times (e.g. 30 seconds) already resulted in round microparticles or hydrogel films rather than well-structured microparticles. This indicates that polymerization also occurred in the dark areas. Well-formed hexagonal microparticles could only be obtained when placing the photomask in direct contact with the polymer solution and increasing the vitamin C concentration to 2% (w/v). Likely, due to removal of the upper glass plate, less refraction of the light occurred, and as a result the illumination time could be increased up to 900 seconds (>90% methacrylate conversion). Figure 6B and 6C show well-formed hexagonal microparticles (Ø 100 µm or Ø 30 µm, respectively, with a thickness of 20 µm) obtained using this direct contact method.

After UV-polymerization for 330, 160 or 900 seconds (structures of 700x1400 µm, rectangles of 200x400 µm and hexagons of Ø 100 µm or Ø 30 µm, respectively) the photomask and / or the upper glass plate were removed and the formed microparticles could easily and quantitatively be washed off with water.

3.3. Swelling of HyPG-MA microparticles

The HyPG-MA microgels, obtained after photolithography or after release from SU-8 or PDMS grids, were characterized for their swelling behavior. Microparticles prepared by the rigid-micromolding technique (using SU-8 grids) were dried prior to being released from the grid. It was observed that upon rehydration these dried particles did not reach their initial size (data not shown). This indicates that dehydration followed by rehydration is not fully reversible. Swelling studies were therefore only performed with non-dehydrated microparticles obtained after soft-micromolding (using PDMS grids) and photolithography. Assuming that the hydrogel particles are isotropic, the total swelling of the particles can be evaluated using the results of the 1-D swelling.

Figure 7A shows the swelling behavior of microgels (DS 11) with varying percentages of initial solid content. It was observed that swelling of micromolded gels decreased (equilibrium swelling ratio 1.6, 1.5 and 1.2; Fig. 7A) with increasing solid content (30%, 50% and 100% (w/w), respectively). Herewith the equilibrium water content of the microgels decreased from 76% to 69% to 42%, respectively. A similar trend was observed for gels obtained by photolithography (equilibrium swelling ratio 1.6, 1.5 and 1.3, respectively; Fig. 7A). For these gels the equilibrium water content decreased from 76% to 68% to 51%, respectively. This decrease in swelling can be explained by the increasing solid content: the concentration of methacrylate groups increases, which results in a higher crosslink density of the UV polymerized HyPG-MA gels.

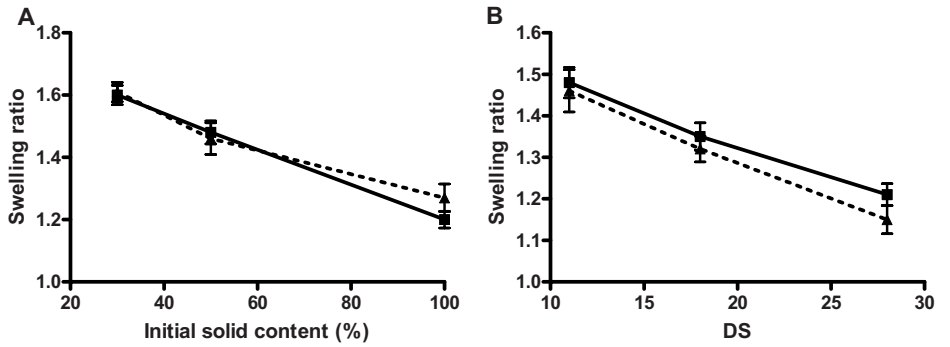

Figure 7. *Swelling ratio of HyPG-MA microgels prepared by soft-micromolding (■) or by photolithography (▲) as function of the initial solid content (A) and as function of the degree of substitution (DS, the percentage of derivatized hydroxyl groups; B). The data are shown as average ± SD, n = 3. The swelling ratio (D_t/D_0) is defined as the ratio between the diameter of the gel at time t (D_t) and its initial diameter (D_0).*

The microparticles rapidly absorbed water and equilibrium swelling was obtained within 2 min. Figure 7B shows that the swelling of micromolded gels decreased (equilibrium swelling ratio 1.5, 1.4 and 1.2) with increasing DS (DS 11, 18 and 28, respectively; 50% (w/w) initial solid content). Herewith the equilibrium water content of the microgels decreased from 69% to 59% to 44%, respectively. Microgels prepared by photolithography showed the same swelling trend (equilibrium swelling ratio 1.5, 1.3 and 1.2, respectively; Fig. 7B). For these gels the equilibrium water content decreased from 68% to 57% to 34%, respectively. No significant differences were observed in the swelling ratio between both preparation methods, which can be ascribed to the similar polymerization kinetics and methacrylate conversion. The restricted swelling implies that the HyPG-MA microgels are dimensionally stable, as was observed previously for HyPG-MA macroscopic hydrogels [4]. In addition, a similar trend as for the macroscopic hydrogels was observed regarding the total swelling of the microgels (results not shown), which was determined assuming that the hydrogel particles are isotropic.

Soft-micromolding and photolithography are efficient methods to fabricate isolated, monodisperse HyPG-MA microgels with various shapes and sizes (size range: 30-1400 µm), which are comparable to hydrogel microparticles obtained with similar techniques previously described in the literature [13, 26]. The shapes and sizes in this work were chosen arbitrarily, but could easily be adjusted to any specific request. Both methods are easy to implement but might need optimization when using other polymers than HyPG-MA. Moreover, soft-micromolding and photolithography can be used to manufacture microparticles for a variety of applications, for example, drug delivery devices and tissue engineering.

4. Conclusions

In this paper, we report on the preparation and characterization of the swelling properties of methacrylated hyperbranched polyglycerol (HyPG-MA) structured microgels with uniform sizes prepared using different preparation methods.

The three preparation techniques rigid-micromolding, soft-micromolding and photolithography could all be applied to obtain structured microparticles. However, with the rigid-micromolding only a restricted percentage of well-defined particles (>90% conversion) could be obtained. The other particles remained adhered to the SU-8 grid or broke into smaller particles due to the drying process. Moreover, after this drying procedure, the obtained microgels did not rehydrate completely.

With the soft-micromolding technique a high yield (80 to 90%; >90% conversion) of well-defined HyPG-MA microparticles could be obtained. Although a number of particles showed a less-defined shape, as not all grids could be filled well, the microgels showed restricted swelling implying that these gels are dimensionally stable.

In addition, an efficient photolithographic method was developed to obtain HyPG-MA microgels with well-defined sizes and shapes and additionally gain 100% yield (>90% conversion). HyPG-MA microparticles in the size-range of 30 µm to 1400 µm could easily be prepared by adding an inhibitor (e.g. vitamin C) to the polymer solution to inhibit dark polymerization. Moreover, the microgels showed limited swelling indicating that dimensionally stable particles were obtained.

It was shown that both soft-micromolding and photolithography resulted in HyPG-MA microgels with well-defined size and shape. Consequently, these gels offer excellent opportunities for potential drug delivery matrices or for tissue engineering purposes.

References

1. Wan D, Li Z, Huang Z. Synthesis of a new type of core-shell particle from hyperbranched polyglycerol. *J Polymer Sc* 2005; 43: 5458-5464.
2. Sunder A, Kramer M, Hanselmann R, Mulhaupt R, Frey H. Molecular Nanocapsules Based on Amphiphilic Hyperbranched Polyglycerols. *Angew Chem Int Ed Engl* 1999; 38(23): 3552-3555.
3. Haag R, Sunder A, Stumbe J. An approach to glycerol dendrimers and pseudo-dendritic polyglycerols. *J Am Chem Soc* 2000; 122: 2954-2955.
4. Oudshoorn MHM, Rissmann R, Bouwstra JA, Hennink WE. Synthesis and characterization of hyperbranched polyglycerol hydrogels. *Biomaterials* 2006; 27(32): 5471-5479.
5. Sunder A, Quincy MF, Mulhaupt R, Frey H. Hyperbranched Polyether Polyols with Liquid Crystalline Properties. *Angew Chem Int Ed Engl* 1999; 38(19): 2928-2930.
6. Hyperpolymers. http://www.hyperpolymers.com.
7. Garcia-Bernabe A, Kramer M, Olah B, Haag R. Syntheses and phase-transfer properties of dendritic nanocarriers that contain perfluorinated shell structures. *Chemistry* 2004; 10(11): 2822-2830.
8. Sunder A, Mulhaupt R, Haag R, Frey H. Hyperbranched Polyether Polyols: A Modular approach to complex Polymer Architectures. *Adv Mater* 2000; 12(3): 235-239.
9. Stiriba SE, Kautz H, Frey H. Hyperbranched molecular nanocapsules: comparison of the hyperbranched architecture with the perfect linear analogue. *J Am Chem Soc* 2002; 124(33): 9698-9699.
10. Hoffman AS. Hydrogels for biomedical applications. *Adv Drug Deliv Rev* 2002; 54(1): 3-12.
11. Li L, James Lee L. Photopolymerization of HEMA/DEGDMA hydrogels in solution. *Polymer* 2005; 46(25): 11540-11547.
12. Stenekes RJ, Franssen O, van Bommel EM, Crommelin DJ, Hennink WE. The preparation of dextran microspheres in an all-aqueous system: effect of the formulation parameters on particle characteristics. *Pharm Res* 1998; 15(4): 557-561.
13. Guan J, Ferrell N, James Lee L, Hansford DJ. Fabrication of polymeric microparticles for drug delivery by soft lithography. *Biomaterials* 2006; 27(21): 4034-4041.
14. Bryant SJ, Hauch KD, Ratner BD. Spatial patterning of thick poly(2-hydroxyethyl methacrylate) hydrogels. *Macromolecules* 2006; 39(13): 4395-4399.
15. Hahn MS, Taite LJ, Moon JJ, Rowland MC, Ruffino KA, West JL. Photolithographic patterning of polyethylene glycol hydrogels. *Biomaterials* 2006; 27(12): 2519-2524.
16. Khademhosseini A, Suh KY, Jon S, Eng G, Yeh J, Chen GJ, Langer R. A soft lithographic approach to fabricate patterned microfluidic channels. *Anal Chem* 2004; 76(13): 3675-3681.
17. Falconnet D, Csucs G, Grandin HM, Textor M. Surface engineering approaches to micropattern surfaces for cell-based assays. *Biomaterials* 2006; 27(16): 3044-3063.
18. Maynor BW, LaRue I, Hu Z, Rolland JP, Pandya A, Fu Q, Liu J, Spontank RJ, Sheiko SS, Samulski RJ, DeSimone JM. Supramolecular nanomimetics: replication of micelles, viruses, and other naturally occurring nanoscale objects. *Small* 2007; 3(5): 845-849.

19. Wang B, Hong Y, Feng J, Gong Y, Gao C. Rings of hydrogel fabricated by a micro-transfer technique. *Macromol J* 2007; 28: 567-571.
20. Rolland JP, Maynor BW, Euliss LE, Exner AE, Denison GM, DeSimone JM. Direct fabrication and harvesting of monodisperse, shape-specific nanobiomaterials. *J Am Chem Soc* 2005; 127(28): 10096-10100.
21. Gratton SE, Pohlhaus PD, Lee J, Guo J, Cho MJ, DeSimone JM. Nanofabricated particles for engineered drug therapies: A preliminary biodistribution study of PRINT(trade mark) nanoparticles. *J Control Release* 2007; 121(1-2): 10-18.
22. Wang X, Yan Y, Pan Y, Xiong Z, Liu H, Cheng J, Liu F, Lin F, Wu R, Zhang R, Lu Q. Generation of three-dimensional hepatocyte/gelatin structures with rapid prototyping system. *Tissue Eng* 2006; 12(1): 83-90.
23. Zguris JC, Itle LJ, Koh W-G, Pishko MV. A novel single-step fabrication technique to create hetergoneous poly(ethylene glycol) hydrogel microstructures containing multiple phenotypes of mammalian cells. *Langmuir* 2005; 21: 4168-4174.
24. Fukuda J, Khademhosseini A, Yeo Y, Yang X, Yeh J, Eng G, Blumling J, Wang CF, Kohane DS, Langer R. Micromolding of photocrosslinkable chitosan hydrogel for spheroid microarray and co-cultures. *Biomaterials* 2006; 27(30): 5259-5267.
25. Allcock HR, Phelps MVB, Barrett EW. Ultraviolet photolithographic development of polyphosphazene hydrogel microstructures for potential use in microarray biosensors. *Chem Mater* 2006; 18: 609-613.
26. Kuckling D, Hoffman J, Plötner M, Ferse D, Kretschmer K, Adler H-JP, Arndt K-F, Reichelt R. Photo cross-linkable poly(N-isopropylacrylamide) copolymers III: micro-fabricated temperature responsive hydrogels. *Polymer* 2003; 44: 4455-4462.
27. Stenekes RJ, Hennink WE. Polymerization kinetics of dextran-bound methacrylate in an aqueous two phase system. *Polymer* 2000; 41: 5563-5569.
28. Franzesi GT, Ni B, Ling Y, Khademhosseini A. A controlled-release strategy for the generation of cross-linked hydrogel microstructures. *J Am Chem Soc* 2006; 128(47): 15064-15065.
29. Schillemans JP, Flesch FM, Hennink WE, van Nostrum CF. Synthesis of bilayer-coated nanogels by selective cross-linking of monomers inside liposomes. *Macromolecules* 2006; 39: 5885-5890.

Mimicking vernix caseosa - preparation and characterization of synthetic biofilms

Robert Rissmann[a], Marion H.M. Oudshoorn[b], Raphaël Zwier[c], Maria Ponec[a], Joke A. Bouwstra[a], Wim E. Hennink[b]

[a] Department of Drug Delivery Technology, Leiden/Amsterdam Center for Drug Research (LACDR), Leiden University, Leiden, The Netherlands
[b] Department of Pharmaceutics, Utrecht Institute for Pharmaceutical Sciences (UIPS), Utrecht University, Utrecht, The Netherlands
[c] Fine Mechanical Department, Leiden University, Leiden, The Netherlands

Submitted for publication

5

Abstract

The multiple protecting and barrier-supporting properties of the creamy, white biofilm vernix caseosa (VC) before and after birth suggest that a VC biomimetic could be an innovative barrier cream for barrier-deficient skin. The aim of this study was the rational design and preparation of synthetic biofilms mimicking the unique composition and properties of natural VC.

Hexagonal, highly hydrated hyperbranched polyglycerol microgel particles (30 µm in diameter) were embedded in a synthetic lanolin-based lipid mixture using a micromixer. In these formulations, the water content of the particles (i.e. 50% and 80%), an additional lipid coating of the particles and different particle:lipid ratios were varied. Characterization with confocal laser scanning microscopy showed a homogeneous distribution of the labeled particles in the lipid matrix. Regarding structural appearance, particle density and distribution, the formulations with a high particle:lipid ratio (5:1) resembled native VC very closely. Concerning water handling-properties, the formulation with the pre-coated particles (80% water content) and a particle:lipid ratio of 2:1 exhibited a sustained water release for 140 h, mimicking VC most closely. The formulations were stable for at least one month at 4°C and exhibited - similar to VC - two overlapping phase transitions at a physiological temperature range as investigated by differential scanning calorimetry. Rheological properties showed a comparable tan δ (i.e. quotient of viscosity and elasticity) between the formulations and native VC. In conclusion, our formulations closely mimic natural VC and are promising candidates for *in vivo* studies.

1. Introduction

Vernix caseosa (VC) is the creamy white skin-surface biofilm which covers the skin of the fetus and the newborn. It is suggested to have multiple biological functions such as waterproofing and facilitation of skin formation in utero [1, 2]. During delivery it is suggested to act as a lubricant, while exhibiting anti-infective [3], anti-oxidant [4] and skin cleansing properties postnatally [5]. Moreover, the dehydration profile of VC shows a strong temperature-dependence, which enables VC to hydrate the newborn's skin in a sustained manner [6, 7]. These multiple biological functions and unique properties of VC suggest that the generation of a synthetic VC equivalent could lead to a new generation of biofilms. The biofilms might be applicable for extremely low birth weight infants with deficient barrier function and absence of VC [5, 8] but may also be beneficial for adult skin to enhance wound healing [9].

VC consists of dead cells (corneocytes) that are embedded in lipids. Hence, the structure is very similar to that of the stratum corneum (SC), the uppermost layer of the skin. VC is composed of 80% water, about 10% proteins and 10% lipids [1, 8]. The most abundant protein present in VC is keratin, which forms the scaffold of the corneocytes. These dead cells are the main water reservoir of VC and are mostly polygonal and flat in shape with a diameter of approximately 30 µm. Additionally, VC contains antibiotic peptides and polypeptides with innate immune functions [3, 10, 11]. VC lipids consist of a large variety of different lipid classes, including squalene, sterol esters/wax esters, triglycerides and free sterols [12]. Similar to SC, also barrier lipids -cholesterol, fatty acids, and ceramides- are present but they comprise only between 10% and 30% of the total amount of VC lipids [8, 13]. At the interface between the corneocytes and the free lipids, a monolayer of covalently linked lipids is present [13].

Because of the excellent properties of VC for the treatment of barrier-deficient skin [14], the aim of the present study is the generation of synthetic biofilms mimicking the unique composition and properties of natural VC. Previously, the thermal transitions and lipid organization of series of lanolin-derived, synthetic lipid mixtures were examined [15]. From these studies the lipid mixture mimicking most closely the physical properties of VC lipids was selected and used in the present study. Furthermore, it was reported that hydrated hydrogel microparticles can be prepared from hyperbranched polyglycerol [16, 17]. This biocompatible polymer [18] enabled us to reconstruct synthetic corneocytes (referred to as particles), similar to natural corneocytes in shape and size (i.e. hexagonal, Ø 30 µm) [17]. In the present study, these particles were embedded in a lipid mixture composed of the synthetic lipids mentioned above using a specially designed micromixer. Compositions with various particle:lipid ratios as well as particles with different water content in the absence and presence of a surrounding lipid coating were studied to obtain the most optimal biofilm. The homogeneity of these biofilms was

characterized by confocal laser-scanning microscopy (CLSM). Moreover, stability, water handling-properties, rheology and thermotropic behavior of these VC mimetics were investigated.

2. Experimental section

2.1. Materials

HyPG (M_n 2000 g/mol, on the average 32 hydroxyl groups per molecule) was obtained from Hyperpolymers GmbH (Freiburg, Germany). Dimethyl sulfoxide (DMSO, $H_2O \leq 0.005\%$), glycidyl methacrylate (GMA) were purchased from Fluka (Buchs, Switzerland). 4-(*N*,*N*-dimethylamino)pyridine (DMAP) was purchased from Acros Chimica (Geel, Belgium). 2-hydroxy-4'-(2-hydroxyethoxy)-2-methylpropiophenone (Irgacure 2959, purity 98%), triolein, tripalmitolein, trinervonin, squalene, cholesterol, palmitic acid, palmitoleic acid, oleic acid, methyl sulfoxide-d_6 (99.9% atom D) and fluorescein isothiocyanate (FITC)-dextran (M_W = 70 kDa) were provided by Sigma-Aldrich (Zwijndrecht, The Netherlands). Ascorbic acid (vitamin C, purity 99%) was obtained from BUFA B.V. (Uitgeest, The Netherlands). Diethylether was purchased from Biosolve Ltd. (Valkenswaard, The Netherlands). Hydrous lanolin was purchased from Caesar & Loretz (Bonn, Germany). The synthetic ceramides were kindly provided by Cosmoferm B.V. (Delft, The Netherlands). DOPC (dioleoyl phosphatidylcholine) and DOTAP (dioleoyl trimethylammoniumpropane) were obtained from Avanti Polar Lipids Inc (Alabaster, AL, USA). Texas Red and Nile Red were manufactured by Molecular Probes Europe BV (Leiden, The Netherlands). The commercial cream 'Zwitsal – protective cream with vernix protection' was purchased from Sara Lee (The Hague, The Netherlands).

2.2. Synthesis of hyperbranched polyglycerol derivatized with glycidyl methacrylate

Photocrosslinkable HyPG-MA was prepared as described previously [16]. The degree of substitution (DS, the percentage of derivatized hydroxyl groups) of the obtained product was 11 as determined by proton nuclear magnetic resonance spectroscopy (^{1}H NMR; Gemini 500 MHz spectrometer, Varian Associates Inc. NMR Instruments, Palo Alto, CA) in dimethyl sulfoxide-d_6.

2.3. Preparation of particles (synthetic corneocytes)

Structured HyPG-MA hydrogel microparticles were prepared by photolithography [17]. In brief, HyPG-MA (50% or 20% (w/w)) was dissolved in phosphate buffer (10 mM, pH 7.2) also containing 1% (w/v) Irgacure 2959 and 2% (w/v) vitamin C and flushed with nitrogen. To obtain fluorescent labeled particles a few drops of 4.5% FITC-dextran solution in phosphate buffer were added to 1 ml of the HyPG-MA solution. This solution

was applied between a glass plate (40x40x0.7 mm) and a patterned mask (Philips Research Laboratories, Micro Fabrication Center, Eindhoven, The Netherlands; hexagons of Ø 30 µm) using a spacer of 20 µm. Then, the HyPG-MA was polymerized via exposure to UV light (intensity of 11 mW/cm^2, UV light model Bluepoint 4 UVC, Dr. Hoenle AG, UV-Technology, Gräfelfing, Germany) for 120 seconds. Subsequently, the mask was removed and the microparticles were collected by rinsing the plate with water.

2.4. Lipid coating of particles

Preparation of lipid vesicles and subsequent coating of the microparticles was performed as described previously [19]. In short, to prepare the lipid vesicles, DOPC (20 mM) and DOTAP (35 mM) were dissolved in 2 ml chloroform. Next, 4 µl Texas Red solution was added to 190 µl of the DOPC-DOTAP solution as fluorescent label. The chloroform was evaporated from the lipid matrix yielding a lipid film on a glass vial with cylindrical shape (Ø 3 cm). HEPES buffer (2 ml, 10 mM, pH 7) was added to yield a lipid concentration of 1 mg/ml and the mixture was sonicated (Braun Labsonic tip-sonicator; Braun Biotech, Melsungen, Germany) on ice for 10 min to obtain the lipid vesicles (liposomes). These liposomes (500 µl) were mixed with a suspension (100 µl) of HyPG-MA microgels and shaken (1000 rpm) for 1 h at room temperature to allow adsorption of the lipid vesicles onto the surface of the microgels. The samples were centrifuged for 10 min at 2000 rpm, the supernatant removed and the particles were redispersed in 1 ml MilliQ-water. The centrifugation and resuspension was repeated three times. Finally, the microparticles were redispersed in 150 µl of MilliQ-water and directly used for further studies. Visualization of the lipid coated HyPG-MA microparticles was performed by confocal laser scanning microscopy (CLSM).

2.5. Preparation of the lipid matrix

The composition and preparation of the lipid mixture has been described previously [15]. Briefly, the non-polar sterol ester and wax ester fractions of lanolin were isolated by column-chromatography. Subsequently, chloroform/methanol 2:1 lipid solutions were pipetted into a glass tube with following composition: combined sterolester/waxester/dihydroxywaxester 48%, trinervonin 11.9%, tripalmitolein 11.9%, triolein 11.9%, squalene 6.8%, cholesterol 3.5%, ceramide EOS (C30) 0.7%, ceramide NS (C24) 1.0%, ceramide NP (C24) 0.4%, ceramide NP (C16) 0.4%, ceramide AS (C24) 0.8%, ceramide AP (C24) 1.5%, palmitic acid 0.8%, palimoitoleic acid 0.3%, stearic acid 0.1%, oleic acid 0.3% (w/w). Then, the lipid solution was dried under a flow of nitrogen at 40°C.

2.6. Preparation and visualisation of synthetic vernix caseosa

2.6.1. Mixing of the particles with lipids

In order to homogeneously distribute the particles within the lipid matrix, an automatic ointment-mixer Topitec® (WEPA, Germany) was modified in-house for small-scale purpose. A small amount of lipids (~10 mg) was first transferred into the small mixing tube (Fig. 1), in order to coat the surface of the mixing tube and to prevent the breaking of the particles. Then, the suspension of fully hydrated microgels was added, centrifuged (5 min, 500 rpm) and the supernatant removed. Subsequently, the microgels were dispersed in a minimal amount of water. The rest of the lipids were added and the mixing tube was mounted onto the stirrer of the mixing device. Various formulations were prepared by using two particle:lipid ratios (i.e. 2:1 and 5:1 (w/w)). Particles with an initial water content of either 50% (w/w) or 80% (w/w) were selected for the studies. The particles were mixed with the lipids until a homogeneous mixture was obtained while particles were still intact. For this purpose rotating speed and mixing time could be adjusted. The composition of the various formulations is given in Table 1. The biofilms are denoted in the text by an acronym presented in the first column (Table 1).

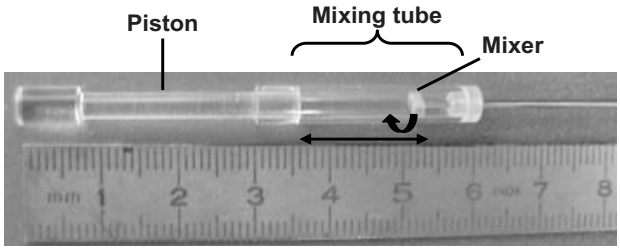

Figure 1. *A custom-designed micromixer for sample sizes between 25 and 220 mg was designed to embed particles within the lipid matrix. During the mixing process, the mixer moves within the mixing tube (arrows). After mixing, the piston can be moved to eject the obtained biofilm.*

2.6.2. Visualization of the biofilms by means of confocal laser scanning microscopy

The homogeneity of the biofilms was characterized by CLSM. For this purpose, we labeled the lipids with Nile Red (0.1 µg/mg lipid) whereas the particles contained FITC-dextran as a label. Immediately after mixing the biofilm was transferred onto a microscopic glass-slide, covered with a glass cover slip and visualized by CLSM. Images were processed using a Bio-Rad Radiance 2100 CLSM equipped with a Nikon Eclipse TE2000-U inverted microscope and a 40x S Fluor (NA 1.30; Nikon, Japan) oil-immersion objective. The images were captured using a helium neon laser with a wavelength of 543 nm. An emission filter excluded fluorescence with a wavelength below 570 nm.

Table 1. *Composition of the various biofilms prepared in this study*

Entry	Sample*	Composition		
		Particle:lipid ratio	Initial water content particles (% w/w)	Lipid coated particles
B1	2:1_50	2:1	50	No
B1c	2:1_50_coated	2:1	50	Yes
B2	2:1_80	2:1	80	No
B2c	2:1_80_coated	2:1	80	Yes
B3*	5:1_50	5:1	50	No
B3c	5:1_50_coated	5:1	50	Yes
B4**	5:1_80	5:1	80	No
B4c	5:1_80_coated	5:1	80	Yes

* *only for visualization study*

** *only for follow-up study*

FITC-labeled particles were visualized after excitation with an Argon laser (488 nm) combined with a 515/30 nm emission filter. At least 3 images of different sites in the biofilm were acquired with the Laser Sharp 2000 software (Bio-Rad, Hercules, USA). For stability studies two biofilms (i.e. B1 and B3; n = 2) were re-evaluated by CLSM after storage for 1 month at 4°C in a closed eppendorf tube.

2.7. Thermotropic behavior by differential scanning calorimetry

The thermotropic behavior of various biofilms was examined by differential scanning calorimetry (DSC). The measurements were carried out on a Q-1000 calorimeter (TA Instruments, New Castle, Delaware, USA). An aluminum pan was filled with ~5 mg of biofilm and subsequently hermetically sealed. After 5 min equilibration at 5°C, DSC analysis was performed with a heating rate of 2°C/min and a modulation of ± 1°C/min up to 50°C.

2.8. Water-handling properties

2.8.1. Water content by means of thermogravimetric analysis

The water content of the various biofilms was determined by thermogravimetric analysis *(*TGA; Q50 thermogravimetric analyzer, TA Instruments, New Castle, Delaware, USA). Approximately 30 mg of sample was placed into an open platinum crucible. Samples were then heated at a rate of 10°C/min from 20 to 200°C. The balance was purged with a constant flow of nitrogen (40 ml/min). The water content was calculated from the weight loss which occurred during the heating process.

2.8.2. Dehydration of synthetic VC

The water-holding capacity of the biofilms was assessed gravimetrically and compared to natural VC. For the dehydration study, custom-made weighing boats were filled with the formulation and dried over P_2O_5 in a desiccator at room temperature (21-24°C). During dehydration, the samples were weighed (Microbalance, Mettler TG50, Switzerland) at various intervals until a constant weight was achieved. The percentage of water release was calculated using the following equation: m (evaporated water)/m (total water) × 100%.

2.9. Rheology

Rheological properties of VC were studied on a rheometer (AR1000-N, TA instruments, Etten-Leur, The Netherlands) with a steel cone (1°, 20 mm diameter). In order to prevent evaporation of water, a solvent trap was installed above the cone. The shear storage modulus (*G'*, correlated to the elasticity) and the shear loss modulus (*G"*, correlated to the viscosity) of the different biofilms were recorded in the oscillation mode with a controlled strain of 0.1% at a frequency of 1 Hz. Temperature-induced changes were studied between 10 and 40°C with a heating/cooling rate of 2°C/min.

3. Results and discussion

3.1. Visualization of coated particles

HyPG-MA microgels [17] were selected as mimetic of the highly hydrated corneocytes in natural VC. These microgels were labeled with FITC-dextran to enable visualization by CLSM (Fig. 2A). The hexagonal shape, as well as the Ø 30 µm particle size is apparent. The lipid coating of the microparticles was intended to facilitate embedding of the hydrophilic particles and to control water release from the biofilm. The coating lipids were labeled with the lipophilic dye Texas Red, which enables the distinction in another channel of the microscope (Fig. 2B). A uniform lipid coating surrounding the entire particle is observed. When merging both channels, the successful coating can be easily perceived (Fig. 2C).

3.2. Homogeneity of biofilm formulations as observed by confocal laser scanning microscopy

A suspension of highly hydrated microparticles was embedded in the lipids using a modified Topitec® micromixer (Fig. 1). The obtained CLSM pictures of the synthetic biofilms and natural VC are depicted in Figure 3. VC is characterized by corneocytes that show only little auto-fluorescence (Fig. 3A). The Nile Red labeled lipids of VC are surrounding the corneocytes (black) and the structure of VC is clearly visible (Fig. 3B and 3C).

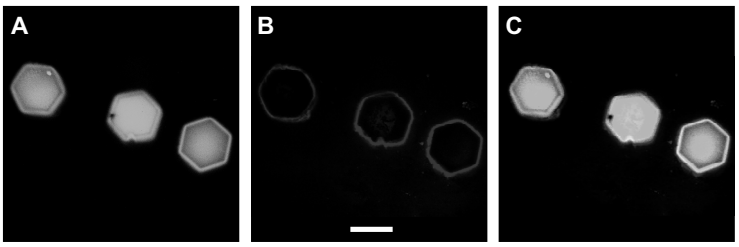

Figure 2. *HyPG-MA microgels labeled with FITC-dextran (A) and lipid coating (labeled with Texas Red) surrounding the microgels (B). Both images can be superposed (C) to visualize the labels of particles and lipids simultaneously. Scale bar represents 25 µm.*

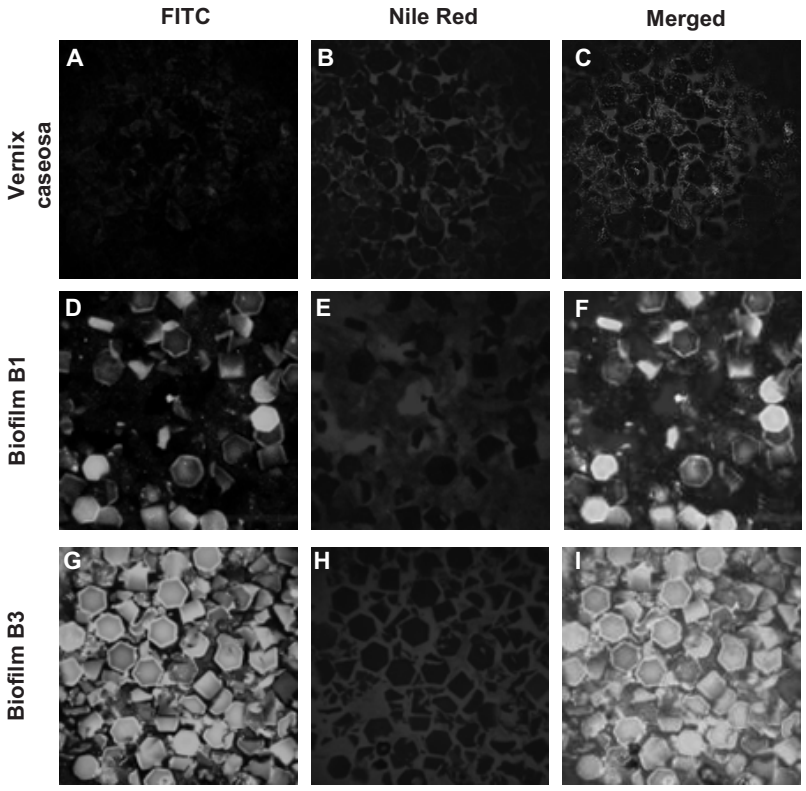

Figure 3. *Photomicrographs of native VC and various biofilm formulations, obtained by CLSM, are depicted. VC is characterized by corneocytes (black) which are embedded in Nile Red-labeled lipids (A-C). Synthetic biofilms, with particle:lipid ratios of 2:1 (biofilm B1; Fig. 3D-F) and 5:1 (biofilm B3; Fig. 3G-I), exhibit red labeled lipids and FITC-labeled synthetic particles. The particles (synthetic corneocytes) are intact and are randomly distributed within the lipid mixture. Scale bar represents 50 µm.*

The size of the corneocytes varies between 15 and 40 µm and they are randomly distributed within the lipid matrix. The synthetic biofilms are characterized by the FITC-dextran labeled particles (50% initial water content of the particles) embedded in the Nile Red labeled lipids (Fig. 3F and 3I). At the optimal mixing condition (i.e. 5 min and 400 rpm) the particles (synthetic corneocytes) remained intact and were homogenously distributed within the lipid matrix. When mixing longer (e.g. 10 min at 400 rpm) or with higher mixing speeds (e.g. 5 min at 800 rpm) fragmented particles were visible, whereas shorter mixing times (e.g. 2 min at 400 rpm) resulted in a visually inhomogeneous biofilm (data not shown). In Figure 3G the hexagonal top view of the particles (cross section of 30 µm) and the side view of the particles with a thickness of 20 µm and a rectangular shape is clearly visible. When comparing natural VC (Fig. 3A - 3C) and the synthetic biofilm B1 (Fig. 3D - 3F) it can be clearly observed that the corneocytes density is higher in natural VC. Increasing the particle:lipid ratio to 5:1 (Fig. 3G - 3I) resulted in a biofilm (B3) with a particle distribution similar to the natural counterpart. VC consists of 80% water, 10% lipid and 10% proteins [1, 8], whereas formulation B3 consists of 61% water, 22% HyPG-MA and 17% lipids. Although this difference in composition is noticed and our biofilms lack proteins, a very nice resemblance in structure was obtained.

3.3. Stability

After storage of various biofilms in a closed eppendorf tube for one month at 4°C, the obtained confocal images revealed a similar particle distribution in the lipid matrix (data not shown). Neither sedimentation nor separation occurred during storage, indicating that our biofilms have an excellent stability.

3.4. Thermotropic behaviour of the biofilms

The thermotropic behavior of the various biofilms was evaluated by DSC (Fig. 4). The depicted biofilms (B1 and B2) are characterized by two overlapping lipid transitions with onset temperatures at 21°C and ~25°C and corresponding enthalpies of -0.17 J/g and 0.28 J/g (biofilm B2), respectively. The formulations with a higher particle:lipid ratio (5:1) and formulations containing the pre-coated particles showed similar onset temperatures of the transitions (data not shown). The enthalpies and temperatures of the observed lipid transitions are very similar to the thermotropic behavior of natural VC (Fig. 4) and the synthetic lipid mixtures without corneocytes in the formulation [15]. In conclusion, the mixing of lipids and hydrogels did not affect the onset

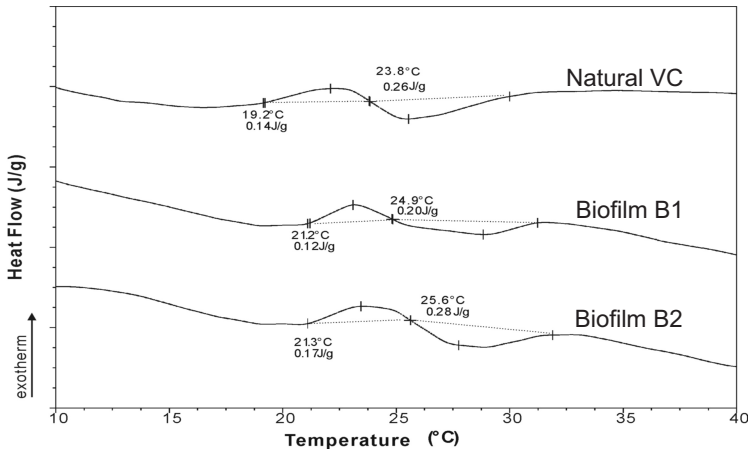

Figure 4. *DSC of natural VC (upper trace) and synthetic VC biofilms (lower two traces).*

temperatures of the transitions. Previously, it has already been speculated that these thermotropic transitions and the resulting reduced dehydration rate of VC at lower temperatures may play an important role in minimizing the evaporative heat and water loss from the skin of the newborn [6]. Taken this into account, the presence of these transitions in the biofilms might also be of beneficial character for the skin.

3.5. Water handling properties - water content and dehydration studies

The water content of natural VC and different biofilm formulations is depicted in Table 2. Natural VC is characterized by the highest amount of water (77.8 ± 0.6%) whereas the commercial formulation Zwitsal contains a little less water (73.4 ± 0.5%). The biofilms with particle:lipid ratio 2:1 using lipid coated or uncoated particles (i.e. B1, B1c, B2 and B2c) exhibited a water content ranging from 51.0 ± 0.0% up to 59.8 ± 0.1%, respectively. A substantial difference between the theoretically calculated water level and experimental water was observed for biofilms containing particles with 50% water. The calculated water content was 33%, while the measured value was between 50 and 60%. In the biofilm preparation procedure, the microgels are dispersed in a minimal volume of 'free' water and subsequently mixed with the lipids using a micromixer. This might result in an excess of water in the external lipid phase and explains the difference between expected and experimentally obtained amounts of water in the formulations as shown in Table 2. An increase in initial water content from 50% (w/w) to 80% (w/w) in the microgels did not show a considerable influence on total water content of the biofilms (55.7 ± 3.5% and 57.0 ± 1.4% for B2 and B2c, respectively) but showed a better correlation between experimental and calculated values (52.8%) indicating that less excess of external water was present.

Table 2. *Theoretical and experimental water content (w/w) of VC, a commercial formulation (Zwitsal) and biofilms by means of TGA.*

Samples*	Theoretical water content (%)	Experimental water content (%)
VC	N.A.	77.8 ± 0.6
Zwitsal	-	73.4 ± 0.5
B1	33.3	59.8 ± 0.1
B1c	33.3	51.0 ± 0.0
B2	52.8	55.7 ± 3.5
B2c	52.8	57.0 ± 1.4
B3c	41.7	61.2 ± 1.3
B4c	66.7	68.0 ± 0.0

** HyPG-MA microgels (synthetic corneocytes) with 50% or 80% (w/w) initial water content, with or without lipid coating, were embedded in the lipid mixture with a 2:1 or 5:1 particle:lipid ratio. Experimental data are presented as mean ± SD (n = 3).*

When increasing the particle:lipid ratio to 5:1, maintaining the use of coated particles, the formulations showed 61.2 ± 1.3% and 68.0 ± 0.0% water content for B3c and B4c, respectively. The high water content of the latter biofilm is close to that of natural VC, however, also at higher particle levels the 50% formulation resulted in higher water levels than the predicted values.

Water release profiles of VC and the biomimetics are presented in Figure 5. As was already described previously [6], VC is characterized by an initial rapid water loss prior to a sustained, steady dehydration at room temperature (Fig. 5). In contrast, a very fast release of water was observed with the biofilm B1 with non-coated particles and the dehydration process was completed within 24 h. Interestingly, lipid coating of the microgels (B1c) prolonged the dehydration period to 48 h (Fig. 5). Furthermore, the increase of the initial water content of the microgels from 50% to 80% (w/w) (i.e. biofilm B2c) slowed down the complete water release to 140 h. This formulation was also mimicking the dehydration behavior of the natural biofilm most closely. The increase in the particle:lipid ratio to 5:1 did not result in a further retardation in water release kinetics.

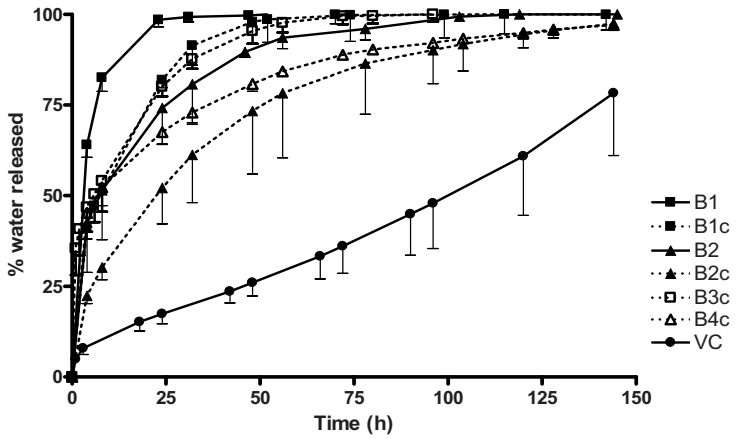

Figure 5. *Water release profiles of native VC (●) and various biofilms were obtained by monitoring the weight loss of the specimen in a desiccator over P_2O_5 at room temperature. Various parameters were changed in the formulations: the initial water content of the particles was either 50% (■, □) or 80% (▲,Δ). The particles were coated with a lipid layer (dashed lines) or kept uncoated (solid lines) prior to embedding in the lipid matrix. The particle:lipid ratio was either 2:1 (■,▲) or 5:1 (□,Δ). Data is presented as mean (w/w) -SD (n = 3).*

As the postnatal water-handling properties of VC [6] are an important aspect, it should be considered to achieve similar high skin hydration [7] with the synthetic VC. Hence, the water release from our synthetic biofilms could elegantly be controlled by the adjustment of the particle:lipid ratio and by the pre-coating of the particles. However, there is still a difference between the water-holding properties of synthetic and native VC. This might be due to I) the polymer used to prepare the microgel, i.e. HyPG-MA, which might be less efficient in binding water than keratin, the most important biopolymer for water-binding present in the corneocytes of VC [20], II) the thick and highly cross-linked cornified envelope in native corneocytes [21] being absent in the biofilms and III) the presence of long chain ceramides and fatty acids [13] chemically bound to the cornified envelope in natural VC, while in synthetic VC shorter chain phospholipids were used to coat the hydrogels. Although some differences are observed between the water holding properties of VC and the biofilm, the water release could be extended from 24 to 140 h by adjusting the composition of the biofilms. This prolonged water-release from the optimized biofilm is also much longer than observed for the Zwitsal formulation which completed dehydration after 72 h (not shown).

3.6. Rheological characterization

The biofilms were characterized for their viscoelastic properties by means of rheology. The shear storage modulus (*G'*) and the shear loss modulus (*G"*) of the different biofilms were measured as function of temperature. A representative rheogram of a biofilm (i.e. B1) is shown in Figure 6. Both *G'* and *G"* decrease with increasing temperature from 10 to 28°C (closed symbols) where a plateau is reached. Upon cooling from 40°C to 10°C, *G'* and *G"* returned to the original values (open symbols) demonstrating that the temperature induced changes in the biofilm were reversible. The tan *δ* (i.e. the quotient of *G"* and *G'*) of this formulation varied between 0.11 and 0.18 during the heating/cooling cycle, underlining the viscoelastic behavior of this formulation. Other biofilm formulations showed a similar reversible profile (data not shown). For comparison, *G'*, *G"* and tan *δ* of the various biofilms and VC at 32ºC (skin temperature) are listed in Table 3. Natural VC shows a higher *G'* and *G"* at skin temperature than all biofilm formulations. This is presumably due to the difference of water localization within the specimen, i.e. higher amount of external water in the biofilms. However, several similarities between natural VC and synthetic formulations are noticed: I) before and after the heating/cooling cycle, biofilms exhibit *G'* and *G"* values in a similar range indicating a reversible process as was also reported for VC [6]. II) the observed plateau of *G'* and *G"* in the biofilms was also described for VC to occur approximately at (adult) skin temperature [6]. III) The tan *δ* of native and synthetic VC is within the similar range indicating that both natural VC and synthetic counterpart exhibit viscoelastic properties.

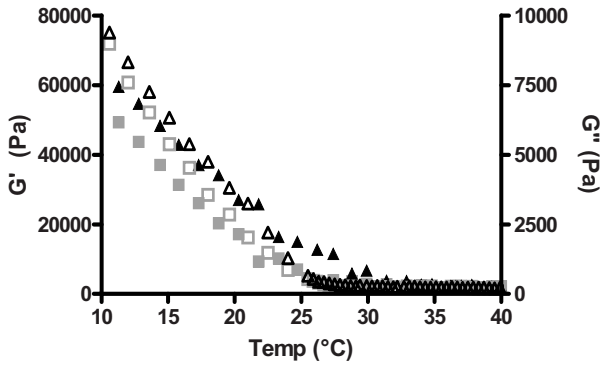

Figure 6. *Rheological properties of a representative biofilm (B1) as a function of temperature. The shear storage modulus (G',■) is correlated to the elasticity whereas the shear loss modulus (G",▲) is correlated to the viscosity. The heating values are depicted by closed symbols while the open symbols represent the cooling cycle.*

Table 3. *Rheological properties (32°C) of VC, a commercial formulation (Zwitsal) and biofilms.*

Samples*	*G'* (Pa)[§]	*G"* (Pa)[§]	tan *δ*[§]
VC	19,000 / 20,000	4,000 / 2,000	0.22 / 0.10
Zwitsal	80 / 1	60 / 6	0.70 / 8.20
B1	3,000 / 2,000	500 / 300	0.17 / 0.15
B1c	1,500 / 1,300	500 / 300	0.35 / 0.25
B2	2,000 / 2,000	300 / 300	0.15 / 0.14
B2c	2,000 / 1,600	500 / 300	0.27 / 0.20
B3c	4,000 / 4,000	600 / 600	0.22 / 0.43
B4c	2,000 / 1,600	500 / 300	0.27 / 0.20

** HyPG-MA microgels (synthetic corneocytes) with 50% and 80% (w/w) water content and with or without lipid coating were embedded in the lipid mixture with a 2:1 or 5:1 particle:lipid ratio. Experimental data is presented as mean ± SD (n = 3).*

§ G', G" and tan δ at 32°C at heating / cooling step

The Zwitsal cream was characterized by a much lower *G'* and *G"* compared to natural VC and all biofilms, indicating a very different rheological behavior. In conclusion, the rheological study showed that natural VC was mimicked very well by the synthetic formulations. Moreover, the lower *G'* and *G"* of the biofilms might result in a better patient acceptance and compliance, since the biofilms are more tractable than the natural counterpart.

4. Conclusion

In conclusion, an excellent resemblance was achieved in composition, structure and properties between native VC and synthetic biofilms. Our in vitro optimization demonstrates that the biofilms with a particle: lipid ratio of 5:1 mimics VC most closely concerning the structural appearance whereas B2c exhibits water handling properties that mimics those of native VC most closely. In future, additional hydrophilic (into the microgels) and lipophilic (into the lipids) compounds could be added, e.g. drug substances, to apply our biofilms as drug delivery matrix.

References

1. Pickens WL, Warner RR, Boissy YL, Boissy RE, Hoath SB. Characterization of vernix caseosa: water content, morphology, and elemental analysis. *J Invest Dermatol* 2000; 115(5): 875-881.
2. Tansirikongkol A, Wickett RR, Visscher MO, Hoath SB. Effect of vernix caseosa on the penetration of chymotryptic enzyme: potential role in epidermal barrier development. *Pediatr Res* 2007; 62(1): 49-53.
3. Akinbi HT, Narendran V, Pass AK, Markart P, Hoath SB. Host defense proteins in vernix caseosa and amniotic fluid. *Am J Obstet Gynecol* 2004; 191(6): 2090-2096.
4. Pickens WL, Zhou Y, Wickett RR, Visscher MO, Hoath SB. Antioxidant defense mechanisms in vernix caseosa: potential role of endogenous vitamin E. *Pediatr Res* 2000; 47: 425A.
5. Moraille R, Pickens WL, Visscher MO, Hoath SB. A novel role for vernix caseosa as a skin cleanser. *Biol Neonate* 2005; 87(1): 8-14.
6. Rissmann R, Groenink HW, Gooris GS, Oudshoorn MHM, Hennink WE, Ponec M, Bouwstra JA. Temperature-Induced Changes in Structural and Physicochemical Properties of Vernix Caseosa. *J Invest Dermatol* 2008; 128: 292-299.
7. Visscher MO, Narendran V, Pickens WL, LaRuffa AA, Meinzen-Derr J, Allen K, Hoath SB. Vernix caseosa in neonatal adaptation. *J Perinatol* 2005; 25(7): 440-446.
8. Hoeger PH, Schreiner V, Klaassen IA, Enzmann CC, Friedrichs K, Bleck O. Epidermal barrier lipids in human vernix caseosa: corresponding ceramide pattern in vernix and fetal skin. *Br J Dermatol* 2002; 146(2): 194-201.
9. Haubrich KA. Role of Vernix caseosa in the neonate: potential application in the adult population. *AACN Clin Issues* 2003; 14(4): 457-464.
10. Tollin M, Bergsson G, Kai-Larsen Y, Lengqvist J, Sjovall J, Griffiths W, Skuladottir GV, Haraldsson A, Jornvall H, Gudmundsson GH, Agerberth B. Vernix caseosa as a multi-component defence system based on polypeptides, lipids and their interactions. *Cell Mol Life Sci* 2005; 62(19-20): 2390-2399.
11. Tollin M, Jagerbrink T, Haraldsson A, Agerberth B, Jornvall H. Proteome analysis of vernix caseosa. *Pediatr Res* 2006; 60(4): 430-434.
12. Kaerkkaeinen J, Nikkari T, Ruponen S, Haahti E. Lipids of Vernix Caseosa. *J Invest Dermatol* 1965; 44: 333-338.
13. Rissmann R, Groenink HW, Weerheim AM, Hoath SB, Ponec M, Bouwstra JA. New insights into ultrastructure, lipid composition and organization of vernix caseosa. *J Invest Dermatol* 2006; 126: 1823-1833.
14. Oudshoorn MHM, Rissmann R, van der Coelen D, Hennink WE, Ponec M, Bouwstra JA. Development of a Murine Model to Evaluate the Effect Vernix Caseosa on Skin Barrier Recovery. Accepted for publication in *Exp Dermatol* 2008.
15. Rissmann R, Oudshoorn MHM, Kocks E, Hennink WE, Ponec M, Bouwstra JA. Lanolin-derived lipid mixtures mimic closely the lipid composition and organization of vernix caseosa lipids. Accepted for publication in *BBA Biomembranes* 2008.

16. Oudshoorn MHM, Rissmann R, Bouwstra JA, Hennink WE. Synthesis and characterization of hyperbranched polyglycerol hydrogels. *Biomaterials* 2006; 27(32): 5471-5479.
17. Oudshoorn MHM, Penterman R, Rissmann R, Bouwstra JA, Broer DJ, Hennink WE. Preparation and characterization of structured hydrogel microparticles based on cross-linked hyperbranched polyglycerol. *Langmuir* 2007; 23(23): 11819-11825.
18. Kainthan RK, Janzen J, Levin E, Devine DV, Brooks DE. Biocompatibility testing of branched and linear polyglycidol. *Biomacromolecules* 2006; 7(3): 703-709.
19. De Geest BG, Stubbe BG, Jonas AM, Van Thienen T, Hinrichs WL, Demeester J, De Smedt SC. Self-exploding lipid-coated microgels. *Biomacromolecules* 2006; 7(1): 373-379.
20. Tansirikongkol A, Hoath SB, Pickens WL, Visscher MO, Wickett RR. Equilibrium water content in native vernix and its cellular component. *J Pharm Sci* 2008; 97(2): 985-994.
21. Candi E, Schmidt R, Melino G. The cornified envelope: a model of cell death in the skin. *Nat Rev Mol Cell Biol* 2005; 6(4): 328-340.

Development of a murine model to evaluate the effect of vernix caseosa on skin barrier recovery

Marion H.M. Oudshoorn[a], Robert Rissmann[b], Dennis van der Coelen[b], Wim E. Hennink[a], Maria Ponec[b], Joke A. Bouwstra[b]

[a] Department of Pharmaceutics, Utrecht Institute for Pharmaceutical Sciences (UIPS), Utrecht University, Utrecht, The Netherlands
[b] Department of Drug Delivery Technology, Leiden/Amsterdam Center for Drug Research (LACDR), Leiden University, Leiden, The Netherlands

Accepted for publication in Experimental Dermatology

6

Abstract

The aim of this study was twofold, that is generation of a reliable model for skin barrier disruption and repair and to evaluate recovery of damaged skin after application of vernix caseosa (VC). VC was selected as its wound healing properties were suggested previously but never clearly demonstrated.

Five different levels of barrier disruption in mice, accomplished by tape-stripping, were evaluated. Disruption models moderate, severe #1 and #2 (TEWL of 31 ± 2, 59 ± 4 and 66 ± 3 g/m^2/h, respectively) showed complete recovery within 72 h. However, not all corneocytes were removed after tape-stripping. Additionally models severe #3 and #4 (TEWL of 73 ± 5 and 79 ± 6 g/m^2/h, respectively) with a more severe disruption were evaluated. After tape-stripping, all corneocytes were removed and the remaining epidermis was intact. However, model #3 still showed complete recovery within 72 h. With model #4 a crust was formed and almost complete recovery (~90%) was obtained within only 8 days.

The effect of VC application on recovery of disrupted skin was evaluated with model #3 and #4. Model #3 showed that application of VC predominantly influenced initial recovery. Therefore this model is merely appropriate to study the effect of formulations in the initial recovery period. Topical application of VC on model #4 considerably increased initial and long-term recovery. Moreover, VC application promoted rapid formation of stratum corneum and prevented epidermal thickening. These observations not only confirm the ability of VC to enhance barrier recovery, but also suggest potential use of this treatment clinically.

1. Introduction

The cutaneous permeability barrier is an essential defense system against exogenous agents on the one hand, and prevents dehydration on the other. The stratum corneum (SC), the outermost layer of the epidermis, forms the main barrier for diffusion of substances across the skin [1, 2]. One of the commonly used methods to remove SC is sequential tape stripping [2-5]. Increasing the number of tape strips increases the amount of corneocytes removed. Once the barrier function is impaired, a homeostatic repair response is initiated within the epidermis, which results in a recovery of the skin barrier [3, 6]. By measuring the changes in transepidermal water loss (TEWL), the barrier recovery can be monitored non-invasively [3, 5, 7, 8].

Epidermal barrier perturbation can be a consequence of various environmental factors such as burns or injuries. Furthermore, an impaired barrier function is also encountered in diseased skin and in skin of preterm infants. These infants have an ineffective skin barrier due to a deficient or even absent SC [9-11]. Importantly, in preterm infants the protective natural biofilm vernix caseosa (VC) is also lacking. VC is a lipid-rich material that covers the skin surface of the fetus and the newborn. The structure of VC is very similar to that of SC. VC consists of dead cells with high water binding capacity, nevertheless, it lacks intercorneocyte desmosomal connections and might therefore be referred to as a 'mobile phase' SC [12-14]. It is suggested that VC promotes the formation of the horny layer of the fetus [12, 13] and, moreover, that it acts as a lubricant and moisturizer. Additionally, VC shows a temperature-dependent dehydration behavior [15] and exhibits anti-infective [16], anti-oxidant [17], skin hydrating [18] and skin cleansing properties postnatally [10]. These multiple biological functions of VC imply that this natural biofilm is an excellent candidate to promote the repair of the skin barrier of preterm infants [10, 11] and may enhance wound healing in adult skin as well [12].

The purpose of the present study is twofold, namely to generate a reliable model for skin barrier disruption and repair and to evaluate the recovery of damaged skin after application of VC. As previous studies [3, 8, 19, 20] only examined barrier disruption models that resulted in a very fast recovery (i.e. a few hours), it was difficult to design and study formulations that would accelerate skin barrier repair. Our study therefore focused on a skin barrier disruption model with slow recovery. Disruption of the skin barrier was accomplished by tape stripping, which induces skin damage similar to a variety of clinically relevant situations [3]. VC was applied topically on the disrupted mouse skin to determine whether the barrier recovery could be accelerated. This natural biofilm was selected as its wound healing properties were suggested previously [9, 12, 13, 21], but were never clearly demonstrated. Results of VC were compared to the oil-based ointment Vaseline (petrolatum; Vas). Changes in TEWL were selected to monitor

barrier recovery. Additionally, biopsies were harvested to evaluate the recovery of the SC by histology.

2. Experimental section

2.1. Materials

Tissue-Tek® O.C.T.™ Compound was obtained from Sakura Finetek Europe B.V. (Zoeterwoude, The Netherlands). Black D-squame (rectangles from 70 mm x 25 mm) was obtained from CuDerm (Dallas, USA). Gelatin capsules were provided by Spruyt-Hillen (IJsselstein, The Netherlands). Safranin O was purchased from Sigma (Schnellendorf, Germany). Vaseline (petrolatum) was purchased from Elida Fabergé (London, UK).

2.2. Vernix caseosa collection

Vernix caseosa (VC) was scraped off gently immediately after vaginal delivery or cesarean section of healthy full-term neonates. The samples were transferred into sterile plastic tubes and stored at 4ºC until use. The collection of VC was approved by the ethical committee of the Leiden University Medical Center and informed consent was given by the parents.

2.3. Model for skin barrier disruption

Nude male mice (Skh-1), 7-9 weeks old and 28 ± 2 g in weight, were purchased from Charles River Laboratories (Saint-Aubin-les-Elbeuf, France). All animal experiments were conducted in conformity with the Public Health Service Policy on use of laboratory animals and had been approved by the Research Ethical Committee of Leiden University (UDEC, no. 07002). The mice were maintained in the animal care facility of the Gorlaeus Laboratories, Leiden University, in temperature- and humidity-controlled rooms and fed standard laboratory chow and tap water *ad libitum*.

The animals were anaesthetized using a mixture of Ketamine (150 mg/kg body weight; Nimatek®, Euovet Animal Health B.V., Bladel, The Netherlands) and Xylazine (10 mg/kg body weight; Rompun®, Bayer B.V., Mijdrecht, The Netherlands) by intraperitoneal injection (i.p.). During anaesthesia, the mice were kept on a warm mattress faced down and their eyes wetted with Visagel® (Eurovet, Bladel, The Netherlands). The mice were grouped randomly (six per group), with each group receiving a different treatment. The skin of the mice was washed carefully with deionized water prior to marking two areas (~1 cm^2, both left and right) on the upper flank of the back of the mice, near the head. The skin barrier was disrupted by sequential tape stripping by a single individual. For this purpose, tape strips (black D-squame) of ~1 cm^2 were cut and applied on the marked areas. The strips were compressed with finger tips for 5 seconds before rapid removal in

alternated stripping direction. An increase in the number of tape strips led to an increase in number of removed SC cells and consequently reduces the skin barrier function. Several levels of barrier disruption were induced: from moderate (defined as TEWL (transepidermal water loss) of 30 g/m^2/h; 4 tape strips) to severe (defined as TEWL of ≥60 g/m^2/h; 12 tape strips). After treatment, the mice were housed individually to avoid fight-induced skin injury. No scratching of the treated area or any abnormal behavior was observed during the studies.

2.4. Application

Immediately after disruption of the skin barrier, one test area per mouse was treated with either 5 mg/cm^2, twice 5 mg/cm^2 (second application 4 h after first application), 15 mg/cm^2 VC or 5 mg/cm^2 Vaseline. VC from 3 different donors was used; VC was not pooled but VC from different donors was applied on different mice. A single individual rubbed the samples onto the treatment area with a spatula. Untreated contralateral disrupted sites served as controls.

2.5. Biophysical evaluation of the skin

2.5.1. Transepidermal water loss

The level of barrier disruption and the repair rate were assessed by measuring the TEWL at regular intervals using a Tewameter TM 210 (Courage & Khazaka, Cologne, Germany). The TEWL was measured by holding the probe lightly against the test area until a constant TEWL value was obtained. The pressure applied to the probe was just enough to prevent leakage of air between the lower rim of the Teflon cylinder and the skin.

The percentage of barrier recovery was calculated using the following equation: 1 – ((TEWL at indicated time point – TEWL of average control 'undamaged skin')/(TEWL immediately after stripping – TEWL of average control 'undamaged skin')) × 100%.

2.5.2. Histology

Biopsies were taken, using a pair of scissors in conjunction with metal tweezers, from the central part of the (treated) sites. The biopsies were immediately placed in a gelatin capsule, processed by fixation in Tissue-Tek®, frozen in liquid nitrogen and stored in liquid nitrogen prior to slicing. Samples (thickness 5 µm) were sliced perpendicular to the skin surface with a cryotome (Leica CM 3050S, Wetzlar, Germany). After fixation in cold acetone (4°C), the sections were stained for 1 min with a 1% (w/v) aqueous safranin solution for contrast. Subsequently, the sections were washed with deionized water. To allow the corneocytes to swell, a 2% (w/v) KOH solution was applied to the sections during 20 min. Visualization was performed using a light microscope combined with a digital camera (Carl Zeiss axioskop, Jena, Germany).

The thickness of the viable epidermis was measured in at least 18 different locations of the stained cross-sections. Statistical differences between the groups (i.e. VC treated, Vas treated and untreated) were determined by a one-way ANOVA with a Bonferroni post-test. All data analysis was performed using GraphPad Prism 4.0.

3. Results and discussion

3.1. Skin barrier disruption

Disruption of the skin barrier was accomplished by tape stripping. The mice were grouped in several grades of barrier perturbation (i.e. varying from moderate to severe disruption), which simulate a variety of clinically relevant situations [3]. In table 1 the various characteristics of the different skin barrier disruption models are listed. The moderate (4 tape strips) and severe #1 (6 tape strips) barrier disruption model resulted in a TEWL of respectively 31 ± 2 g/m^2/h and 59 ± 4 g/m^2/h. In comparison, normal (undisrupted and untreated) skin has a TEWL of ~9 g/m^2/h. Both models did not show any sign of redness or irritation. The recovery of the skin was monitored by TEWL measurements at regular time intervals and it was observed that complete recovery occurred already within 72 h for both moderate and severe #1 (data not shown). Importantly, histological images of the cross-sections clearly revealed that not all corneocytes were removed directly after tape stripping (Fig. 1a and 1b). As the skin repair process occurred within 3 days and not all corneocytes were removed, additional models with a more severe barrier disruption were evaluated: the number of sequential tape strips was increased to 7 (severe #2; mean TEWL of 66 ± 3 g/m^2/h), 8 (severe #3; mean TEWL of 73 ± 5 g/m^2/h) or 12 (severe #4; mean TEWL of 79 ± 6 g/m^2/h).

Table 1. *Applied levels of barrier disruption by tape stripping with their characteristics.*

Disruption level	No. of strips applied	TEWL* (g/m^2/h)	Appearance skin	Corneocytes present	Recovery (24 h)	Recovery (72 h)
Moderate	4	31 ± 2	normal	Yes	70%	95%
Severe #1	6	59 ± 4	normal	Yes	70%	95%
Severe #2	7	66 ± 3	shiny	Yes	70%	95%
Severe #3	8	73 ± 5	shiny, slightly red	No	64%	95%
Severe #4	12	79 ± 6	very shiny, very red	No	4%[§]	50%[§]

** Undamaged skin has a TEWL of ~9 g/m^2/h*

[§] After disruption a crust was formed within a few hours

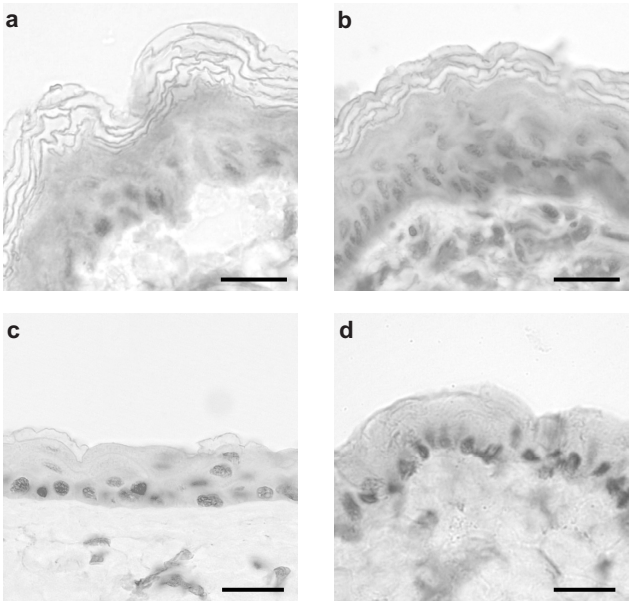

Figure 1. *Cross-sections of hairless mouse skin prior to (a) and directly after tape stripping to obtain the barrier disruption model moderate (b), severe #2 (c) or severe #4 (d). Scale bar is 20 µm.*

Disruption model severe #2 did not show any sign of redness or irritation but showed a slight glistening of the skin, which is indicative for complete removal of the SC [5]. However, still some corneocytes were visible by histology (Fig. 1c). Between disruption model severe #3 and #4 a considerable difference in both skin appearance and barrier recovery was observed. With model severe #3, the skin was glistening and showed some initial redness indicating an irritation of the skin. The skin of model severe #4 was clearly glistening and an intense redness of the skin was observed.

Light microscopic images of the biopsies, taken directly after tape stripping, confirmed that the SC was completely removed for both severe #3 (not shown) and severe #4 (Fig. 1d) and that the remaining epidermis was intact. Although the SC was completely removed, model severe #3 still showed complete recovery of the TEWL within 72 h. However, with model severe #4 a crust was formed on the disrupted area within a few hours. As a result only 50% recovery of the TEWL was observed in 72 h. No scratching of the treated area or any abnormal behavior was observed. Therefore, the recovery was monitored for an additional 5 days and an almost complete recovery (~90%) of the skin barrier was obtained within this time period, although some scars developed. As the light microscopic images of both model severe #3 and model severe #4 showed complete

removal of SC, and severe #4 showed a rather long recovery time, both models were assessed to study the changes in barrier repair rate after topical application of VC.

3.2. Effect of treatment with vernix caseosa on barrier recovery

To study the effect of VC on the recovery of tape stripped skin, both models, severe #3 and severe #4, were employed. Model severe #3 typically resembles the models previously described in literature that have a very fast recovery (i.e. several hours) [3, 8, 19, 20], whereas severe #4 is an innovative model with extensively damaged skin resulting in substantial slower recovery (i.e. 200 h). Macroscopic observations of the VC application site of the damaged skin of model severe #3 are shown in Figure 2. Immediately after tape stripping, the skin was glistening and slightly red (Fig. 2b). However, upon VC application, the redness disappeared within a few minutes (applied on left side; Fig. 2c). Four hours after application, VC was not visible anymore at the skin surface and the skin had a normal appearance (Fig. 2d and 2e). Although the untreated area (right side; Fig. 2) was glistening and slightly red after tape stripping, the skin visually recovered within a few hours as well. The recovery of the skin was also monitored by TEWL measurements (Fig. 3).

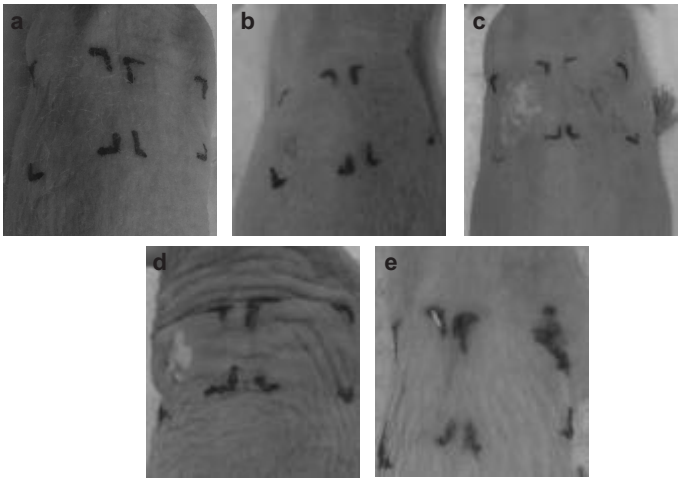

Figure 2. *Representative macroscopic observations of undisrupted skin (a), disrupted skin (model severe #3) directly after tape stripping (b) and the effect of topical application of VC (c, d and e; 5 mg/cm^2) on the disrupted skin after 1 min, 3 h and 8 h.*

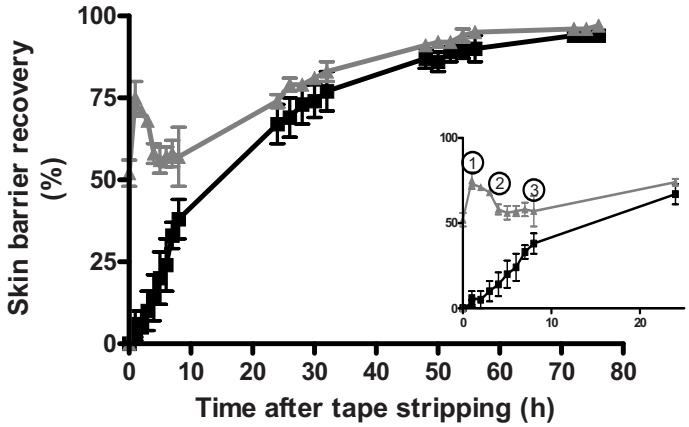

Figure 3. *Skin barrier recovery after tape stripping (barrier disruption model severe #3) as function of time: VC application (▲; 5 mg/cm^2) and untreated, disrupted skin (■). The inset shows the recovery of the first 24 h after disruption. In the initial phase (phase 1) VC is applied and covers the skin. VC disappears within 3 to 4 h (phase 2). As the skin is not fully recovered, skin barrier repair is further monitored (phase 3) until complete recovery. Data are shown as average ± SD (n = 6).*

Application of VC (5 mg/cm^2) immediately increased barrier recovery (TEWL decreased from 73 ± 5 g/m^2/h to 23 ± 1 g/m^2/h after application of VC), indicated as phase 1 in Figure 3. Once applied, VC disappeared visually within 3 to 4 h (phase 2, Fig. 3). As the skin was not fully recovered a high TEWL was measured (36 ± 1 g/m^2/h; barrier recovery of 58 ± 3%). Subsequently, skin barrier repair was monitored (phase 3, Fig. 3) and complete recovery occurred within 72 h. As the disrupted, untreated skin of this severe #3 model also showed a recovery in 72 h, application of VC predominantly influenced initial barrier recovery. Moreover, the application of a higher dose (i.e. 15 mg/cm^2) of VC on the disrupted skin did not improve barrier recovery significantly (based on TEWL data; data not shown). Due to its fast recovery, this model is appropriate to study the effect of formulations in the initial recovery period, as described in literature [3, 8, 19, 20].

In Figure 4 light microscopic images of the damaged skin without treatment, collected at several time intervals, are depicted. Normal skin is characterized by stained nuclei of the viable epidermis cells, while swollen corneocytes are also clearly visible (Fig. 4a). After complete barrier disruption (model severe #3) corneocytes were absent (Fig. 4b). During the recovery phase, cell layers of corneocytes gradually reappeared: after 2 h and 6 h one up to two corneocyte layers were observed (Fig. 4c and 4d).

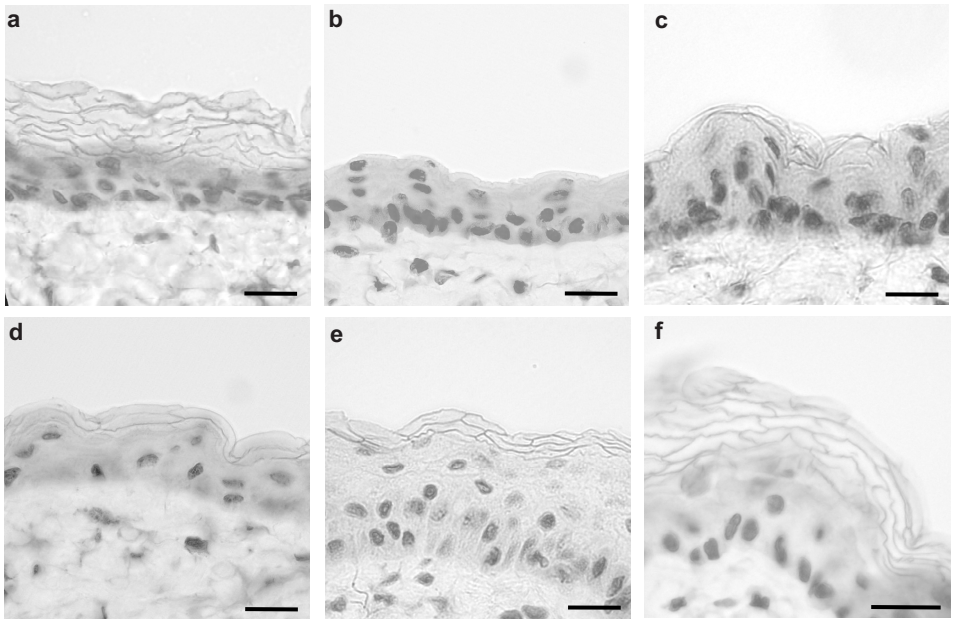

Figure 4. *Cross-sections of undisrupted mouse skin (a), disrupted skin (model severe #3) directly after stripping (b) and the recovery of skin after 2 h, 6 h, 24 h and 72 h (c to f, respectively). Scale bar is 20 µm.*

After one day, three corneocyte layers were present, whereas a complete SC (4 to 6 cell layers) was observed again after 72 h of recovery. Upon application of VC, histological images did not differ from those of skin which was not treated with VC: an equal number of stratum corneum layers could be observed at the various time intervals (results not shown). As the barrier repair model severe #3 is merely appropriate to study the effect of formulations in the initial recovery period, because of its fast recovery, the effect of VC treatment on a more extensively damaged skin (severe #4) was also evaluated. Figure 5 shows that the skin was very red and glistening after tape stripping and subsequently a crust was formed within a few hours (Fig. 5b-5i, right side). This crust was still present 100 h (Fig. 5i; right side) after stripping but was fully absent within 168 h (Fig. 5j; right side), although some scars developed. However, when VC was applied directly after stripping (Fig. 5c, the left side) the redness disappeared in a few minutes and no crust formation occurred (Fig. 5b-5i, left side). Furthermore, the skin recovered much faster (visually: ~72 h in stead of ~168 h; see Fig. 5) and no scars were formed as compared to untreated skin (Fig. 5j). As seen in Figure 6, disrupted skin treated with VC showed fast and complete recovery after approximately 100 h. Initially, the skin is covered with VC (phase 1, Fig. 6) decreasing the TEWL from 79 ± 6 g/m^2/h to 29 ± 2 g/m^2/h.

Subsequently, VC disappeared visually within 3 to 4 h (phase 2, Fig. 6). As the skin was not fully recovered a TEWL of 57 ± 5 g/m^2/h was measured (barrier recovery of 37 ± 5%). Next, the skin barrier repair is monitored (phase 3, Fig. 6) and complete recovery occurred within 100h.

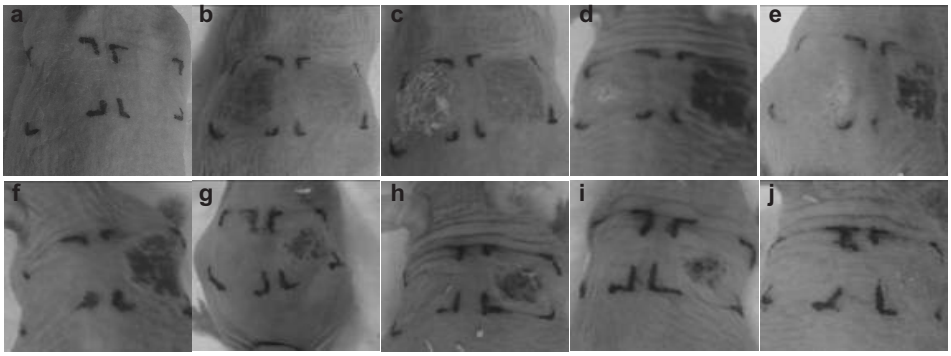

Figure 5. *Representative macroscopic observations of undisrupted skin (a), skin barrier disruption (model severe #4) immediately after tape stripping (b) and the effect of topical application of vernix caseosa after 1 min, 3 h, 5 h, 8 h, 24 h, 72 h, 100 h and 168 h (c, d, e, f, g, h, i, j, respectively) on the disrupted skin.*

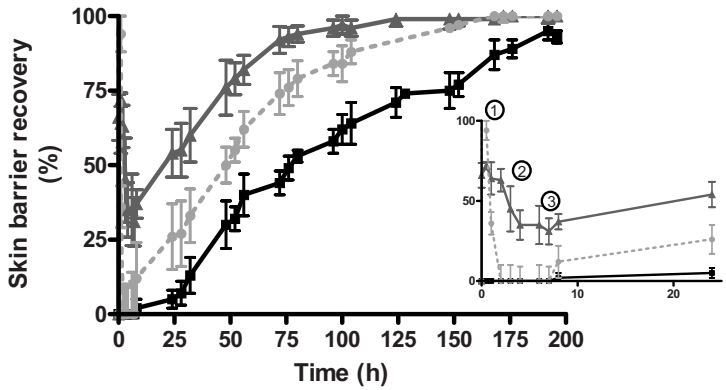

Figure 6. *Skin barrier recovery of disrupted skin (model severe #4) as function of time: VC application (▲; 5 mg/cm^2), Vaseline treated (●; dashed line) and untreated, disrupted skin (■; continuous line). The inset shows the recovery of the first 24 h after disruption. In the initial phase (phase 1) VC and Vaseline are applied and cover the skin. Both VC and Vas disappear within 3 to 4 h (phase 2). As the skin is not fully recovered, skin barrier repair is further monitored (phase 3) until complete recovery. Data are shown as average ± SD (n = 6).*

Neither application of a higher dose (i.e. 15 mg/cm^2) nor multiple applications (i.e. twice 5 mg/cm^2; second dose applied 4 h after first dose) of VC did further accelerate the skin barrier recovery (based on TEWL data; data not shown) compared to a single application of 5 mg VC. VC was obtained from 3 different donors; VC from different donors were not pooled but was applied on different mice. However, no donor-to-donor variation was observed (based on TEWL data). Untreated disrupted skin showed an initial lag time of 7 h after which barrier repair developed slowly and nearly complete recovery (~90%) only occurred after 200 h. These observations not only confirm the ability of VC to enhance initial and long-term barrier recovery [12] of extensively damaged skin, but they also suggest the potential use of this treatment clinically for wound healing purposes. To date, these wound healing properties of VC were only shown in adult patients with trophic ulcers [22]. One can speculate whether the suggested mechanism of action, i.e. the stimulation of tissue metabolism, is also valid for our study.
The effect of VC on the recovery of extensively disrupted skin was also histologically studied (Fig. 7). A number of corneocytes could already be perceived on the VC treated skin (Fig. 7a) 6 h after tape stripping, whereas no SC was visible on untreated, disrupted skin at the same time point (Fig 7b). After 24 h even more corneocytes were present on the VC treated skin whereas the untreated damaged skin was still free from corneocytes (Fig. 7c and 7d, respectively). The SC was clearly visible (Fig. 7e) after 48 h on untreated, disrupted skin and no major difference could be observed between VC treated and untreated skin (Fig. 7e and 7f, respectively). When the skin was fully recovered (after 8 days; Fig. 7g and 5 h) the histology was similar to that prior the disruption procedure. Hence, VC application promotes a fast recovery of the SC. Moreover, when analyzing the dermal areas in the histological sections no abnormalities of the appearance, i.e. signs of inflammation, could be observed.

The oil-based ointment Vaseline (Vas) already has been speculated to accelerate barrier recovery in mice [23]. Therefore the effect of Vas was investigated with model severe #4 and compared to VC. When Vas was applied directly after stripping (data not shown), the treated site remained red. Moreover, 3 days post application the disrupted treated site was still slightly red and minor crust formation was observed. These observations indicate an improved wound healing compared to untreated skin (strong crust development), however less effective compared to VC treated skin (absence of crust). Application of Vas (5 mg/cm^2) immediately restored the barrier function of the skin (indicated as phase 1 in Fig. 6; TEWL decreased from 79 ± 6 g/m^2/h to 3 ± 0.5 g/m^2/h) demonstrating the occlusive properties of Vas. Vas disappeared visually within 2 h, which was associated with loss of its barrier function (phase 2, Fig. 6). As a result, the TEWL raised again to 77 ± 7 g/m^2/h, which is comparable to disrupted untreated skin (i.e. 79 ± 6 g/m^2/h).

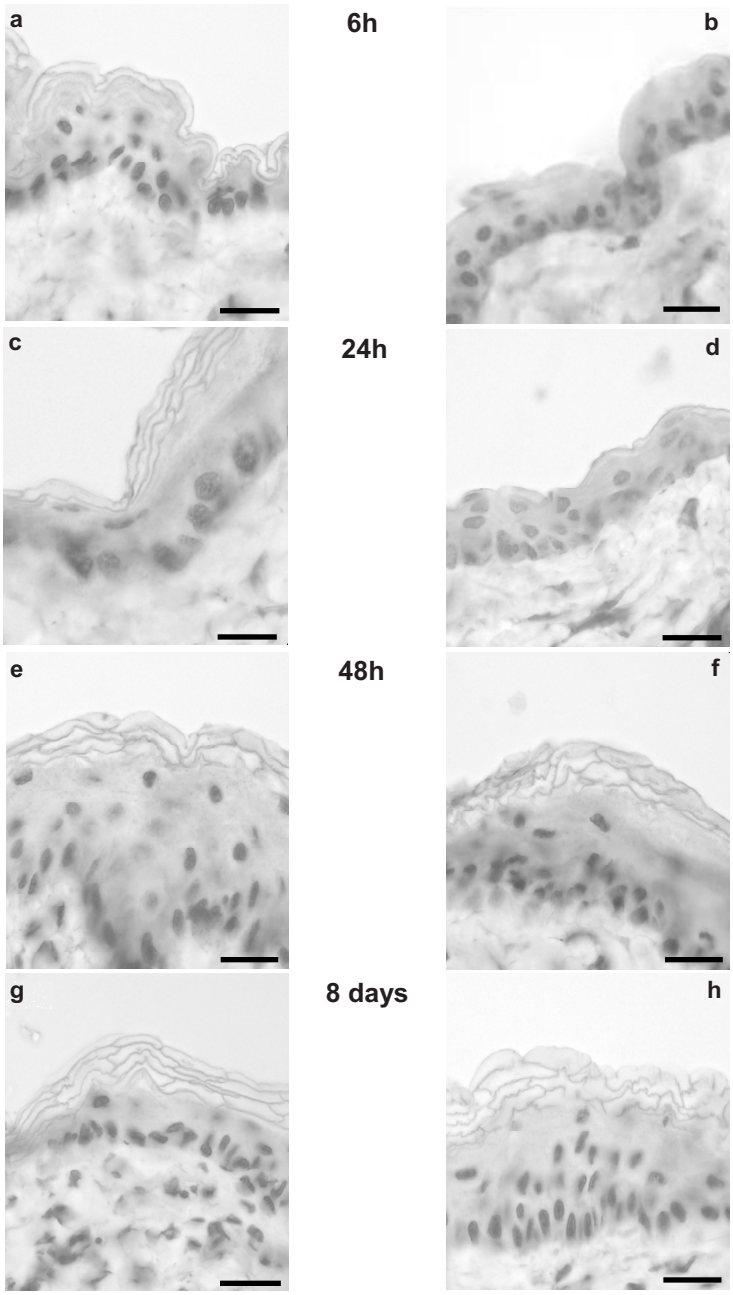

Figure 7. *Representative histological cross-sections of mouse skin after disruption (model severe #4): with VC application (a, c, e, g) or without treatment (b, d, f, h) 6 h, 24 h, 48 h and 8 days after tape stripping, respectively. Scale bar is 20 µm.*

Subsequent monitoring of the skin barrier showed that complete recovery occurred within 150 h (phase 3, Fig. 6). Since the disrupted untreated skin showed nearly complete recovery within 200 h, application of Vas did enhance barrier recovery however to a lesser extent than VC (i.e. 100 h). A histological study of the effect of Vas on the recovery of extensively disrupted skin revealed a similar trend in SC recovery (data not shown) as was observed after VC treatment (Fig. 7). These results clearly indicate that occlusion of the skin (i.e. upon application of Vas) is not sufficient to elucidate the effect of VC. Hence, the water content of VC and/or the presence of specific groups of lipids/proteins may play a role in the favorable effects of VC on skin barrier recovery.

In addition, the occurrence of epidermal thickening was evaluated. Epidermal thickening has been partly associated with hyperproliferation [24] and is an indication for different skin diseases such as atopic dermatitis and psoriasis [5]. Figure 8 shows the thickness of the viable epidermis of untreated, VC or Vas treated disrupted mouse skin after 3 and 8 days of recovery in comparison to undisrupted untreated skin. The thickness of the viable epidermis of undamaged and untreated hairless mouse skin is 16 ± 6 µm. Three and 8 days after recovery the disrupted but untreated epidermis is much thicker (68 ± 20 µm and 43 ± 20 µm, respectively). This is significantly different (P<0.05) from the VC treated site after 3 and 8 days where the epidermis exhibited a thickness of 25 ± 5 µm and 18 ± 6 µm, respectively, which is comparable to undamaged untreated skin.

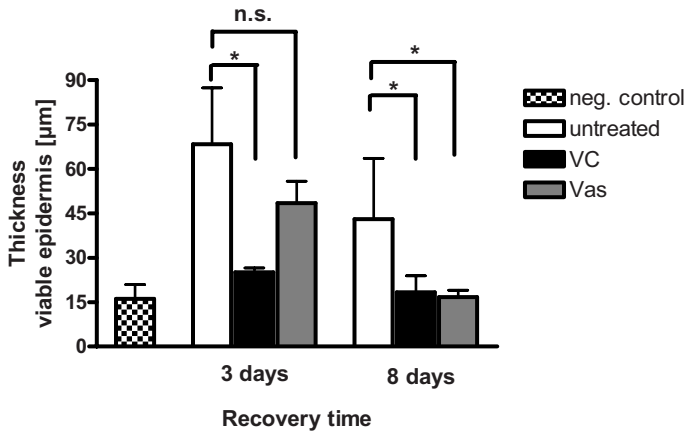

Figure 8. *Thickness of viable epidermis of untreated, VC or Vas treated disrupted mouse skin after 3 or 8 days of recovery compared to undisrupted untreated skin (negative control). Per treatment, at least 18 different locations of the cross-sections were measured. The error bars show SD. *P<0.05; n.s. = not significant.*

The Vas treated site, however, showed a thickened epidermis after 3 days (48 ± 10 µm) similar to disrupted untreated skin. Moreover, this is significantly different (P<0.05) from the VC treated site. Eight days after treatment, the Vas treated skin showed a less thickened epidermis (17 ± 5 µm), which is comparable to VC. Epidermal thickening of disrupted untreated skin and of Vas treated skin after 3 days of recovery is likely due to hyperproliferation that is not observed on disrupted, VC treated areas. Therefore, application of VC not only accelerates barrier recovery but also effectively prevents epidermal thickening after severe barrier insults.

4. Conclusions

The present study demonstrates that sequential tape stripping is an efficient method to generate reliable models for skin barrier disruption and repair. By increasing the number of tape strips different models could be obtained with a disrupted skin varying from moderate to severe. Only extensively damaged skin (i.e. model severe #4) showed a rather slow recovery, whereas all other models resulted in a very fast skin barrier repair. It was observed that topical application of VC on severely disrupted skin (model severe #4) considerably increased the skin barrier recovery and was more efficient than Vas treatment. Moreover, VC application promoted a rapid formation of SC and prevented most effectively epidermal thickening. These observations not only confirm the ability of VC to enhance barrier recovery, but it also suggests the potential use of this treatment clinically.

References

1. Madison KC. Barrier function of the skin: "la raison d'etre" of the epidermis. *J Invest Dermatol* 2003; 121(2): 231-241.
2. Breternitz M, Flach M, Prassler J, Elsner P, Fluhr JW. Acute barrier disruption by adhesive tapes is influenced by pressure, time and anatomical location: integrity and cohesion assessed by sequential tape stripping. A randomized, controlled study. *Br J Dermatol* 2007; 156(2): 231-240.
3. Yang L, Mao-Qiang M, Taljebini M, Elias PM, Feingold KR. Topical stratum corneum lipids accelerate barrier repair after tape stripping, solvent treatment and some but not all types of detergent treatment. *Br J Dermatol* 1995; 133(5): 679-685.
4. Uhoda E, Piérard-Franchimont C, Debatisse B, Wang X, Piérard G. Repair kinetics of the stratum corneum under repeated insults. *Exog Dermatol* 2004; 3: 7-11.
5. van de Kerkhof PC, de Mare S, Arnold WP, van Erp PE. Epidermal regeneration and occlusion. *Acta Derm Venereol* 1995; 75(1): 6-8.
6. Hachem JP, Houben E, Crumrine D, Man MQ, Schurer N, Roelandt T, Choi EH, Uchida Y, Brown BE, Feingold KR, Elias PM. Serine protease signaling of epidermal permeability barrier homeostasis. *J Invest Dermatol* 2006; 126(9): 2074-2086.
7. Fluhr JW, Feingold KR, Elias PM. Transepidermal water loss reflects permeability barrier status: validation in human and rodent in vivo and ex vivo models. *Exp Dermatol* 2006; 15(7): 483-492.
8. Grubauer G, Elias PM, Feingold KR. Transepidermal water loss: the signal for recovery of barrier structure and function. *J Lipid Res* 1989; 30(3): 323-333.
9. Bautista MI, Wickett RR, Visscher MO, Pickens WL, Hoath SB. Characterization of vernix caseosa as a natural biofilm: comparison to standard oil-based ointments. *Pediatr Dermatol* 2000; 17(4): 253-260.
10. Moraille R, Pickens WL, Visscher MO, Hoath SB. A novel role for vernix caseosa as a skin cleanser. *Biol Neonate* 2005; 87(1): 8-14.
11. Hoeger PH, Schreiner V, Klaassen IA, Enzmann CC, Friedrichs K, Bleck O. Epidermal barrier lipids in human vernix caseosa: corresponding ceramide pattern in vernix and fetal skin. *Br J Dermatol* 2002; 146(2): 194-201.
12. Haubrich KA. Role of Vernix caseosa in the neonate: potential application in the adult population. *AACN Clin Issues* 2003; 14(4): 457-464.
13. Pickens WL, Warner RR, Boissy YL, Boissy RE, Hoath SB. Characterization of vernix caseosa: water content, morphology, and elemental analysis. *J Invest Dermatol* 2000; 115(5): 875-881.
14. Rissmann R, Groenink HW, Weerheim AM, Hoath SB, Ponec M, Bouwstra JA. New insights into ultrastructure, lipid composition and organization of vernix caseosa. *J Invest Dermatol* 2006; 126: 1823-1833.
15. Rissmann R, Groenink HW, Gooris GS, Oudshoorn MHM, Hennink WE, Ponec M, Bouwstra JA. Temperature-Induced Changes in Structural and Physicochemical Properties of Vernix Caseosa. *J Invest Dermatol* 2008; 128: 292-299.
16. Akinbi HT, Narendran V, Pass AK, Markart P, Hoath SB. Host defense proteins in vernix caseosa and amniotic fluid. *Am J Obstet Gynecol* 2004; 191(6): 2090-2096.

17. Pickens WL, Zhou Y, Wickett RR, Visscher MO, Hoath SB. Antioxidant defense mechanisms in vernix caseosa: potential role of endogenous vitamin E. *Pediatr Res* 2000; 47: 425A.
18. Visscher MO, Narendran V, Pickens WL, LaRuffa AA, Meinzen-Derr J, Allen K, Hoath SB. Vernix caseosa in neonatal adaptation. *J Perinatol* 2005; 25(7): 440-446.
19. Amano T, Takeda T, Yano H, Tamura T. Olopatadine hydrochloride accelerates the recovery of skin barrier function in mice. *Br J Dermatol* 2007; 156(5): 906-912.
20. Ikeyama K, Fuziwara S, Denda M. Topical application of neuronal nitric oxide synthase inhibitor accelerates cutaneous barrier recovery and prevents epidermal hyperplasia induced barrier disrupted. *J Invest Dermatol* 2007; 127: 1713-1719.
21. Hoath SB, Pickens WL, Visscher MO. The biology of vernix caseosa. *Int J Cosmetic Sci* 2006; 28: 319-333.
22. Zhukov BN, Neverova EI, Nikitin KE, Kostiaev VE, Myshentsev PN. [A comparative evaluation of the use of vernix caseosa and solcoseryl in treating patients with trophic ulcers of the lower extremities]. *Vestn Khir Im I I Grek* 1992; 148(6): 339-341.
23. Ghadially R, Halkier-Sorensen L, Elias PM. Effects of petrolatum on stratum corneum structure and function. *J Am Acad Dermatol* 1992; 26(3 Pt 2): 387-396.
24. Porter RM, Reichelt J, Lunny DP, Magin TM, Lane EB. The relationship between hyperproliferation and epidermal thickening in a mouse model for BCIE. *J Invest Dermatol* 1998; 110(6): 951-957.

Effect of synthetic vernix biofilm on barrier recovery of damaged mouse skin

Marion H.M. Oudshoorn[a], Robert Rissmann[b], Dennis van der Coelen[b], Wim E. Hennink[a], Maria Ponec[b], Joke A. Bouwstra[b]

[a] Department of Pharmaceutics, Utrecht Institute for Pharmaceutical Sciences (UIPS), Utrecht University, Utrecht, The Netherlands
[b] Department of Drug Delivery Technology, Leiden/Amsterdam Center for Drug Research (LACDR), Leiden University, Leiden, The Netherlands

Submitted for publication

7

Abstract

The aim of this work was to investigate whether topical application of synthetic biofilms supports and accelerates the recovery of the murine skin barrier, disrupted by sequential tape stripping. Therefore, various biofilms were applied topically on disrupted mouse skin to determine which formulation could improve barrier function, as was observed previously for the natural biofilm vernix caseosa (VC). The biofilms (i.e. particles (synthetic corneocytes) embedded in a synthetic lipid matrix) closely mimic the physical properties of VC, which consists of corneocytes (dead cells) surrounded by a lipid matrix. Various formulations were prepared using different particle:lipid ratios, particles with different initial water-content and uncoated or lipid-coated particles. It was observed that application of all tested formulations improved the skin barrier recovery and reduced crust formation and epidermal hyperproliferation. However, only one of the biofilms (i.e. B1; composed of uncoated particles with 50% (w/w) initial water content and particle:lipid ratio of 2:1) mimicked the effects of native VC most closely. This indicates the importance of the presence of individual components, i.e. barrier lipids and water, as well as the ratio of these components. Consequently, these observations suggest the potential clinical use of this biofilm treatment.

1. Introduction

Vernix caseosa (VC) is a lipid-rich, natural biofilm which normally covers the skin of the developing fetus during the final stage of the gestational period [1, 2]. However, in premature infants this protective surface film is absent [3, 4]. Macroscopically, VC is a thick, viscous and white cream that consists of hydrated dead cells (corneocytes) dispersed in a lipid matrix. Lipids covalently bound to the cornified envelope of the cells form the interface between the corneocytes and the lipid matrix. The structure of VC is very similar to that of stratum corneum (SC), the outermost layer of the skin, although VC lacks intercorneocyte desmosomal connections and the lipids are in a less ordered state [1, 5]. Consequently, VC exhibits a viscous fluid character and might therefore be perceived as mobile SC [1, 2, 5, 6].

A variety of biological properties has been assigned to VC. In utero it is suggested to act as a waterproof film promoting the formation of the horny layer of the fetus [1, 6]. During delivery it acts as a lubricant and postnatally it exhibits anti-infective [7], anti-oxidant [8], skin hydrating [9] and skin cleansing properties [4]. Moreover, VC shows a temperature-dependent dehydration behavior, enabling the hydration of the newborn's skin in a sustained manner [9, 10]. Because of these excellent properties, VC holds promise as an effective clinical therapeutic agent promoting the repair of the skin barrier of preterm infants [3, 4] or enhancing wound healing in adult skin [6]. Previously, it was already shown that topical application of native VC on disrupted mouse skin considerably increased the skin barrier recovery, promoted a rapid formation of SC and prevented epidermal hyperproliferation [11]. Application of VC in clinics, however, is restricted by the limited availability of VC and the risk of disease transmission. Therefore, the generation of a synthetic VC equivalent could lead to new biofilms, mimicking closely the unique composition and properties of natural VC. Recently, we presented the development of synthetic VC closely resembling the physicochemical properties of natural VC [12]. These biofilms were composed of particles embedded in a lipid matrix. The particles, structured hydrogel microparticles based on hyperbranched polyglycerol, were prepared by photolithography [13] and used as synthetic corneocytes (referred to as particles) in our biofilms. The lipid matrix consisted of a lanolin-derived synthetic lipid mixture and showed similar composition and organization as natural VC [14]. Various formulations were prepared using different particle:lipid ratios, particles with different initial water-content and uncoated or lipid-coated particles to obtain a biofilm mimicking natural VC [12]. In order to test these new formulations, the use of an animal model is essential to investigate efficacy and safety. An excellent mice model for severe skin barrier disruption and repair was developed previously for this purpose [11]. This model showed a slow recovery (i.e. 8 days) and is appropriate to evaluate the effect of formulations on recovery.

The present study aims to investigate whether topical application of our synthetic biofilms supports and accelerates the recovery of the murine skin barrier, disrupted by sequential tape stripping. Various biofilms were applied topically on the disrupted mouse skin to determine which formulation could improve and accelerate, such as VC, the skin barrier repair. Changes in transepidermal water loss (TEWL) were used to monitor barrier recovery. In addition, biopsies were harvested to evaluate the recovery of the SC by histology. Results were compared to the effect on disrupted mouse skin of the natural biofilm VC, which showed previously the ability to enhance skin barrier recovery [11], and to that of the commonly used oil-based ointments Vaseline (petrolatum; Vas) and Eucerin cum aqua (Euc).

2. Experimental section

2.1. Materials

Black D-squame (rectangles from 70 mm x 25 mm) was obtained from CuDerm (Dallas, USA). Vaseline (petrolatum) was purchased from Elida Fabergé (London, UK) and Eucerin cum aqua (unguentum alcoholum lanae aquosum; consisting of petrolatum, wool wax alcohols, cetylstearyl alcohol and water) was supplied by Pharminnova B.V. (Warregem, Belgium). Gelatin capsules were provided by Spruyt-Hillen (IJsselstein, The Netherlands). Tissue-Tek® O.C.T.™ Compound was obtained from Sakura Finetek Europe B.V. (Zoeterwoude, The Netherlands). Safranin O was purchased from Sigma (Schnellendorf, Germany).

2.2. Collecting vernix caseosa and extracting its lipids

Vernix caseosa (VC) was scraped off gently immediately after vaginal delivery or cesarean section of healthy full-term neonates. The samples were transferred into sterile plastic tubes and stored at 4ºC until use. The collection of VC was approved by the ethical committee of the Leiden University Medical Center and informed consent was given by the parents.

2.3. Preparation of biofilms

Synthetic biofilms, mimicking closely the unique composition and properties of natural VC, were prepared as described previously [12]. In brief, fully hydrated particles (structured HyPG-MA hydrogel microparticles acting as synthetic corneocytes [13]) were mixed with lipids (mimicking closely lipid composition and organization of natural VC [14]) using an automatic ointment-mixer Topitec® (WEPA, Germany) modified for small-scale purpose. Various formulations were prepared using different particle:lipid ratios (i.e. 2:1 and 5:1) and particles with different initial water-content (i.e. 50% (w/w) and 80% (w/w). Additionally, uncoated or lipid-coated particles were used to obtain biofilms.

The composition of the various formulations is given in Table 1. The particles and lipids were mixed for 5 min with a rotation speed of 400 rpm to obtain a homogeneous biofilm formulation.

2.4. Skin barrier disruption

Nude male mice (Skh-1), 7-9 weeks old and 28 g ± 2 g in weight, were purchased from Charles River Laboratories (St Aubin Les Elbeuf, France). All animal experiments were conducted in conformity with the Public Health Service Policy on use of laboratory animals and had been approved by the Research Ethical Committee of Leiden University (UDEC, no. 07002). The mice were maintained in the animal care facility of the Gorlaeus Laboratories, Leiden University, with temperature- and humidity-controlled room, and fed standard laboratory chow and tap water *ad libitum*.

The animals were anaesthetized using a mixture of Ketamine (150 mg/kg body weight; Nimatek®, Euovet Animal Health B.V., Bladel, The Netherlands) and Xylazine (10 mg/kg body weight; Rompun®, Bayer B.V., Mijdrecht, The Netherlands) by intraperitoneal injection (i.p.). During anaesthesia, the mice were kept on a warm mattress with their face down and their eyes wetted with Visagel® (Eurovet, Bladel, The Netherlands).

Table 1A. *Composition of the various biofilms applied on the disrupted skin*

Entry	Sample	Composition		
		Particle:lipid ratio	**Initial water content particles (% w/w)**	**Lipid coated particles**
B1	2:1_50	2:1	50	No
B1c	2:1_50_coated	2:1	50	Yes
B2	2:1_80	2:1	80	No
B2c	2:1_80_coated	2:1	80	Yes
B3	5:1_50	5:1	50	No
B4	5:1_80	5:1	80	No

Table 1B. *List of the lipid mixtures, natural biofilm and commercially available creams applied on the disrupted skin.*

Entry	Sample
VC lipids	Natural VC lipids without corneocytes
L1	Synthetic lipid mixture
L2	Synthetic mixture without barrier lipids
VC	Vernix caseosa
Vas	Vaseline
Euc	Eucerin

The mice were grouped randomly (six per group), with each group receiving a different treatment. The skin of the mice was washed carefully with deionized water prior to marking two areas (~1 cm^2, both left and right) on the upper flank of the back of the mice, near the head. An impaired skin barrier was induced by sequential tape stripping by a single individual. Tape strips (black D-squame) of ~1 cm^2 were cut and applied on the marked areas. The strips were compressed for 5 seconds before being removed in alternated stripping direction. A severe barrier disruption (i.e. model severe #4 as described in our previous paper) [11], defined as TEWL of 79 ± 6 $g/m^2/h$ (12 tape strips), was induced. After treatment, the mice were housed individually to avoid fight-induced skin injury. No scratching of the treated area or any abnormal behavior was observed during the studies.

2.5. Topical applications

Immediately after disruption of the skin barrier, one test area per mice was treated with natural VC, Vaseline, Eucerin cum aqua or with one of the biofilm formulations (Table 1; 5 mg/cm^2). Additionally, various lipid mixtures were evaluated: synthetic lipid mixtures (synthetic counterpart of isolated VC lipids; L1) and a similar synthetic mixture without the barrier lipids ceramides, free fatty acids and cholesterol (L2) and isolated VC lipids [14]. A single individual applied the samples onto the treatment area with a spatula. The bilateral untreated site served as control.

2.6. Biophysical evaluation of the skin

2.6.1. Macroscopic observations

Digital photographs were taken at predetermined time points using a canon ixus 40 (Canon Inc., Japan). The photographs of at least three mice were blinded and then independently scored by three independent investigators. The redness as well as the formation of a crust was classified into four different levels: obvious (++), intermediate (+), slight (+/-) or absent (-). The mean of the data was used for interpretation.

2.6.2. Transepidermal water loss

The level of barrier disruption and the repair rate were assessed by measuring the transepidermal water loss (TEWL) at regular time intervals using the Tewameter TM 210 (Khazaka Courage, Cologne, Germany). The TEWL was measured by holding the probe lightly against the test area until a constant TEWL value was obtained. The pressure applied to the probe was just enough to prevent leakage of air between the lower rim of the Teflon cylinder and the skin.

The percentage of barrier recovery was calculated using the following equation: 1 – ((TEWL at indicated time point – TEWL of average control ‘undamaged skin’)/(TEWL immediately after stripping – TEWL of average control ‘undamaged skin’)) × 100%.

The AUC (area under the curve) of the recovery curve was calculated at the initial phase (1 day), at an intermediate period (3 days) and after full recovery (8 days). The different treatments were compared using a one-way ANOVA with a Bonferroni post-test; $P<0.05$ was considered as statistically significant. All data analysis was performed using GraphPad Prism 4.0.

2.6.3. Histology

After the animals were sacrificed, biopsies were taken after 3 and 8 days using a pair of scissors in conjunction with metal tweezers, from the central part of the (treated) sites. The biopsies were immediately placed in a gelatin capsule, processed by fixation in Tissue-Tek®, frozen in liquid nitrogen and stored in liquid nitrogen prior to slicing. Samples (thickness 5 µm) were sliced perpendicular to the skin surface with a cryotome (Leica CM 3050S, Wetzlar, Germany). After fixation in cold acetone (4°C), contrast staining of the sections was performed for 1 min with a 1% (w/v) aqueous safranin solution. Subsequently, the sections were washed with deionized water. To allow the corneocytes to swell, a 2% (w/v) KOH solution was applied on the sections during 20 min [15, 16]. Visualization was performed with a light microscope combined with a digital camera (Carl Zeiss axioskop, Jena, Germany). The thickness of the viable epidermis was measured in at least 12 different locations of the stained cross-sections to obtain the mean.

3. Results and Discussion

3.1. Topical application of various synthetic biofilms on disrupted skin

The disruption of the skin was performed as described previously [11]. After sequential tape stripping (i.e. 12 tape strips) the skin was damaged in a controlled manner yielding a TEWL of 79 ± 6 g/m^2/h. In comparison, normal (undisrupted and untreated) skin has a TEWL of ~9 g/m^2/h. In our previous study we showed that the SC was completely removed after tape stripping while the remaining epidermis was intact. Moreover, a rather slow recovery (i.e. 200 h) was obtained, which makes it an excellent model to study the effect of formulations on both the initial and long-term barrier recovery. In a previous study, topical application of natural VC on this disrupted skin showed that complete recovery was enhanced, suggesting the potential use of VC treatment clinically [11]. Therefore, we studied the effect of formulations mimicking VC on skin barrier recovery in comparison to natural VC and commonly used oil-based ointments (Vas and Euc). The various synthetic formulations and commercially available creams used in this study are given in Table 1.

The base of our synthetic biofilms consisted of particles embedded in a lipid matrix [12]. The various components as well as the particle:lipid ratio, the water content in the particles and the absence or presence of a lipid coating on the particles (Table 1) were varied to select the most optimal biofilm. The various formulations had different effects on redness and crust formation (Table 2), which were rated concerning their severity. The disrupted untreated site was clearly glistening and red following tape stripping, after which a crust was formed. Upon application of natural VC, redness disappeared in a few minutes and crust formation was prevented. Application of the various biofilms on the disrupted skin resulted in different observations (Table 2). The biofilms B1c and B2 (Fig. 1) showed predominantly intermediate crust formation (Table 2), whereas B2c showed both redness and major crust formation. However, it was clearly observed that application of B1 prevented largely both redness and crust formation (Fig. 1; Table 2): only after 1 and 3 days a slight crust formation was observed. Macroscopic observations (Fig. 1) showed once more that B1 improved skin conditions compared to the other biofilms, in which B2 was selected as representative.

Table 2. *Rating of redness and crust formation of the disrupted sites followed in time. The average evaluation of digital pictures from three independent investigators is presented.*

Treatment	**Rating in time***			
	8h	**1d**	**3d**	**5d**
untreated	++	++	++	+
VC	-	-	-	-
B1	-	+/-	+/-	-
B1c	+/-	+/-	+	-
B2	+/-	+/-	+	-
B2c	+/-	+/-	+/-	+/-
B3	+/-	+	+	-
B4	+/-	+/-	+	-
Vas	+/-	+/-	+/-	-
Euc	+/-	+/-	+/-	-
L1	-	+/-	+/-	-
L2	+/-	+/-	+/-	-

** Redness and crust formation on skin were assessed as obvious (++), intermediate (+), slight (+/-) or absent (-)*

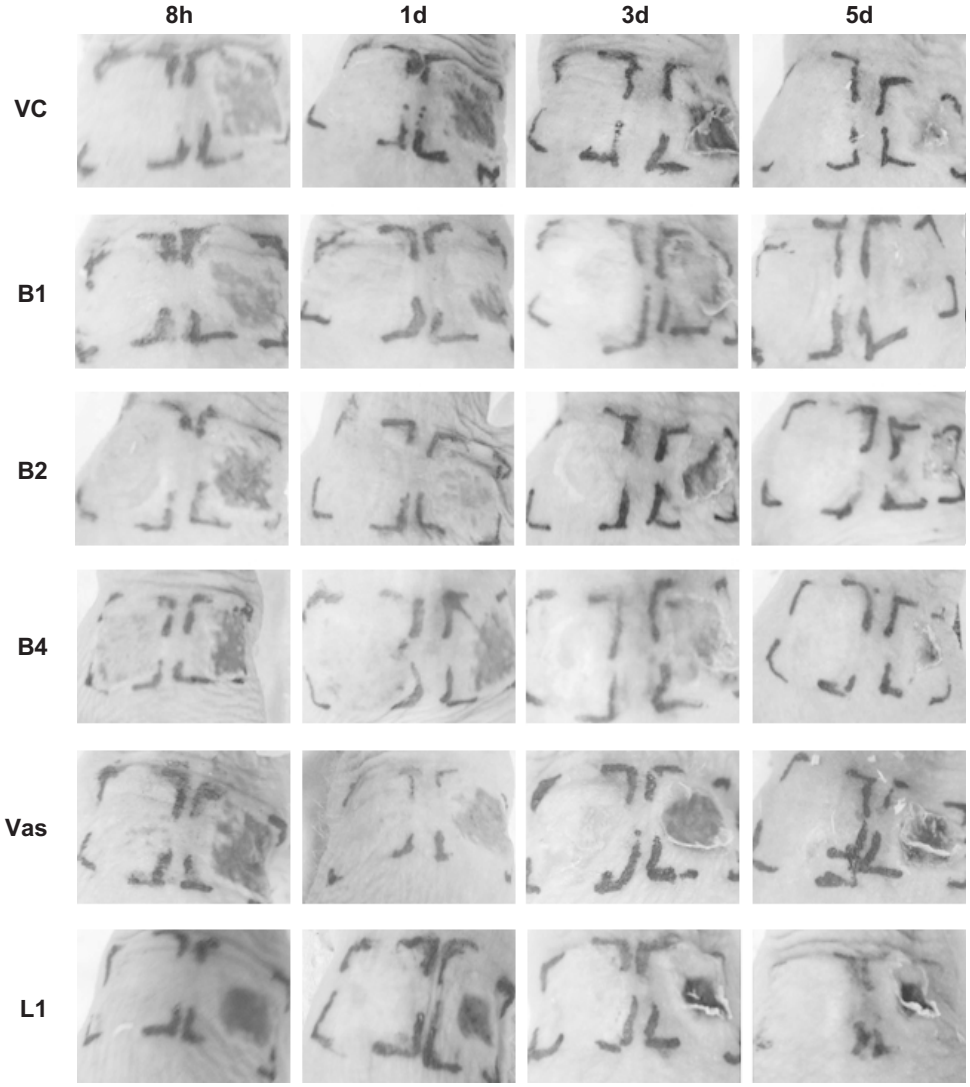

Figure 1. *Representative macroscopic observations of the effect of topically applied native VC, the biofilms B1, B2 and B4, Vas and lipid mixture L1 on disrupted skin after 8 h, 1 day, 3 days and 5 days. Formulations were applied on the left side and the right side served as disrupted, untreated control.*

The recovery of the skin was also monitored by TEWL measurements (Fig. 2). Initially the effect of the biofilm mimicking most closely the properties (in terms of water level in the particles, lipid composition and the presence of a lipid coating) of VC on barrier

recovery was studied. This biofilm, referred to as biofilm B2c, consisted of a particle:lipid ratio of 2:1 using lipid coated particles with an initial water content of 80% (w/w). It was observed that upon application of this biofilm B2c (5 mg/cm^2) on disrupted skin, complete recovery occurred already within ~100 h as compared to ~200 h for untreated disrupted skin (Fig. 2A). The inset (Fig. 2A) shows the initial recovery period (phase 1) where a rapid barrier recovery was observed (TEWL decreased from 79 ± 6 g/m^2/h to 38 ± 6 g/m^2/h). Visually, the biofilm B2c disappeared within 3 to 4 h (phase 2, Fig. 2A). As the skin was not fully recovered a high TEWL was measured (56 ± 5 g/m^2/h; barrier recovery of 34 ± 6%). Further monitoring of the skin barrier (phase 3, Fig. 2A) showed complete recovery within 100 h. Upon application of biofilm B2c, the initial recovery was similar to VC treated skin, whereas the recovery period between 3 and 75 h was slower. Complete recovery, however, occurred within the same time span (i.e. 100 h) as VC treated skin. When decreasing the initial water content of the particles to 50% (w/w) and maintaining other components equal including the particle coating (biofilm B1c; Table 1), a similar barrier recovery profile as for biofilm B2c was obtained (Fig. 2A). A comparable skin barrier repair outcome was also obtained (Fig. 2A) when applying biofilm B2 on disrupted skin. B2 is very similar to B2c, except that uncoated particles were used. The particle:lipid ratio of this biofilm B2 was 2:1 and the initial water content of the microgels 80% (w/w; Table 1). A biofilm composed of uncoated particles with 50% (w/w) initial water content and particle:lipid ratio of 2:1 (biofilm B1; Table 1), however, showed a different profile. Up to 10 h, the barrier recovery profile was still comparable to the biofilms B1c, B2, B2c and VC (see inset Fig. 2A). However, from that moment (i.e. 10 h after stripping) until complete recovery the profile was similar to that of VC and, hence, more rapid compared to the other biofilms. Moreover, complete recovery was already obtained within 75 h, which is slightly faster than VC (i.e. 100 h). Overall, B1 mimics most closely the barrier recovery profile of VC (based on TEWL data).

Aforementioned, only the effect of various formulations with a particle:lipid ratio of 2:1 was shown. However, we observed previously that biofilms with a 5:1 particle:lipid ratio showed a more dense and random particle distribution and a higher water content more closely mimicking the corneocyte distribution and water level in VC [12]. Therefore, the topical application of biofilms with a particle:lipid ratio of 5:1 with an initial water content of 80% (w/w) or 50% (w/w) in the particles (biofilm B3 and B4, respectively; Table 1) was also evaluated. Lipid coating on the particles was omitted as this did not increase barrier recovery for the 2:1 particle:lipid formulations (Fig. 2A). Topical application of B3 and B4 on disrupted skin resulted predominantly in intermediate crust formation (Table 2; Fig 1). TEWL measurements showed a complete recovery within 150 h after application of both biofilms (Fig. 2B). Application of B3 and B4 (5 mg/cm^2) decreased only slightly the TEWL from 79 ± 6 g/m^2/h to 62 ± 7 g/m^2/h and 61 ± 8 g/m^2/h, respectively (barrier recovery increased to 20 ± 7% and 21 ± 8%, respectively, indicated as phase 1 in Fig. 2B).

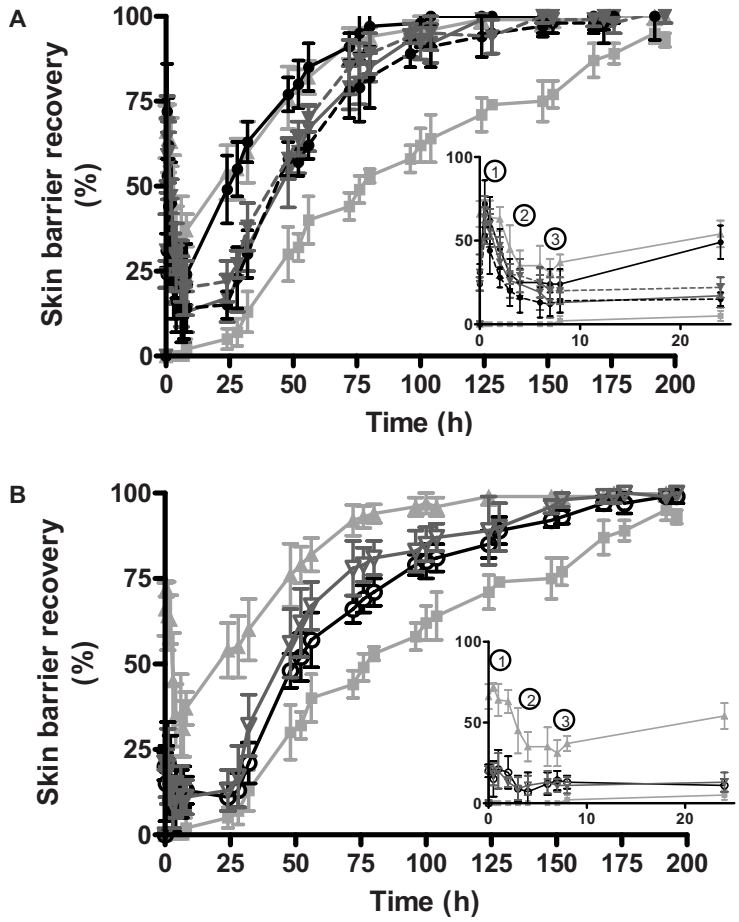

Figure 2. *Skin barrier recovery after tape stripping as function of time and after application of various formulations. (A) Formulations with particle:lipid ratio 2:1, B1 (●; continuous line), B1c (●; dotted line), B2 (▼; continuous line) and B2c (▼; dotted line) are depicted and compared to VC (▲; 5 mg/cm^2) and undisrupted skin (■). (B) Formulations with particle:lipid ratio 5:1, B3 (o), B4 (▽), are depicted and compared to VC (▲; 5 mg/cm^2) and undisrupted skin (■). The inset shows the recovery during the first 24 h that can be divided into three distinct stages: in phase 1 the formulations covered the skin, in phase 2 the formulations disappeared and in phase 3 further monitoring of the skin barrier was performed. Data are shown as average ± SD (n = 6).*

Within 1 to 2 h the biofilms B3 and B4 disappeared visually (phase 2, Fig. 2B). The skin was not fully recovered as indicated by a TEWL of 71 ± 6 and 69 ± 4 g/m^2/h, respectively. Further skin barrier repair was monitored (phase 3, Fig. 2B) until complete recovery was achieved (i.e. 150 h). Apparently, increasing the initial water content of the particles (i.e. B4 compared to B3; Fig. 2B) or increasing the amount of particles (e.g. B4 compared to B2; Fig. 2) did not further improve the skin barrier repair. This might also be due to the lower lipid content of the formulations B3 and B4, as these biofilms contain less lipids compared to the formulations B1, B1c, B2 and B2c (i.e. 16.7% vs. 33.3%) as was shown previously [12]. Moreover, when comparing water release from the biofilms as was described previously [12], it is observed that initial high water release from the biofilms resulted in more enhanced barrier repair compared to the sustained water release from the pre-coated microgels (i.e. B1 vs. B1c, respectively).

The effect of the biofilms on the recovery of extensively disrupted skin was also histologically studied. Normal skin is characterized by viable epidermal cells and stratum corneum containing 4 to 6 corneocyte layers (Fig. 3a). After complete barrier disruption, using the tape stripping method applied in this study, the SC was removed (Fig. 3b) [11]. Three days after tape stripping, corneocytes gradually reappeared on disrupted, untreated skin (Fig. 3c) whereas only 8 days after recovery, similar to normal murine SC, untreated skin exhibits 3-5 corneocyte layers (Fig. 3d). Morphological features of biofilm-treated skin after 3 and 8 days are depicted in Figure 3: biofilms B1, B2 and B4 were chosen as representative for this purpose. After 3 days, the presence of 3-5 corneocyte layers was observed (Fig. 3) for all biofilms. However, the viable epidermis was largely thickened for B2 and B4, similar to disrupted, untreated skin (Fig. 3c). Epidermal thickening has been partly associated with hyperproliferation [17]. Application of B1 on the disrupted skin showed a normal thickness of the viable epidermis (Fig. 3e, f) indicating a higher stage in the healing process. After 8 days, the various treatments (Fig. 3) showed similar results in SC and viable epidermis appearance compared to normal hairless mouse skin (Fig. 3a). In addition, the average thickness of the viable epidermis was determined by measuring 12 random locations of the biopsies. The data obtained 3 and 8 days after treatment are presented in Figure 4. After 3 days, the viable epidermis of B2 and B4 was up to 4 times thicker compared to the negative control (undisrupted, untreated skin). Upon treatment with B1, however, the thickness of the epidermis after 3 days was 31.0 ± 8.9 µm and comparable to VC treated skin (i.e. 25.2 ± 4.8 µm). After 8 days, the thickness of the epidermis of all biofilm-treated areas was similar to undisrupted untreated skin. In comparison, the disrupted untreated skin still showed a 2 times thicker epidermis compared to undisrupted skin.

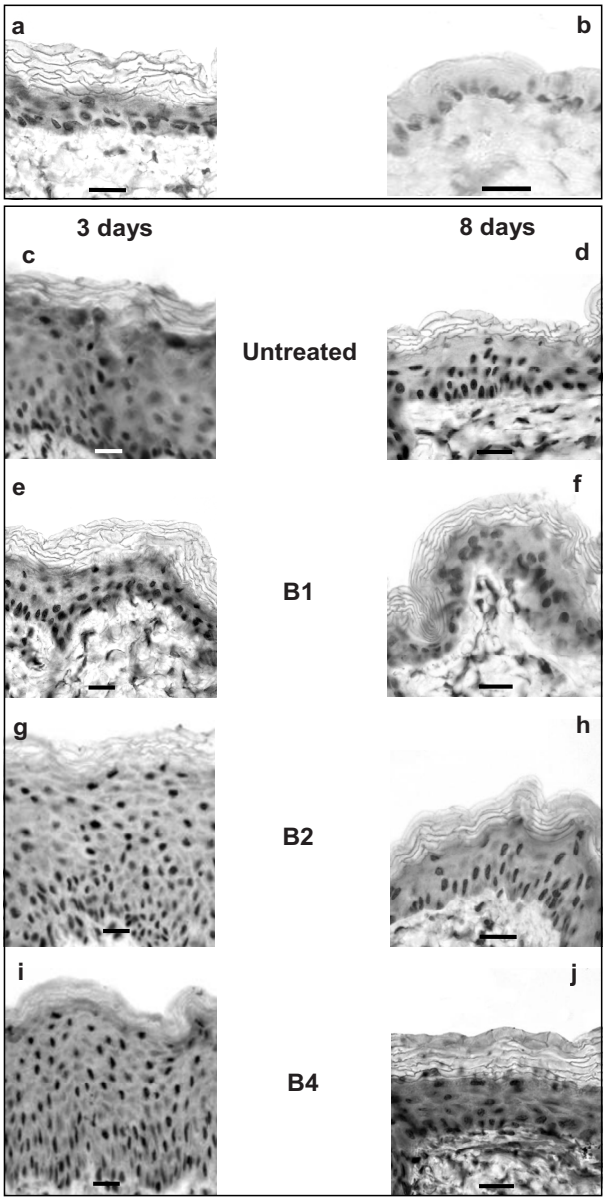

Figure 3. *Cross-sections of hairless mouse skin prior to (a) and directly after tape stripping (b). And cross-sections of tape stripped hairless mouse skin without treatment (c, d) or treated with B1 (e, f), B2 (g, h) or B4 (i, j) after 3 days and 8 days of recovery, respectively. Scale bar is 20 µm.*

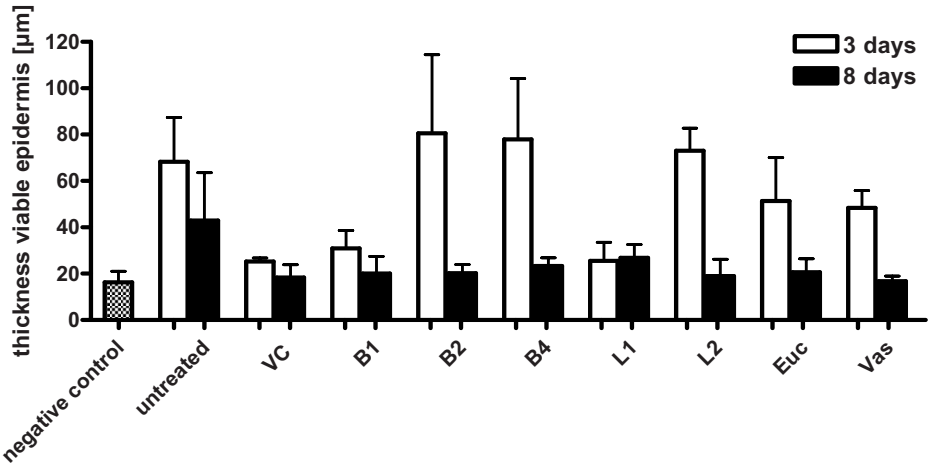

Figure 4. *Thickness of the viable epidermis of undisrupted untreated (negative control), disrupted untreated or disrupted treated hairless mouse skin after 3 (white) and 8 days (black) of recovery. At least 12 different random locations of the cross-sections were measured per treatment. Data is shown as average ± SD.*

3.2. Topical application of lipid formulations on disrupted skin

B1, the biofilm inducing the most accelerated barrier recovery, was also applied on the disrupted skin using 15 mg/cm^2. TEWL measurements showed a similar barrier recovery profile (data not shown) as was obtained for the biofilm B1 applied at 5 mg/cm^2 (Fig. 2A). To determine whether the lipids play a role in the recovery, the effect of lipids in the absence of particles (formulation L1, 5 mg/cm^2; Table 1) on barrier recovery was evaluated as well. It was observed that application of L1 showed similar effect as B1: redness and crust formation were largely prevented (Fig. 1; Table 2) and hence only slight curst formation was observed after 1 and 3 days. However, when omitting the barrier lipids (i.e. cholesterol, fatty acids, and ceramides [12, 14]) from the lipid matrix (lipid mixture L2), prevention of redness and crust formation was less effective compared to L1 and B1 (Table 2). Treatment with L2 resulted in occurrence of a crust and/or redness after 8 h to 3 days.

TEWL measurements showed that application of L1 (Fig. 5) on the disrupted skin resulted in a similar barrier recovery as observed for the biofilms B1c, B2 and B2c (Fig. 2A). Application of L2, which has similar lipid composition as L1 but without the barrier lipids, on disrupted skin, decreased clearly the barrier recovery (Fig. 5): complete barrier recovery was obtained within 150 h compared to 100 h for L1. The histological assessment also indicates an improved recovery with L1 compared to L2 (Fig. 6).

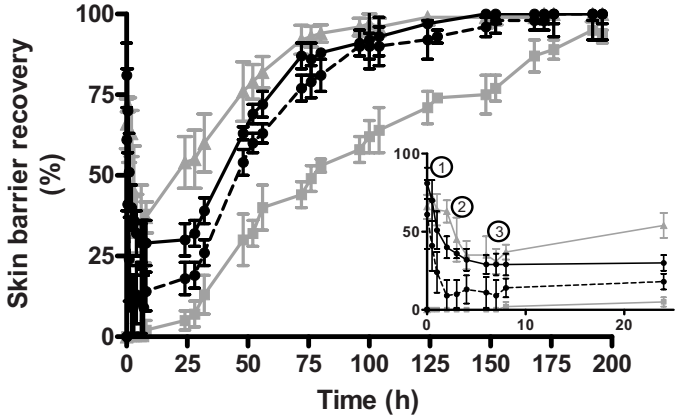

Figure 5. *Skin barrier recovery after tape stripping as function of time and after application of various formulations. Synthetic lipid mixture L1 (●; continuous line) and synthetic lipid mixture without barrier lipids L2 (●; dotted line) are depicted and compared to VC (▲; 5 mg/cm^2) and undisrupted skin (■). The inset shows the recovery during the first 24 h. In the initial phase (phase 1) the formulations covered the skin and in phase 2 the formulations disappeared (phase 2). In phase 3 further monitoring of the skin barrier was performed. Data are shown as average ± SD (n = 6).*

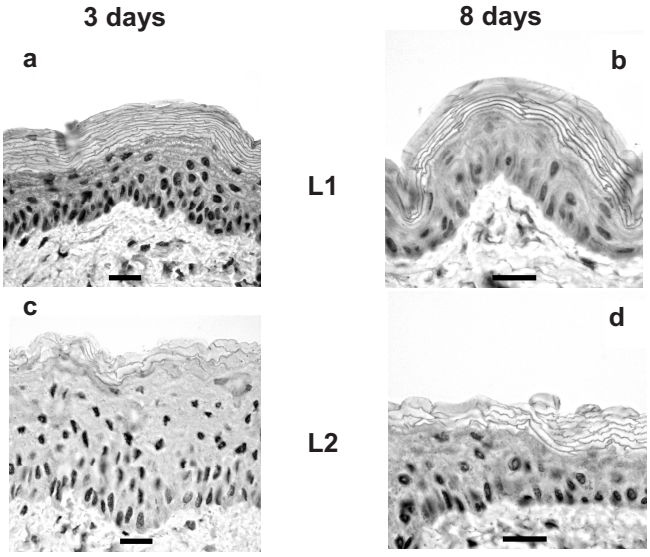

Figure 6. *Cross-sections of tape stripped hairless mouse skin treated with L1 (a, b) and L2 (c, d) after 3 days or 8 days of recovery. Scale bar represents 20 µm.*

In addition, a very thick SC (~10 layers; Fig. 6a) was observed after 3 days of recovery for L1 whereas L2 only showed 3 layers (Fig. 6c). Despite the thick SC, the TEWL is still increased indicating a perturbed barrier. Upon application of L2 also the viable epidermis was thicker compared to L1-treatment after 3 days (Fig. 4), which in turn was comparable to undisrupted, untreated skin. After 8 days the thickness of the epidermis with both treatments (Fig. 6b, 6d, respectively) are similar to normal skin (Fig. 3a). Hence, it was showed that microscopic observations and rating after topical application of L1 on disrupted skin were similar to the most optimal biofilm B1, although the skin barrier recovery profile was not as effective (i.e. 100 h and 75 h, respectively, for complete barrier recovery). Moreover, the presence of barrier lipids (L1 vs. L2) is of major importance as they promoted barrier repair as was observed previously [18, 19]. The lipid formulation L1 contains about 10% of barrier lipids [12]. It was shown in literature that lipid mixtures containing ceramides (using acyl-ceramides isolated from mouse skin), fatty acids and cholesterol, increase the barrier recovery in acetone disrupted, hairless mouse skin [18]. Although our lipid mixture contains synthetic (acyl-) ceramides, also a clearly improved barrier recovery rate was observed between these lipid mixtures and lipids without barrier lipids (Fig. 5). Mechanistically, this effect can be attributed to the uptake of the barrier lipids by the viable epidermal cell layers where they can be incorporated in the lamellar bodies and at a latter stage may be involved in the formation of the intercellular lamellae [20, 21].

3.3. Topical application of Vaseline and Eucerin on disrupted skin

The effect of the aforementioned formulations mimicking VC on skin barrier recovery where also compared to the commonly used oil-based ointments Vaseline (Vas) and Eucerin cum aqua (Euc). Vas has been speculated to be occlusive and to increase barrier recovery [22, 23]. Euc is a water-in-oil emulsion that contains large amounts of water (i.e. 50%) [1], which is known to be of high importance in wound healing. It was observed that upon application of Vas on disrupted skin the redness did not disappear within the first hours as opposed to VC. Two hours after application, Vas was not visible anymore at the skin surface and the skin had a similar appearance as disrupted, untreated skin although crust formation was largely prevented (Fig. 2). Upon application of Euc, the emulsion was not visible anymore after 2 h and the redness almost completely disappeared (not shown). Crust formation, however, was not completely prevented. The treatments showed a slight crust development, indicating an improved wound healing compared to untreated but clearly less effective than native VC (Table 2).
The recovery of the disrupted skin, untreated and after application of Vas and Euc, was also monitored by TEWL measurements at various time points (Fig. 7). Application of Vas (5 mg/cm^2) immediately restored the barrier function of the skin (indicated as phase 1 in Fig. 7; TEWL decreased from 79 ± 6 g/m^2/h to 3 ± 0.5 g/m^2/h) demonstrating

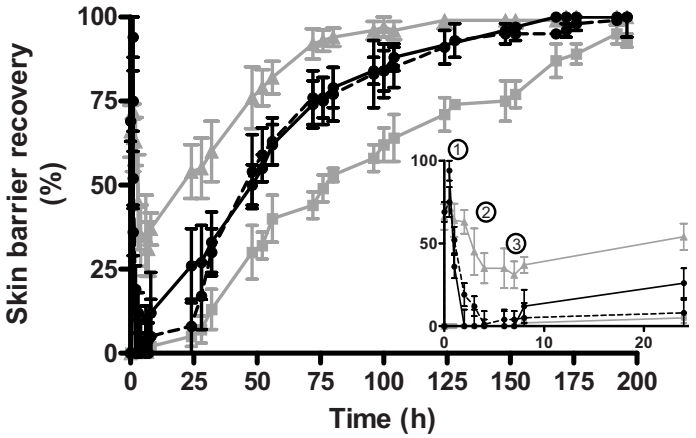

Figure 7. *Skin barrier recovery after tape stripping as function of time and after application of various formulations. The commonly used oil-based ointments Vas (●; continuous line) and Euc (●; dotted line) are depicted and compared to VC (▲; 5 mg/cm^2) and undisrupted skin (■). The inset shows the recovery during the first 24 h. In the initial phase (phase 1) the formulations covered the skin and in phase 2 the formulations disappeared (phase 2). In phase 3 further monitoring of the skin barrier was performed. Data are shown as average ± SD (n = 6).*

the occlusive properties of Vas. As mentioned, Vas disappeared visually within 2 h, which was associated with a higher TEWL (phase 2, Fig. 7). Four hours after application the TEWL was 77 ± 7 g/m^2/h; for untreated disrupted skin the TEWL was in the same range. Subsequent monitoring of the skin barrier showed that complete recovery occurred within 150 h (phase 3, Fig. 7). An immediate restored skin barrier function was observed as well upon application of Euc (TEWL decreased from 73 ± 5 g/m^2/h to 25 ± 8 g/m^2/h; phase 1 in Fig. 7). Four hours after application Euc disappeared visually and TEWL increased to 74 ± 8 g/m^2/h (phase 2, Fig. 7). The subsequent recovery profile (phase 3, Fig. 7) was similar to Vas and complete recovery was observed within 150 h. Since the disrupted, untreated skin showed nearly complete recovery within 200 h, application of both Vas and Euc did enhance barrier recovery to some extent. However, when comparing the effect of Vas and Euc to natural VC (Fig. 7; [11]) or to our biofilms (Fig. 2), barrier recovery was slower (i.e. 150 h compared to 75-100 h, respectively).

Subsequently, the effect of Vas and Euc on the recovery of extensively disrupted skin was histologically studied. Vas and Euc treated skin showed the presence of 5-6 corneocyte layers 3 days after recovery and after 8 days no major differences in SC could be observed (data not shown). However, it was observed that both Vas and Euc showed thickened viable epidermis (i.e. 2.5 times thicker epidermis compared to undisrupted skin) after 3 days of recovery (Fig. 4). The average thickness of the viable epidermis was determined by measuring 12 random locations of the biopsies. After

8 days, the thickness of the epidermis of the Vas and Euc treated areas was similar to undisrupted untreated skin (Fig. 3a). In comparison, the disrupted untreated skin still showed a 2 times thickened epidermis compared to undisrupted skin.
In summary, macroscopic observations, TEWL measurements as well as histological analysis showed that barrier recovery was enhanced and that crust formation was partly prevented upon application of Vas or Euc on disrupted skin, however, not as effective as VC or the most optimal biofilm B1. In agreement with the literature [21], our results indicate that the barrier lipid containing biofilms perform better than Vas (from 8 h onwards), whereas in the initial recovery phase Vas treatment shows lower TEWL values which can be attributed to the occlusive nature of Vas.

3.4. Comparison of the recovery after the various treatments

In order to evaluate the recovery curves of the various treatments in a statistic manner, the AUC's of the individual treatments were calculated and compared. The results after 1, 3 and 8 days of recovery are presented in Figure 8. In general, the same trends can be observed for all 3 time points: disrupted untreated skin (white bars) exhibits the lowest AUC compared to disrupted treated (applied for all treatments) skin, indicating the lowest recovery rate. After 3 and 8 days, natural VC showed significant better recovery than Vas and Euc, however, no significant difference to the best biofilm, i.e. B1. In turn, B1 demonstrated a significant improved recovery versus B1c, B3, B4, L2, Vas and Euc after both 3 and 8 days. Moreover, B1 showed a significant improvement of barrier recovery after 3 days compared to L1, although after 8 days the difference between both formulations was not significant.
It has been suggested that the water-handling properties are of major importance for the proper functioning of a VC substitute [24]. We therefore optimized the water release from the biofilms in our previous study [12], mimicking as closely as possible the water release rate from VC. When focusing on the water release rate from the various biofilms, no clear correlation was observed between the skin barrier repair rate and the water release rate from the biofilms. However, it was observed that the biofilm with the fastest water release rate, biofilm B1, resulted in a better performance than the other biofilms concerning crust formation (table 2), epidermal thickening (Fig. 4) and barrier recovery (Fig. 2A). When comparing the biofilms with a different particle/lipid ratio, it is obvious that the biofilms with a 2:1 particle/lipid ratio resulted in a better performance than the biofilms with a 5:1 particle lipid ratio. This indicates that the amount of lipids might play an important role for the biological effect. Therefore, also with respect to natural VC, the question arises how important are the water-handling properties as well as the presence of corneocytes for barrier recovery? Therefore, we examined also the barrier recovery of VC lipids in the absence of water and corneocytes. These studies revealed that VC lipids resulted in a similar barrier recovery as was observed for natural VC (Fig. 6). This is very

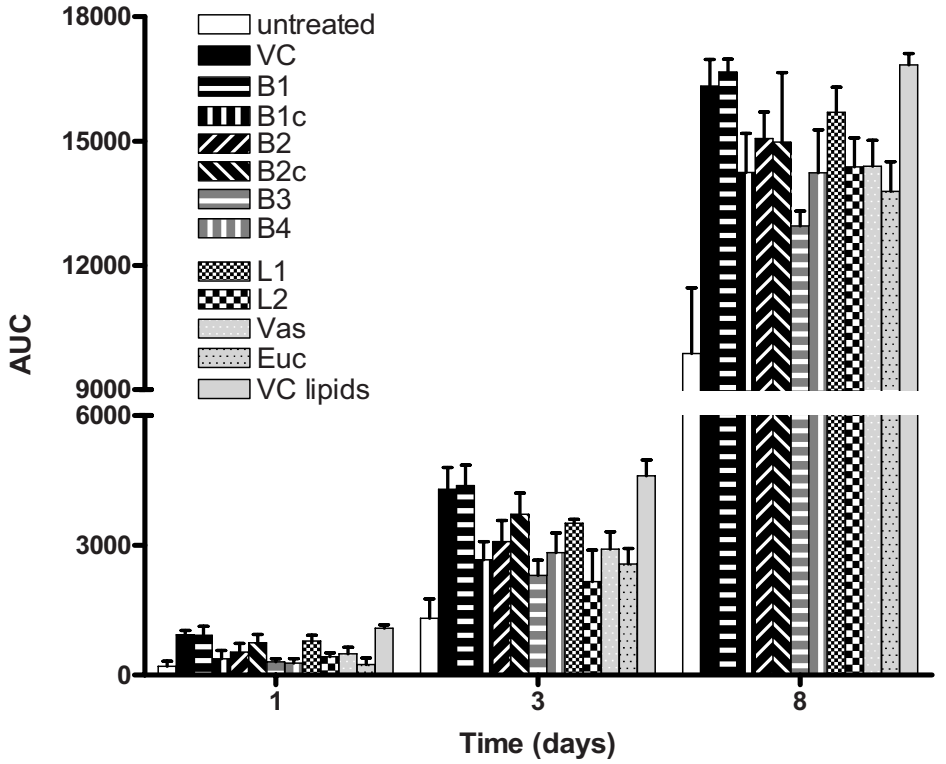

Figure 8. *Area under the curve (AUC) of the recovery curves after tape stripping of hairless mouse skin after 1, 3 and 8 days of recovery. All treatments are depicted: untreated (white), VC treated (black), B1-B1c-B2-B2c (black and white; striped), B3-B4 (grey and white; striped), L1-L2 (black and white; checked), Vas-Euc (grey; dotted) and isolated VC lipids (grey). Data is represented as average ± SD (n = 6).*

similar to the results that were obtained for the synthetic biofilms vs. the lipid formulation without water and particles (L1), but in the presence of barrier lipids. This demonstrates that the lipids, including barrier lipids, play a more prominent role in barrier recovery than the water content and the presence of corneocytes. However, the water-containing corneocytes may be very beneficial for increasing skin hydration, especially important for the treatment of dry and diseased skin. Importantly, the particles (synthetic corneocytes) can also be used as drug delivery matrix in our biofilm formulation. Incorporation of e.g. growth factors or natural moisturizing factor is an attractive approach and will be subject of future studies.

The obtained results indicate that for an improved barrier recovery several aspects are important for the formulation. I) Besides the presence of barrier lipids, the initial high

water release from the formulations as observed for B1 (likely due to a low particle:lipid ratio and particles without lipid coating) [12] appears to be beneficial. In contrast, native VC exhibited a fast barrier recovery rate, although a very slow water release and only little water in the external lipid matrix was reported for the natural biofilm [5]. This enhancement of barrier recovery might be explained by the fact that VC comprises a number of components (e.g. antioxidants such as alpha-tocopherol) that might stimulate the epidermal metabolism [8]. II) Occlusion of impaired skin (i.e. application of Vas) only enhances recovery to a small extent whereas a more permeable formulation (i.e. lipid mixtures) seems more suitable. III) A balanced ratio of particles, water and lipids is necessary to obtain barrier recovery. This clearly indicates that the presence of both the barrier lipids and the highly hydrated particles (initial water content 50% (w/w)) in a specific ratio are necessary to obtain the most optimal biofilm inducing a fast skin barrier repair similar to native VC.

4. Conclusion

A clear improvement of skin barrier recovery, reduced crust formation and epidermal hyperproliferation was demonstrated upon application of all tested formulations. However, the synthetic VC analogues showed stronger effects concerning the recovery rate than Vas and Euc, especially biofilm B1 mimicked the effects of native VC most closely. The importance of the presence of individual components, i.e. barrier lipids and water, as well as the ratio of these components was observed. In future, these biofilms will be tested in humans to demonstrate their beneficial effect with a potential use of the particles as drug delivery system.

References

1. Pickens WL, Warner RR, Boissy YL, Boissy RE, Hoath SB. Characterization of vernix caseosa: water content, morphology, and elemental analysis. *J Invest Dermatol* 2000; 115(5): 875-881.
2. Hoath SB, Pickens WL, Visscher MO. The biology of vernix caseosa. *Int J Cosmetic Sci* 2006; 28: 319-333.
3. Hoeger PH, Schreiner V, Klaassen IA, Enzmann CC, Friedrichs K, Bleck O. Epidermal barrier lipids in human vernix caseosa: corresponding ceramide pattern in vernix and fetal skin. *Br J Dermatol* 2002; 146(2): 194-201.
4. Moraille R, Pickens WL, Visscher MO, Hoath SB. A novel role for vernix caseosa as a skin cleanser. *Biol Neonate* 2005; 87(1): 8-14.
5. Rissmann R, Groenink HW, Weerheim AM, Hoath SB, Ponec M, Bouwstra JA. New insights into ultrastructure, lipid composition and organization of vernix caseosa. *J Invest Dermatol* 2006; 126: 1823-1833.
6. Haubrich KA. Role of Vernix caseosa in the neonate: potential application in the adult population. *AACN Clin Issues* 2003; 14(4): 457-464.
7. Akinbi HT, Narendran V, Pass AK, Markart P, Hoath SB. Host defense proteins in vernix caseosa and amniotic fluid. *Am J Obstet Gynecol* 2004; 191(6): 2090-2096.
8. Pickens WL, Zhou Y, Wickett RR, Visscher MO, Hoath SB. Antioxidant defense mechanisms in vernix caseosa: potential role of endogenous vitamin E. *Pediatr Res* 2000; 47: 425A.
9. Visscher MO, Narendran V, Pickens WL, LaRuffa AA, Meinzen-Derr J, Allen K, Hoath SB. Vernix caseosa in neonatal adaptation. *J Perinatol* 2005; 25(7): 440-446.
10. Rissmann R, Groenink HW, Gooris GS, Oudshoorn MHM, Hennink WE, Ponec M, Bouwstra JA. Temperature-Induced Changes in Structural and Physicochemical Properties of Vernix Caseosa. *J Invest Dermatol* 2008; 128: 292-299.
11. Oudshoorn MHM, Rissmann R, van der Coelen D, Hennink WE, Ponec M, Bouwstra JA. Development of a Murine Model to Evaluate the Effect Vernix Caseosa on Skin Barrier Recovery. Accepted for publication in *Exp Dermatol* 2008.
12. Rissmann R, Oudshoorn MHM, Kocks E, Ponec M, Bouwstra JA, Hennink WE. Mimicking vernix caseosa - preparation and characterization of synthetic biofilms. *Submitted* 2008.
13. Oudshoorn MHM, Penterman R, Rissmann R, Bouwstra JA, Broer DJ, Hennink WE. Preparation and characterization of structured hydrogel microparticles based on cross-linked hyperbranched polyglycerol. *Langmuir* 2007; 23(23): 11819-11825.
14. Rissmann R, Oudshoorn MHM, Kocks E, Hennink WE, Ponec M, Bouwstra JA. Lanolin-derived lipid mixtures mimic closely the lipid composition and organization of vernix caseosa lipids. Accepted for publication in *BBA Biomembranes* 2008.
15. Ya-Xian Z, Suetake T, Tagami H. Number of cell layers of the stratum corneum in normal skin - relationship to the anatomical location on the body, age, sex and physical parameters. *Arch Dermatol Res* 1999; 291(10): 555-559.
16. Sakai S, Endo Y, Ozawa N, Sugawara T, Kusaka A, Sayo T, Tagami H, Inoue S. Characteristics of the epidermis and stratum corneum of hairless mice with experimentally induced diabetes mellitus. *J Invest Dermatol* 2003; 120(1): 79-85.

17. Porter RM, Reichelt J, Lunny DP, Magin TM, Lane EB. The relationship between hyperproliferation and epidermal thickening in a mouse model for BCIE. *J Invest Dermatol* 1998; 110(6): 951-957.
18. Man MM, Feingold KR, Thornfeldt CR, Elias PM. Optimization of physiological lipid mixtures for barrier repair. *J Invest Dermatol* 1996; 106(5): 1096-1101.
19. Yang L, Mao-Qiang M, Taljebini M, Elias PM, Feingold KR. Topical stratum corneum lipids accelerate barrier repair after tape stripping, solvent treatment and some but not all types of detergent treatment. *Br J Dermatol* 1995; 133(5): 679-685.
20. Menon GK, Feingold KR, Elias PM. Lamellar body secretory response to barrier disruption. *J Invest Dermatol* 1992; 98(3): 279-289.
21. Mao-Qiang M, Brown BE, Wu-Pong S, Feingold KR, Elias PM. Exogenous nonphysiologic vs physiologic lipids. Divergent mechanisms for correction of permeability barrier dysfunction. *Arch Dermatol* 1995; 131(7): 809-816.
22. Bautista MI, Wickett RR, Visscher MO, Pickens WL, Hoath SB. Characterization of vernix caseosa as a natural biofilm: comparison to standard oil-based ointments. *Pediatr Dermatol* 2000; 17(4): 253-260.
23. Ghadially R, Halkier-Sorensen L, Elias PM. Effects of petrolatum on stratum corneum structure and function. *J Am Acad Dermatol* 1992; 26(3 Pt 2): 387-396.
24. Tansirikongkol A, Visscher MO, Wickett RR. Water-handling properties of vernix caseosa and a synthetic analogue. *J Cosmet Sci* 2007; 58(6): 651-662.

Synthesis and characterization of hyperbranched polyglycerol substituted with biodegradable and polymerizable side groups

Marion H.M. Oudshoorn, Geert J.W.Segers, Marijn Zeemijer, Wim E. Hennink

Department of Pharmaceutics, Utrecht Institute for Pharmaceutical Sciences (UIPS),
Utrecht University, Utrecht, The Netherlands

8

Abstract

The aim of this work was to develop biodegradable hyperbranched polyglycerol (HyPG) gels, which can potentially be used in biofilms as described in this thesis as well as for drug delivery matrices. HyPG was derivatized with succinylated HPMA ((2-hydroxypropyl) methacrylamide) in dimethyl sulfoxide using *N,N*-dicyclohexylcarbodiimide (DCC) as coupling agent, yielding HyPG-SA-HPMA. HyPG-SA-HPMA hydrogels were obtained by radical polymerization using potassium peroxodisulfate (KPS) as initiator and *N,N,N',N'*-tetramethylethylenediamine (TEMED) as catalyst. The degree of substitution (DS; defined as the percentage of derivatized hydroxyl groups) could be tailored from 7 to 35 by varying the molar ratio of succinylated HPMA to HyPG in the reaction mixture. In these hydrogels two hydrolysable esters were present in the spacer connecting the HPMA and HyPG. A degradation study showed that the ester between the spacer and HyPG was more prone to hydrolysis than the ester between the spacer and HPMA, which is explained by the faster hydrolysis of an ester of a primary alcohol versus an ester of a secondary alcohol.

Rheological analysis showed that the elastic modulus of the gels increased with higher substitution degree. Importantly, it was observed that the gels degrade under physiological conditions (pH 7.2 and 37°C) although rather slowly (i.e. 158 days for DS 7 gels). Hydrogels with DS 20, however, showed a slower swelling and did not reach their maximal swelling after 200 days. To accelerate degradation, the study was repeated at pH 9.6, 37°C: complete degradation was reached after 2 days and 6 days for DS 7 and DS 20 gels, respectively. Consequently, this indicates that degradable systems were obtained.

1. Introduction

In recent years, hyperbranched polymers [1-4] have been introduced as alternative to dendrimers, which are perfectly branched structures but have a labor-intensive synthesis. These hyperbranched structures were previously regarded as poorly-defined due to their relatively broad molecular weight distribution and random branching. Nevertheless, novel synthetic methods have been developed in which substantially better-defined hyperbranched polymers with low polydispersities and predetermined molecular weight were obtained [1, 2, 5, 6]. An example of such a molecule is hyperbranched polyglycerol (HyPG; M_W ranging from $1x10^3$ to $1.4x10^6$ g/mol; $M_W/M_n < 1.5$) [7, 8]. HyPG consists of an inert polyether-backbone with functional hydroxyl-groups at every branch-end. This structural feature resembles the well-known poly(ethylene glycol) (PEG), one of the most studied biocompatible polymers that is widely used in the pharmaceutical and biomedical field [9-12]. It has already been reported in literature that HyPG's are highly biocompatible and moreover thermally and oxidatively more stable than PEG [13-15]. These characteristics make HyPG a promising material for biomedical and pharmaceutical applications [3, 6, 14-16]. Additionally, the large number of reactive functional groups makes HyPG very suitable for further chemical derivatization, e.g. for the design of hydrogels, hydrophilic polymeric networks [17-20]. In this thesis, we reported on HyPG hydrogels both in the form of macro- and microgels that were obtained by radical polymerization of methacrylated HyPG (HyPG-MA; Chapter 3 and 4) [21, 22]. These HyPG-MA hydrogels, however, were essentially non-degradable under physiological conditions because the methacrylate units are directly coupled to the hydroxyl functionalities of HyPG [23]. The development of biodegradable HyPG gels intended for use in biofilms as described in this thesis as well as for drug delivery applications would be advantageous as the degradation kinetics, which in turn will likely depend on the DS and the initial water content of the gel, can be used to control the release kinetics of loaded substances.
This introductory study reports on the development of biodegradable HyPG gels. The prepared hydrogels were characterized for their swelling and degradation properties as well as for their rheological behavior.

2. Experimental section

2.1. Materials

Hyperbranched polyglycerol (M_n 2,000 g/mol, 32 hydroxyl groups per molecule) was purchased from Hyperpolymers GmbH (Freiburg, Germany). Dimethyl sulfoxide (DMSO, $H_2O \leq 0.005\%$), hydroquinone monomethyl ether (MeHQ), methacryloyl chloride, *N,N,N',N'*-tetramethylethylenediamine (TEMED) were purchased from Fluka (Buchs,

Switzerland). 4-(*N,N*-dimethylamino)pyridine (DMAP), DL-1-amino-2-propanol (99+%), *N,N*-dicyclohexylcarbodiimide (DCC, 99%) and succinic anhydride (99+%) were obtained from Acros Chimica (Geel, Belgium). *N,N'*-carbonyldiimidazole (CDI), trifluoroacetic acid (TFA, 99+%, spectrophotometric grade), methyl sulfoxide-d_6 (99.9% atom D) and chloroform-*d* (99.8% atom D) were provided by Sigma-Aldrich (Zwijndrecht, The Netherlands). Sodium hydroxide (NaOH) pellets, triethylamine and potassium peroxodisulfate (KPS) were obtained from Merck (Darmstadt, Germany). Tetrahydrofuran (THF, HPLC grade), diethylether, ethyl acetate, dichloromethane (DCM) and acetonitrile (ACN; HPLC grade) were purchased from Biosolve Ltd. (Valkenswaard, The Netherlands). Magnesium sulphate ($MgSO_4$, 30-38% H_2O) was obtained from BUFA B.V. (Uitgeest, The Netherlands).

2.2. Synthesis of hydroxypropyl methacrylamide

The synthesis of hydroxypropyl methacrylamide (HPMA) was based on the method described by Song et al. for the synthesis of hydroxyethyl methacrylamide [24]. In detail, DL-1-amino-2-propanol (19 ml; 235 mmol) was mixed with 100 ml 1 M NaOH in a cooled round bottom flask and kept on ice. A spatula tip of MeHQ was added to this mixture to prevent premature polymerization of methacryloyl chloride. Next, a mixture of methacryloyl chloride (25 ml; 258 mmol) in DCM (75 ml) was added drop wise to the DL-1-amino-2-propanol solution. Simultaneously, NaOH pellets were added to the mixture to maintain the pH at 8.5, the optimal pH for this reaction. After addition of all methacryloyl chloride, the reaction mixture was allowed to warm to room temperature after which the reaction mixture was stirred overnight at room temperature.

Subsequently, the aqueous and DCM fractions were separated and the DCM fraction was extracted twice with water. MeHQ (~10 mg) was added to the pooled aqueous fractions after which the pH was adjusted to neutral by the addition of 1 M HCl and water was removed at 50ºC under reduced pressure. The remaining oil was dissolved in 200 ml DCM and dried with $MgSO_4$. After filtration, DCM was evaporated to obtain HPMA (72% yield; white solid). The obtained HPMA was characterized by ^{1}H NMR. NMR spectra were obtained on a Gemini 300 MHz spectrometer (Varian Associates Inc. NMR Instruments, Palo Alto, CA, USA).

^{1}H NMR ($CDCl_3$, δ in ppm): 6.32 (s, 1H, CON<u>H</u>CH_2), 5.73 (s, 1H$_\alpha$, $CH_3CC\underline{H}_2CO$), 5.35 (s, 1H$_\beta$, $CH_3CC\underline{H}_2CO$), 3.96 (m, 1H, $CH_2C\underline{H}OHCH_3$), 3.50 (m, 1H$_\alpha$, $NHC\underline{H}_2CHOH$), 3.19 (m, 1H$_\beta$, $NHC\underline{H}_2CHOH$), 1.95 (s, 3H, $C\underline{H}_3CCH_2$), 1.20 (d, 3H, $CH_2CHOHC\underline{H}_3$).

2.3. Attempted derivatization of HyPG with HPMA using carbonyldiimidazole (CDI)

N,N'-carbonyldiimidazole (CDI; 6 g; 37 mmol) was dissolved in 60 ml DCM under a nitrogen atmosphere at room temperature. Additionally, HPMA (2 g; 14 mmol) was dissolved in 20 ml DCM and added dropwise to the CDI solution. After 1 h stirring at

room temperature, the mixture was washed 3 times with an equal amount of water and subsequently the DCM-layer was dried with $MgSO_4$. After filtration, DCM was evaporated and the obtained product (HPMA-Cl) put under vacuum for 1 h. The obtained product was characterized by ^{1}H NMR.

In the next step, HPMA-Cl was coupled to the hyperbranched polyglycerol (HyPG). Therefore, 1 g HyPG (16 mmol OH groups) was dissolved in 9 ml DMSO at room temperature under a nitrogen atmosphere. Next, DMAP (0.2 g; 2 mmol) and a certain amount of HPMA-Cl (0.2 to 2.2 g; 1 to 10 mmol), depending on the aimed degree of substitution, was added. The mixture was stirred at various temperatures (4°C, 20°C and 50°C) and samples were taken at regular time intervals. Samples were added to diethyl ether to precipitate the product that was subsequently was washed three times with the same solvent. The obtained product was analyzed by ^{1}H NMR.

2.4. Derivatization of HyPG with HPMA using succinic anhydride (SA)

2.4.1. Synthesis of succinylated HPMA

Succinic anhydride (3.5 g; 35 mmol), HPMA (5 g; 35 mmol) and triethylamine (9 ml; 64 mmol) were dissolved in 100 ml freshly distilled THF. Next, MeHQ (~10 mg) was added to prevent premature polymerization and the reaction mixture was stirred overnight at room temperature under a nitrogen atmosphere. Next, the reaction mixture was concentrated under reduced pressure. This crude mixture was dissolved in 100 ml carbonate solution (50 mM) and washed three times with 25 ml DCM. The pH of the aqueous fraction was lowered to 3, using 1 M HCl, and subsequently extracted twice with 100 ml DCM. The DCM fractions were pooled and dried with $MgSO_4$, filtrated and concentrated under reduced pressure to obtain succinylated HPMA (HPMA-SA; 74% yield). The obtained product was analyzed by ^{11}H NMR ($CDCl_3$, δ in ppm): 6.32 (s, 1H, CON$\underline{H}$CH$_2$), 5.70 (s, 1H$_\alpha$, CH$_3$CC$\underline{H}_2$CO), 5.33 (s, 1H$_\beta$, CH$_3$CC$\underline{H}_2$CO), 5.08 (m, 1H, CH$_2$C$\underline{H}$OCH$_3$), 3.55 (m, 1H$_\alpha$, NHC$\underline{H}_2$CHO), 3.38 (m, 1H$_\beta$, NHC$\underline{H}_2$CHO), 2.69 (m, 2H, COC$\underline{H}_2$CH$_2$COOH), 2.60 (m, 2H, COCH$_2$C$\underline{H}_2$COOH), 1.95 (s, 3H, C$\underline{H}_3$CCH$_2$), 1.22 (d, 3H, CH$_2$CHOC$\underline{H}_3$).

2.4.2. Synthesis of HyPG-SA-HPMA using succinylated HPMA

HyPG (0.3 g; 4.8 mmol OH groups) and HPMA-SA (1 g; 4.2 mmol; for quantitative conversion of the OH groups) were dissolved in 5 ml DMSO (H_2O≤0.005%) at room temperature. Next, DMAP (0.1 g; 1 mmol) and DCC (1 g; 5 mmol) were added and the reaction mixture was stirred overnight at room temperature under a nitrogen atmosphere. Next, the mixture was filtrated, to remove the formed dicyclohexylurea. The HyPG derivatized with succinylated HPMA (referred to as HyPG-SA-HPMA) was precipitated in 50 ml diethyl ether and washed three times with the same solvent. The DS, defined as the percentage of derivatized hydroxyl groups, of the obtained product was determined

by ^{1}H NMR spectroscopy. The reaction kinetics was evaluated by taking samples of 0.3 ml at regular time intervals. Samples were filtered, added to diethyl ether to precipitate the product, which was subsequently washed three times with the same solvent. The degree of HPMA substitution was determined by ^{1}H NMR spectroscopy. The substituted HPMA-SA groups were identified by the signals of the methacryloyl group at 5.33 and 5.70 ppm (protons of the double bond H_{α} and H_{β}, respectively). With the protons of HyPG detected between 3.1 and 3.6 ppm (H_p, on average 5 protons per repeating unit) the degree of substitution is calculated as follows:

$$DS = \frac{(H_a + H_b)/2}{H_p/5} * 100\%$$

2.5. Degradation kinetics of HyPG-SA-HPMA

The degradation kinetics of unpolymerized HyPG-SA-HPMA (DS 7) was studied by dissolving 20 mg HyPG-SA-HPMA in 100 ml 100 mM carbonate buffer pH 9.6 (polymer concentration 200 µg/ml) and subsequently incubating this polymer solution at 37˚C.

At regular time intervals, samples (500 µl) were taken and mixed with 300 µl 1 M acetate buffer (pH 5) to prevent further degradation. Five microlitres of this mixture was injected onto a BEH300 C18 column (Acquity UPLC™ Waters Corp.; column oven set at 50°C). Analysis was carried out by Ultra Performance Liquid Chromatography (UPLC; Acquity™, Waters Corp.). A gradient was run from 100% A (H_2O/ACN, 95/5 (w/w) containing 0.1% TFA) to 50% B (100% ACN with 0.1% TFA) in 10 min at a flow rate of 0.25 ml/min. Peaks were detected by UV at 210 nm. Calibration curves were obtained by injecting varying volumes (0.5 µl to 7.5 µl) of a 150 µg/ml HPMA solution in eluent or a 300 µg/ml HPMA-SA solution in eluent. The chromatograms were analyzed using Empower software (Empower Pro, Waters Corp.).

2.6. Preparation of HyPG-SA-HPMA hydrogels

HyPG-SA-HPMA's (150 mg) with varying DS (7, 20 and 35) were dissolved in 10 mM phosphate buffer pH 7.2 (315 µl; 30% (w/w) solid content) transferred into cylindrical moulds of 10 x 7 mm (diameter x height) and polymerized after the addition of 25 µl KPS (50 mg/ml) and 10 µl TEMED ((20% (v/v) adjusted to pH 7 with 2 M HCl) for 1 hour at room temperature.

2.7. Rheological characterization of HyPG-SA-HPMA hydrogels

Rheological characterization of the hydrogels was performed on an AR1000-N rheometer (TA instruments, Etten-Leur, The Netherlands) equipped with a 1˚ steel cone geometry of 20 mm diameter. Directly after addition of the polymerizing agents KPS and

TEMED, the HyPG-SA-HPMA solutions were placed between the plates of the rheometer. Oscillatory time sweep, strain sweep and creep experiments were performed at 20˚C to monitor the rheological properties of the gels. The time sweep, performed with a constant strain of 1% and a constant frequency of 1 Hz, was used to measure the shear storage modulus (G') and the loss modulus (G") for 1 hour. The viscoelastic deformation of a 30% (w/w) HyPG-SA-HPMA hydrogel (DS 20) was evaluated with a strain sweep with a strain range of 0.02% to 10%. The creep experiments were performed to evaluate the deformation of the samples when applying a shear stress of 100 Pa for 2 min. Next, the stress was stopped and the recovery of the gels followed for 2 min.

2.8. Swelling and degradation behavior of HyPG-SA-HPMA hydrogels

Hydrogels were prepared, using HyPG-SA-HPMA with various DS (30% (w/w); DS 7 and 20), as described in section 2.6. The gels were transferred to pre-weighed glass vials (gels in vials were set as initial weight, W_0) and incubated in 10 ml isotonic 100 mM PBS, pH 7.2, containing 0.02% NaN_3 at 37˚C. A number of HyPG-SA-HPMA gels (30% (w/w); DS 7 and 20) were also incubated in 10 ml isotonic 100 mM carbonate buffer, pH 9.6, containing 0.02% NaN_3. To determine the swelling ratio (defined as W_t/W_0) the gels were weighed at regular time intervals (W_t). The buffer was replaced by fresh PBS or carbonate buffer, depending on the pH at which the experiment was performed, at regular times.

3. Results and Discussion

3.1. Synthesis and characterization of hydroxypropyl methacrylamide derivatized HyPG

3.1.1. Attempted synthesis of HyPG-HPMA using CI-activated HPMA

To obtain polymerizable HyPG with polymerizable methacrylamide groups coupled via a hydrolytically sensitive bond, first the synthesis of HyPG-HPMA using CDI as activating agent was attempted. Therefore, HPMA was activated with *N,N'*-carbonyldiimidazole (CDI) and the formed HPMA-CI was coupled to HyPG (Fig. 1) using essentially the same synthetic method as described for both HPMA and hydroxyethyl methacrylate modified dextrans [25, 26]. ^{1}H NMR analysis of the obtained products demonstrated that under the selected reaction conditions, at room temperature under a nitrogen atmosphere with DMSO as solvent and DMAP as catalyst, the HPMA groups were coupled to HyPG.

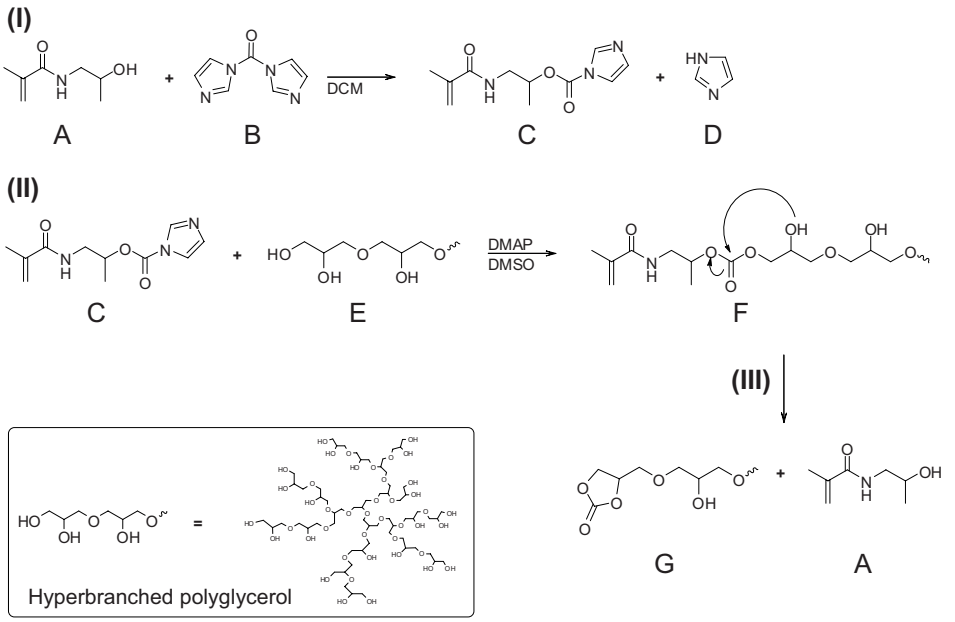

Figure 1. *Synthesis of hydroxypropyl methacrylamide (HPMA) derivatized hyperbranched polyglycerol using carbonyldiimidazole (CDI). (I) HPMA (A) was activated with CDI (B) in dichloromethane (DCM) resulting in HPMA-CI (C) and imidazole (D). (II) HPMA-CI (C) reacted with hyperbranched polyglycerol (HyPG; E) in dimethyl sulfoxide (DMSO), using 4-(N,N-dimethylamino)pyridine (DMAP) as a catalyst, to obtain the crosslinkable product HyPG-HPMA (F). (III) Likely a cyclic carbonate (G) was formed due to the attack of HyPG-hydroxyl groups on the carbonyl groups of the carbonate linker.*

However, many other peaks, which could not be assigned, were present in the spectrum as well (data not shown) indicating that side reactions had occurred. A possible explanation is that, as described previously for the reaction of dextrans and nitrophenyl chloroformate [27], a cyclic carbonate was formed due to the attack of HyPG-hydroxyl groups on the carbonyl groups of the carbonate linker (Fig. 1). Independent of the reaction conditions (i.e. 4°C, 20°C and 50°C, various HPMA-CI concentrations or absence of DMAP), these side reactions still occurred. When analyzing the obtained products by infrared spectroscopy, the formation of a cyclic compound was confirmed (Fig. 2).

3.1.2. Synthesis of HyPG-SA-HPMA using succinylated HPMA

As the synthesis of HyPG-HPMA using CDI as activating agent was not successful, we developed an alternative method for the derivatization of HyPG with HPMA with full control over the degree of substitution (DS). The procedure consists of the derivatization

of HPMA with succinic anhydride in THF using triethylamine (TEA) as a base (Fig. 3). Subsequently, the obtained succinylated HPMA (HPMA-SA) was coupled to HyPG in DMSO using DMAP as a catalyst and DCC as a coupling agent, under dry and oxygen free conditions, yielding HyPG derivatized with succinylated HPMA (referred to as HyPG-SA-HPMA) (Fig. 3).

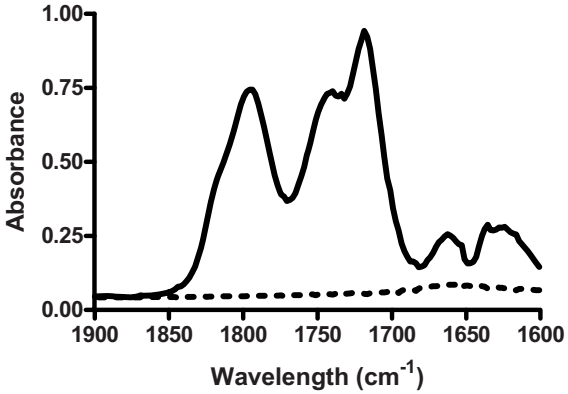

Figure 2. *Infrared spectrum of hyperbranched polyglycerol (dotted line) and hyperbranched polyglycerol derivatized with CI-activated HPMA (continuous line). The peak at 1800 cm^{-1} is indicative for a cyclic carbonate [27], confirming the formation of a cyclic compound (see reaction scheme of Fig. 1). The peaks at around 1720 cm^{-1} and 1650 cm^{-1} are characteristic for the non-cyclic carbonate ester and the amide.*

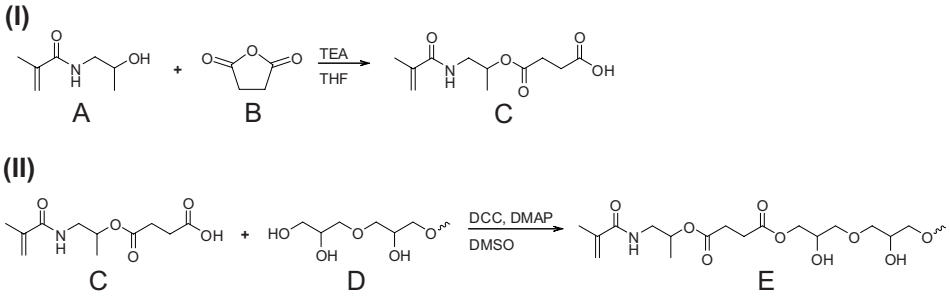

Figure 3. *Synthesis of hydroxypropyl methacrylamide (HPMA) derivatized hyperbranched polyglycerol using succinic anhydride (SA). (I) HPMA (A) was activated with SA (B) in tetrahydrofuran (THF), using triethylamine (TEA), resulting in HPMA-SA (C). (II) HPMA-SA (C) reacted with hyperbranched polyglycerol (HyPG; D) in dimethyl sulfoxide (DMSO), using 4-(N,N-dimethylamino)pyridine (DMAP) and N,N'-dicyclohexylcarbodiimide (DCC), to obtain the crosslinkable product HyPG-SA-HPMA (E).*

The DS, defined as the percentage of derivatized hydroxyl groups, of the obtained product was determined by ^{1}H NMR spectroscopy. In Figure 4A and 4B the spectra of HyPG and HyPG-SA-HPMA are displayed, respectively. The ^{1}H spectrum of HyPG (Fig. 4A) shows the methylene and methine protons of HyPG as one broad resonance around 3.4 ppm, whereas the hydroxyl protons give a signal at 4.6 ppm. The two signals observed at 0.9 and 1.2 ppm are due to the methyl and methylene group, respectively, of the initiator 1,1,1-tris(hydroxymethyl)propane used for the synthesis of HyPG [28]. In the spectrum of HyPG-SA-HPMA (Fig. 4B) the methacrylate moiety gives signals at 1.8 ppm (methyl protons) and at 5.3 and 5.6 ppm (protons of de double bond) having a ratio of 3:2 as expected. The DS was determined by comparing the characteristic peaks of the methacrylate moiety (5.3 and 5.6 ppm) to the broad band of the polymer (ranging from 3.2 to 3.9 ppm). A study of the kinetics of the reaction of HPMA-SA with HyPG (aimed DS 50) showed that a DS of 20 was obtained within 6 h after which no further increase in DS was observed. A DS of 20 indicates that ~6 out of the 32 hydroxyl groups of HyPG were substituted with a HPMA-SA group. The relation between the aimed DS (ratio of HPMA-SA and HyPG) and the DS of the obtained product is depicted in Figure 5. It was shown that the DS can accurately and reproducibly be tailored in the range of 7 to 35 and that an incorporation of about 50% was obtained.

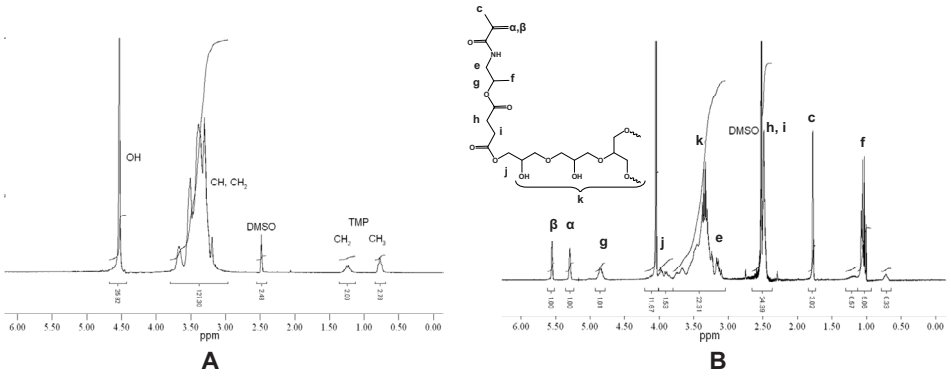

Figure 4. *^{1}H NMR spectra of (A) hyperbranched polyglycerol and (B) hydroxypropyl methacrylamide derivatized hyperbranched polyglycerol (HyPG-SA-HPMA). The polymers were dissolved in DMSO-d_6.*

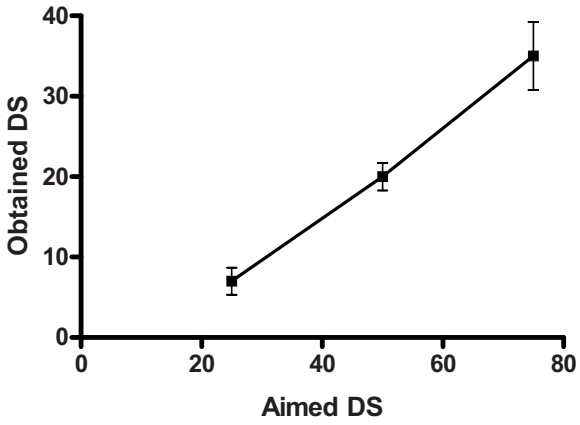

Figure 5. *Relation between the aimed DS and the DS of the obtained material. The data are shown as average ± SD, n = 3.*

3.1.3. Degradation of HyPG-SA-HPMA

The degradability of HyPG-SA-HPMA before radical polymerization was studied by incubation in carbonate buffer pH 9.6 at 37˚C. Figure 6A shows the degradation profile of HyPG-SA-HPMA. The calculated curves (drawn lines; Fig. 6B) are obtained according to the model described by Neradovic [29]. It was observed that the ester between HyPG and the linker is more sensitive to hydrolysis than to the ester between HPMA and the linker (k_1 (9.7 ± 0.7)x10^{-5} s^{-1} and k_2 (5.5 ± 0.2)x10^{-5} s^{-1}, respectively, corresponding to a half life of 2.0 h and 3.5 h)). Consequently, the half lives at physiological pH will be 504 h and 1008 h, respectively, assuming that in this pH range the hydrolysis is first order in hydroxyl ion concentration. Additionally, if the ester between HyPG and the linker hydrolyses, a reaction rate constant of (9.0 ± 2)x10^{-6} s^{-1} (k_3; corresponding to a half life of 21h; Fig. 6) is found for the ester between HPMA and the linker. The lower stability of esters of primary alcohols (i.e. between HyPG and the linker) compared to esters of secondary alcohols (i.e. between HPMA and the linker) can be ascribed to less steric hindrance resulting in the attack of the first mentioned ester bond by a hydroxyl ion, as was reported previously by Rijcken [30].

3.2. Preparation and characterization of HyPG-SA-HPMA hydrogels

3.2.1. Rheological characterization of HyPG-SA-HPMA hydrogels

HyPG-SA-HPMA was crosslinked by radical polymerization, using KPS as initiator and TEMED as catalyst. The obtained hydrogels were characterized by rheology. It was observed that, for HyPG-SA-HPMA gels (DS 20, 30% (w/w) solid content), within 30 min a fully elastic network (Fig. 7A; *G'* = 73 kPa; *G"* = 1 kPa; *tan δ* = 0.02) was obtained.

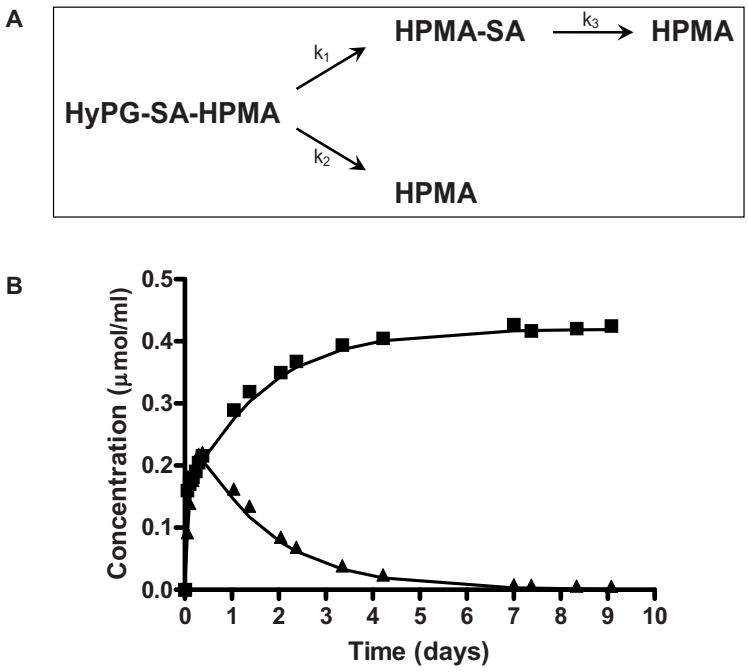

Figure 6. *Possible degradation routes (A) and degradation profile (B) of HyPG-SA-HPMA at 37˚C at pH 9.6 (symbols represent the experimental data; drawn lines are fitted according to model [29]): HPMA-SA (▲); HPMA (■).*

Before addition of KPS and TEMED, an aqueous solution of HyPG-HPMA showed mainly viscous behavior (*tan δ* > 1.5, and both *G'* and *G"* were low, 0.1 and 0.15 Pa, respectively), demonstrating that the elastic properties of the HyPG-SA-HPMA gels are due to polymerization of the methacrylamide groups by which a network was obtained. After the time sweep experiment, a frequency sweep and strain sweep experiment were performed (results not shown). It was shown that when a frequency of 1 Hz and a strain of 1% were applied, the gel was in the linear viscoelastic deformation range. This range was maintained up to a frequency of 10 Hz and a strain of 6%. The viscoelastic properties of HyPG-SA-HPMA gels (DS 20, 30% (w/w) solid content) were also investigated with creep experiments. The hydrogel was deformed up to 0.15% strain when a shear stress of 100 Pa was applied. After removal of the stress the gel recovered completely (Fig. 7B), confirming the fully elastic properties of the network. Rheological analysis showed that, as was observed for HyPG-HPMA DS 20 gels, also the HyPG-SA-HPMA DS 7 and DS 35 hydrogels were fully elastic (Fig. 8). Figure 8 shows the storage modulus of the formed HyPG-SA-HPMA gels. It was observed that the storage modulus of the HyPG-SA-HPMA gels increased with increasing degree of substitution. Hydrogels

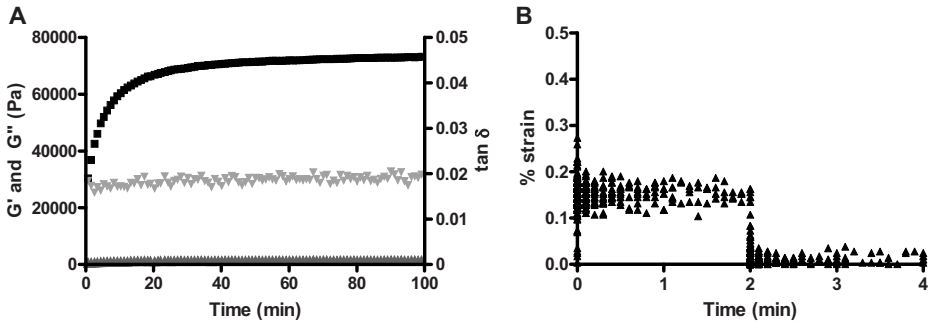

Figure 7. *(A) Storage modulus G' (■) loss modulus G" (▲) and tan δ (▼) of a gelating 30% (w/w) HyPG-SA-HPMA DS 20 solution as function of time after addition of KPS and TEMED. (B) Creep experiment (applied stress 100 Pa) on a 30% (w/w) HyPG-SA-HPMA DS 20 hydrogel as function of time.*

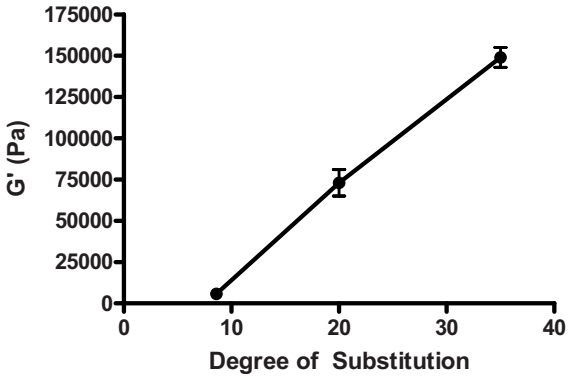

Figure 8. *Storage modulus (G') as function of the substitution degree of 30% (w/w) HyPG-SA-HPMA hydrogels obtained after polymerization with KPS and TEMED. The data are shown as average ± SD, n = 3.*

consisting of HyPG with a higher DS have a higher crosslink density and consequently higher storage modulus (*G'* 6.0 ± 1.7 kPa for gels with DS 7 and *G'* 149 ± 6 kPa for gels with DS 35, respectively).

3.2.2. Swelling and degradation of HyPG-SA-HPMA hydrogels

The swelling and degradation behavior of HyPG-SA-HPMA hydrogels with varying substitution degrees (DS 7 and 20; 30% (w/w) solid content) was evaluated by incubating the gels in an aqueous buffer of pH 7.2 at 37˚C. For HyPG-SA-HPMA DS 7 gels it was observed (Fig. 9A) that a progressive swelling profile was followed by a degradation phase. However, maximal swelling (2.8 times its initial weight) was reached after 142 days after which the gels degraded rather fast (i.e. 158 days). Hydrogels with

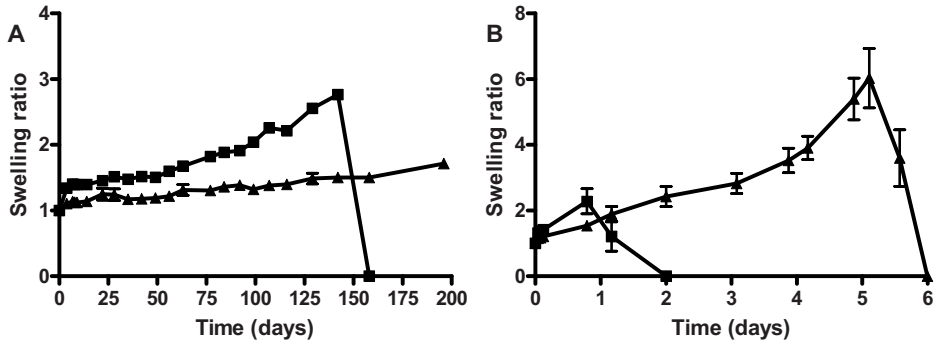

Figure 9. *Swelling/degradation ratio of HyPG-SA-HPMA hydrogels (30% (w/w) initial solid content; DS 7 (■) and DS 20 (▲)) in aqueous buffer of pH 7.2 (A) and pH 9.6 (B) at 37˚C as function of the time.*

DS 20 showed a slower swelling and did not reach their maximal swelling after 200 days (1.8 times its initial weight was reached at that time; Fig. 9A). As swelling and degradation were rather slow at pH 7.2, a study was performed in aqueous buffer of pH 9.6 at 37˚C to accelerate degradation. The HyPG-SA-HPMA gels (DS 7 and 20) both showed an initial progressive swelling followed by a fast degradation phase (Fig. 9B). At lower DS, the gels showed faster swelling and degradation kinetics although the maximal swelling was lower. A maximal swelling of 2.3 times was reached after 19 h (i.e. 4 times $t_{1/2}$ of unpolymerized HyPG-SA-HPMA) for gels with DS 7. For gels with DS 20 a maximal swelling of 6.0 its initial weight was reached after 5 days. The time that HyPG-SA-HPMA started to dissolve was longer with increasing DS, likely due to more crosslinks that have to be hydrolyzed, which requires more time. Hydrogels were fully dissolved after 2 and 6 days for DS 7 and DS 20 gels, respectively.

4. Conclusion

In this introductory story we report on the development of biodegradable HyPG gels. An efficient method was presented to modify HyPG with succinylated HPMA with full control over the DS. Two hydrolyzable esters were present: the ester between the spacer and HyPG was more prone to hydrolysis than the ester between the spacer and HPMA. HyPG-SA-HPMA hydrogels were obtained by radical polymerization. Rheological characterization of these hydrogels showed that the elastic modulus of the gels increased with higher DS. Moreover, it was observed that the gels degraded slower with increasing DS and lower pH (i.e. pH 7.2 compared to pH 9.6). Consequently, this study indicates that degradable HyPG-SA-HPMA hydrogels can potentially be used in biofilms as described in this thesis as well as drug delivery matrices.

References

1. Haag R, Stumbe JF, Sunder A, Frey H, Hebel A. An approach to core-shell-type architectures in hyperbranched polyglycerols by selective chemical differentiation. *Macromolecules* 2000; 33(22): 8158-8166.
2. Stiriba SE, Slagt MQ, Kautz H, Klein Gebbink RJ, Thomann R, Frey H, van Koten G. Synthesis and supramolecular association of immobilized NCN-pincer platinum(II) complexes on hyperbranched polyglycerol supports. *Chemistry* 2004; 10(5): 1267-1273.
3. Sunder A, Mulhaupt R, Haag R, Frey H. Hyperbranched Polyether Polyols: A Modular approach to complex Polymer Architectures. *Adv Mater* 2000; 12(3): 235-239.
4. Garcia-Bernabe A, Kramer M, Olah B, Haag R. Syntheses and phase-transfer properties of dendritic nanocarriers that contain perfluorinated shell structures. *Chemistry* 2004; 10(11): 2822-2830.
5. Sunder A, Quincy MF, Mulhaupt R, Frey H. Hyperbranched Polyether Polyols with Liquid Crystalline Properties. *Angew Chem Int Ed Engl* 1999; 38(19): 2928-2930.
6. Sunder A, Kramer M, Hanselmann R, Mulhaupt R, Frey H. Molecular Nanocapsules Based on Amphiphilic Hyperbranched Polyglycerols. *Angew Chem Int Ed Engl* 1999; 38(23): 3552-3555.
7. Haag R, Sunder A, Stumbe J. An approach to glycerol dendrimers and pseudo-dendritic polyglycerols. *J Am Chem Soc* 2000; 122: 2954-2955.
8. Kainthan RK, Muliawan EB, Hatzikiriakos SG, Brooks DE. Synthesis, characterization, and viscoelastic properties of high molecular weight hyperbranched polyglycerols. *Macromolecules* 2006; 39: 7708-7717.
9. West JL, Hubbell JA. Comparison of covalently and physically cross-linked polyethylene glycol-based hydrogels for the prevention of postoperative adhesions in a rat model. *Biomaterials* 1995; 16(15): 1153-1156.
10. Sperinde JJ, Griffith LG. Synthesis and characterization of enzymatically-crosslinked poly(ethylene glycol) hydrogels. *Macromolecules* 1997; 30: 5255-5264.
11. DiRamio JA, Kisaalita WS, Majetich GF, Shimkus JM. Poly(ethylene glycol) methacrylate/dimethacrylate hydrogels for controlled release of hydrophobic drugs. *Biotechnol Prog* 2005; 21(4): 1281-1288.
12. Frey H, Haag R. Dendritic polyglycerol: a new versatile biocompatible-material. *J Biotechnol* 2002; 90(3-4): 257-267.
13. Kainthan RK, Hester SR, Levin E, Devine DV, Brooks DE. In vitro biological evaluation of high molecular weight hyperbranched polyglycerols. *Biomaterials* 2007; 28(31): 4581-4590.
14. Kainthan RK, Brooks DE. In vivo biological evaluation of high molecular weight hyperbranched polyglycerols. *Biomaterials* 2007; 28(32): 4779-4787.
15. Kainthan RK, Janzen J, Levin E, Devine DV, Brooks DE. Biocompatibility testing of branched and linear polyglycidol. *Biomacromolecules* 2006; 7(3): 703-709.
16. Stiriba SE, Kautz H, Frey H. Hyperbranched molecular nanocapsules: comparison of the hyperbranched architecture with the perfect linear analogue. *J Am Chem Soc* 2002; 124(33): 9698-9699.

17. Smeds KA, Pfister-Serres A, Miki D, Dastgheib K, Inoue M, Hatchell DL, Grinstaff MW. Photocrosslinkable polysaccharides for in situ hydrogel formation. *J Biomed Mater Res* 2001; 54(1): 115-121.
18. Jin Y, Yamanaka J, Sato S, Miyata I, Yomota C, Yonese M. Recyclable characteristics of hyaluronate-polyhydroxyethyl acrylate blend hydrogel for controlled releases. *J Control Release* 2001; 73(2-3): 173-181.
19. Hoffman AS. Hydrogels for biomedical applications. *Ann N Y Acad Sci* 2001; 944: 62-73.
20. Drury JL, Mooney DJ. Hydrogels for tissue engineering: scaffold design variables and applications. *Biomaterials* 2003; 24(24): 4337-4351.
21. Oudshoorn MHM, Rissmann R, Bouwstra JA, Hennink WE. Synthesis and characterization of hyperbranched polyglycerol hydrogels. *Biomaterials* 2006; 27(32): 5471-5479.
22. Oudshoorn MHM, Penterman R, Rissmann R, Bouwstra JA, Broer DJ, Hennink WE. Preparation and characterization of structured hydrogel microparticles based on cross-linked hyperbranched polyglycerol. *Langmuir* 2007; 23(23): 11819-11825.
23. van Dijk-Wolthuis WNE, Kettenes-van den Bosch JJ, van der Kerk-van Hoof A, Hennink WE. Reaction of dextran with glycidyl methacrylate: an unexpected transesterification. *Macromolecules* 1997; 30(11): 3411-3413.
24. Song J, Saiz E, Bertozzi CR. A new approach to mineralization of biocompatible hydrogel scaffolds: an efficient process toward 3-dimensional bonelike composites. *J Am Chem Soc* 2003; 125(5): 1236-1243.
25. van Dijk-Wolthuis WN, Tsang SKY, Kettenes-van den Bosch JJ, Hennink WE. A new class of polymerizable dextrans with hydrolyzable groups: hydroxyethyl methacrylated dextran with and without oligolactate spacer. *Polymer* 1997; 38(25): 6235-6242.
26. Vlugt-Wensink KD, Oudshoorn M, Verrijk R, Jiskoot W, Crommelin DJ, Hennink WE. Synthesis and characterization of dextrans substituted with hydrophilic polymerizable side groups and their application in protein-releasing microspheres - an introductory story, in: Vlugt-Wensink K. (thesis), Dextran-based microspheres as controlled drug delivery systems for proteins. Utrecht, The Netherlands. 2007; Chpt-7: 130-144.
27. Vandoorne F, Vercauteren R, Permentier D, Schacht EH. Re-investigation of the 4-nitrophenyl chloroformate activation of dextran. Evidence for the formation of different types of carbonate moieties. *Die Makromolekulare Chemie* 1985; 186: 2455-2460.
28. Sunder A, Hanselmann R, Frey H, Mulhaupt R. Controlled synthesis of hyperbranched polyglycerols by ring-opening multibranching polymerization. *Macromolecules* 1999; 32: 4240-4246.
29. Neradovic D, van Steenbergen MJ, Vansteelant L, Meijer YJ, van Nostrum CF, Hennink WE. Degradation mechanism and kinetics of thermosensitive polyacrylamides containing lactic acid side chains. *Macromolecules* 2003; 36: 7491-7498.
30. Rijcken CJ, Veldhuis TF, Ramzi A, Meeldijk JD, van Nostrum CF, Hennink WE. Novel fast degradable thermosensitive polymeric micelles based on PEG-block-poly(N-(2-hydroxyethyl)methacrylamide-oligolactates). *Biomacromolecules* 2005; 6(4): 2343-2351.

Summary & Perspectives

Summary

The mature epidermis is an effective barrier which prevents the body from dehydration and protects it against various environmental influences. If the natural barrier is immature or damaged, the skin barrier is impaired and desiccation occurs [1-4]. Hence, the regeneration of impaired skin is an essential process for survival. In patients, the natural recovery is sometimes rather slow, in particular in the cases of large defects. To support skin regeneration, a large variety of skin creams is presently available, aiming to modify the hydration level of the skin and to protect the body against excessive water loss and thus to enhance epidermal barrier function. However, these creams clearly have a different structure than stratum corneum (SC), resulting in low water binding capacity and uncontrolled hydration of the skin. The basic mechanism of these skin creams is that they act as moisturizer and increase the hydration of SC by either blocking the TEWL (transepidermal water loss) or by delivering exogenous hygroscopic substances to the SC [5-8]. Therefore, it has been suggested that the development of barrier creams with high water-holding capacity and thus controlled water transport, such as the natural cream VC (vernix caseosa) [9, 10], might help in the development and/or restoration of the SC barrier.
The aim of this thesis was the development of a new generation of skin-surface biofilms, combining the structure and properties of VC, to protect diseased, dry and premature skin and to facilitate wound healing. These biofilms were based on synthetic cells embedded in a lipid matrix. The development of the synthetic corneocytes from crosslinked hydrophilic polymers is presented in this thesis. Combined with the work of Rissmann (presented in thesis R. Rissmann), who mainly focused on characterization of VC and the development of a synthetic lipid mixture, we were able to prepare biofilms. The preparation, characterization and subsequent *in vivo* testing of these biofilms are also described in this thesis.

Chapter 1 provides a general introduction to the structure and function of the human skin and available models to mimic human skin. Additionally, the preparation and characteristics of hydrogels, that will mimic the corneocytes in the newly generated biofilms, are described.

To mimic the water binding properties of the natural corneocytes and to ensure dimensional stability, crosslinked hydrophilic polymers were investigated in this project. The modification and subsequent crosslinking of the hydrophilic polymer hyaluronic acid (HyA) is described in **Chapter 2**. HyA was derivatized with polymerizable methacrylate residues in dimethyl sulfoxide (DMSO) using glycidyl methacrylate (GMA) and 4-(*N,N*-dimethylamino)pyridine (DMAP) as a catalyst. By exchanging the Na^+ ions of HyA by the

more lipophilic tetrabutylammonium ions, the polymer was rendered soluble in DMSO. The obtained product, methacrylated HyA (HyA-MA), was obtained with precise control over the substitution degree in the range of 5 to 30 by varying the molar ratio of GMA to HyA in the reaction mixture. Radical polymerization of aqueous solutions of HyA-MA, using potassium peroxodisulfate (KPS) as initiator and *N,N,N',N'*-tetramethylethylenediamine (TEMED) as catalyst, resulted in opaque and elastic hydrogels. Rheological analysis and swelling experiments showed that the elastic modulus and the dimensional stability of the gels increased with higher substitution degree. These results show that HyA-MA hydrogels with tailorable characteristics can be prepared and thus could be utilized for the preparation of synthetic corneocytes. Additionally, these hydrogels have potential as drug delivery systems and for tissue engineering purposes.

As alternative to HyA, the application of hyperbranched polyglycerol (HyPG) for the preparation of hydrogels was studied. **Chapter 3** reports on the derivatization of HyPG with GMA in DMSO using DMAP as a catalyst to obtain methacrylated HyPG (HyPG-MA). This method allowed tailoring of the substitution degree by varying the molar ratio of GMA to HyPG. Hydrogels were obtained by crosslinking methacrylated HyPG in aqueous solutions using KPS and TEMED as initiator and catalyst, respectively. Alternatively, HyPG-MA could also be crosslinked by photopolymerization using Irgacure 2959 as photoinitiator. Rheological analysis showed that, for both polymerization methods, the elastic modulus of the gels could be tailored by varying the concentration of HyPG-MA in the aqueous solution as well as by the DS (degree of substitution). In addition, the obtained hydrogels had a limited swelling capacity showing that rather dimensionally stable networks were obtained. Important for possible applications, e.g. synthetic corneocytes, drug delivery or tissue engineering, it was shown that HyPG-MA hydrogels could be prepared with high concentrations of solid content, demonstrating that the characteristics of the gels could easily be adjusted to the requirements.

In **Chapter 4** the development of the synthetic corneocytes from crosslinked hydrophilic polymers is described. For this purpose, HyPG-MA (Chapter 3) was used because the handling properties of aqueous solutions in terms of e.g. viscosity are superior to those of HyA-MA (Chapter 2). Well-defined HyPG-MA microparticles with uniform sizes and shapes were prepared using rigid-micromolding, soft-micromolding or photolithography. For the rigid-micromolding technique, SU-8 (a photoresist based on epoxies) grids were used. Independent of the surface treatment of the grids, only a restricted percentage of well-defined particles could be obtained. The other particles remained adhered to the SU-8 grid or broke into smaller particles due to drying during the release process.

Moreover, after this drying procedure, the obtained microgels did not rehydrate completely. The soft-micromolding technique, using elastomeric PDMS (poly(dimethyl siloxane)) grids, resulted in a high yield of microgels with well-defined size and shape (squares of 100x100x50 µm or hexagons with ∅ 30 µm and a thickness of 20 µm). Although a number of particles showed deviating dimensions, as not all grids could be filled well, the microgels showed restricted swelling implying that these gels are rather dimensionally stable. Good results were obtained using a photolithographic method to prepare well-defined HyPG-MA microparticles in a high yield. Microparticles in the size-range of 30 µm to 1400 µm could easily be prepared by adding an inhibitor (e.g. vitamin C) to the polymer solution to inhibit dark polymerization. Moreover, the microgels showed limited swelling indicating that rather dimensionally stable particles were obtained. It was concluded that photolithography and soft-micromolding, as compared to rigid-micromolding, are the most appropriate techniques to fabricate structured HyPG-MA microgels with a tailorable and well-defined size and shape.

The preparation and characterization of biofilms, mimicking the unique composition and properties of natural VC, is presented in **Chapter 5**. The base of our biofilms consisted of synthetic cells embedded in a lipid matrix. Structured HyPG-MA microgels prepared by photolithography (Chapter 4) were used as synthetic corneocytes. The development of the lanolin-derived synthetic lipid matrix, with very similar composition and organization as found for VC, is described in the thesis of R. Rissmann. Hexagonal, highly hydrated microgels (Ø 30 µm) were embedded in a synthetic lipid mixture using a micromixer. Various formulations were prepared using different particle:lipid ratios (i.e. 2:1 and 5:1), particles with different initial water-content (i.e. 50% (w/w) and 80% (w/w)) and uncoated or lipid-coated synthetic corneocytes. Characterization with confocal laser scanning microscopy showed a homogeneous distribution of the FITC (fluorescein isothiocyanate) labeled particles in the Nile Red stained lipids, indicating a successful embedment. Formulations with a higher particle:lipid ratio (5:1) showed a better resemblance to VC in terms of ultrastructural appearance compared to biofilms with a lower particle:lipid ratio (2:1). Additionally the formulations were stable for at least one month at 4°C and exhibited similar thermotropic behavior as VC. Water-handling properties were tailorable using lipid coated particles, whereas rheological analysis of the formulations showed that a similar tan δ (i.e. quotient of viscosity and elasticity) as for VC was obtained. Hence, an excellent resemblance was achieved in composition, ultrastructure and properties between native VC and synthetic biofilms.

The efficacy of new wound healing strategies needs to be tested under well-controlled conditions. The availability of a suitable model is, therefore, essential to investigate product efficacy and safety. In **Chapter 6** we focused on the generation of a reliable

mice model for skin barrier disruption and repair. Five different levels of skin barrier disruption in mice, accomplished by sequential tape stripping, were evaluated. By increasing the number of tape strips different models were obtained with a disrupted skin varying from moderate to severe. The skin barrier disruption models moderate and severe #1 to #3 showed complete recovery of the TEWL within 72 h. Extensively damaged skin (i.e. model severe #4), however, showed a rather slow recovery and within 72 h only 50% recovery was obtained and complete recovery occurred within 8 days. The effect of VC application on the recovery of tape stripped skin was evaluated with both model severe #3 and severe #4. Model severe #3 typically resembles the models previously described in literature that have a very fast recovery (i.e. several hours), whereas severe #4 is an innovative model with extensively damaged skin resulting in a substantial slower recovery. Topical application of VC on the severe #3 disruption model showed that predominantly the initial barrier recovery was enhanced. Hence, this model is merely appropriate to study the effect of formulations in the initial recovery period. When VC was applied on the disrupted skin of model severe #4, both initial and long-term barrier recovery was accelerated. In addition, VC application promoted a rapid formation of SC and prevented epidermal hyperproliferation. The obtained results not only show that a suitable mice model for skin barrier disruption and repair was generated, but they also confirm the ability of VC to enhance barrier recovery, as was suggested previously [11-13].

In vivo studies with the biofilms, which are described in Chapter 5, on disrupted mice skin are presented in **Chapter 7**. Various biofilm formulations were applied topically on mice skin, disrupted by sequential tape stripping (model severe #4). Changes in TEWL were used to monitor barrier recovery. It was observed that application of biofilm B4 (lipid:particle ratio 2:1, using uncoated particles with 50% (w/w) initial water content) resulted in an increased skin barrier recovery comparable to VC. Other biofilm formulations and lipid mixtures showed less enhanced skin barrier recovery, similar to the commonly used oil-based ointments Vaseline and Eucerin. Biopsies were harvested to evaluate the recovery of the SC by histology. All formulations promoted a rapid formation of SC and prevented epidermal hyperproliferation. In general the synthetic VC analogues showed strong effects concerning the recovery rate and especially biofilm B4 mimicked the effects of native VC the most closely.

The synthetic corneocytes, i.e. structured HyPG-MA microgels, described in Chapter 4 and 5 were essentially non-degradable under physiological conditions because the methacrylate units are directly coupled to the hydroxyl functionalities of HyPG [14]. In **Chapter 8** we reported on an introductory study on the development of biodegradable HyPG gels, which can potentially be used as drug delivery matrices in the biofilms. The

presence of hydrolysable bonds can, in addition to the DS and the initial water content of the gel, control the release of loaded substances. HyPG was modified in DMSO using succinilated HPMA ((2-hydroxypropyl) methacrylamide) with *N,N*-dicyclohexylcarbodiimide (DCC) as coupling agent. HyPG-HPMA hydrogels were obtained by radical polymerization using KPS and TEMED. In these hydrogels two hydrolysable esters are present in the spacer: one connecting the spacer and HPMA and one connecting the spacer and HyPG. Rheological analysis showed that the elastic modulus of the gels increased with higher substitution degree. Importantly, it was observed that the gels degrade under physiological conditions. The degradation time was slower with increasing DS and lower pH (i.e. pH 7.2 compared to pH 9.6). Consequently, this indicates that degradable systems were obtained.

In conclusion, this thesis describes the development of a new generation of skin-surface biofilms mimicking closely the structure and properties of VC. These biofilms act as skin protectants and facilitate the restoration of the SC barrier. These unique systems have therefore great potential to protect diseased, dry and premature skin and to facilitate wound healing in humans.

Perspectives

In this thesis we reported on the (micro)fabrication and characterization of novel hydrogels and their application as synthetic cells (in particular corneocytes) in a new generation of biofilms. Hydrogels were prepared by polymerization of methacrylated hyaluronic acid (HyA-MA; Chapter 2) and methacrylated hyperbranched polyglycerols (HyPG-MA; Chapter 3). The fabrication of microgels was done with HyPG (Chapter 4) because the handling properties of aqueous solutions in terms of e.g. viscosity were superior to those of HyA. The obtained HyPG-based microgels were assembled and mixed with a lipid matrix resulting in biofilms that mimicked not only the unique composition and physicochemical properties of natural VC (Chapter 5) but also the skin barrier recovery properties in an animal model (Chapter 6 and 7). In these chapters it was shown that the application of the various biofilms on disrupted skin improved the skin barrier recovery. One biofilm in particular, mimicked the effects of native VC very closely. In future, these biofilms might further be tested in human skin models and in humans (i.e. prematures or superficial wound healing in adults) to demonstrate their possible beneficial effect whereby the corneocytes can also be used as drug delivery system, e.g. to release growth factors to modulate the wound healing process. Prior to clinical application, however, some general issues need to be tackled. The first aspects are related to the development of the biofilm itself, regarding further characterization, upscaling, sterility and safety. An additional characterization concerning the biofilms, more specific the lipid coating surrounding the synthetic cells, is already reported in section 1. Furthermore, the introduction of therapeutically active components (e.g. natural moisturizing factor, growth factors or drugs) in the synthetic corneocytes and their release and biological effect needs to be evaluated as well. In a next step, the large scale production of synthetic corneocytes should be studied and optimized as well as upscaling of the preparation of the lipid matrix and the biofilm. To circumvent several safety concerns regarding bacterial contamination, the aseptic preparation of the biofilms and biofilm components needs attention. Moreover, the biocompatibility and possible irritancy and toxicity of the biofilm and its degradation products (i.e. when using degradable synthetic corneocytes as described in Chapter 8) should be studied. It is however recommended that prior to application of our biofilms on prematures or superficial wounds, artificial human skin models or cultured human skin are used to assess skin irritation and percutaneous absorption of drugs. Moreover, cellular functions as well as tissue repair can be tested using such models.

In addition to the medical field, these biofilms can also find application in the cosmetic field. The biofilms offer possibilities to improve the hydration level in the SC in a controlled way. For instance, people with dry skin and/or with skin that is regularly

exposed to detergents (e.g. hair-dressers) likely can profit from it. Moreover, they will also be of benefit in sun-care products as an increased hydration will prevent drying of the skin during sun exposure. It should be noted that although the application of these biofilms in the cosmetic field is promising, it is restricted as *in vivo* animal studies (described in Chapter 7 for the biofilms) for cosmetics are banned in the European Union.

As mentioned above, two new hydrogel systems are described in this thesis. Hydrogels, in general, have been widely used in the biomedical and pharmaceutical field because of their tailorable chemical structure, tailorable 3D structure, good mechanical properties, high water content and biocompatibility. These unique properties offer potential for using hydrogels as drug delivery devices, tissue engineering purposes and artificial organs/implants [15-20]. Hydrogels can be in the form of macroscopic networks or restricted to smaller dimensions such as microgels. Microfabrication of hydrogels is used increasingly for various applications, because their tailorable properties and uniform particle distribution have more potential compared to the classical macroscopic-sized hydrogels. Ideally, the morphology of the gels (i.e. size and shape) should be adjusted in accordance to their aimed application and function.
In the first part of this thesis we described the application of two different polymers, i.e. hyaluronic acid (HyA) and hyperbranched polyglycerol (HyPG) (Chapter 2 and 3, respectively), for the preparation of hydrogels. Moreover, an introductory study was reported (Chapter 8) on the development of biodegradable HyPG gels, which can potentially be used in biofilms as described in this thesis as well as drug delivery matrices. For further development of the above described polymers for tissue engineering and drug delivery purposes, some general issues need to be considered, such as biocompatibility, cytotoxicity and safety. To assess their potential as cell supporting matrices (both HyA and HyPG) and as protein release matrix (degradable HyPG), preliminary studies were performed and described in section 2 and 3, respectively.

1. Characterization of lipid coating surrounding hyperbranched polyglycerol microgels by atomic force microscopy

The preparation and characterization of HyPG-MA based microscopic particles with size and shape similar to natural corneocytes was described in this thesis (Chapter 4). These microgels were used as synthetic corneocytes in our biofilms (Chapter 5), which mimicked the unique composition and properties of natural VC. The biofilms were obtained by embedding the microgels in a synthetic lanolin-based lipid mixture using a micromixer. Various formulations were prepared using different particle/lipid ratios,

particles with different initial water-content and uncoated or lipid-coated synthetic corneocytes to obtain the most optimal biofilm. The lipid coating of the synthetic corneocytes, which is also present in SC and VC coating the natural corneocytes, was intended to facilitate embedding of the particles and to control water release from the biofilm.

Preparation of lipid vesicles and subsequent coating of the microparticles was performed as described in literature [21]. In brief, DOPC-DOTAP liposomes were mixed with a suspension of HyPG-MA microgels and shaken for 1 h at room temperature to allow adsorption of the lipid vesicles onto the surface of the microgels. After centrifugation and resuspension, microparticles were directly used for further studies. Visualization of the lipid coated HyPG-MA microparticles was performed by confocal laser scanning microscopy (shown in Chapter 5). With this technique the presence of a lipid coating could be confirmed, however, the thickness could not be determined. For this purpose preliminary studies were performed using atomic force microscopy (AFM). These studies were done in collaboration with the group of Prof. A.E. Rowan (Dep. of Molecular Materials, Institute for Molecules and Materials, University of Nijmegen, The Netherlands). AFM is a well-known technique to visualize surfaces of materials with the highest spatial resolution [22]. Taking advantage of the sharpness of the tips and strong and localized tip-surface interactions, AFM can also be applied to nanopattern the surfaces. The procedure of the AFM-based surface patterning, known as nanoshaving, is illustrated in Figure 1. In nanoshaving the AFM tip exerts a high local pressure at the contact. This pressure results in a high shear force during the scan, which causes displacement of the lipids. The AFM measurements were done using a Nanoscope IV multimode instrument (Veeco, Santa Barbara, California, USA) equipped with a 12 µm E-scanner. Both imaging and nanoshaving were performed with 350 µm standard contact-mode tips with a typical force constant of 0.03 N/m (CSG01, NT-MDT, Zelenograd, Moscow, Russia). The pristine surfaces were first contacted with the AFM tip and imaged with only a small force applied by the tip on the sample (low setpoints).

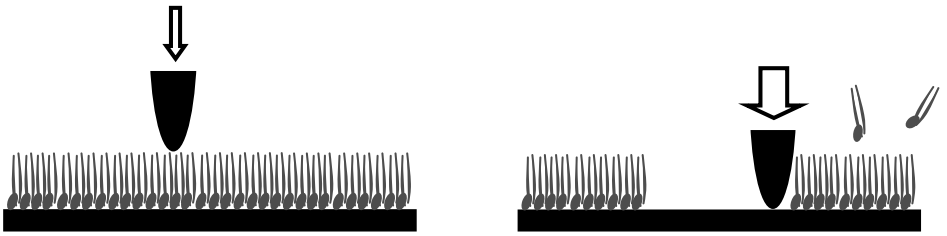

Figure 1. *Schematic representation of the nanoshaving technique. Initially the surface is characterized under a low force. Next, the AFM tip exerts a high local force at the contact, causing displacement of the lipids. (Adapted from [22]).*

For the nanoshaving, the setpoint (force) was increased, typically to about 3 V, while scanning only a small area (typically between 100x100 nm^2 and 500x500 nm^2). After zooming out, the subsequent imaging was again done at very low setpoints. The surface of a lipid coated microgel before and after nanoshaving is shown in Figure 2A and 2B, respectively. A typical 3-D surface representation of lipid-coated HyPG-MA particles after nanoshaving two distinct areas (i.e. one square of 200x200 nm^2 and one of 300x300 nm^2) is shown in Figure 3. Squares were shaved into the lipid surface after which the depth of the pattern was determined. It was observed that upon increasing the applied force, the depth of the shaved pattern reached a maximum of 24 nm, indicating that most likely 4 bilayers were present on the surface of the microgels. This number was surprisingly consistent for several different particles and two different particle preparations. Moreover, after shaving the surface of uncoated HyPG-MA microparticles no patterns could be detected (data not shown), even after applying higher forces on the surface. This indicates that the shaved patterns observed on lipid-coated microgel surfaces correspond to the displacement of the lipids. It can be concluded that nanoshaving is an appropriate technique to evaluate the thickness of the lipid coating on HyPG-MA microgels.

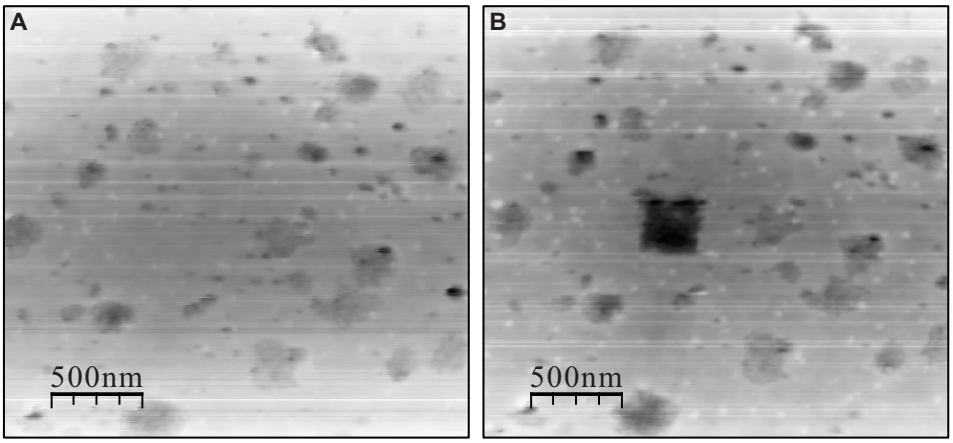

Figure 2. *Surface of lipid-coated HyPG-MA particles before (A) and after nanoshaving (B).*

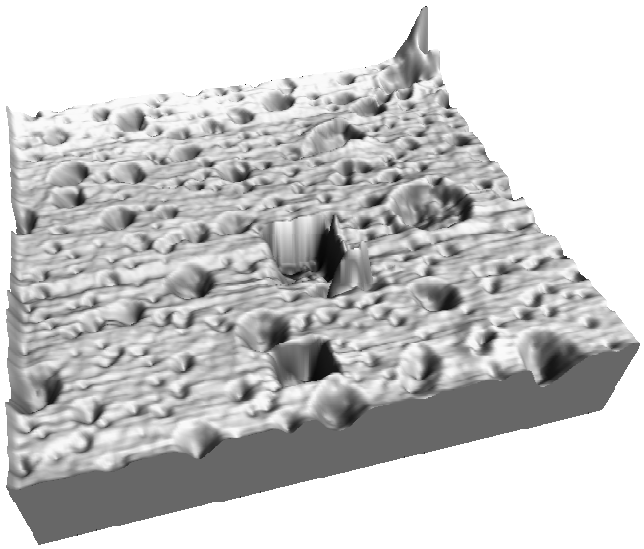

Figure 3. *A three dimensional surface representation of lipid-coated HyPG-MA particles after nanoshaving two areas of 200x200 nm^2 and 300x300 nm^2.*

2. Tissue engineering

Photopolymerizable hydrogels have already been widely employed in tissue engineering for release of growth factors and as scaffolds for entrapment of cells. Injectable (cell-laden) formulations that can be polymerized in situ are currently under clinical investigation for cartilage replacement therapy [20, 23, 24]. Hydrogels are attractive candidates for the design of scaffolds because of their biocompatibility and controllable degradability. Moreover, the high water-absorbing capacity of hydrogels gives them physical characteristics similar to soft tissues [15-17, 20, 25, 26]. Photopolymerization is fast and can be performed at room or physiological temperature with minimal heat production. This technique offers spatial and temporal control over polymerization and yields stable and mechanically strong hydrogels [17].

A novel approach in tissue engineering is organ- or tissue printing, which creates layered, cell-laden hydrogel scaffolds with a defined three-dimensional structure and organized cell placement [26]. Photopolymerizable hydrogels have great potential for this purpose. This organ printing technique is under investigation in the group of Prof. W.J.A. Dhert (Dep. of Orthopaedics, University Medical Center Utrecht, The Netherlands) to engineer bone grafts with osteoprogenitor cells, embedded in hydrogel matrices. In collaboration with our group, the effect of the photopolymerization process on behavior of encapsulated cells, with regard to cell-survival and differentiation, was investigated. The

cells were encapsulated in two different photopolymerizable hydrogels described in this thesis (Chapter 2 and 3). Cell-laden hydrogels were composed of goat bone marrow stromal cells (gBMSC's) encapsulated in HyA-MA (2% (w/w)) and HyPG-MA (30% (w/w)) hydrogels. The hydrogels were obtained after exposure to UV for 300 seconds in the presence of 0.05% (w/v) or 0.1% (w/v) Irgacure. The viability of the embedded cells was measured after 1, 2 or 3 weeks of incubation with a live/dead assay. Osteogenic differentiation of the cells was determined by evaluating the activity of the osteogenic marker alkaline phosphatase after 1 and 2 weeks of incubation in cell-laden HyA-MA or HyPG-MA hydrogels.

The results of the cell viability study and the differentiation study are shown in Figure 4 and 5, respectively. When using cells embedded in photopolymerized hydrogels, around 60% of cells were viable in HyA-MA hydrogels, as compared to 50% viability in HyPG-MA hydrogels after 1 week of encapsulation. After 2 weeks, up to 30% of the embedded cells were positive for alkaline phosphatase in HyA-MA gels, as compared to 5% positive cells in HyPG-MA gels. In conclusion, both the viability and the differentiation of the photoencapsulated cells depend on the hydrogel material used, with HyA-MA gels providing a more suitable matrix than HyPG-MA gels to the embedded gBMSC's. To further improve the gels it is suggested to couple e.g. RGD (arginine-glycine-aspartic acid) sequences to the hydrogel matrix in order to increase cell viability. Binding of the RGD sequence to integrins on cell surfaces is known to support cell adhesion and might enhance cell survival [27, 28], hence improving the applicability of the hydrogels as cell-supporting scaffolds.

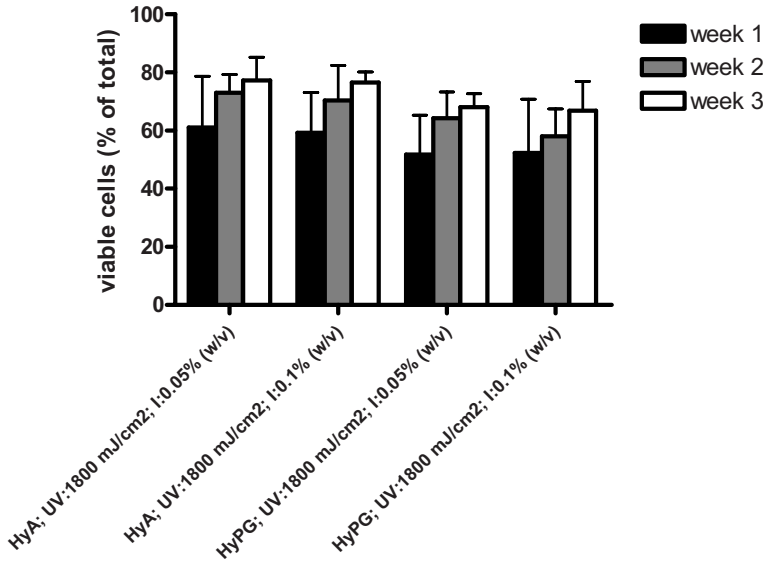

Figure 4. *Viability of embedded gBMSC's in HyA-MA or HyPG-MA hydrogels, as measured with a live/dead staining.*

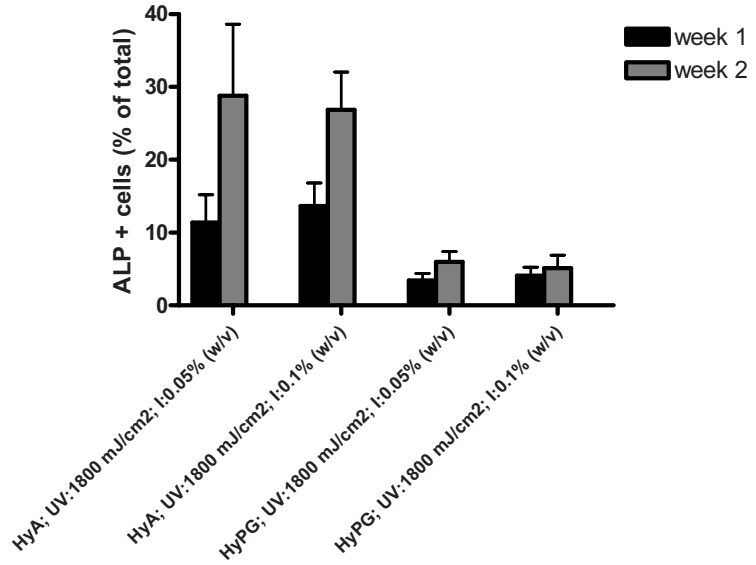

Figure 5. *Osteogenic differentiation of the embedded gBMSC's in HyA-MA or HyPG-MA hydrogels, analyzed with an alkaline phosphatase (ALP) assay.*

3. Controlled release of a model protein from degradable HyPG hydrogels

For drug delivery application it is advantageous to use biodegradable hydrogels as the degradation kinetics, which in turn will likely depend on the DS and the initial water content of the gel, can be used to control the release kinetics of loaded substances. Importantly, the formed degradation products should possess low toxicity. Degradability can be established by introducing labile bonds whereas the formed degradation products can be tailored by selecting the appropriate hydrogel building blocks. This polymer composition of hydrogels together with crosslink density and water content determine the release kinetics of entrapped proteins. In Chapter 8 we reported on novel biodegradable hyperbranched polyglycerol (HyPG) gels that can potentially be used as drug delivery system. Preliminary studies were performed on the release of the model protein lysozyme (M_W 14000 g/mol) from these degradable hydrogels. HyPG-HPMA (SA) gels (DS 20; 30% (w/w)) were prepared as described in Chapter 8. For loading of the gels with lysozyme, a protein solution in PBS was added to the polymer solution prior to polymerization, yielding a concentration of 1 mg lysozyme per 100 mg gel. The protein loaded gels were incubated at 37°C in carbonate buffer of pH 9.6 (to accelerate degradation) and the release of the lysozyme was evaluated using a BCA® Protein Assay.

In Figure 6 the release profile of lysozyme from HyPG-HPMA (SA) hydrogels is shown. After an initial fast release, a slow release of lysozyme was observed in which the release is mainly determined by diffusion. However, a second phase followed in which fast release was observed.

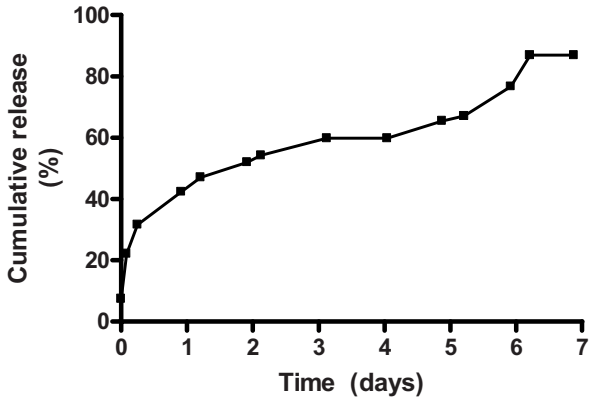

Figure 6. *Cumulative release of lysozyme from a HyPG-HPMA (SA) hydrogel (DS 20) in carbonate buffer, pH 9.6, at 37°C.*

This can be attributed to the degradation of the gel, which is associated with an exponential increase in hydrogel pore size. A maximal release of 85% was reached after 6 days for HyPG-HPMA (SA) gels. These results indicate that HyPG-HPMA (SA) gels have great potential as drug delivery matrices, although these systems still need to be optimized to control swelling and degradation, and consequently also protein release, at physiological pH.

References

1. Bouwstra JA, Ponec M. The skin barrier in healthy and diseased state. *Biochim Biophys Acta* 2006; 1758(12): 2080-2095.
2. Fartasch M. The nature of the epidermal barrier: structural aspects. *Adv Drug Deliv Rev* 1996; 18: 273-282.
3. Chuong CM, Nickoloff BJ, Elias PM, Goldsmith LA, Macher E, Maderson PA, Sundberg JP, Tagami H, Plonka PM, Thestrup-Pederson K, Bernard BA, Schroder JM, Dotto P, Chang CM, Williams ML, Feingold KR, King LE, Kligman AM, Rees JL, Christophers E. What is the 'true' function of skin? *Exp Dermatol* 2002; 11(2): 159-187.
4. Wilson DR, Maibach HI. Transepidermal water loss in vivo. Premature and term infants. *Biol Neonate* 1980; 37(3-4): 180-185.
5. Vernon HJ, Lane AT, Wischerath LJ, Davis JM, Menegus MA. Semipermeable dressing and transepidermal water loss in premature infants. *Pediatrics* 1990; 86(3): 357-362.
6. Lane AT, Drost SS. Effects of repeated application of emollient cream to premature neonates' skin. *Pediatrics* 1993; 92(3): 415-419.
7. Hoath SB, Narendran V. Adhesives and emollients in the preterm infant. *Semin Neonatol* 2000; 5(4): 289-296.
8. Okan D, Woo K, Ayello EA, Sibbald G. The role of moisture balance in wound healing. *Adv Skin Wound Care* 2007; 20(1): 39-53; quiz 53-35.
9. Pickens WL, Warner RR, Boissy YL, Boissy RE, Hoath SB. Characterization of vernix caseosa: water content, morphology, and elemental analysis. *J Invest Dermatol* 2000; 115(5): 875-881.
10. Hoath SB, Pickens WL, Visscher MO. The biology of vernix caseosa. *Int J Cosmetic Sci* 2006; 28: 319-333.
11. Moraille R, Pickens WL, Visscher MO, Hoath SB. A novel role for vernix caseosa as a skin cleanser. *Biol Neonate* 2005; 87(1): 8-14.
12. Haubrich KA. Role of Vernix caseosa in the neonate: potential application in the adult population. *AACN Clin Issues* 2003; 14(4): 457-464.
13. Hoeger PH, Schreiner V, Klaassen IA, Enzmann CC, Friedrichs K, Bleck O. Epidermal barrier lipids in human vernix caseosa: corresponding ceramide pattern in vernix and fetal skin. *Br J Dermatol* 2002; 146(2): 194-201.
14. van Dijk-Wolthuis WNE, Kettenes-van den Bosch JJ, van der Kerk-van Hoof A, Hennink WE. Reaction of dextran with glycidyl methacrylate: an unexpected transesterification. *Macromolecules* 1997; 30(11): 3411-3413.
15. Peppas NA, Bures P, Leobandung W, Ichikawa H. Hydrogels in pharmaceutical formulations. *Eur J Pharm Biopharm* 2000; 50(1): 27-46.
16. Hoffman AS. Hydrogels for biomedical applications. *Adv Drug Deliv Rev* 2002; 54(1): 3-12.
17. Nguyen KT, West JL. Photopolymerizable hydrogels for tissue engineering applications. *Biomaterials* 2002; 23(22): 4307-4314.
18. Peppas NA, Hilt JZ, Khademhosseini A, Langer R. Hydrogels in biology and medicine: from molecular principle to bionanotechnology. *Adv Mater* 2006; 18: 1345-1360.

19. Hennink WE, van Nostrum CF, Crommelin DJ, Bezemer JM. Hydrogels for the controlled release of proteins, in: Kwon G.S. (Ed.), Polymeric drug delivery systems, Taylor & Francis Group, Boca Raton, FL. 2005; 148: 215-249.
20. Anseth KS, Metters AT, Bryant SJ, Martens PJ, Elisseeff JH, Bowman CN. In situ forming degradable networks and their application in tissue engineering and drug delivery. *J Control Release* 2002; 78(1-3): 199-209.
21. De Geest BG, Stubbe BG, Jonas AM, Van Thienen T, Hinrichs WL, Demeester J, De Smedt SC. Self-exploding lipid-coated microgels. *Biomacromolecules* 2006; 7(1): 373-379.
22. Liu G-Y, Xu S, Qian Y. Nanofabrication of self-assembled monolayers using scanning probe lithography. *Acc Chem Res* 2000; 33: 457-466.
23. Yun K, Moon HT. Inducing chondrogenic differentiation in injectable hydrogels embedded with rabbit chondrocytes and growth factor for neocartilage formation. *J Biosci Bioeng* 2008; 105(2): 122-126.
24. Tessmar JK, Gopferich AM. Matrices and scaffolds for protein delivery in tissue engineering. *Adv Drug Deliv Rev* 2007; 59(4-5): 274-291.
25. Fedorovich NE, Alblas J, De Wijn JR, Hennink WE, Verbout AJ, Dhert WJA. Hydrogels as extracellular matrices for skeletal tissue engineering: state-of-art and novel application in organ printing. *Tissue Eng* 2007; 13(8): 1905-1925.
26. Fedorovich NE, De Wijn JR, Verbout AJ, Alblas J, Dhert WJA. Three-dimensional fiber deposition of cell-laden, viable, patterned constructs for bone tissue printing. *Tissue Eng: Part A* 2008; 14(1): 127-133.
27. Ruoslahti E, Reed JC. Anchorage dependence, integrins, and apoptosis. *Cell* 1994; 77(4): 477-478.
28. Nuttelman CR, Tripodi MC, Anseth KS. Synthetic hydrogel niches that promote hMSC viability. *Matrix Biol* 2005; 24(3): 208-218.

Appendix

Colour figures

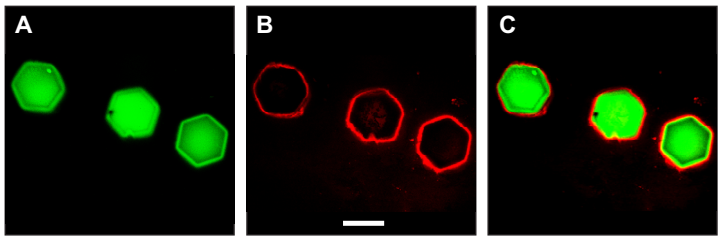

Figure 2. *HyPG-MA microgels labeled with FITC-dextran (A) and lipid coating (labeled with Texas Red) surrounding the microgels (B). Both images can be superposed (C) to visualize the labels of particles and lipids simultaneously. Scale bar represents 25 µm. (Chapter 5, page 81)*

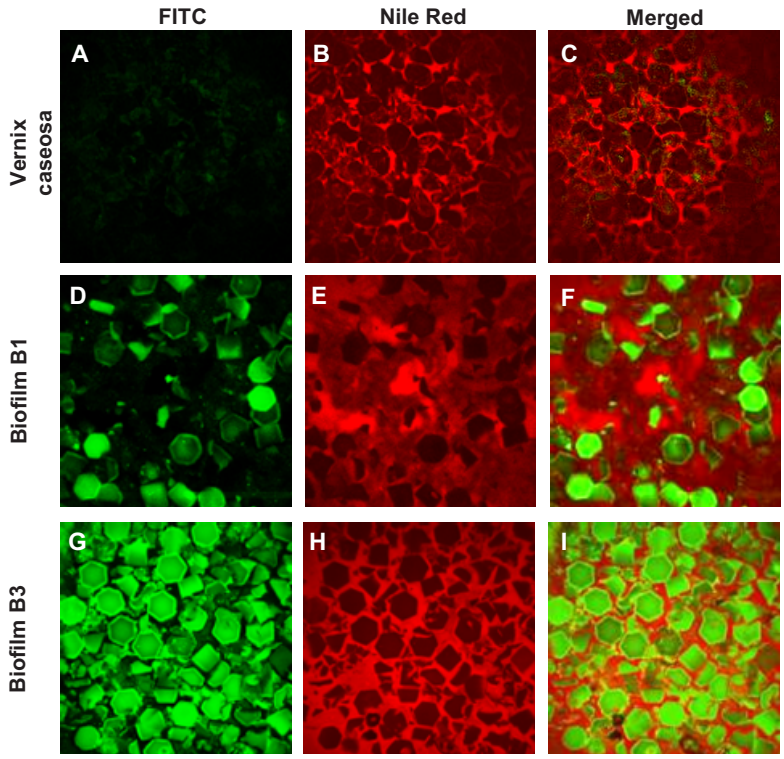

Figure 3. *Photomicrographs of native VC and various biofilm formulations, obtained by CLSM, are depicted. VC is characterized by corneocytes (black) which are embedded in Nile Red-labeled lipids (A-C). Synthetic biofilms, with particle:lipid ratios of 2:1 (biofilm B1; Fig. 3D-F) and 5:1 (biofilm B3; Fig. 3G-I), exhibit red labeled lipids and FITC-labeled synthetic particles. The particles (synthetic corneocytes) are intact and are randomly distributed within the lipid mixture. Scale bar represents 50 µm. (Chapter 5, page 81)*

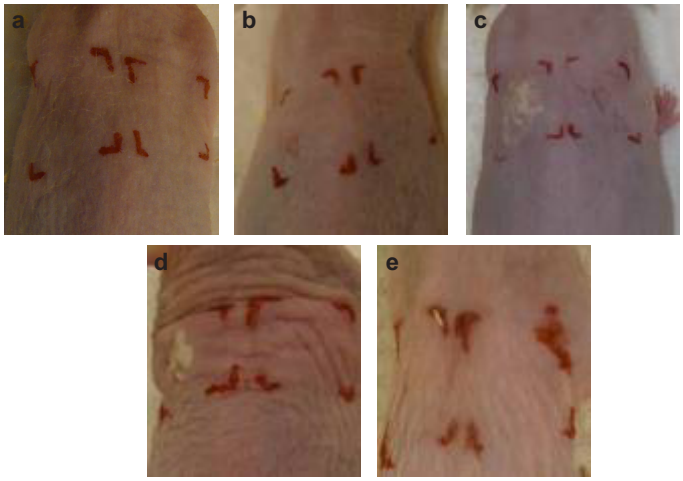

Figure 2. *Representative macroscopic observations of undisrupted skin (a), disrupted skin (model severe #3) directly after tape stripping (b) and the effect of topical application of VC (c, d and e; 5 mg/cm^2) on the disrupted skin after 1 min, 3 h and 8 h. (Chapter 6, page 98)*

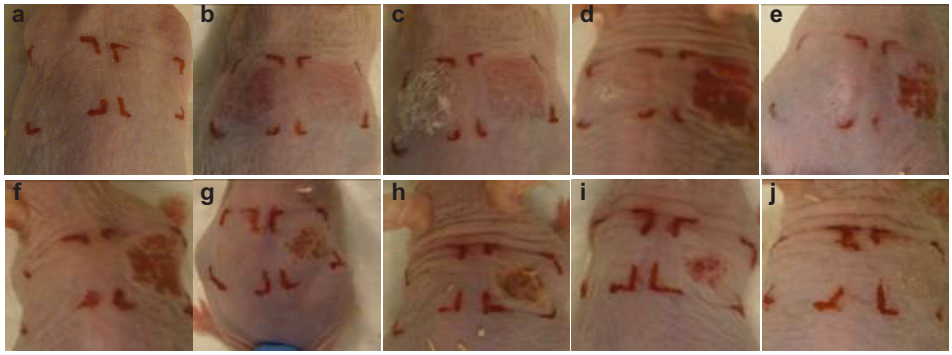

Figure 5. *Representative macroscopic observations of undisrupted skin (a), skin barrier disruption (model severe #4) immediately after tape stripping (b) and the effect of topical application of vernix caseosa after 1 min, 3 h, 5 h, 8 h, 24 h, 72 h, 100 h and 168 h (c, d, e, f, g, h, i, j, respectively) on the disrupted skin. (Chapter 6, page 101)*

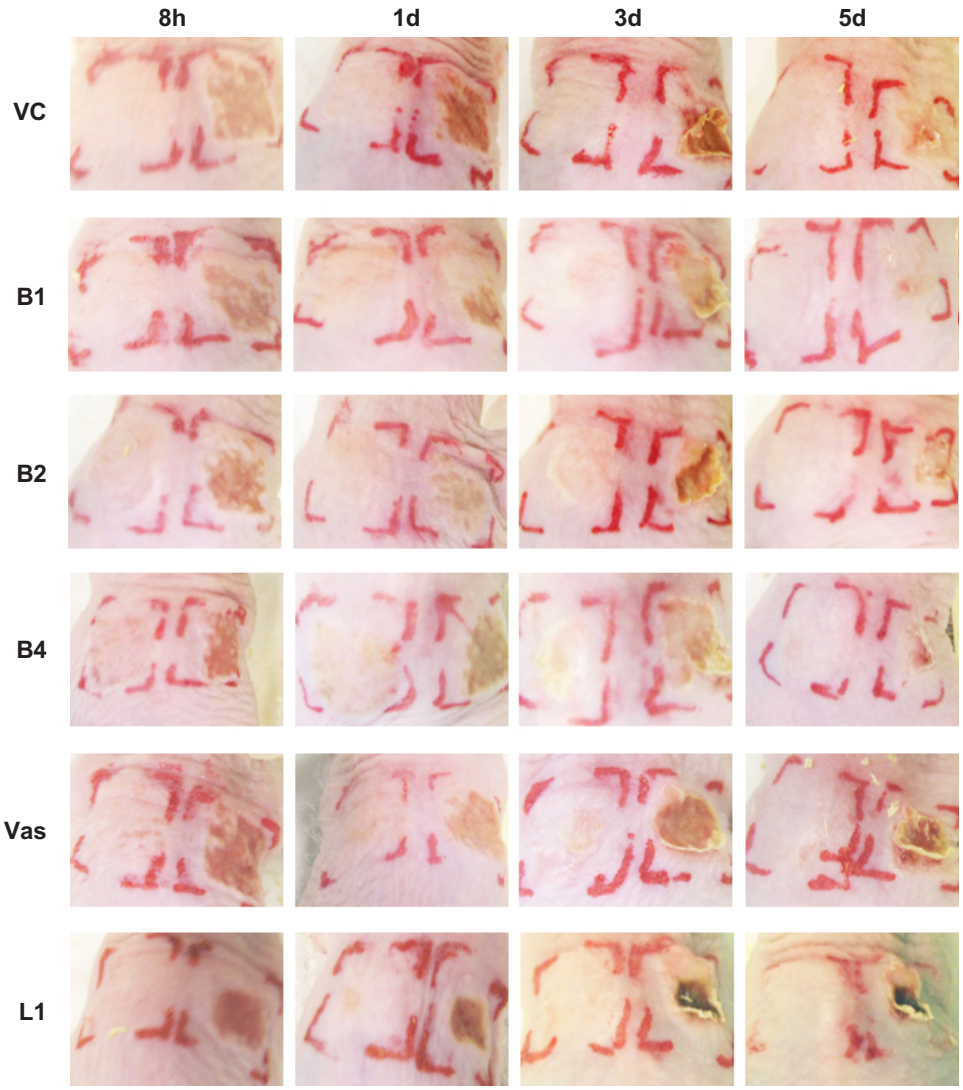

Figure 1. *Representative macroscopic observations of the effect of topically applied native VC, the biofilms B1, B2 and B4, Vas and lipid mixture L1 on disrupted skin after 8 h, 1 day, 3 days and 5 days. Formulations were applied on the left side and the right side served as disrupted, untreated control. (Chapter 7, page 117)*

Nederlandse samenvatting

De functie van de huid is de bescherming van het lichaam tegen uitdrogen en het binnendringen van ongewenste stoffen. De belangrijkste barrière wordt gevormd door de buitenste huidlaag, het stratum corneum (SC). Het SC is opgebouwd uit verhoornde cellen (corneocyten) ingebed in een matrix van lipiden. Verstoring van de huidbarrière kan door verschillende factoren veroorzaakt worden, zoals omgevingsfactoren, brandwonden of verwondingen. Bovendien kan een verminderde barrière ook bij een zieke en/of premature huid voorkomen. Een belangrijke factor voor een voorspoedig herstel en voor het behoud van een optimale barrière functie is de hydratatiegraad van het SC. Een evenwichtig vochtgehalte behoudt de flexibiliteit van de huid en voorziet enzymen van voldoende water om het continue vernieuwingsproces van het SC in stand te houden. Een gebrek of overmaat aan hydratatie zal deze processen belemmeren.
Veel barrière- en vochtinbrengende crèmes zijn op de markt gebracht met het doel het lichaam te beschermen tegen een te groot waterverlies via het huidoppervlak en om de hydratatiegraad van de huid te moduleren. Deze crèmes lijken echter in het geheel niet op het SC. De waterbindende capaciteit in deze crèmes is vaak laag. Crèmes die wel een hoge waterbindende capaciteit hebben, veranderen drastisch van eigenschappen door verdamping van water. Hierdoor is het niet mogelijk een gecontroleerde en langdurige afgifte van water te bewerkstelligen. Om deze reden is gesuggereerd dat een crème, die een hoge waterbindende capaciteit combineert met een constante structuur tijdens waterverdamping, zou kunnen helpen in de ontwikkeling en/of herstel van de huidbarrière. In omstandigheden waar SC nog wel aanweizg is (bijvoorbeeld een droge huid), zou de applicatie van deze crèmes kunnen resulteren in een gecontroleerde afgifte van water. Wanneer bovendien de structuur van het SC nauwkeurig nagebootst wordt, dan zouden deze crèmes ook als beschermende laag kunnen dienen voor beschadigde huid waar het SC grotendeels afwezig is.

Een voorbeeld van een natuurlijke crème met soortgelijke structuur als het SC is vernix caseosa (VC). VC is een witte, vettige natuurlijke biofilm, die gedurende het laatste trimester voor de geboorte door de humane fetus uitgescheiden wordt en die zich over het gehele huidoppervlakte uitspreidt. VC bestaat uit dode cellen ingebed in een lipiden matrix. De cellen vertonen veel gelijkenis met de cellen in het SC. De laatste jaren zijn verschillende biologische eigenschappen toegekend aan VC: er zijn bijvoorbeeld veel aanwijzingen dat VC de vorming van het SC in de fetus stimuleert. Vanwege deze biologsche functies is gesuggereerd dat VC veelbelovend is als therapeutische crème ter bevordering van het herstel van de beschadigde volwassen huid en/of premature huid. Klinische toepassing van VC is echter beperkt, vanwege de gelimiteerde beschikbaarheid en de kans op het overdragen van ziektes.

De ontwikkeling van een synthetisch VC equivalent zal tot een nieuwe generatie biofilms kunnen leiden die op een unieke manier de samenstelling en eigenschappen van VC nabootsen. In tegenstelling tot bestaande crèmes zal de structuur van deze nieuwe biofilms wel de structuur van het SC kunnen benaderen wanneer deze crèmes op een rationele wijze worden ontworpen. De innoverende biofilms zouden de barrière-herstelprocessen kunnen bevorderen. Deze processen worden in literatuur ook aan VC toebedeeld.

Het onderzoek beschreven in dit proefschrift betreft de ontwikkeling en karakterisering van een nieuwe generatie synthetische biofilms die de structuur en eigenschappen van natuurlijke VC nabootsen. De biofilms zullen hun toepassing kunnen vinden in het beschermen van de huid en/of bevorderen van het herstel van aangetaste huid.
Deze biofilms zijn gebaseerd op synthetische waterhoudende cellen (synthetische corneocyten) ingebed in een lipiden matrix. De ontwikkeling van de synthetische corneocyten, bestaande uit gecrosslinkte polymeren, staat beschreven in het eerste deel van dit proefschrift. Gecombineerd met het werk van Rissmann (gepresenteerd in zijn proefschrift; publicatie voorzien voor eind 2008), dat voornamelijk gebaseerd is op de karakterisering van VC en de ontwikkeling van de synthetische intercellulaire lipiden matrix, was het mogelijk biofilms te creëeren. De ontwikkeling, karakterisering en vervolgens het testen *in vivo* van de biofilms is beschreven in het tweede deel van dit proefschrift.

In **Hoofdstuk 1** wordt een algemene inleiding gegeven en worden de doelen van het onderzoek in dit proefschrift uiteen gezet.
De corneocyten zijn één van de belangrijkste elementen in VC en zijn verantwoordelijk voor de waterbindende eigenschappen. In een synthetisch VC model, kan de rol van corneocyten overgenomen worden door hydrogel deeltjes. Hydrogelen zijn 3-dimensionale netwerken die opgebouwd zijn uit hydrofiele polymeren. Ze zijn in staat grote hoeveelheden water te absorberen waarbij de 3-D structuur gehandhaafd blijft, wat ze bijzonder aantrekkelijk maakt voor tal van farmaceutische en biomedische toepassingen. Om het oplossen van de polymeren in een waterige omgeving te voorkomen, is de aanwezigheid van crosslinks (vernettingen) in een hydrogel nodig. Crosslinks kunnen tot stand gebracht worden via chemische (permanent) of fysische (reversibel) bindingen. In **Hoofdstuk 2** is de modificatie en de daaropvolgende chemische crosslinking van het hydrofiele polymeer hyaluronzuur (HyA) beschreven. HyA werd gemodificeerd met methacrylaatgroepen in een geschikt organisch oplosmiddel. Het verkregen product, hyaluronzuur methacrylaat (HyA-MA), werd chemisch vernet wat resulteerde in elastische hydrogelen. De netwerkeigenschappen (elasticiteit en zwelling) van de gelen konden worden gevarieerd door de methacrylaat-substitutiegraad van het HyA. Als alternatief voor HyA werd in **Hoofdstuk 3** ingegaan op

het polymeer hyperbranched polyglycerol (HyPG) dat op een zelfde manier als HyA werd gemodificeerd. Van deze gesubstitueerde HyPG's werden hydrogelen gemaakt door middel van chemische crosslinking. Ook hier konden de netwerkeigenschappen gevarieerd worden. De verwerkingseigenschappen van HyPG (bijvoorbeeld viscositeit) was superieur aan die van HyA en daarom werd dit polymeer gebruikt in verdere studies. De ontwikkeling van microscopische hydrogelen, vervaardigd van gecrosslinkt HyPG-MA, is beschreven in **Hoofdstuk 4**. Deze deeltjes zullen toegepast worden als synthetische corneocyten in biofilms, zoals in andere hoofdstukken van dit proefschrift beschreven wordt. De vervaardiging van goed-gedefinieerde HyPG-MA microdeeltjes met uniforme grootte en vorm werd met verschillende technieken onderzocht. Goede resultaten en een hoge opbrengst aan deeltjes werden verkregen met fotolithografie. Fotolithografie is een techniek waarbij de polymere oplossing gecrosslinkt wordt d.m.v. UV-licht dat door een masker met motieven valt. Na het stoppen van de belichting en verwijderen van het masker werden de deeltjes verzameld. Afhankelijk van het masker, variëerden de deeltjes in vorm (bijvoorbeeld zeshoeken en rechthoeken) en grootte (bijvoorbeeld van 30 µm tot 1400 µm). Om de natuurlijke corneocyten zo goed mogelijk na te bootsen, werden HyPG-MA deeltjes vervaardigd in de vorm van een zeshoek met een diameter van 30 µm en een dikte van 20 µm. De ontwikkeling van biofilms door deze deeltjes te mengen met een lipiden matrix is onderzocht in **Hoofdstuk 5**. De bereiding van de lipiden matrix staat beschreven in het proefschrift van R. Rissmann. Diverse formuleringen werden gemaakt door gebruik te maken van verschillende deeltjes:lipid (d.w.z. 2:1 en 5:1) verhoudingen. Tevens werden deeltjes met verschillend watergehalte (d.w.z. 50% en 80%) en ongecoate of lipid-gecoate deeltjes gebruikt. De biofilms met een deeltjes:lipid verhouding van 5:1 vertoonden een zelfde homogeniteit als natuurlijke VC. Alle formuleringen waren stabiel gedurende minimaal 1 maand bij 4°C en bovendien waren diverse eigenschappen (d.w.z. dehydratatie, reologie en thermische analyse) van de formuleringen zo te sturen dat ze de eigenschappen van natuurlijke VC zo dicht mogelijk benaderden. Uiteindelijk werd een uitstekende gelijkenis van onze synthetische biofilms met natuurlijk VC verkregen.

Alvorens de veiligheid en werkzaamheid van deze nieuwe biofilms *in vivo* met muizen geëvalueerd kan worden, moet eerst een geschikt model ontwikkeld worden om barriere herstel over een langere periode te onderzoeken. In **Hoofdstuk 6** is daarom ingegaan op de ontwikkeling van een betrouwbaar muismodel voor het herstel van een beschadigde huid. Vijf verschillende niveau's van huidbeschadiging op muizen, tot stand gebracht door consecutief tape strippen (een speciale tape wordt daarbij op de huid aangedrukt en in één beweging verwijderd), werden onderzocht. Door het aantal tape strips te verhogen werden modellen gegenereerd met een beschadigde huid variërend van matig tot ernstig beschadigd. Bij een matig beschadigde huid herstelde de huid binnen 72 uren terwijl daarentegen de ernstig beschadigde huid zich binnen 200 uren

volledig herstelde. De applicatie van VC op dit laatste huidmodel (d.w.z. ernstig beschadigde huid) versnelde aanzienlijk het herstelproces: na 100 uren was de huid volledig hersteld. Deze resultaten laten zien dat een geschikt muismodel voor herstel van beschadigde huid is verkregen. Bovendien wordt het vermogen van VC om het herstelproces te bevorderen, zoals eerder was gesuggereerd in literatuur, bevestigd.
In **Hoofdstuk 7** is beschreven hoe de biofilms werden geëvalueerd op inductie van huidfuctie-herstel op de bovengenoemde muismodellen met ernstig beschadigde huid. Diverse formuleringen werden op de beschadigde huid aangebracht waarna het effect bestudeerd en vergeleken werd met natuurlijke VC en de commercieel verkrijgbare zalf Vaseline. De toepassing van de formuleringen bevorderde in alle gevallen het herstel van de huid. Eén van de biofilms (d.w.z. biofilm B4, bestaande uit ongecoated deeltjes met 50% water-gehalte en een deeltjes:lipid verhouding van 2:1) vertoonde het sterkste effect en kwam het beste overeen met VC. Deze resultaten wijzen op het belang van de aanwezigheid van de verschillende individuele componenten, zoals de typen lipiden en de deeltjes:lipid verhouding.

De synthetische corneocyten (d.w.z. hexagonale HyPG-MA microgelen met een diameter van 30 µm), zoals beschreven in **Hoofdstuk 4** en **5**, zijn niet-degradeerbaar onder fysiologische omstandigheden. In **Hoofdstuk 8** is daarom een inleidende studie gepresenteerd betreffende de ontwikkeling van biodegradeerbare HyPG gelen die potentie hebben als gecontroleerd afgiftesysteem in de biofilms. HyPG werd gemodificeerd met HPMA ((2-hydroxypropyl) methacrylamide)-groepen in een geschikt organisch oplosmiddel. Het verkregen product, HyPG-HPMA, werd chemisch gecrosslinkt wat resulteerde in elastische hydrogelen. De gelen waren inderdaad degradeerbaar: de degradatietijd was te sturen tussen 2 en 6 dagen bij pH 9.6, 37°C). De netwerkeigenschappen (elasticiteit en zwelling) van de gelen konden worden gevarieerd door meer of minder HPMA-groepen aan HyPG te koppelen.

Een Engelse samenvatting en de toepasbaarheid van de biofilms beschreven in dit proefschrift is gepresenteerd in **Hoofdstuk 9**. Hierbij is aandacht gegeven aan de aspecten die nog bestudeerd moeten worden voordat de biofilms klinisch toegepast kunnen worden. Verder worden de resultaten van inleidende studies met betrekking tot eiwitafgifte en weefseltechnologie (of ‘tissue engineering’) kort besproken.

Het onderzoek in dit proefschrift laat zien dat een nieuwe generatie biofilms ontwikkeld is die de structuur en eigenschappen van natuurlijke VC nabootsen. Deze biofilms zijn werkzaam als huidbescherming en bevorderen het herstel van de huidbarrière. Deze unieke systemen hebben veel potentie om zieke, droge en premature huid te beschermen en wondgenezing te bevorderen.

List of abbreviations

ACN	acetonitrile
AUC	area under the curve
CAD	computer-aided design
CDI	*N,N'*-carbonyldiimidazol
CLSM	confocal laser scanning microscopy
CVD	chemical vapor deposition
D_0	initial diameter of a gel
D_t	diameter of a gel at time t
DCC	*N,N*-dicyclohexylcarbodiimide
DCM	dichloromethane
DMA	dynamic mechanical analyzer
DMAP	4-(*N,N*-dimethylamino)pyridine
DMSO	dimethyl sulfoxide
DOPC	dioleoyl phosphatidylcholine
DOTAP	dioleoyl trimethylammoniumpropane
DS	degree of substitution
DSC	differential scanning calorimetry
E	Young's modulus
Euc	Eucerin cum aqua
FITC	fluorescein isothiocyanate
G'	storage modulus
G"	loss modulus
GMA	glycidyl methacrylate
GPC	gel permeation chromatography
^{1}H-NMR	proton nuclear magnetic resonance
HCl	hydrochloric acid
HEPES	4-(2-hydroxyethyl)-1-piperazineethanesulfonic acid
HPLC	high performance liquid chromatography
HPMA	2-hydroxypropyl methacrylamide
HPMA-CI	hydroxypropyl methacrylamide activated with CDI
HPMA-SA	succinilated hydroxypropyl methacrylamide
HyA	hyaluronic acid
HyA-MA	methacrylated hyaluronic acid
HyA-TBA	hyaluronic acid with tetrabutylammonium ion
HyPG	hyperbranched polyglycerol
HyPG-MA	methacrylated hyperbranched polyglycerol

HyPG-HPMA	HyPG derivatized with HPMA (using HPMA activated with CDI)
HyPG-SA-HPMA	HyPG derivatized with succinilated HPMA
i.p.	intraperitioneal
k	reaction rate constant
KOH	potassium hydroxide
KPS	potassium peroxodisulfate
M_c	molecular weight between crosslinks
M_n	number average molecular weight
M_W	weight average molecular weight
MA	methacrylate
MEHQ	hydroquinone monomethyl ether
$MgSO_4$	magnesium sulphate
NaOH	sodium hydroxide
NMR	nuclear magnetic resonance
PBS	phosphate buffered saline
PDMS	poly(dimethylsiloxane)
PEG	poly(ethylene glycol)
PRINT	particle replication in nonwetting templates
R	gas constant
RO	reversed osmosis
ROMBP	ring-opening multibranching polymerization
RP-HPLC	reversed phase-high performance liquid chromatography
SC	stratum corneum
SD	standard deviation
tan δ	tangens (delta)
T	absolute temperature
TBA-F	tetrabutylammonium fluoride trihydrate
TEMED	*N,N,N',N'*-tetramethylethylenediamine
TEWL	transepidermal water loss
TFA	trifluoroacetic acid
TGA	thermogravimetric analysis
THF	tetrahydrofuran
UV	ultraviolet
UPLC	ultra performance liquid chromatography
Vas	Vaseline
VC	vernix caseosa
W_0	initial weight of a gel
W_t	weight of a gel at time t

List of publications

Papers

Bivas-Benita M, **Oudshoorn MHM**, Romeijn S, Van Meijgaarden K, Koerten H, Van der Meulen H, Lambert G, Ottenhof T, Benita S, Junginger H, Borchard G. Cationic submicron emulsions for pulmonary DNA immunization. *J Control Release* 2004;100(1):145-155

Oudshoorn MHM, Rissmann R, Bouwstra JA, Hennink WE. Synthesis and characterization of hyperbranched polyglycerol hydrogels. *Biomaterials* 2006;27(32):5471-5479

Oudshoorn MHM, Rissmann R, Bouwstra JA, Hennink WE. Synthesis of methacrylated hyaluronic acid with tailored degree of substitution. *Polymer* 2007;48:1915-1920

Oudshoorn MHM, Penterman R, Rissmann R, Bouwstra JA, Broer DJ, Hennink WE. Preparation and characterization of structured hydrogel microparticles based on crosslinked hyperbranched polyglycerol. *Langmuir* 2007;23:11819-11825

Rissmann R, Groenink HW, Gooris GS, **Oudshoorn MHM**, Hennink WE, Ponec M and Bouwstra JA. Temperature-induced changes in structural and physicochemical properties of vernix caseosa. *J Invest Dermatol* 2008; 128(2):292-299

Rissmann R, **Oudshoorn MHM**, Kocks E, Hennink WE, Ponec M, Bouwstra JA. Lanolin-derived lipid mixtures mimic closely the lipid composition and organization of vernix caseosa lipids. Accepted for publication in *Biochim Biophys Acta - Biomembranes*

Oudshoorn MHM, Rissmann R, van der Coelen D, Hennink WE, Ponec M, Bouwstra JA. Development of a Murine Model to Evaluate the Effect Vernix Caseosa on Skin Barrier Recovery. Accepted for publication in *Exp Dermatol*

Rissmann R, **Oudshoorn MHM**, Kocks E, Ponec M, Bouwstra JA, Hennink WE. Mimicking vernix caseosa - preparation and characterization of synthetic biofilms. *Submitted for publication*

Oudshoorn MHM, Rissmann R, van der Coelen D, Hennink WE, Ponec M, Bouwstra JA. Effect of synthetic vernix biofilm on barrier recovery of damaged mice skin. *Submitted for publication*

Rissmann R, **Oudshoorn MHM**, Hennink WE, Ponec M, Bouwstra JA. Skin barrier disruption by acetone – observations in a hairless mouse skin model. *Submitted for publication*

Fedorovich NE, **Oudshoorn MHM**, van Geemen D, Hennink WE, Alblas J, Dhert WJ. Stem cell fate after photoexposure in cell-laden hydrogels. *Submitted for publication*

Selected abstracts

Oudshoorn MHM, Rissmann R, Bouwstra JA, Hennink WE. Synthesis and characterization of hyperbranched polyglycerol hydrogels. Dutch Polymer Days, February 2007, Lunteren, The Netherlands.

Oudshoorn MHM, Rissmann R, Bouwstra JA, Hennink WE. Synthesis and characterization of hyperbranched polyglycerol hydrogels. Pre-satellite meeting of the Pharmaceutical Sciences World Congress, April 2007, Amsterdam, The Netherlands.

Oudshoorn MHM, Rissmann R, Bouwstra JA, Hennink WE. Synthesis and characterization of hyperbranched polyglycerol hydrogels. Pharmaceutical Sciences World Congress, April 2007, Amsterdam, The Netherlands.

Oudshoorn MHM, Rissmann R, Bouwstra JA, Hennink WE. Methacrylated hyperbranched polyglycerol hydrogels: preparation and physical characterization. 34th Controlled Release Society Annual Meeting, July 2007, Long Beach (California), USA.

Oudshoorn MHM, Penterman R, Rissmann R, Bouwstra JA, Broer DJ, Hennink WE. Structured hydrogel microparticles based on crosslinked hyperbranched polyglycerol. Dutch Polymer Days, February 2008, Lunteren, The Netherlands.

Oudshoorn MHM, Penterman R, Rissmann R, Bouwstra JA, Broer DJ, Hennink WE. Fabrication of uniformly shaped hydrogel microparticles based on crosslinked hyperbranched polyglycerol by micromolding and photolithographic methods. 10th European Symposium on Controlled Drug Delivery, April 2008, Noordwijk, The Netherlands.

Oudshoorn MHM, Penterman R, Rissmann R, Bouwstra JA, Broer DJ, Hennink WE. Structured hydrogel microparticles based on crosslinked hyperbranched polyglycerol. 8th World Biomaterials Congress, May-June 2008, Amsterdam, The Netherlands.

Oudshoorn MHM, Penterman R, Rissmann R, Bouwstra JA, Broer DJ, Hennink WE. Monodisperse Hydrogel Microparticles based on crosslinked hyperbranched polyglycerol prepared by micromolding and photolithographic methods. 35th Controlled Release Society Annual Meeting, July 2008, New York (NY), USA.

Rissmann R, Groenink HWW, **Oudshoorn MHM**, Hennink WE, Ponec M, Bouwstra JA. New insights into the lipid composition, lipid phase behavior and ultrastructure of vernix caseosa. Perspectives of percutaneous penetration conference, April 2006, La Grande Motte, France.

Rissmann R, Groenink HWW, **Oudshoorn MHM**, Hennink WE, Ponec M, Bouwstra JA. Lipid organization and ultrastructure of vernix caseosa. Autumn Meeting of the Belgian-Dutch Biopharmaceutical Society, December 2006, Leiden, The Netherlands.

Rissmann R, Groenink HWW, **Oudshoorn MHM**, Hennink WE, Ponec M, Bouwstra JA. Temperature-dependent characterization of vernix caseosa. Pre-satellite meeting of the Pharmaceutical Sciences World Congress, April 2007, Amsterdam, The Netherlands.

Rissmann R, Groenink HWW, **Oudshoorn MHM**, Hennink WE, Ponec M, Bouwstra JA. Temperature-dependent characterization of vernix caseosa. Pharmaceutical Sciences World Congress, April 2007, Amsterdam, The Netherlands.

Rissmann R, Groenink HWW, **Oudshoorn MHM**, Hennink WE, Ponec M, Bouwstra JA. Physicochemical features of vernix caseosa change within physiological temperature range. 34th Controlled Release Society Annual Meeting, July 2007, Long Beach (California), USA.

Rissmann R, Groenink HWW, **Oudshoorn MHM**, Hennink WE, Ponec M, Bouwstra JA. Temperature-induced changes in structural and physicochemical properties of vernix caseosa. Gordon research conference: Barrier function of the mammalian skin, August 2007, Newport (Rhode Island), USA.

Rissmann R, Groenink HWW, **Oudshoorn MHM**, Hennink WE, Ponec M, Bouwstra JA. Temperature-induced changes in structural and physicochemical properties of vernix caseosa. Annual meeting of the American Association for Pharmaceutical Scientists, November 2007, San Diego (California), USA.

Rissmann R, Groenink HWW, **Oudshoorn MHM**, Hennink WE, Ponec M, Bouwstra JA. Investigations of the thermotropic properties of vernix caseosa. Spring Meeting of the Belgian-Dutch Biopharmaceutical Society, May 2008, Leuven, Belgium.

Curriculum Vitae

Date of birth	9th November 1981
Place of birth	Delft, The Netherlands

Education

1999-2004	Bio- Pharmaceutical Sciences at Leiden University (The Netherlands).
1993-1999	Atheneum at Stanislas College, Delft (The Netherlands).

Work experience

09/2004 – 09/2008	PhD student at the Dpt. of Pharmaceutics, Utrecht University (The Netherlands). Title: Composite of microgels and lipids as biofilm to restore skin barrier function. Promotor: Prof. Dr. Ir. W.E. Hennink.
01/2004 – 07/2004	Internship at OctoPlus N.V., Leiden (The Netherlands). Subject: Synthesis and characterization of alternatives to dex-HEMA.
10/2003 – 01/2004	Internship at Novagali Pharma, Paris (France). Subject: Evaluation of the current treatments for age-related macular degeneration.
08/2003 – 09/2003	Essay at the Dpt. of Pharmacology, Leiden University (The Netherlands). Subject: Mechanisms underlying the generation of temporal lobe epilepsy and the emergence of pharmacoresistance.
07/2002 – 07/2003	Internship at the Dpt. of Pharmaceutical Technology, Leiden University (The Netherlands). Subject: Cationic carriers for the pulmonary delivery of DNA vaccines against tuberculosis.

Achievements

Anselmus award in pharmaceutical technology (The Netherlands, 2003).

Acknowledgements / Dankwoord

Alle begin is moeilijk...
Zelfs het begin van een dankwoord is lastig. Want waar begin je? Er zijn zoveel mensen die ik wil bedanken. Zoveel nieuwe mensen die ik heb leren kennen en oude bekenden die ik beter heb leren kennen. Voor al die mensen bij voorbaat:

'Bedankt!'

Natuurlijk zijn er altijd mensen die een bijzondere bijdrage hebben geleverd en die wil ik hier graag persoonlijk bedanken. Allereerst Wim Hennink, mijn begeleider en geestelijk vader van deze promotie. Beste Wim, bedankt voor uw inzet en vertrouwen. Ik weet dat ik nogal koppig ben en u aardig "op de huid heb gezeten". Daardoor heb ik het u misschien niet altijd even makkelijk gemaakt, maar als ik zo terug kijk denk ik dat we allebei tevreden kunnen zijn over het eindresultaat. Met veel respect ben ik begonnen. Het respect is gebleven, maar tegen het einde van de promotie heb ik ervan genoten dat ik niet meer zozeer onder begeleiding, maar veel meer samen met u aan dit onderzoek mocht werken. Heel veel dank voor de goede begeleiding!
Vanaf het begin waren ook geestelijke 'moeders' Joke Bouwstra, mijn tweede promotor, en Maja Ponec bij mijn project betrokken. Pas aan het eind werd het contact met jullie intensiever. Ik wil jullie allebei bedanken voor de begeleiding bij het project, maar ook voor de goede gesprekken. Behalve vakinhoudelijk hebben jullie mij ook geholpen bij het beter leren kennen van de wereld en mezelf. Het heeft mij zeker geholpen bij mijn oriëntatie naar een nieuwe baan. Bedankt voor alles! Naast deze begeleiding was er nog een andere AIO met wie ik dit project deelde. Robert, het is dan eindelijk zover! In het begin deden we allebei ons eigen deel, daarna kwam alles bij elkaar en hebben we veel samengewerkt. Gelukkig konden we het goed met elkaar vinden, want anders was het niet gelukt om samen zoveel werk te verzetten. Met de nodige humor (en wederzijds geduld....) gingen we er toch altijd weer tegenaan. Ik denk dat we zeker trots kunnen zijn op onze proefschriften! Ik wil je heel veel succes wensen met je nieuwe baan en heel veel geluk met Sylvia en de kleine (al vind ik wel dat je een erg omslachtige manier hebt gekozen om aan nieuwe vernix te komen). We zullen zeker contact houden!

Twee keer per jaar hadden we voor dit project een gebruikerscommissie vergadering, waar we de voortgang van ons project besproken. Ik zou graag alle deelnemers aan deze vergadering willen bedanken voor hun inzet en goede discussiepunten: Sicco Scherjon (LUMC), Dick Broer (Philips), Chris Dederen (Croda), Kees Korevaar (Cosmoferm) en Paul Boontje (STW). Met dank aan Sicco hadden we voor ons onderzoek altijd genoeg vernix. In het bijzonder zou ik Dick willen bedanken die mij de mogelijkheid heeft gegeven een deel van mijn onderzoek bij Philips uit te voeren. Daar

werd ik begeleid door Roel Penterman. Dick, Roel, bij jullie was ik altijd welkom en ook met mijn vragen kon ik altijd bij jullie terecht. Bedankt voor alles! Tenslotte wil ik Johann Wiechers niet vergeten. Bij de eerste vergaderingen zat jij er ook nog bij, daarna heeft Chris het van je overgenomen. Bij deze wil ik dus jullie beiden bedanken voor jullie input, het was voor mij heel waardevol.
Via Dick en Roel kwam ik terecht bij Jaap den Toonder, aan wie ik dank verschuldigt ben omdat hij me in contact bracht met Lambert van Breemen. Lambert, bedankt voor de tijd en moeite die je in de metingen hebt gestoken. Helaas was het toch allemaal ingewikkelder dan verwacht en zijn de resultaten niet in dit boekje opgenomen, maar het is zeker niet voor niks geweest. Jij bent nu bezig met de laatste loodjes. Succes! Natalja, jij hebt enkele experimenten met mijn polymeren gedaan. Een deel daarvan staat in dit proefschrift. Het was leuk en leerzaam om met je samen te werken. Ik wens je veel succes met je eigen promotie onderzoek, maar het gaat je zeker lukken om wat moois neer te zetten. In the mean time I found another person willing to do some AFM measurements. Kasper, thank you for everything! We only met a few times, but we became good friends. Now you are in Denmark, we keep contact by mail…but for sure we will visit you soon!

Nataša, vier jaar geleden kwam ik als nieuwe collega (baby-AIO...) op het lab naast je werken. Je hebt het niet gemakkelijk gehad, maar juist toen hebben we elkaar beter leren kennen en ik waardeer het in je dat je zo'n sterke vrouw bent. Ik ben blij dat ik je mijn vriendin mag noemen. Ik vind het dan ook super dat ik je paranimf mocht zijn en dat en dat ik deze eer kan retourneren! Barbara, jij wordt mijn andere paranimf. Ben je al zenuwachtig (straks krijg je nog een vraag van Wim....)? En weet je al wat je aan gaat trekken? We gaan wel een keertje samen shoppen en dan komt het helemaal goed! Bedankt dat jullie er altijd voor me waren; even bijkletsen of uitrazen...het kon altijd. En ook al werken we straks alledrie ergens anders, we zullen nog vaak afspreken om samen te gaan eten of shoppen (of allebei)!

Labgenootjes, Z 709 en later Z 711 was echt een gezellig lab! Niels, Sophie, Albert en Frank, zonder jullie was het werk stukken zwaarder geweest. Altijd had iemand wel tijd voor een praatje of grapje en ook een helpende hand was nooit een probleem. Sophie, bedankt voor de vrouwelijke onderonsjes op het voornamelijk 'mannen'-lab. Zowel aan het begin als aan het einde van mijn aio-tijd kon ik bij jou terecht met al mijn vragen. Bedankt voor alles en succes met je nieuwe baan! Albert, jij bent nu ook bezig met de laatste loodjes. Samen hebben we de afgelopen maanden zitten zwoegen in de AIO-kamer. Hoewel onze manier van plannen wel verschilde (maar chaos en orde gaan soms goed samen) hebben we nu wel allebei de eindstreep in zicht. Succes, je bent er bijna! Niels en Frank, nog even maar dan is het voor jullie ook zover. Ik ben blij dat ik met jullie een lab mocht delen, het was erg gezellig!

Natuurlijk wil ook alle andere (ex)collega's van Biofarmacie bedanken voor de gezellige pauzes, bbq's, labuitjes, feestjes ed. Mark en Martin, jullie waren mijn grote broers die mij op het lab overal doorheen sleepten. Ook al zijn jullie nu alweer een tijdje weg, ik hoop dat we nog vaak even zullen bijkletsen over de mail of op de fiets! Maryam, we met in Leiden and then I followed you to Utrecht. Now I stop following you and choose my own path. You're not afraid of giving your opinion, always being honest…you are a great person! I would also like to thank Lidija (keep sending those e-mails), Chantal, Marieke (de pogingen zijn er, maar we gaan nu echt wat afspreken), Lise, Emmy, Roberta and Sjoerd. Not only during working hours, but also afterwards it was always possible to talk and laugh with you! Without you, those 4 years (and especially the end!) would not have been the same.
Mies bij wie sta jij niet in het dankwoord? En terecht! bedankt voor je altijd positieve instelling en al je hulp met de dagelijkse beslommeringen op het lab, je bent er werkelijk voor iedereen en menig AIO, zo ik ook, heeft voor jouw een apart plekje in zijn dankwoord. Raymond en Marcel, bedankt voor jullie hulp bij de opzet van mijn *in vivo* experimenten! Voor de confocal plaatjes kan ik maar één persoon bedanken...Marjan. Niet alle plaatjes staan er in, maar het heeft mij wel geholpen om nog betere resultaten te krijgen. Natuurlijk moet ik ook Frits en zijn vrouw Ilse, maar vooral dochter Laura, niet vergeten! Jullie waren de enige kennissen van wie ik vernix heb mogen ontvangen. Deze beroepsdeformatie betekende voor mij waardevolle input voor dit onderzoek. Ik ben er van overtuigd dat een deel van mijn mooie resultaten rechtstreeks het gevolg is van de vernix van jullie mooie dochter. Bedankt!

Geert, Marijn, jullie hebben allebei je master-stage bij mij gedaan. Ondanks het vele werk, was het nog best lastig om mooie resultaten te krijgen. Uiteindelijk heeft toch nog geleid tot een hoofdstuk en daar mogen jullie best trots op zijn, ik ben het in ieder geval wel! Bedankt voor al het werk! Maarten en Arthur, jullie project was erg kort, maar bedankt voor jullie inzet!

De laatste maanden was ik wekelijks te vinden in Leiden. Ook daar wil ik iedereen bedanken voor de gezelligheid, maar ook voor alle hulp bij de experimenten. Met name Wouter, Dennis en Raphael, zonder jullie hadden we niet zoveel (goede) resultaten verkregen. Fred, Ine en Johan, ook jullie bedankt voor de inzet! Julia, je was altijd in voor een praatje. De laatste maanden zonder jou was het toch wel een beetje stil in Leiden.

At one of the congresses I attend, I met Kim Briggs. Recently we met again in NYC. Kim, thanks for the nice conversations and being such an inspiring person.

Na het werk, heb ik de nodige frustraties en stress heerlijk van mij af kunnen 'ballen' in het zwembad. Een stukje inspanning voor de ontspanning. Zowel mijn oude als nieuwe

teammaatjes, bedankt om mij AIO-perikelen toch altijd maar weer aan te horen. D4 (Christel, Alida, Marinka, Patricia, Mirjam, Maartje, Maud, Henriette, Jose, Willeke, Anita, Sjouck, Sylvia), bedankt dat ik afgelopen seizoen met jullie mee mocht doen. Ik vond het ontzettend gezellig en erg ontspannend. Hopelijk worden we dit jaar wel kampioen! Bianca, Merel, Jolien, Sharon, Maud & Sander, Nienke & Sander en Patrick, even weg van de AIO-stress in het zwembad, in de kantine, tijdens de vrijmarkt, op de piste of in de stad....bedankt voor alle sportiviteit en de leuke gesprekken. Dat er nog veel mogen volgen (gesprekken, wedstrijden en wintersporten)!

Naast het werk (en zwemmen) waren er natuurlijk ook andere vrienden met wie Jeroen en ik regelmatig wat afspraken. Ook jullie, Jiska & Martijn, Imke & Eric, Maartje & Boy, Laura & Remco en Rogier wil ik bedanken voor de gezellige uurtjes die we vaak aan tafel door brachten. En dan Emmani (Emm)...ik zou je niet durven vergeten! Samen gestudeerd en nu allebei aan het promoveren. Het was altijd gezellig als we elkaar weer spraken: bijkletsen, lachen of even klagen, het kan allemaal. Nog heel even doorzetten Emm en dan ben jij aan de beurt!

Bij deze wil ik ook Jan Pater bedanken dat ik één van zijn beelden heb mogen gebruiken voor de omslag van mijn proefschrift.

Nu ik dit dankwoord schrijf, ben ik nog niet begonnen aan mijn nieuwe baan. Maar ik heb al wel kennis mogen maken met mijn nieuwe collega's van Astellas. Dus bij deze wil ik jullie nu al allemaal bedanken voor de warme ontvangst. Ik heb daardoor alleen maar meer zin in gekregen om bij jullie te starten.

Een dankwoord begin je met de mensen die je inhoudelijk het meest bij hebben gestaan en eindig je vaak met de mensen die je het meest nabij hebt. Daarom wil ik hier mijn familie bedanken. Dus ik wil op deze plek mijn ouders bedanken, mijn opa & oma en het fantastische koppel mijn zus Muriel & Benno, die als nieuw lid van de familie wat zuidelijke charme in alle hectiek wist te brengen. Zonder jullie was ik nooit zover gekomen!
Tevens dank aan mijn (toekomstige) schoonouders en Manon en Sven. In vier jaar heeft het warme welkom dat jullie altijd voor me hadden veel voor me betekent.
Ouders en Schoonouders hebben ook altijd goede vrienden die met hun geinteresseerde houding mij ook tot steun waren, waarvoor dank, Koos & Rick en Warda & Peter & Ceasar.

Jeroen, met jou (verreweg de belangrijkste) sluit ik mijn dankwoord af. Promoveren, daar heb ik zelf voor gekozen, maar zonder je steun en onvoorwaardelijk vertrouwen was het nooit zo verlopen (en vast niet zo mooi geworden). Bedankt voor je hulp, begrip, liefde en dat je er gewoon altijd voor me bent!